Study of the development of elastomer nanoparticles and their application as reinforcing agents for poly(lactic acid)

Yuan Fang

CENTRE NATIONAL DE LA RECHERCHE SCIENTIFIQUE(CNRS)

UNIVERSITE DE LORRAINE
ÉCOLE DOCTORALE : RP2E
Laboratoire de LRGP

THÈSE

Présentée et soutenue publiquement le 07/12/2012
pour l'obtention du grade de Docteur de l'UNIVERSITE DE LORRAINE
(Spécialité : Génie des Procédés et des Produits)

par

Yuan FANG

Sujet :

Etude de l'élaboration de nano-particules élastomères et application de celles-ci en tant qu'agents renforçants pour le poly(acide lactique)

Composition du Jury:

Président du jury :	**Serge BOURBIGOT**	**Professeur- Ecole Nationale Supérieure de Chimie de Lille**
Rapporteurs:	**Serge BOURBIGOT**	**Professeur- Ecole Nationale Supérieure de Chimie de Lille**
	Norhafizah ABDULLAH	**Professeur- Université Putra Malaysia**
Examinateurs:	**Guo-Hua HU**	**Professeur -Université de Lorraine**
	Alain DURAND	**Professeur -Université de Lorraine**

REMERCIEMENTS

Ce travail de thèse a été effectué au sein du Laboratoire des Sciences du Génie Chimique (IRGP) devenu en 2012 Laboratoire Réactions et Génie des Procédés (LRGP). Je remercie Monsieur Michel SARDIN, alors directeur du LSGC et Monsieur Gabriel WILD, directeur du LRGP, pour leur accueil.

Je remercie Messieurs Guo-hua HU et Alain DURAND, mes directeurs de thèse, qui m'ont accueilli au sein de l'équipe Génie des Procédés de polymérisation (GP2). Je leur suis très reconnaissant de leurs conseils avisés et la confiance qu'ils m'ont témoignée au long de ces travaux. Ils sont toujours attentifs à la progression de nos travaux, ce en quoi ils ont grandement contribué à ma formation de chercheur.

Je n'oublierais pas d'adresser mes remerciements à Madame Sandrine HOPPE, responsable d'équipe GP2 et Monsieur Richard LAINE, ingénieur d'études d'équipe GP2, pour leur aides permanentes.

Une partie des analyses de ce travail ont été réalisées dans Université du Zhejiang en Chine et Ecole des Mines à Nancy. Je remercie ainsi Monsieur Lianfang FENG, Madame Xueping GU et Monsieur Olivier GODARD pour leur gentillesse et leur aide de la réalisation des tests de propriétés mécanique. Je remercie également Monsieur J. Ghanbaja dans la Service Commun de Microscopies Electroniques et de Microanalyses X (ECMEM) à la faculté des sciences de Nancy pour son savoir faire et son aide aux caractérisations de produits par MET dans ce travail.

Je remercie mes collègues Messieurs Jean-François REMY, Henri LENDA et Olivier FABRE, pour leurs grandes contributions à ces travaux de recherche. Leur appui a été essentiel aux nombreuses caractérisations de produits qui ont été effectuées.

Je tiens à remercier Monsieur Serge BOURBIGOT de l'Ecole Nationale Supérieure de Chimie de Lille et Madame Norhafizah ABDULLAH de l'Université Putra en Malaysia pour avoir accepté d'être rapporteurs de cette thèse, malgré leurs multiples occupations.

La liste de ces remerciements ne saurait être complète sans accorder une attention particulière à mes trois compagnons de bureau Sara, Itab, Salah et Zhenghui pour

leurs nombreuses suggestions et leur bonne humeur.

Un grand merci à tous mes collègues de LRGP qui ont su rendre mon séjour enrichissant et agréable. J'exprime mon amitié à tous les travailleurs de l'ombre au sein du LRGP : Annie, Claudine, de même que Véronique et Christine, sans oublier l'antenne informatique (Gérard et Fabrice).

Je tien à remercier beaucoup mes parents et mon mari pour me soutenir.

Résumé

Le poly(acide lactique) (PLA), est un polymère synthétisé à partir de ressources renouvelables, qui est l'objet de beaucoup d'études à l'heure actuelle mais qui souffre d'une faible résistance au choc. Le but de ce travail est de rechercher des pistes permettant la préparation d'un matériau à base de PLA avec une résistance au choc améliorée tout en minimisant la perte de résistance à la traction.

Les travaux présentés ici ont étudié le rôle de nanoparticules élastomères de poly(acrylate de butyle) (PBA) chargées de laponite (LRD) (PBA-LRD) ainsi que de nanocomposites cœur-écorce (PBA-LRD)/poly(méthacrylate de méthyle) (PMMA) en tant qu'agents de renforcement d'une matrice de PLA. Ces nanoparticules ont été dispersées dans la matrice PLA à l'état fondu. La synthèse de ces nanoparticules a été effectuée par polymérisation en émulsion ou miniémulsion. La laponite a été incorporée dans les nanoparticules afin de minimiser la perte de la rigidité tout en améliorant la résistance au choc de PLA. Trois types de tensioactifs et des modifications de surface de la laponite ont été testées pour améliorer l'adhérence entre les particules de PBA et la matrice de PLA. Enfin une écorce de PMMA a été utilisée pour assurer la bonne adhérence entre les particules de PBA et de matrice PLA. Nous avons montré que les particules cœur-écorce ont permis d'augmenter la résistance au choc au 3 fois du PLA tout en réduisant la diminution du module d'Young et la perte de résistance à la traction (~25%).

Les propriétés de les particules synthétiques et les propriétés des mélange du PLA avec les particules PBA ou particules cœur-écorce ont été étudiées par diverses techniques de caractérisation (DLS, FTIR, ATG, MET, MEB, RMN ^{1}H, DSC, DMTA…).

Mot-clé: Poly(acide lactique); Laponite; Poly(acrylate de butyle), Propriétés mécaniques; Polymérisation en mini-émulsion; Poly(méthacrylate de méthyle); Nanoparticules cœur-écorce.

Abstract

Poly(lactic acid) (PLA), come from renewable resources, one of the most important biopolymers, suffers from weak impact resistance. The aim of this work is to develop a process that will allow preparing a PLA with improved impact resistance while minimizing loss in tensile strength.

The work presented here examined in detail the synthesis of poly(butyl acrylate) (PBA) nanoparticles charged with laponite (LRD) (PBA-LRD) and (PBA-LRD) / poly(methyl methacrylate) (PMMA) core-shell nanocomposites. They were dispersed phase in PLA matrix and were synthesized by emulsion or miniemulsion polymerization. The clay such as laponite was included in these nanoparticles to minimize the loss of rigidity while improving the impact resistance of PLA. Note that three types of surfactants and some modify agents for LRD have been tried to improve the adhesion between the PBA particles and matrix PLA, PMMA was finally used to ensure a good adhesion between the PBA particles and the matrix. To this end, we explored successively the PLA blend, using PBA nanocomposites and the PBA/PMMA core-shell nanoparticles as reinforcing agents, with improved impact resistance, showing that core-shell particles allowed increasing of 3 times of impact strength of the PLA with a minimum amount of loss (~25%) in Young's modulus and tensile strength.

The properties of the synthetic particles and the properties of PLA blends have been demonstrated by various characterization techniques (DLS, FTIR, TGA, TEM, SEM, ^{1}H-NMR, DSC, DMTA ...).

Keyword: Poly(lactic acid); Laponite; Poly(butyl acrylate); Mechanical properties; Miniemulsion polymerization; Poly(methyl methacrylate); Core-shell nanoparticles.

Sommaire

Nomenclature

Symbol	Designation	Unit
$\vec{B}$	Magnetic field	-
CEC	Cationic exchange capacity	mol/g, mequiv/g
CMC	Critical micelle concentration	mol/m^3, mol/L
d	Diameter	m
d_n	Average diameter	m
d_v	Average volume diameter	m
d_i	Diameter of particle i	m
$D_{[3,2]}$	Surface diameter which a spherical droplet from an isometric sample whose surface identical to that of covered by the sample would have	m
$D_{[4,3]}$	Volume average diameter which a spherical droplet from an isometric sample whose volume identical to the volume occupied by the droplets would have	m
E	Young's Modulus	Pa
*E**	Complex elastic modulus	Pa
E'	Storage modulus	Pa
E"	Loss modulus	Pa
ES	The ratio between the quantity of the dried residual solids content and the total quantity of the sample started	-
$\bar{G}_i$	Interfacial partial molar free energy	J
G_c	Impact energy absorbed per square meter	KJ/m^2
ΔH_f	Enthalpy of fusion	J
ΔH_{cr}	Enthalpy of crystallization	J
K_c	Fracture toughness	$MN/4\ m^{2/3}$
k_p	Propagation overall coefficient	$m^3.mol^{-1}.s^{-1}$
ln	Natural logarithm	-
m	Weight of the sample at time t	g
m_0	Initial weight of the sample	g
m_i	Mass of the ingredient i	g
m_{mono}	Quantity of monomer	g
m.p.	Melting point	°C
$[M]_p$	Monomer concentration in the particles	mol/m^3
m_{sol}	Quantity of the various solid residues (initiator, surfactants, co-stabilizer ...)	g
M_{total}	Quantity of the sample at time t	g

$\bar{n}$	Average number of radicals per particle	-
n_i	Number of droplets of diameter d_i	-
N_{pi}	The number of particles containing i radicals	-
R	Gas constant	8.31 $J.mol^{-1}.K^{-1}$
r	Distance between the scattering medium and the detector	m
rpm	Revolutions per minute	$r \cdot min^{-1}$
T	Temperature	°C
T_c	Crystallization temperature	°C
T_g	Glass transition temperature	°C
T_α	Relaxation temperature	°C
T_m	Melting temperature	°C
wt%	Weight percent	-
γ	Polydispersity index	-
τ_1	Molecular diffusion degradation	-
τ_2	Coalescence by collisions	-
ν	Frequency	Hz
φ	Volume fraction of water	-
θ	Viewing angle	rad
Δ	Precedes the symbol of a parameter to denote finite change	-
ε^*	Sinusoidal strain	-
σ^*	Sinusoidal stress	Pa
δ	Shift phase	-

Acronym	Designation
AMBN	2,2'-Azobis (2-methylbutyronitrile)
BA	Butyl acrylate
CA	Cetyl alcohol
CTAB	Hexadecyltrimethylammonium bromide
DDAC	Dimethyldioctadecylammonium chloride
DLS	Dynamic light scattering
DMTA	Dynamic mechanical thermal analysis
DSC	Differential scanning calorimetry
FTIR	Fourier transform infrared spectroscopy
HD	Hexadecane
KPS	Potassium persulfate
LRD	Laponite RD
LRD-Si	Laponite RD modified by 3-Methacryloxypropyltrimethoxysilane
MMT	Montmorillonite
MMA	Methyl methacrylate
MPTMS	3-Methacryloxypropyltrimethoxysilane
NMR	Nuclear magnetic resonance
NR	Non-reactive
OMMT	Organic-montmorillonite
OTAB	Octadecyltrimethylammonium bromide
PBA	Poly (butyl acrylate)
PDI	Polydispersity index
PEGMEM	Poly (ethylene glycol) methyl ether methacrylate
PLA	Poly (lactic acid)
PLS	Polymer-layered silicate
PMMA	Poly (methyl methacrylate)
PS	Poly styrene
PSD	Particle size distribution
PVC	Polyvinyl chloride
QSSA	Quasi-steady-state approximation
SEM	Scanning electron microscopy
SLS	Sodium lauryl surfate
SDS	Sodium dodecyl sulfate
TEM	Transmission electron microscopy
TGA	Thermogravimetric analysis
UAc	Uranyl acetate
3A	3-Aminopropyltriethoxy silane
3G	(3-Glycidoxypropyl)trimethoxy silane

Résumé long

1. Introduction

1.1Le poly(acide lactique) et son renforcement mécanique

La fabrication de matériaux biodégradables propose une solution intéressante pour l'impact des matières plastiques. Une grande partie de l'augmentation de la consommation devrait provenir de ces polyesters comme poly(acide lactique) (PLA) et de ses mélanges. PLA, un polymère thermoplastique biocompatible et biodégradable dérivé de l'acide lactique (2-hydroxy-acide propionique) a attiré beaucoup d'attention des scientifiques lors de la dernière décennie comme un biopolymère susceptible de remplacer les plastiques à base de pétrole conventionnels, car il est un produit à partir ressources renouvelables tel que l'amidon. PLA pur peut être dégradé en dioxyde de carbone, eau et méthane en utilisant à long terme, par rapport aux autres plastiques pétroliers. Il a été largement utilisé pour des applications biomédicales telles que les sutures et dispositifs d'administration de médicaments en raison de sa nature biodégradable et biocompatible. Il peut facilement être transformé en pièces moulées, films, ou des fibres, et ainsi de suite. Malheureusement, le PLA est un polymère relativement fragile et rigide avec une faible déformation à la rupture, avec une température de transition vitreuse allant de 55 à 65 °C, sa robustesse et sa résistance à la chaleur ne sont pas satisfaisantes pour des applications à température ambiante dans de nombreux cas [1-11].

L'unité constitutionnelle de PLA, l'acide lactique, peut être fabriquée par fermentation de glucides ou synthèse chimique. L'acide lactique existe dans deux configurations optiquement actives, le L (+) et D (-) isomères (Schéma 1).

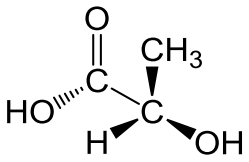

L-Acide Lactique
m.p. 16.8 °C

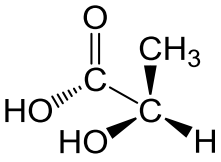

D-Acide Lactique
m.p. 16.8 °C

Schéma 1 Structure chimique de L et D-acide lactique (m.p. est le point de fusion) [12].

Le lactide, le dimère cyclique de l'acide lactique, est formé par la condensation de deux molécules d'acide lactique, comme suit: L-lactide (deux molécules de L-acide lactique), le D-lactide (deux molécules de D-acide lactique) et de méso-lactide (un L-acide lactique et une molécule de D-acide lactique).

Les unités répétées sont soit ajoutées sous forme de dimères lactide au cours de la polymérisation par ouverture de cycle ou sont ajoutées au polymère final comme monomères d'acide lactique par polymérisation en condensation directe, et une unité constitutionnelle de -[OCH(CH_3)CO-O-CH(CH_3) -CO]- est formée. L'unité répétée de PLA (72 g / mol) contient un stéréocentre qui est soit L (S) ou D (R) en configuration (Schéma 2).

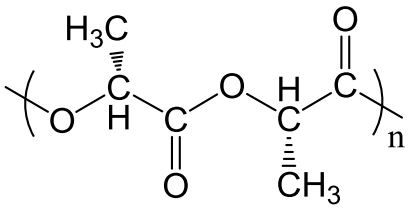

Polylactide, PLA

Schéma 2 Unité constitutionnelle de polylactide [12] .

Parmi ces trois formes isomères possibles, le poly(L-acide lactique) et le poly(D-acide lactique) sont semi-cristallins, et le poly(méso-acide lactique) ou poly(d, l-acide lactique) est amorphe. Les grades amorphes de PLA sont transparents.

Les propriétés physiques et mécaniques du PLA peuvent être modifiées par le contrôle des chaînes de PLA et la combinaison avec d'autres additifs et / ou des charges. Des efforts importants ont été consacrés à la modification de la fragilité du PLA par

copolymérisation de lactides avec d'autres monomères. Bien que la copolymérisation puisse être efficace dans l'amélioration des propriétés mécaniques du PLA, la commercialisation d'un nouveau copolymère est souvent un processus long et coûteux, ce qui rend cette option moins attractive pour les applications du PLA. Des charges minérales telles que le carbonate de calcium, les biocéramiques, la fibre de bambou; plastifiant tel que le polyéthylène glycol (PEG) et glucosemonoesters ou des polymères de la seconde phase tels que des caoutchoucs, la polycaprolactone (PCL), ont déjà été utilisés en combinaison avec PLA pour améliorer la résistance aux chocs et la ténacité du PLA. Les plastifiants sont souvent utilisés non seulement pour accroître la flexibilité et la ductilité des polymères vitreux, mais aussi pour améliorer la facilité de mise en œuvre ou bien la dispersion des charges. L'inconvénient majeur de plastifiants, c'est que pendant utilisation de la matière à long terme, ils ont tendance à migrer vers la surface du matériau, causant la fragilité de PLA. Le PLA peut aussi être mélangé avec un polymère solide pour améliorer efficacement sa résistance, mais cela nécessite généralement une quantité relativement élevée du polymère plus résistant, ce qui peut conduire à une réduction significative du module et la résistance. La plupart de ces mélanges PLA sont non miscibles et des compatibilisants sont nécessaires pour améliorer le mélange. Pendant ce temps, leur résistance au choc avait augmenté, mais normalement au dépens de la rigidité inhérente de la matière [1-3, 5, 7-10].

1.2 Renforcement par élastomère ou de l'argile

Le mélange du PLA avec d'autres polymères représente une méthode souple et économique d'obtenir des produits renforcés mécaniquement. Une méthode efficace pour durcir intrinsèquement le PLA est de mettre à profit la ténacité du caoutchouc. Bien que l'incorporation de particules de caoutchouc améliore la ténacité à la rupture de PLA, elle conduira également à une réduction du module de traction et de la résistance à la traction. En général, les particules sphériques de caoutchouc agissent en tant que concentrateurs de contraintes, en initiant et de terminant des manies dans les matrices polymères fragiles, qui sont responsables pour l'absorption de l'énergie de

fracture [1, 5, 13-14].

Certains auteurs [15] ont tenté d'améliorer la ténacité du PLA par le mélange de poly(acrylate de butyle) (PBA). Dans leur étude, une interface réactive (type R) entre le caoutchouc et le PLA a été formée, mais le système multiphasé n'a pas réussi à produire le durcissement souhaité. La résistance aux chocs et le module de flexion de la matrice PLA sont gravement détériorés par la présence de PBA. Les valeurs enregistrées pour le mélange non-réactif (type NR) étaient encore plus faibles que celles du matériau de type R.

La principale raison des propriétés mécaniques médiocres des mélanges PBA / PLA est que le PBA a une mauvaise compatibilité avec le PLA. PBA ne peut pas être dispersé convenablement dans la matrice PLA, ce qui provoque une mauvaise adhérence interfaciale. Il a été rapporté que l'interaction interfaciale affecte les propriétés mécaniques du composite [4].

D'un point de vue de l'application, on préfère naturellement d'avoir des matériaux qui sont durs et les propriétés de traction maintenue. Le choix naturel serait l'incorporation de charges rigides (comme les particules inorganiques ou des fibres de verre) et des inclusions d'élastomères simultanément.

Ces dernières années, les nanocomposites polymère/nanoparticules inorganiques ont reçu une attention importante car ils présentent des améliorations remarquables de propriétés mécaniques, thermiques, optiques, électriques et magnétiques par rapport à la matière pure ou les composites conventionnels. Les nanocomposites polymère/argile sont intéressants car ils combinent la structure, les propriétés physiques et chimiques de ces deux matériaux inorganiques et organiques [16-21].

Les propriétés du nanocomposite polymère/silicate dépendent notamment de la distribution et de la dispersion du silicate dans la matrice polymère. Des efforts considérables ont été faits pour développer des méthodes de synthèse dans le but de contrôler les dispersions de la charge inorganique au sein du polymère hôte.

Il existe trois méthodes de préparation principales de nanocomposites polymère / silicate, qui peuvent être résumées comme polymère / pré-polymère intercalation de la solution, fusion intercalation, et polymérisation in situ, qui comprend masse, en

solution, et la polymérisation en suspension, polymérisation en émulsion, et polymérisation en miniémulsion.

Le mélange poly(L-lactide) + argile a révélé une mauvaise dispersion de l'argile dans le polymère. Bien que les nanocomposites peuvent être préparées par simple mélange des nanoparticules avec les matrices polymères par agitation à haut cisaillement ou broyage à billes, le degré de dispersion de nanoparticules et l'adhérence interfaciale sont évidentes insuffisante pour obtenir les propriétés souhaitables [9, 12, 18].

En outre, dans les dernières années, le procédé de polymérisation in situ qui comprend principalement polymérisation en émulsion, a gagné beaucoup d'intérêt parce que ce procédé de polymérisation hétérophasé offre de nombreux avantages par rapport à polymérisation en solution comme une faible viscosité du milieu de suspension, de haute masses moléculaires des polymères, la simplicité de la polymérisation et la possibilité de contrôler la morphologie des particules.

Pour la production de nanocomposites à base d'eau pour les applications de revêtements et d'adhésifs, de polymérisation en émulsion in situ est la meilleure solution adaptée, en particulier lorsque la Na-MMT (montmorillonite naturelle) hydrophile non modifiée est utilisé. Dans la plupart des cas, l'argile non-modifiée préfère rester dans la phase aqueuse ou à l'interface huile-eau, mais pas dans la phase huileuse. L'argile non-modifiée simplement mélangés dans la phase aqueuse ou d'ajouter de l'argile dans une étape de post-polymérisation réalisés les produits finaux obtenus sont pas un latex thermodynamiquement stable, mais sont aptes à former des agrégats. D'autres travaux ont également montré qu'il est possible de synthétiser des nanocomposites à base d'eau utilisant des plaquettes d'argile comme le seul agent de stabilisation, qui soi-disant émulsions de Pickering. Cependant, la stabilité de ces dispersions d'argile dans les émulsions de Pickering est très faible et ils sont très sensibles à ce type d'initiateurs utilisés lors de la polymérisation.

En outre, si les argiles organophiles (où les cations des argiles naturelles ont été substitués par échange cationique avec des sels d'ammonium alkyle) sont employées, polymérisation en émulsion n'est pas la meilleure solution parce que l'argile ne sera pas incorporée dans les particules de polymère. Par polymérisation en émulsion, les

particules nanocomposites avec cœur-écorce, de framboise, de type marguerite-forme, et de type multipod morphologie ont été obtenus en fonction de la chimie de surface et la taille des particules inorganiques. La polymérisation en émulsion n'est également pas disponible en raison de la contradiction entre le mécanisme de nucléation de cette approche et l'emplacement de l'argile à encapsuler, même si elle a été un outil puissant pour manipuler une large gamme de produits en latex. Si une particule d'argile doit être conservée séparément dans une des gouttelettes, il faut résister à la coalescence et la coagulation provoquée par la collision des gouttelettes sous cisaillement élevé. Il doit y avoir aucun transfert de radicaux oligomères à partir des micelles gonflées dans la phase aqueuse à la phase huileuse, où l'argile existe, pour ce qui inévitablement provoquer la coagulation, si le mécanisme de nucléation dans un procédé de polymérisation en émulsion normale est suivie. Dans un procédé de polymérisation en émulsion classique, l'argile organophile ne peut pas être incorporée dans les particules de polymère car la diffusion de l'argile organophile à travers la phase aqueuse n'est pas favorisée.

Une approche prometteuse pour la synthèse de polymères/argile nanocomposites (dans la gamme submicronique) en utilisant argiles modifiées est la polymérisation en miniémulsion, où les gouttelettes de monomère peut contenir des piles d'argile hydrophobes lors de la polymérisation (la nucléation et la polymérisation se produit dans les gouttelettes de miniémulsion) pourrait conduire à des nanostructures exfoliées. Pendant ce temps, la polymérisation en miniémulsion présente de nombreux avantages pour la synthèse de polymères/nanocomposites inorganiques encapsulé en raison de son excellente stabilité à la fois avant et après la polymérisation, la taille des gouttelettes submicroniques entre 50 et 500 nm, et son mécanisme unique de nucléation des gouttelettes durant la polymérisation.

Si les particules inorganiques peuvent être bien dispersées dans la phase monomère suivie par minemulsification, chaque gouttelette inférieure au micron peut en effet agir en tant que nanoréacteur, qui produit des particules nanocomposites avec des rendements élevés d'encapsulation des particules inorganiques.

Il a été constaté que, dans un procédé de polymérisation en miniémulsion, la taille

moyenne des particules, la distribution granulométrique et les propriétés de surface de l'argile jouent un rôle remarquable dans l'encapsulation et l'exfoliation ainsi que la stabilité du produit final. Toutes les stratégies proposées nécessitent un prétraitement de l'argile afin d'améliorer sa compatibilité avec la matrice polymère et obtenir une bonne dispersion.

L'hydrophobicité de la surface des particules d'argile est importante pour la polymérisation en miniémulsion. Une argile hydrophobe, par rapport à son hydrophilie intrinsèque, est donc nécessaire pour favoriser son séjour dans la phase huileuse avant la polymérisation. Cette hydrophobie aidera l'entrée de monomère dans les galeries interfoliaires de l'argile et exfolier l'argile à partir d'un face à face d'empilage à une forme dispersés individuellement plaquettaire après polymérisation. Il est bien connu que les surfaces basales d'argiles sont hydrophobes et leurs surfaces de bord sont hydrophiles. Le caractère hydrophobe des surfaces basales à cause du fait que les atomes exposés à la surface sont reliés entre eux par des liaisons siloxane (Si-O-Si) et, par conséquent, ne peuvent pas former de liaisons hydrogène avec de l'eau. Par ailleurs, le caractère hydrophobe des surfaces basales est aussi important pour l'intercalation des particules d'argile, car des surfaces basales hydrophobes faciliter l'entrée du monomère dans les galeries intérieures de l'argile. Les surfaces de bord, d'autre part, sont constitués d'ions hydroxyle, le magnésium, le silicium, et des cations substitués, qui tous subissent une hydrolyse. Par conséquent, les bords sont hydrophiles et peut former de fortes liaisons hydrogène avec de l'eau. Il est souvent nécessaire de rendre la charge d'argile naturellement hydrophile pour augmenter sa compatibilité avec un matériau polymère organique [21] [22] .

Les composés organiques peuvent être incorporés dans les galeries interfoliaires par un processus d'échange d'ions. Réactions d'échange d'ions avec des agents tensioactifs cationiques, notamment les ions ammonium primaire, tertiaire et quaternaire rendre la surface de silicate hydrophobe, ce qui rend l'insertion ultérieure d'une variété de monomères et / ou polymères possible.

En outre, Norma et al. [20] ont intégré l'argile avec les cations alkylammonium qui peuvent fournir des groupes fonctionnels réactifs (par exemple, des monomères, des

initiateurs, catalyseurs, etc.) qui peuvent participer à la polymérisation et promouvoir l'exfoliation des couches d'argile.

Il a été signalé que le nano-composites polymère-silicate (PLS) délaminé est plus efficace pour améliorer la résistance de la matrice polymère par rapport à un nano-composites PLS intercalé. La concentration d'argile dans les composites est très important, que les argiles seront re-agrégés à une plus grande agglomération au-dessus de 2-3% en poids de matières solides. Prendre en considération, le nanocompsoite final ne doit pas avoir plus de teneur d'argile de 2-3% en poids pour obtenir une argile exfoliée vraiment dans la matrice polymère [23-25].

1.3 Polymérisation en émulsion et miniémulsion

La polymérisation en émulsion est le moyen le plus courant pour former des latex de polymère. Dans la version la plus simple, les ingrédients comprennent de l'eau, un monomère de faible solubilité dans l'eau (par exemple le styrène), un amorceur soluble dans l'eau (par exemple le persulfate de potassium) et un tensioactif (latex peut également être synthétisée sans ajouter agent tensioactif et / ou un initiateur, mais ce n'est pas commun). Une nouvelle phase est rapidement formé: d'un polymère colloïdal, comprenant une phase discrète de particules de latex colloïdalement stable, dispersée dans une phase aqueuse continue. La polymérisation se produit au sein de ces colloïdes. À la fin de la réaction, chaque colloïde contient de nombreuses chaînes de polymère. Les stabilisants peuvent être électrostatiques (par exemple avec un agent tensioactif ionique tel que le dodécylsulfate de sodium), stériques (avec un tensioactif non ionique, ou un polymère, un stabilisant tel que le poly (oxyde d'éthylène) éther de nonylphényle), ou électrostérique. Plusieurs chercheurs [24, 26-28] ont utilisé la polymérisation en émulsion classique en présence de plaquettes d'argile-modifiées pour préparer composites polymère-argile particules.

Dans une polymérisation en émulsion, le monomère est dispersé dans une solution aqueuse de tensioactif avec une concentration supérieure à la concentration micellaire critique (CMC) et la polymérisation est démarrée à l'aide d'un système amorceur soluble dans l'eau. En principe, les particules de polymère peuvent être formées par

des radicaux entrés dans les micelles (nucléation hétérogène), la précipitation des oligomères de croissance dans la phase aqueuse (nucléation homogène), et l'entrée de monomère radicalaire dans gouttelettes. Toutefois, des gouttelettes de monomère sont relativement grandes (1-10 µm) par rapport à la taille des micelles gonflées de monomère (10-20 nm), et donc l'aire de surface des micelles est de plusieurs ordres de grandeur supérieure à celle des gouttelettes de monomère. Par conséquent, la probabilité pour un radical d'entrer dans les gouttelettes de monomère est relativement faible, et la plupart des particules sont formées par nucléation soit homogène ou hétérogène. Une fois formées, les particules de polymère subissent une croissance importante par polymérisation. Le monomère requis pour la polymérisation doit être transporté à partir des gouttelettes de monomère par diffusion à travers la phase aqueuse. Il s'agit d'une caractéristique essentielle de la polymérisation en émulsion qui peut parfois être aussi une limitation.

La nécessité du transport de monomère dans la phase aqueuse serait fortement diminuée si tous les gouttelettes de monomère (ou au moins une grande partie) étaient directement le siège de la nucléation. La nucléation des gouttelettes ne peut avoir lieu que si la surface des gouttelettes de monomère est grande par rapport à celle des micelles, ce qui nécessite que la taille des gouttelettes soit submicronique et que le nombre de micelles soit très réduit voire nul. Le mot miniémulsion a été inventé par Chou et al. [29] pour décrire des dispersions submicroniques huile-dans-eau stables pendant une période allant de quelques heures à plusieurs mois. Il a été montré [30] que l'addition d'une petite quantité d'un composé insoluble dans l'eau dans les gouttes d'une miniémulsion ralentit significativement la diffusion moléculaire. En effet, la lenteur de la diffusion du composé insoluble dans l'eau permet au monomère d'atteindre un potentiel chimique sensiblement dans les gouttes de différentes tailles.

Durbin et al. [31] ont étudié de façon systématique l'influence de la taille des gouttes de monomère sur la nucléation directe des gouttes pour un styrène + tensioactif anionique dans l'eau. Il a été constaté qu'en l'absence d'alcool cétylique ou d'hexadécane, la nucléation des gouttelettes était négligeable. Ces premiers travaux ont établi la base pour le procédé de polymérisation en miniémulsion, à savoir que

l'homogénéisation énergique doit être appliquée pour réduire la taille des gouttelettes de monomère, et que ces gouttelettes doivent être protégées à la fois contre la dégradation par diffusion moléculaire et vis-à-vis de la coagulation via l'utilisation d'un composé insoluble dans l'eau et d'un agent tensioactif efficace.

Le composé à stabiliser les gouttelettes de monomères contre mûrissement d'Ostwald a également été appelé un ultra-hydrophobe. Cependant, bien que tout composé insoluble dans l'eau puisse retarder la dégradation de diffusion, son efficacité dépend fortement de la masse molaire. Ainsi des composés insolubles dans l'eau de faible masse molaire sont beaucoup plus efficaces. Par conséquent, le terme co-stabilisant est utilisé dans cette thèse et se référera à des composés insolubles dans l'eau de faible masse molaire, qui sont très efficaces dans la stabilisation des gouttelettes de monomères contre la dégradation de diffusion.

Selon l'état de l'art, il peut être conclu que miniémulsions sont une forme de dispersions de gouttelettes de taille entre 50 et 500 nm dans la phase aqueuses et sont opaques et d'apparence laiteuse. Elle est généralement obtenue par application d'un cisaillement élevé au mélange diphasique, fourni par un appareil à ultrasons ou un homogénéiseur mécanique. La stabilité de ces gouttelettes résulte de l'utilisation d'un tensioactif ionique ou non ionique couplée avec un co-stabilisant qui est hautement soluble dans monomère, hautement insoluble dans l'eau.

Dans une miniémulsion correctement formulée, tous les micelles initialement présentes sont dissociées pour recouvrir la surface des gouttelettes. Par conséquent, laissant la nucléation des gouttelettes est bien le processus de nucléation majoritaire et la nucléation homogène a été considérée comme mineure. Dans une polymérisation en miniémulsion idéale, il n'y a pas de transport monomère dans la phase aqueuse et les particules de latex obtenues doivent avoir environ la même distribution de tailles que les gouttelettes initiales.

Il a été montré [32] que la taille des gouttelettes diminue également avec le temps d'agitation, la puissance sonication, le temps de sonication et la quantité de tensioactif utilisé, et augmente avec la fraction volumique de la phase dispersée.

1.4 Les mélanges de PMMA et PLA

Les propriétés des mélanges de polymères dépendent non seulement de la composition chimique du mélange, mais également de la compatibilité ou la miscibilité des constituants. Par conséquent, comme PBA et le PLA ne sont pas miscibles, le mélange de PBA/PLA ne pourrait pas atteindre les propriétés mécaniques souhaitées. De plus l'addition d'une grande quantité de PBA dans une matrice de PLA certes améliorerait la résistance aux chocs du mélange, mais aurait l'inconvénient de diminuer le module d'élasticité. Le poly(méthacrylate de méthyle) (PMMA) est utilisé dans divers domaines de notre vie quotidienne, c'est à dire, dans les industries du bâtiment et des aspects médicaux. Le PMMA est reconnu partiellement miscible à PLA, et la présence de PMMA a amélioré le module de Young des mélanges PLA/PMMA [5, 14, 15, 33-35].

Avella et al. [14] ont examiné l'utilisation du PMMA comme phase dispersée dans des mélanges avec le PLA. L'augmentation de la T_g du PLA est l'indication d'interactions entre PLA et PMMA. Le mélange PLA/PMMA 70/30 non-réactif est très homogène et aucune particule de PMMA dispersée n'est visible. Les propriétés de flexion et de l'impact de mélanges ont été analysées et le module de Young a été amélioré pour les mélanges PLA/PMMA.

1.5 Les particules cœur-écorce PMMA/PBA

Les nanoparticules cœur-écorce sont utilisées dans une grande variété d'applications afin de maîtriser des propriétés très diverses : augmenter la résistance à l'usure du polymère, la résistance à l'abrasion, la résistance aux intempéries, la résistance aux UV, la résistance à la traction, la résistance aux chocs, améliorer la transparence, réduire la température minimale de formation de film ou encore faciliter la mise en œuvre [36] [37].

Les performances des particules polymères composites formées par polymérisation en émulsion dépendent fortement de leur morphologie. La structure des particules de latex dépend, par exemple, du choix des monomères ou comonomères, des conditions

de synthèse telles que la température, le type d'initiateur et de tensioactif, la densité de réticulation et d'autres variables. La synthèse de latex cœur-écorce ne mène habituellement pas à une morphologie idéale cœur-écorce avec une séparation de phase complète. Dans la plupart des cas, la morphologie des particules résultant ne peut pas être décrite simplement comme un type cœur-écorce. Cela est dû à l'interaction de thermodynamique ainsi que les paramètres cinétiques pendant le processus de polymérisation. Les structures possibles de ces latex composites cœur-écorce sont diverses (figure 1) selon la compatibilité des deux polymères et les conditions de réaction [36] [38] [39] [40] [41].

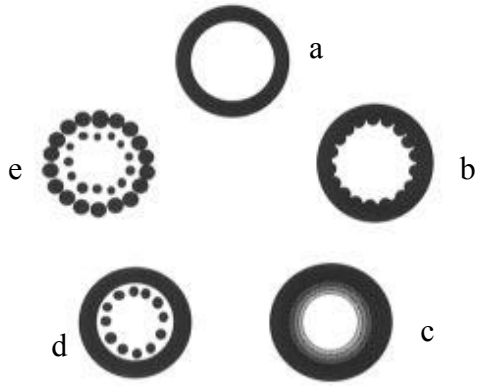

Figure 1 Morphologies différentes de (a) à cœur-écorce idéale: (b) d'interface avec une structure ondulée, (c) d'interface avec un gradient des deux composants, (d) d'interface avec des microdomaines; (e) microdomaines dans l'interface et un structure de l'île comme écorce [36].

Des particules cœur-écorce peuvent être préparées par diverses voies telles que un procédé en deux étapes de polymérisation en émulsion ensemencée, réticulation suspension, la coacervation, la polymérisation interfaciale, l'évaporation du solvant et polymérisation des vésicules. Il est aussi possible de combiner polymérisation mini-et micro-émulsion avec les techniques mentionnées.

La polymérisation en émulsion ensemencée devient peu à peu le moyen le plus largement utilisé et le procédé le plus courant pour préparer des nanocomposites cœur-écorce. Avec la quantité croissante de la deuxième étape, un type cœur-écorce est plus favorable. La couverture des particules synthétisées dans la première étape est

augmentée en augmentant la quantité de monomère polymérisé durant la deuxième étape.

Dans la plupart des cas, il faut choisir un monomère peu hydrophile pour former le matériau de cœur et un monomère avec une plus grande hydrophilie pour former le matériau d'écorce. Dans le cas contraire, le cœur monomère ou polymère plus hydrophile va migrer vers la phase aqueuse et former des particules de structure non régulière. Les paramètres de solubilité du PBA est de 8,8 $[cal/cm^3]^{1/2}$ et du PMMA est de 9,25 $[cal/cm^3]^{1/2}$. L'écorce en PMMA est plus hydrophile que la PBA, une particule de structure cœur-écorce est attendue [36] [38] [40] [42].

Les latex poly(acrylate de butyle) / poly(méthacrylate de méthyle) (PBA/PMMA) cœur-écorce sont largement utilisés dans diverses applications industrielles comme modificateurs d'impact, ainsi que pour les applications touchant à la résistance à l'eau, la résistance à la traction et la force adhésive. Dans le cas spécifique des modificateurs d'impact, le cœur doit être fait d'un matériau hautement élastique tel que le poly(acrylate de butyle) (PBA) pour offrir une résistance aux chocs. Il est généralement admis que la forte adhérence interfaciale est essentielle pour les propriétés mécaniques supérieures, alors une écorce PMMA peut améliorer la compatibilité avec la matrice et la ténacité du matériau. Les améliorations des propriétés mécaniques dynamiques d'un modificateur d'impact directement fonctionne des propriétés du cœur caoutchouteux, l'épaisseur de l'écorce PMMA et la distribution de taille des particules du latex (aussi bien définie que possible, et de préférence pas plus grande que 200 nm). Cependant, la raison de l'existence d'une taille optimale des particules n'a pas été clairement expliquée. Si l'écorce est trop épaisse, le comportement caoutchouteux requis pour un modificateur d'impact est perdu. D'autre part, lorsque la couche d'écorce est trop mince, elle est tout simplement incapable de protéger et de couvrir le cœur interne de caoutchouc dans des conditions de traitement agressives [43] [44].

Le cœur caoutchouteux constitué de PBA est légèrement réticulé, afin de maintenir sa forme et sa taille au cours du mélange à l'état fondu. Les particules de cœur PBA sont d'abord formées et séquentiellement atteint la taille désirée. Pour obtenir la structure

cœur-écorce par polymérisation en émulsion ensemencée, la vitesse d'addition de monomère MMA devrait être plus lente que sa vitesse de polymérisation (goutte à goutte au système réactionnel pour le maintenir dans un état affamé). Le MMA a été ajouté dans un processus affamés et une nouvelle quantité d'amorceur a été ajouté en même temps. Avec la présence de l'amorceur nouvellement introduit, l'atome de carbone tertiaire de la chaîne PBA pourra donner lieu à des réactions de transfert de chaîne. De cette manière, des chaînes de PMMA se trouveront greffées à la surface des particules primaires. Par conséquent, les nanocomposites cœur-écorce obtenus sont censés avoir une plus forte adhérence interfaciale entre cœur et matrice. Sous la condition affamée, le produit obtenu a montré une distribution de taille étroite (l'indice de polydispersité-PDI était petit) et une structure cœur-écorce bien définie. Ils en ont déduit que le latex d'ensemencement qui ont suffisamment de temps pour capturer monomère 2 lorsque la vitesse d'alimentation du monomère 2 est suffisamment lente pour que monomère 2 entrer la particule de germe de forme bien définie des particules à cœur-écorce. Si monomère 2 est ajouté dans un état de régime non-affamé, certains monomère 2 serait toujours entré les particules germes et polymériser à la surface de particules d'ensemencement, tandis que les autres pour absorber tensioactif forment des micelles, et enfin polymériser pour former des homopolymères, qui conduit à une plus large distribution de taille une structure irrégulière. Il ne faisait aucune différence dans la conversion finale et de l'efficacité du gel pour augmenter la quantité de l'agent tensioactif, mais la distribution de taille élargie évidemment. Le surfactant micelles formées vides lorsque l'on augmente la quantité de l'agent tensioactif et la grande quantité de micelles vides a donné l'occasion de monomère 2 pour entrer dans les micelles, ce qui a conduit à la formation des particules d'homopolymère de taille différente, de sorte que la distribution de taille se trouvait élargie. Dans ce système, un ratio de 50/50 est nécessaire pour atteindre des particules PBA/PMMA cœur-écorce. Pour les latex ayant une teneur en extérieur au-dessous de 35%, la structure de l'écorce est encore incomplète [38] [43] [45] [46].

L'approche développée dans cette étude pour améliorer la ténacité de PLA, tout en

conservant autant que possible sa résistance à la traction est d'incorporer des nanocomposites PBA/laponite dans le PLA. Les particules sont fonctionnalisées laponite par échange d'ions, afin de promouvoir la formation de polymère sur leur surface et créer des nanocomposites particules colloïdales par polymérisation en miniémulsion. La stratégie suivie et les étapes de réaction pour la préparation de particules nanocomposites sont illustrées sur la Figure 2.

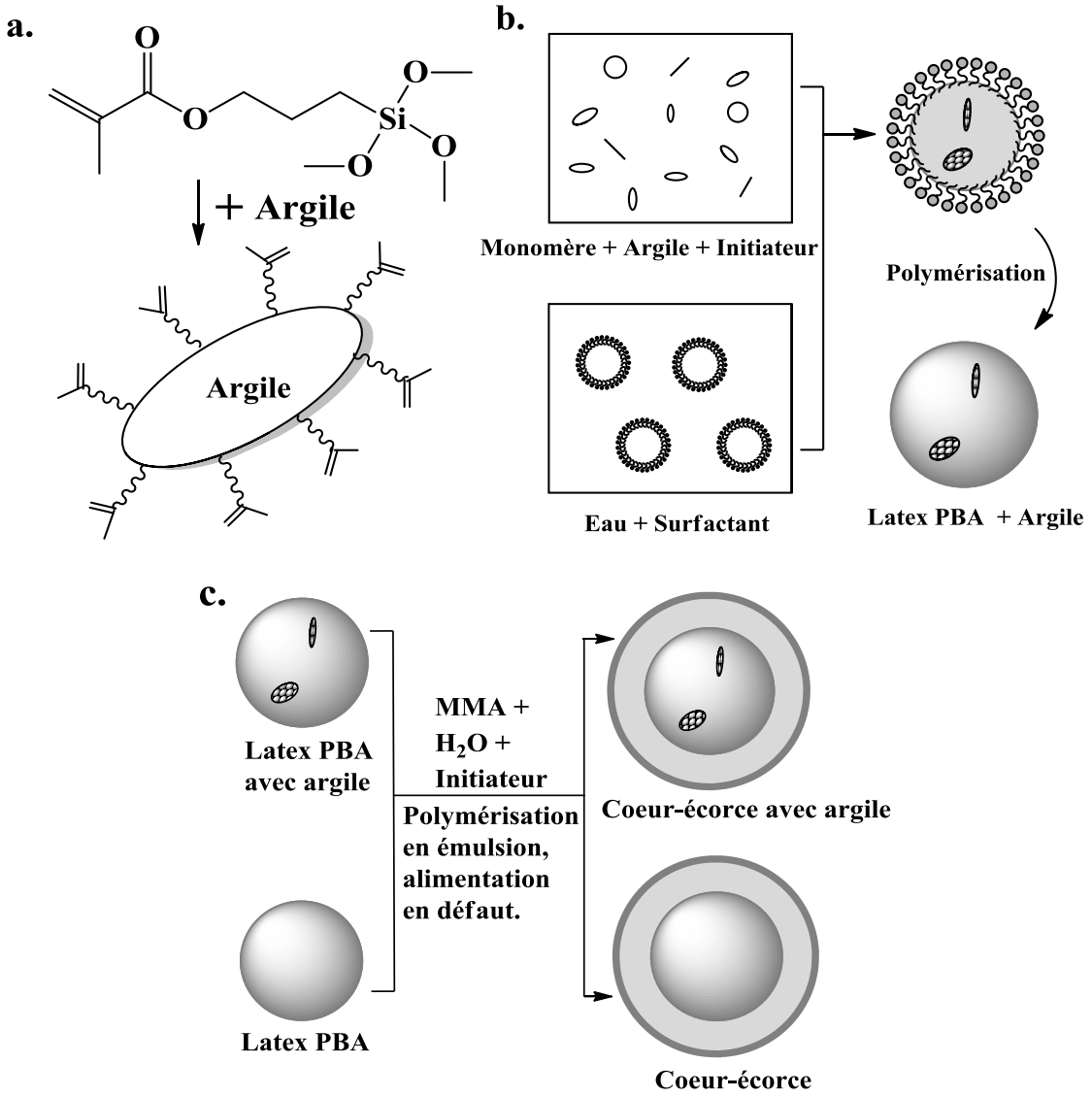

Figure 2 Représentation schématique de (a) la silylation des plaquettes d'argile avec tri-fonctionnel silane, (b) la préparation de la PBA / argile particules composites par polymérisation en mini-émulsion, (c) la préparation particules de cœur (PBA)-écorce (PMMA) par polymérisation en émulsion ensemencée.

2. Partie Expérimental

2.1 Fonctionnalisation

La silylation de la laponite (LRD) a été effectuée dans le toluène. Le LRD (6 g) a été séché à 60 °C pendant 12 heures dans une étuve à vide. Il a été introduit dans un ballon contenant 200 ml de toluène anhydre. L'agent de silylation, le 3-methacryloxypropyltrimethoxysilane (MPTMS) à hauteur de 4,4 g a été introduit dans le ballon et le tout a été agité pendant plusieurs jours à 60 °C. Le LRD résultant (LRD-Si) a été lavé longuement avec du toluène afin d'éliminer le silane non greffé puis séché à 40 °C dans un étuve à vide pendant une nuit pour une utilisation ultérieure.

2.2 Synthèse des particules de latex PBA

Les particules de latex PBA ont été préparées par polymérisation en mini-émulsion. Le Tableau 1 et la Figure 3 montrent les compositions et la procédure de polymérisation en mini-émulsion, respectivement. Celui-ci était composé de deux étapes successives: la préparation de la mini-émulsion et la polymérisation.

Tableau 1 Compositions pour la préparation de particules de latex PBA.

Latex PBA	Mélange A						Mélange B	
	BA (g)	LRD (g)	LRD-Si (g)	CTAB (g)	HD (g)	AMBN (g)	Brij700 ou Brij78(g)	H_2O (g)
PBA	20	-	-	-	0.8	0.4	4	74
PBA-LRD	20	0.4 - 1	-	0.8	0.8	0.4	4	74
PBA-LRD-Si	20	-	0.4 - 1	0.8	0.8	0.4	4	74

Préparation de la miniémulsion

Mélanges A et B ont été introduits dans deux récipients en verre, respectivement, sous l'action d'agitation magnétique. Après 1h d'agitation magnétique dans un bain de glace, le mélange A a été immédiatement soumis à des ultrasons pendant 3 min en utilisant un sonicateur de type Hielscher (0.5s du temps de cycle, 70% de l'amplitude, les

échantillons étant refroidi par un bain de glace). Le mélange B a été préparé avec agitation magnétique à température ambiante pendant 1 h, puis refroidi dans un bain de glace. Finalement, les mélanges A et B ont été mélangés dans un récipient en verre sous agitation magnétique dans un bain de glace pendant 30 min et encore homogénéisé avec l'appareil à ultrasons dans le bain de glace pour un autre 3 min. Le mélange obtenu est prêt pour la polymérisation ultérieure.

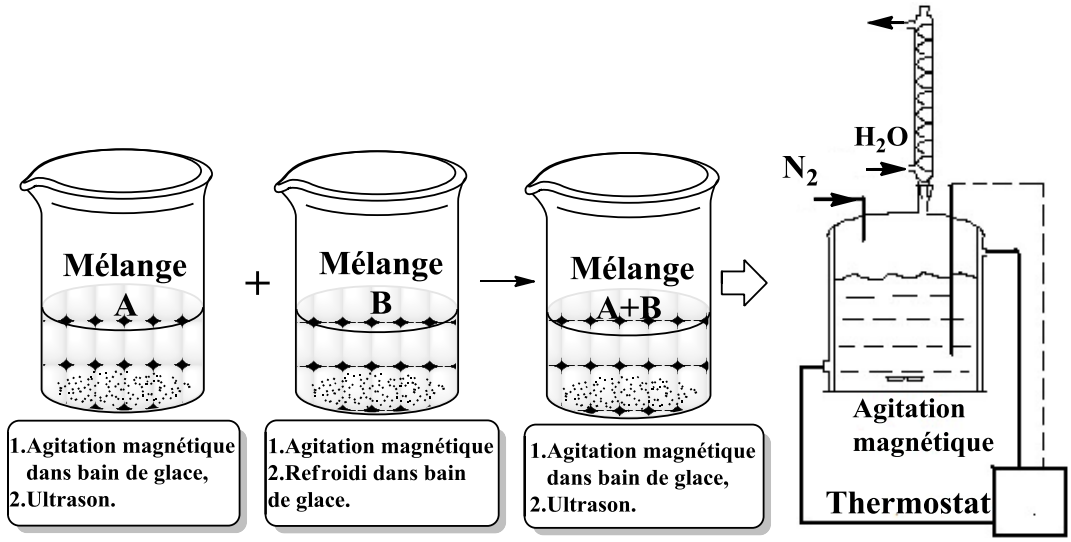

Figure 3 Procédure pour la préparation de la mini-émulsion et sa polymérisation pour obtenir des latex PBA.

Polymérisation

La mini-émulsion telle que préparée a été dégazée par barbotage d'azote pur pendant 30 min sous agitation magnétique dans un réacteur en acier inoxydable à 20 °C. La température du réacteur a été ensuite portée à 75 °C. La polymérisation a été effectuée à cette température pendant plus de 3h sous agitation continue et a été arrêtée par addition d'hydroquinone dans le système. La conversion en polymère a été déterminée par gravimétrie.

2. 3 Particules de PBA avec un tensioactif polymère

Le méthacrylate de poly(éthylène glycol) éther est un tensioactif polymère avec une double liaison en bout de chaîne. La partie poly(oxyde d'éthylène) est un groupe hydrophile et miscible avec le PLA. Une autre partie de la double liaison est le groupe hydrophobe (méthacrylate) qui peut réagir avec la surface des gouttelettes de monomère.

Le tensioactif réactif (PEGMEM, Mn = 950 g/mol) a été ajouté comme un agent tensioactif dans le milieu de polymérisation en mini-émulsion pour préparer des latex PBA.

Tableau 2 Compositions utilisées pour la préparation de particules de latex PBA par polymérisation en mini-émulsion avec le tensioactif PEGMEM.

Mélanges	***Composants***	***Quantité (g)***	***Concentration***
Phase d'huile	BA	20	20 wt%[a]
	AMBN	0.4	2 wt%[b]
	HD	0.8	4 wt%[b]
Phase d'eau	H_2O	70-77	70-77%[a]
	PEGMEM	2-8	0.03-0.12mmol[c]

[a] Basé sur une system totale. [b] Sur la base de monomère. [c] Sur la base aqueuse

2.4 Particule PBA-LRD-Si réactif

2.4.1Traitement au silane

3-aminopropyltriéthoxy silane (silane 1) et le 3-glycidoxypropyltriméthoxysilane (silane 2) ont été utilisés comme agents de couplage pour modifier la surface du LRD. La réaction ayant lieu dans un traitement de surface a été montré sur le schéma 3.

Silane 1: 3-Aminopropyltriethoxy silane

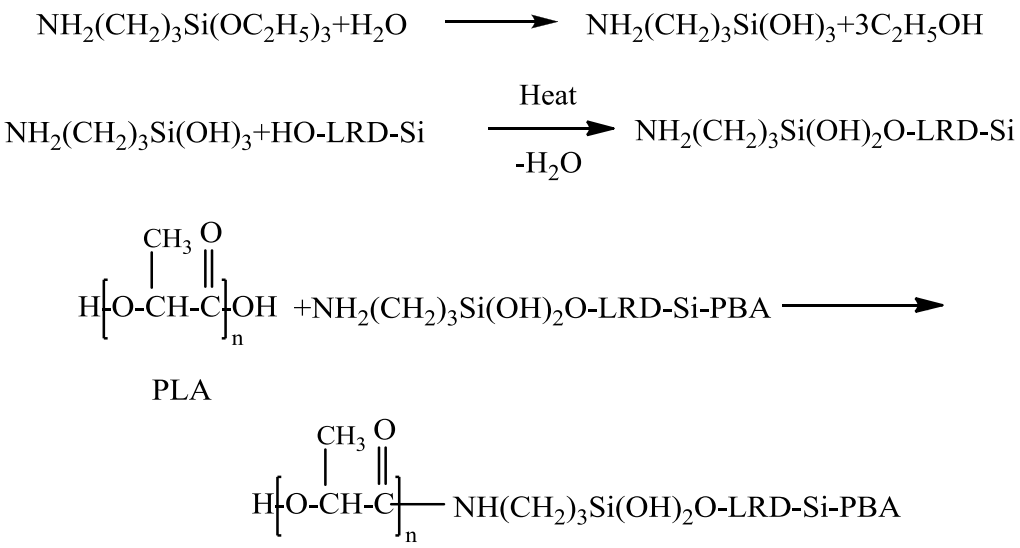

Silane 2: (3-Glycidoxypropyl) trimethoxysilane

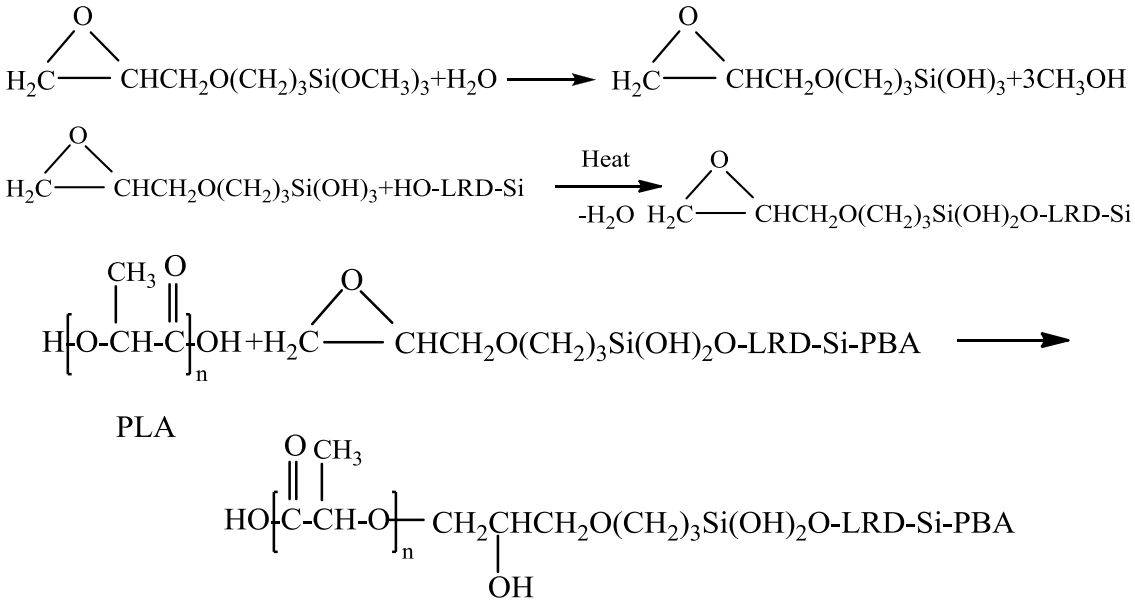

Schéma 3 Réactions de traitement de surface.

Pour le traitement au silane, silane 1 et silane 2 réagit avec l'eau pour former un silanol et de l'alcool tout d'abord. Puis survient la réaction des silanols avec les groupes hydroxyle sur les unités LRD-Si. Lors de l'association avec la matrice de PLA, un autre des groupes fonctionnels de la molécule de silane, tel que des groupes NH_2 pour silane 1 et époxy pour silane 2, réagissent avec les groupes hydroxyle de la résine PLA. Ainsi, la liaison chimique a été établie entre le LRD-PBA et la matrice de PLA. Ceci pourrait améliorer les propriétés interfaciales dans le composite.

2.4.2 Modification des particules LRD-Si et la préparation des particules PBA-LRD-Si-3G ou PBA-LRD-Si-3A

Silane 1 (3A) et le silane 2 (3G) ont été diluées à une concentration de 6% dans de l'acétone avant l'utilisation. Deux parties de modification LRD-Si ont été séparément plongé dans ces deux solutions de silane pendant 24 h, puis nettoyé avec de l'acétone et séché à l'étuve sous vide à 60 °C pendant 4 heures pour éliminer le solvant résiduel. Le 3A-LRD-Si et 3G-LRD-Si ont été obtenus par la modification. Puis, 3A-LRD-Si ou 3G-LRD-Si a pris la place de LRD-Si dans la préparation de PBA-argile composite latex. Tous les processus dans ces expériences étaient les mêmes que la description pour le PBA-LRD-Si. La concentration de 3A-LRD-Si ou 3G-LRD-Si dans le monomère BA a été mise à 3% en poids.

2.5 Synthèse des particules de latex PBA / PMMA

Les particules PBA/PMMA en latex ont été préparées par un procédé classique en deux étapes de polymérisation en émulsion. Les cœurs en élastomère PBA ont été synthétisés selon la recette indiquée dans le tableau 1. Le PMMA écorce rigide a été synthétisé en utilisant LRD-PBA latex ou (LRD-Si)-PBA latex sous forme de semences. Le tableau 3 montre les recettes pour la préparation des particules cœur-écorce composites.

Tableau 3 Compositions en poids pour la préparation du latex PBA/PMMA.

Latex cœur-écorce	*Semence*	*MMA (g)*	*MMA/PBA (p/p)*	*AMBN (g)*	*Brij700 (g)*	*H_2O (g)*
PBA/PMMA	Latex PBA	20	1 : 1	0.2	0.9	10
PBA-LRD/PMMA	Latex PBA-LRD	20	1 : 1	0.2	0.9	10
PBA-LRD-Si/PMMA	Latex PBA-LRD-Si	20	1 : 1	0.2	0.9	10

Les cœurs PBA préparés par polymérisation en mini-émulsion ont été en outre purgée avec de l'azote pur et sous agitation dans le réacteur en acier inoxydable à 60 °C. Un mélange de MMA, de l'eau, un tensioactif et AMBN a été ajouté dans le réacteur dans des conditions affamées (0,25 ml / min). Après l'addition du mélange de monomères, on élève la température à 85 °C et la réaction s'est déroulée pendant 3 heures sous

agitation continue et se termine par l'ajout d'hydroquinone. La conversion du monomère a été déterminée par gravimétrie.

2.6 Préparation des mélanges PLA/PBA et PLA/cœur-écorce

Les latex PBA et PBA / PMMA cœur-écorce ont été coagulés par l'éthanol et lavés par de l'eau, puis séchés à 60 °C pendant 24 heures dans une étuve à vide avant de fondre le mélange. Les mélanges de PLA et latex séchés ont été préparés dans un micro-compoundeur (DSM Xplore) à une vitesse de vis de 60 tours par minute pendant 10 min à 180 °C. Le PLA pur a été soumis au même traitement de mélange de manière à avoir la même histoire thermique que les mélanges.

3. Résultats et discussions

3.1 Choix de l'agent tensio-actif pour la polymérisation en mini-émulsion

Le dodécylsulfate de sodium (SDS) est un tensioactif anionique qui est très fréquent et efficace pour la polymérisation en émulsion ainsi que la polymérisation en mini-émulsion. Néanmoins, des expériences préliminaires ont montré que le SDS ne convenait pas pour la polymérisation en mini-émulsion en présence de LRD ou LRD-Si. Lorsque SDS a été ajouté à la mini-émulsion de BA avec LRD ou LRD-Si, le latex s'est révélé instable et présentait de nombreux agrégats (> 80% en masse du monomère initial) après la polymérisation.

Contrairement au SDS, des tensioactifs non-ioniques tels que le Brij 78 ($C_{18}H_{37}(OCH_2CH_2)_{20}OH$) et Brij 700 ($C_{18}H_{37}(OCH_2CH_2)_{100}OH$) ont stabilisés les mini-émulsions efficacement. En outre, les groupes polaires contenant du poly (oxyde d'éthylène) étaient miscibles avec le PLA. En conséquence, les particules de latex obtenues avec ces deux agents tensioactifs peuvent avoir une meilleure compatibilité avec le PLA. Pour toutes les raisons précédentes, Brij 78 et Brij 700 ont été choisis comme agents tensioactifs pour la polymérisation en mini-émulsion de LRD/PBA composites.

Les figures 4 et 5 montrent la variation de la taille des particules de latex PBA et les quantités correspondantes de précipités après la polymérisation en mini-émulsion, respectivement, en fonction de contenu de Brij 700 ou Brij 78.

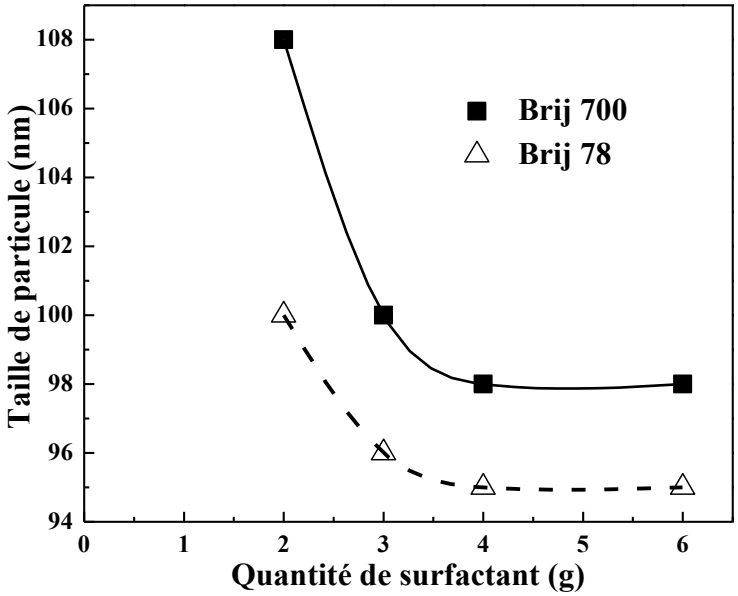

Figure 4 Diamètre moyen des nanoparticules PBA finales en fonction de la quantité de Brij 700 ou Brij 78 dans la charge. La quantité initiale de monomère BA est 20 g.

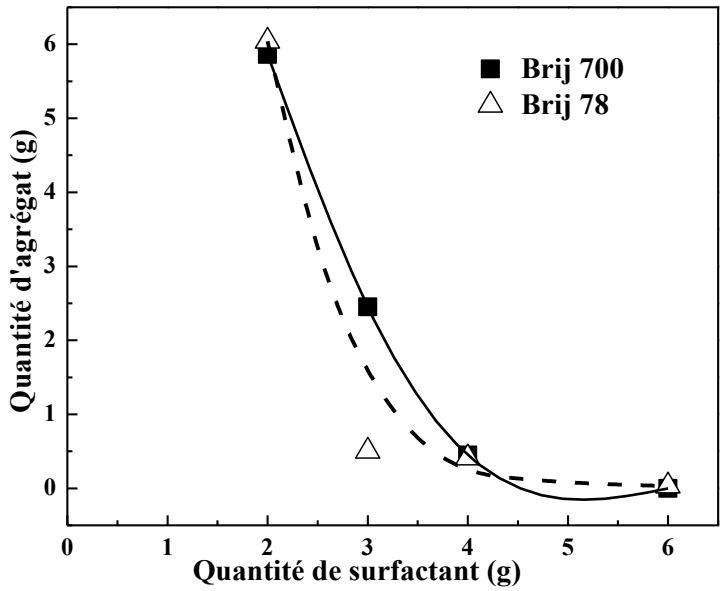

Figure 5 Quantité de précipité récupéré après la polymérisation en mini-émulsion, en fonction de la quantité de surfactant (Brij 700 ou Brij 78) dans l'alimentation. La quantité de monomère BA dans l'alimentation est 20 g.

D'après la figure 4, le diamètre des PBA particules est environ 100 nm et l'efficacité

des deux tensioactifs est similaire. Les deux chiffres donnent à penser que les deux agents tensioactifs sont efficaces lorsque leur concentration dépasse pas 4% en poids (fraction de poids dans le système) et les latex sont stables après la polymérisation.

3.2 Modification hydrophobe de la laponite

La dispersion de la laponite dans monomère BA avant la polymérisation en mini-émulsion rend nécessaire la modification de sa surface. Cette étape a été réalisée en utilisant la réaction de silylation dans le toluène (voir expérimentale). Après un lavage poussé avec du toluène pour éliminer l'agent de couplage γ-MPTMS n'ayant pas réagi et séchage à 40 °C dans un four à vide pendant une nuit, le LRD et LRD-Si poudres ont été caractérisées par FTIR et ATG.

La figure 6 montre le spectre FTIR de la LRD non modifiée et celle de γ-MPTMS greffé LRD notée LRD-Si. Le spectre de la LRD non modifiée présente une bande à environ 3453 cm^{-1}, ce qui indique la présence de l'eau physisorbée. Ceci est corroboré par la présence d'une bande à 1640 cm^{-1} caractéristique des déformations υOH et δOH. Un petit épaulement à environ 3680 cm^{-1} est dû à des hydroxyles sur les surfaces LRD. Après le greffage de γ-MPTMS sur la LRD, le petit épaulement à environ 3680 cm^{-1} correspondant aux groupements hydroxyle sur les surfaces LRD (Mg_s-OH) est décalé vers 3687 cm^{-1}. De plus, il devient plus net et augmente en intensité. Dans le même temps, l'aire sous la bande large à 3450 cm^{-1} diminue. L'existence de groupements résiduels Mg_s-OH dans le spectre LRD-Si IR indique qu'ils ne sont pas accessibles aux molécules γ-MPTMS couplage silane.

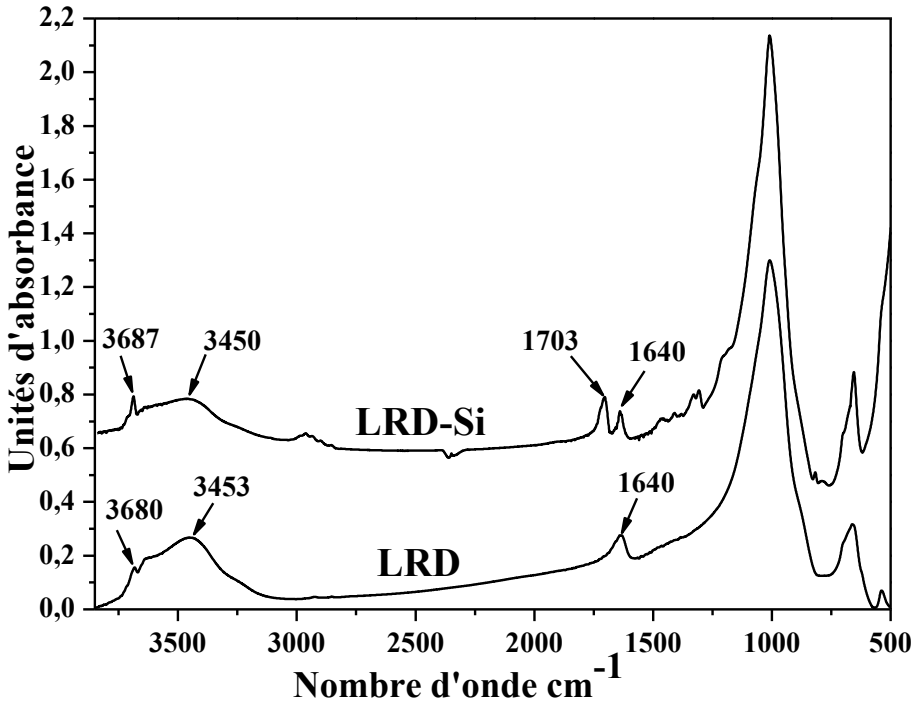

Figure 6 Spectres FTIR de la LRD initiale et greffée par le γ-MPTMS LRD (LRD-Si).

L'ATG a été utilisée pour évaluer la quantité de molécules de silane liées chimiquement sur les bords d'argile. La figure 7 montre les courbes ATG avant et après le greffage des γ-MPTMS sur la LRD.

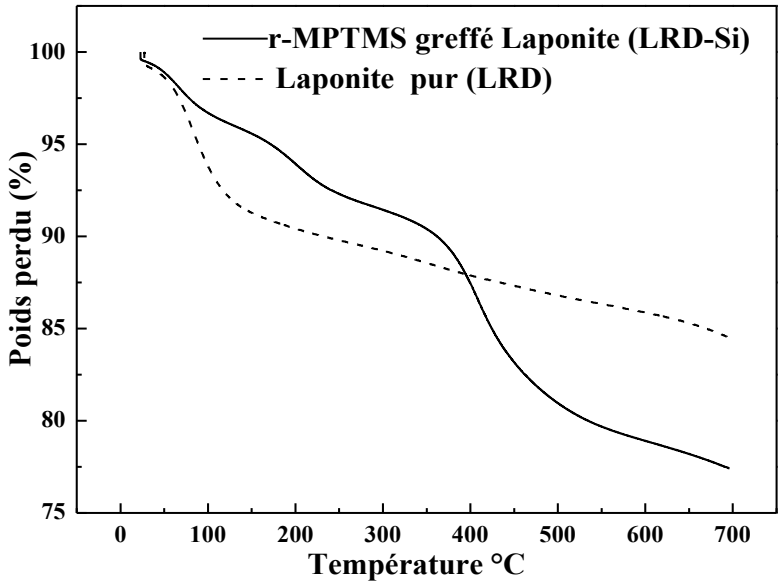

Figure 7 Enregistrements ATG de la LRD initiale et greffée par le γ-MPTMS.

La région comprise entre 200 et 600 °C correspond à la décomposition thermique de

la fraction de silane [47]. A partir des courbes ATG, nous avons calculé que la LRD-Si contient environ 15% en masse de γ-MPTMS greffés sur la LRD. A titre de comparaison, le milieu réactionnel contenait 42% en masse de γ-MPTMS, ce qui montre que près de 24% d'agent de silylation a réagi.

3.3 Contribution des tensioactifs cationiques à la dispersion de Laponite

Plus de 95% de la LRD greffée (LRD-Si) a été précipitée après la polymérisation en l'absence de CTAB ($CH_3(CH_2)_{15}N(Br)(CH_3)_3$), OTAB ($CH_3(CH_2)_{17}N(Br)(CH_3)_3$) ou DDAC ($[CH_3(CH_2)_{17}]_2N(Cl)(CH_3)_2$) parce que dans le mélange préparé avant la polymérisation en mini-émulsion, la dispersion de LRD-Si n'est pas stable sans l'utilisation de ces tensioactifs cationiques. Le tableau 4 montre que, parmi ces trois tensioactifs cationiques, le CTAB a été le plus efficace pour promouvoir la dispersion des LRD-Si dans le monomère BA, en évitant sédimentation massive lors de la polymérisation en mini-émulsion.

Tableau 4 Quantités de précipités après la polymérisation sans ou avec un agent tensioactif cationique dans la mini-émulsion de PBA-3%LRD-Si (quantités initiales de BA: 20g).

Tensioactifs cationiques (0.8 g)	Aucun	DDAC	OTAB	CTAB
Quantités de précipités (g)	18.3	2.2	2.1	0.5

3.4 Caractérisation des latex de PBA

Après polymérisation en mini-émulsion, la MET (microscopie électronique à transmission) a été utilisée pour examiner la morphologie des particules de latex à l'état humide. Latex préparé est passé une centrifugation pour enlever l'agrégat dans le latex avant le test de MET. La figure 8 montre des images représentatives de la PBA latex avec LRD ou LRD-Si. Toutes les PBA particules restent sphériques après la polymérisation et leur diamètre est d'environ 100 nm, ce qui est cohérent avec les diamètres moyens déterminés par diffusion dynamique de la lumière (DLS) (figure 4). La ligne noire et le disque noir dans la figure 8b correspondent aux plaquettes de LRD-Si. Les plaquettes individuelles de LRD sont en forme de disque, d'un diamètre

latéral de 13 à 30 nm et une épaisseur d'environ 1 nm. A partir de ces images, on peut déduire que certaines des particules de latex pourraient être exemptes de plaquettes laponite. Néanmoins, le fait qu'une particule de latex apparaît sans lignes noires ou les disques ne peuvent pas s'assurer qu'il ne contient pas nécessairement de plaquettes de laponite. C'est parce que la visibilité de la laponite sous MET dépend fortement de son orientation dans le plan basal. Si celui-ci est perpendiculaire au faisceau d'électrons, le contraste de diffraction de la plaquette est réduit.

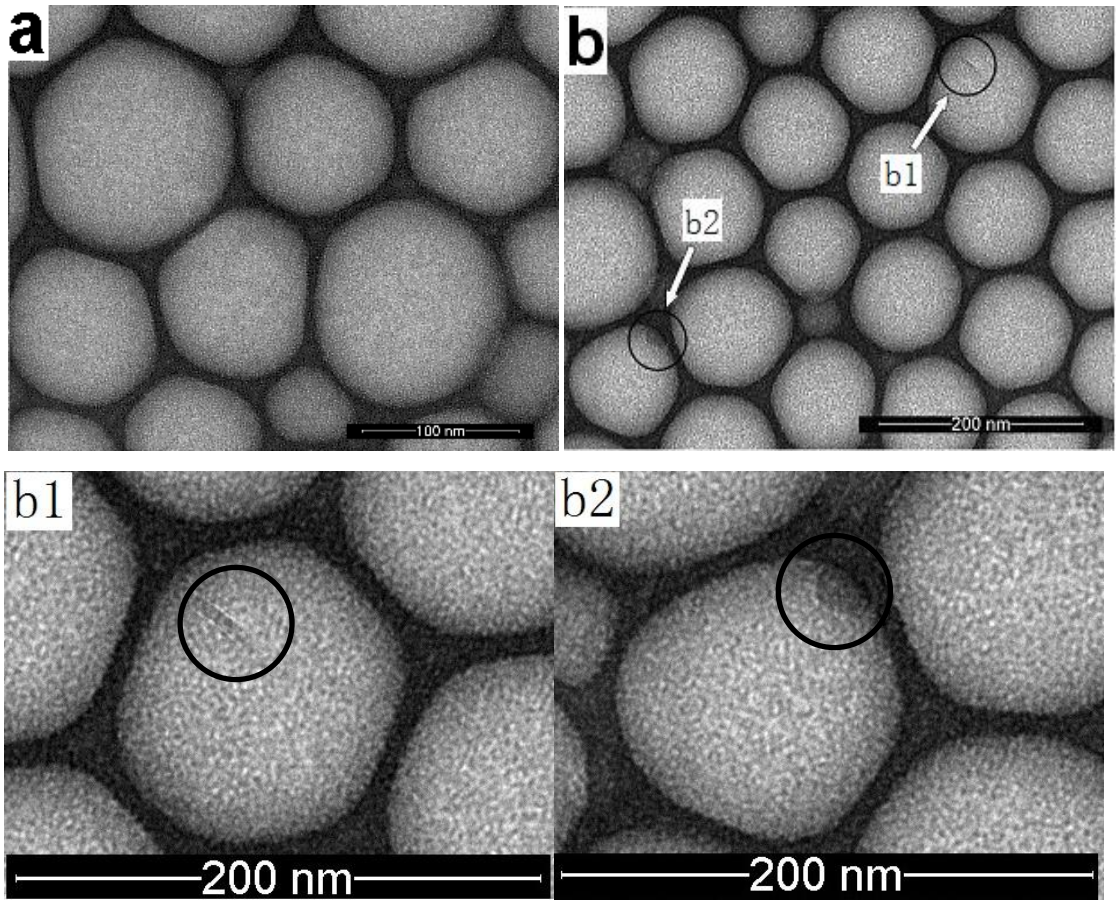

Figure 8 Images MET de (a) latex PBA-3%LRD, (b) latex PBA-3%LRD-Si et deux images agrandies de b. Le contenu laponite en latex est de 3% en poids.

L'ATG a été utilisée pour étudier le contenu en LRD ou LRD-Si dans les précipités après la polymérisation en mini-émulsion. Comme montre dans le tableau 1, la quantité initiale de monomère BA est de 20g et celle de LRD ou LRD-Si est ajouté 0,6 g pour la préparation du nanocomposite latex PBA. Les figures 9 et 10 montrent les analyses ATG du latex PBA et des précipités, respectivement. Conformément à la

figure 9, la quantité de LRD dans le précipité après la polymérisation en mini-émulsion est d'environ 0,3 g. Cela signifie que seulement 50% de la LRD est incorporée dans le latex PBA, même si le CTAB est utilisé comme agent tensioactif. D'autre part, selon la figure 10, 85% du LRD-Si est incorporé dans le latex PBA.

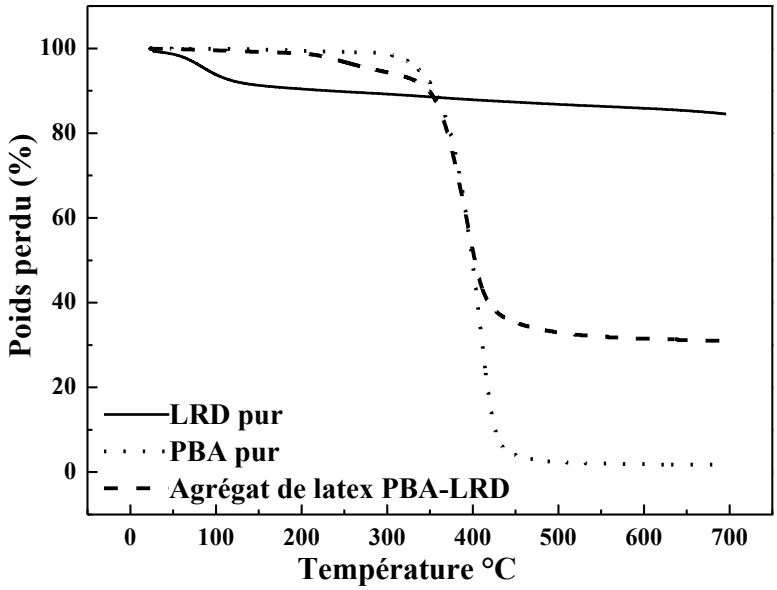

Figure 9 ATG traces de la LRD non modifiée, PBA pur et PBA-3%LRD précipité obtenu par polymérisation en mini-émulsion. La quantité initiale de LRD est de 0,6 g et la quantité de précipité après la polymérisation est de 0,9 g.

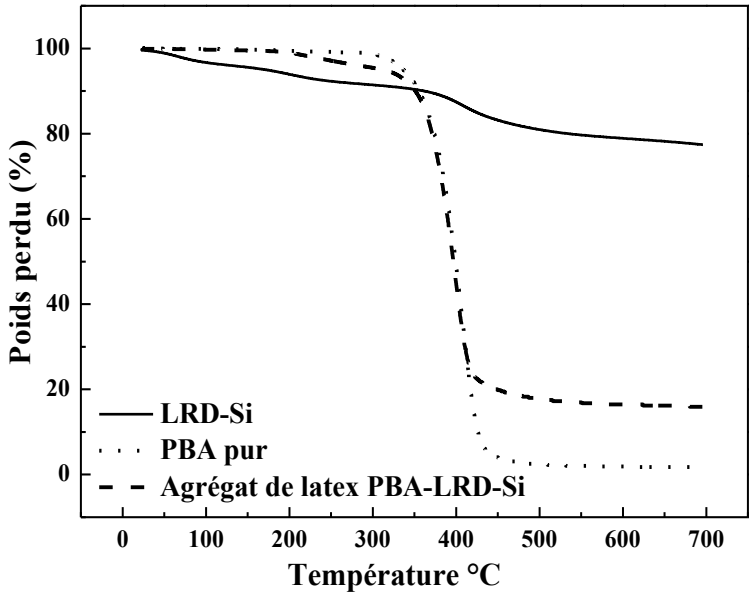

Figure 10 ATG traces de la LRD-Si, du PBA pur et du PBA-3%LRD-Si précipité après la polymérisation en miniémulsion. La quantité initiale de LRD-Si est de 0,6 g et celle du précipité après polymérisation est de 0,5 g.

Les résultats ci-dessus montrent que l'utilisation d'un tensioactif cationique tel que CTAB permet d'obtenir des latex PBA-LRD et PBA-LRD-Si. Comme une question de fait, les silanes greffés LRD-Si nanoparticules sont bien en suspension dans la mini-émulsion de monomère BA et un pourcentage élevé d'entre eux sont incorporés dans les particules de latex PBA après la polymérisation. C'est parce que les molécules de silane sur les nanoparticules LRD-Si peut réagir avec le monomère BA lors de la polymérisation.

3.5 Particules PBA avec tensioactif polymère

L'efficacité de l'agent tensioactif PEGMEM n'était pas aussi bien que le SDS, ni Brij78 ou Brij700. Même si la concentration de PEGMEM dans le système a atteint 8wt% (8g PEGMEM a été ajouté), la viscosité de la mini-émulsion avant la polymérisation est élevée, tandis que le produit final obtenu contenait encore beaucoup d'agrégats de polymère.

En raison de la faible efficacité de tensioactif PEGMEM, par conséquent, PEGMEM a été mélangé avec Brij 700 ou Brij 78 pour former un tensioactif complexe avant d'ajouter dans le milieu de polymérisation en mini-émulsion du PBA. Dans le tensioactif complexe, la quantité de PEGMEM a été fixée à 2 g et la quantité de Brij 700 ou Brij 78 a varié de 0,25 g à 2g.

Lorsque la quantité de Brij 700 ou Brij 78 était inférieure à 0,5 g dans le mélange de stabilisants, l'émulsion n'est pas stable et plus de 70% en poids de la PBA précipitait après la réaction. Bien que la quantité de Brij 700 ou Brij 78 était plus élevée que 0,5 g dans le mélange de stabilisants, la quantité d'agrégats formés après la polymérisation en mini-émulsion est inférieure à 1 g (5% en poids de la PBA). Comme indiqué dans la figure 5, avec seulement 2g de Brij 700 ou Brij 78 dans la polymérisation en mini-émulsion, 6g d'agrégats étaient formés après la polymérisation. Voici les résultats moyens des agents tensioactifs complexes avaient une meilleure influence à stabilité des latex PBA et est plus efficace en tant que tensioactif par rapport à l'efficacité de PEGMEM seul ou Brij78 et Brij700 seuls dans

la polymérisation en mini-émulsion.

3.6 Synthèse et caractérisation de latex cœur-écorce PBA/PMMA

Considérant que PBA et PLA sont non miscibles, les latex cœur-écorce PBA/PMMA, avec ou sans laponite (LRD ou LRD-Si) ont été préparés par polymérisation en émulsion ensemencée, afin d'améliorer la compatibilité entre les nanoparticules et la matrice (par la présence de l'écorce PMMA, miscible à matrice PLA). Les nanoparticules cœur-écorce ont été caractérisées par RMN ^{1}H et MET. Les latex PBA avec ou sans LRD (ou LRD-Si) ont été utilisés comme semences (voir partie expérimentale). Le MMA a été polymérisé en présence de ces semences afin d'obtenir des particules cœur-écorce PBA/PMMA. Le débit d'alimentation du monomère MMA a été maintenu constant et dans des conditions affamées en ce que les particules de latex de semence avaient assez de temps pour polymériser avec le MMA, empêchant ainsi la deuxième génération de particules de PMMA. Le rapport BA/MMA est d'environ 50/50 v/v, pour obtenir des structures ainsi définies à morphologie cœur-écorce.

La figure 11 montre le spectre RMN ^{1}H du latex PBA/PMMA. Le pic à 3.6 ppm (c) et de multiples pics à 4,0 ppm (3) correspondent à la $O\text{-}CH_2$ du PBA et $O\text{-}CH_3$ du PMMA, respectivement. Les pics entre 0,8 et 2.0 ppm peuvent être attribués à des chevauchements entre les protons. La composition en PBA et PMMA a été calculée à partir des aires en intégrant des OCH_2 protons de PBA (3) et des protons OCH_3 de PMMA (c), ce qui donne une composition pondérale PBA/PMMA égale à 51/49 wt/wt [48].

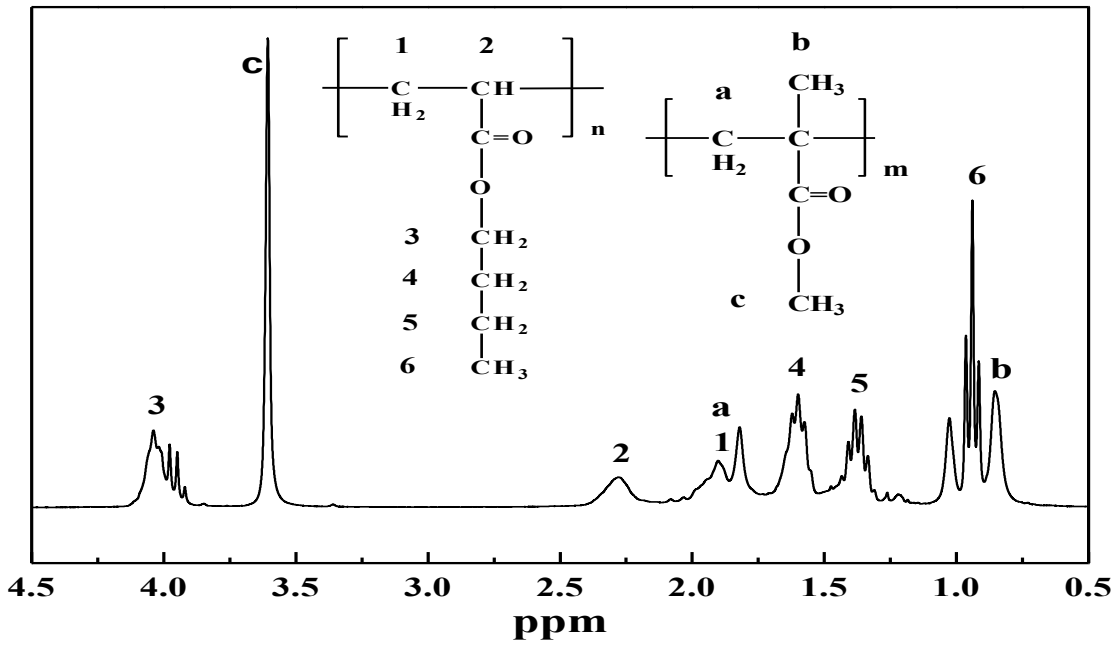

Figure 11 Spectre RMN ^{1}H des particules cœur-écorce PBA/PMMA.

Les tailles de particules ont été déterminées par MET et DLS.

Les diamètres des particules PBA-LRD-Si et composites PBA-LRD-Si/PMMA déterminées par DLS sont représentées sur la figure 12, où le diamètre de latex PBA-LRD-Si est d'environ 100 nm, et la taille des particules de latex PBA-LRD-Si/PMMA est d'environ 120 nm.

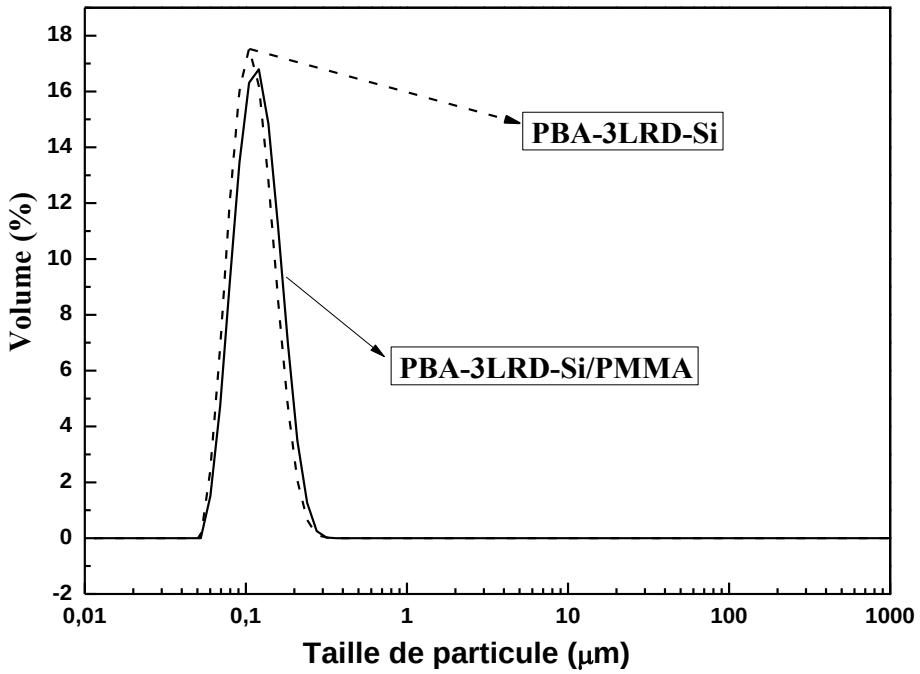

Figure 12 La distribution de taille des particules de PBA-3%LRD-Si et PBA-3%LRD-Si/PMMA.

En outre, en supposant que le nombre de particules composites d'être constant, le diamètre de latex PBA-LRD-Si/PMMA (D_2) peut être calculée à partir de la variation de poids des particules composites selon l'équation 1:

$$\frac{D_2}{D_1} = \left(\frac{V_2}{V_1}\right)^{1/3} \approx \left(\frac{W2}{W1}\right)^{1/3} \quad \textbf{(1)}$$

Lorsque le diamètre de latex PBA-LRD-Si (D_1) est de 100 nm, mesuré par DLS, W2/W1 est le rapport en poids de particules composites PBA-LRD-Si/PMMA et PBA-LRD-Si, qui peut être déterminé par l'analyse du RMN. De la comparaison ci-dessus, on peut voir que le diamètre des particules de latex PBA-LRD-Si/PMMA obtenue à partir de l'observation directe était proche de calcul théorique, en supposant que la polymérisation du MMA a principalement eu lieu sur la surface des particules de PBA-LRD-Si.

La figure 13 montre les images MET des particules cœur-écorce en PBA/PMMA. Le cœur mou de PBA et l'écorce dure en PMMA sont clairement visibles. Le dernier couvre le premier suffisamment et uniformément. L'épaisseur de l'écorce et le diamètre de cœur sont 10-20 et 90 ~ 130 nm, respectivement.

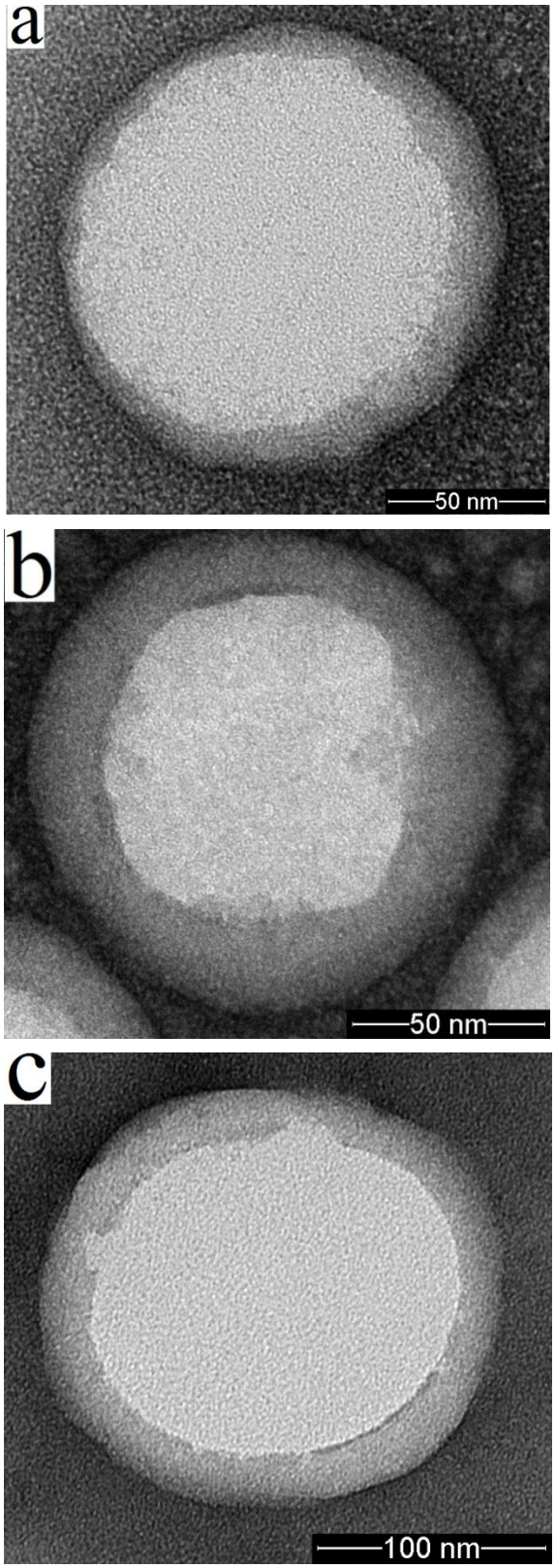

Figure 13 MET images des particules cœur-écorce : (a) PBA/PMMA, (b) PBA/PMMA, PBA-3%LRD/PMMA, et (c) PBA-3%LRD-Si/PMMA.

3.7 Morphologie des mélanges PBA/PLA et PBA/PMMA/PLA

3.7.1 Morphologie des mélanges PBA/PLA

La figure 14 montre les images MEB (microscope électronique à balayage) des mélanges PBA/PLA (10/90), PBA/PLA (20/80), PBA-5%LRD/PLA (20/80), PBA-2%LRD-Si/PLA (20/80), PBA-3%LRD-Si/PLA (20/80) et PBA-5%LRD-Si/PLA (20/80) avec celui du PLA pur. Avant les analyses MEB, les surfaces de ces matériaux sont gravées avec le 2-butanol, un bon solvant de la PBA et un non solvant pour le PLA. Les surfaces des mélanges PBA/PLA (10/90), PBA/PLA (20/80) et PBA-3%LRD/PLA (20/80) allie trous d'exposition tandis que les surfaces de ces trois derniers PBA-LRD-Si/PLA (20/80) des mélanges (d) à (f) tendance à être lisses. Pour le diamètre moyen des trous de ces mélanges qui correspond à des domaines gravés PBA, des trous dans le mélange (a) est d'environ 0.8 µm, de trous dans les mélanges de (b) et (c) est d'environ 1.1 µm et 2.7 µm tandis que de mélange (d) et (e) est de 1,9 µm et 1,4 µm, respectivement. En outre, pour le mélange de (f), qui avec 5% LRD-Si dans la polymérisation en mini-émulsion de PBA, il n'existe presque pas de trous dans la surface après gravure. Ceux-ci confirment que les particules PBA avec LRD-Si sont réticulées au cours de la polymérisation en mini-émulsion par le γ-MPTMS greffé-LRD (LRD-Si) et le degré de réticulation est augmenté lorsque la teneur en LRD-Si dans la polymérisation augmente. En attendant, puisque les valeurs des diamètres de ces trous dans les mélanges sont significativement plus élevées que le diamètre moyen des nanoparticules PBA obtenue par polymérisation en mini-émulsion, ceci pourrait indiquer que l'agrégation des nanoparticules se produit au cours du séchage de suspensions avant mélange avec le PLA et la coalescence des nanoparticules PBA se produit au cours du mélange dans le micro-compoundeur .

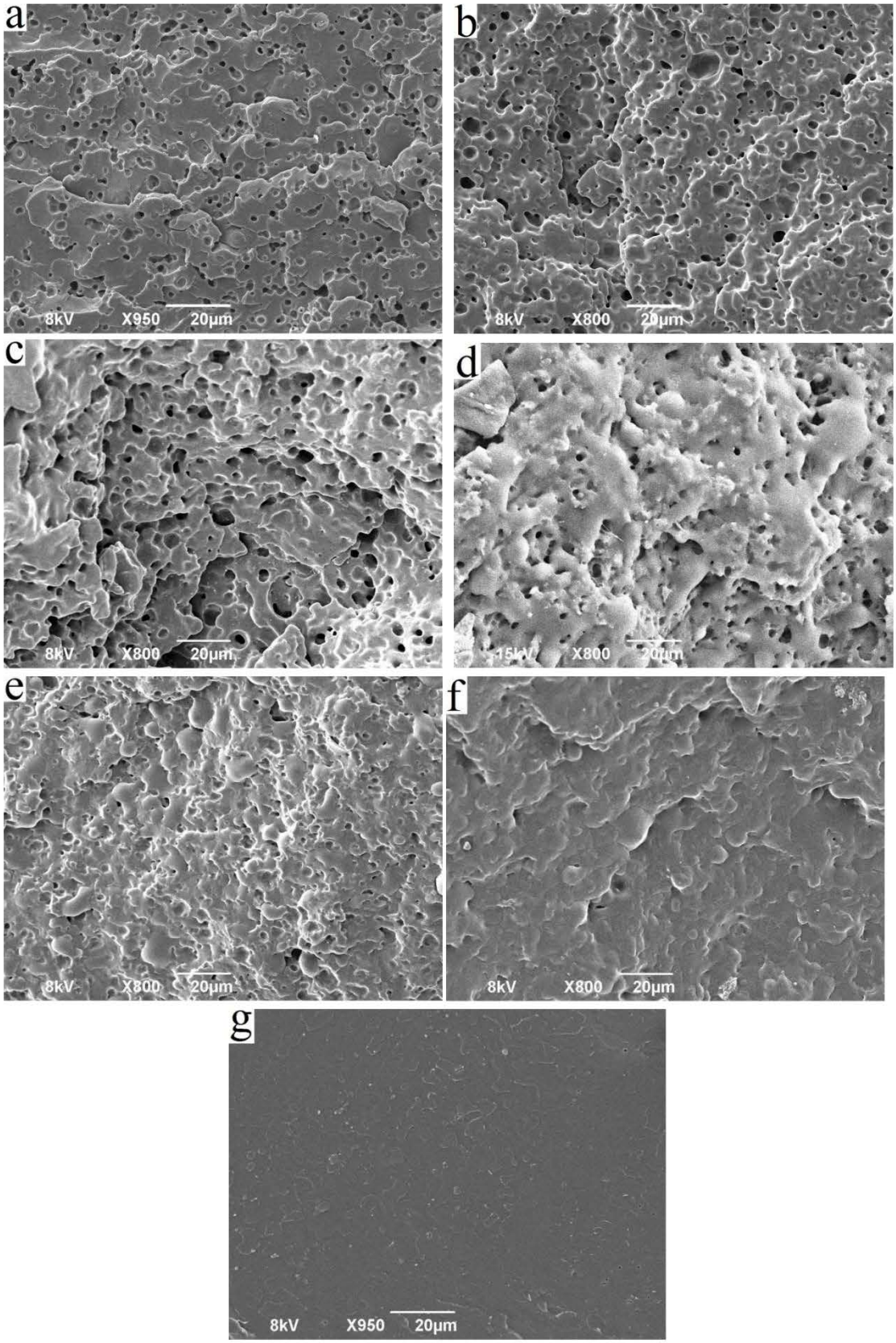

Figure 14 MEB images de (a) mélange PBA/PLA (10/90), (b) mélange PBA/PLA (20/80), (c) mélange PBA-5%LRD/PLA (20/80), (d) mélange PBA-2%LRD-Si/PLA (20/80), (e) mélange PBA-3%LRD-Si/PLA (20/80), (f) mélange PBA-5%LRD-Si/PLA (20/80), et (g) mélange PLA pur.

3.7.2 Morphologie des mélanges PBA /PLA avec un tensioactif polymère

Avec l'ajout du tensioactif PEGMEM, même si le latex PBA a été lavé par de l'éthanol après la réaction, le latex PBA ne précipite pas évidemment après le lavage. Ce qui signifie que certains des PEGMEM restaient à la surface des particules PBA et agissent comme un agent stabilisant même si son efficacité n'a pas été aussi efficace que le SDS ou Brij78.

Après le lavage à l'éthanol, la taille des particules a été examinée par DLS. La taille des particules PBA à l'aide du tensioactif complexe -[0,5g Brij700 avec 2g PEGMEM] était entre 170 nm et 661 nm. Lorsque l'agent tensioactif complexe est [1g Brij700 avec 2g PEGMEM], la taille des particules se situe entre 81 et 193 nm.

Tous les latex PBA ont été coagulés par l'éthanol et lavés fortement par de l'eau déionisée pour diminuer le tensioactif libre dans le latex, puis séché à 60 °C pendant 24 heures dans une étuve à vide avant le mélangeage à l'état fondu. La concentration de PBA dans les mélanges a été fixée à 20 % en poids également.

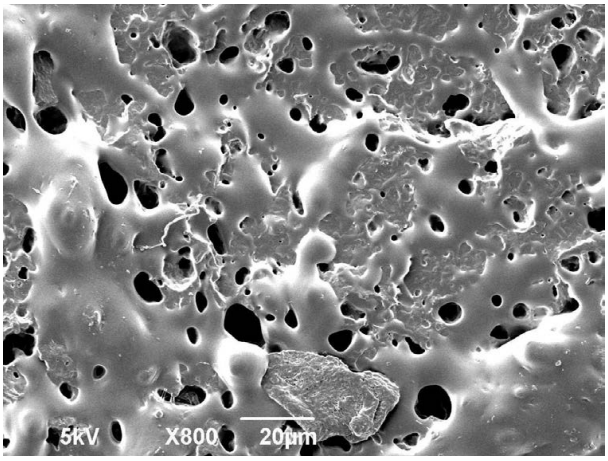

Figure 15 MEB image du mélange PBA/PLA (20/80) quand le tensioactif composite –[0.5gBrij700 avec 2g PEGMEM] a été utilisée dans la préparation de latex PBA. dn =1.57 µm, dv=5.05 µm.

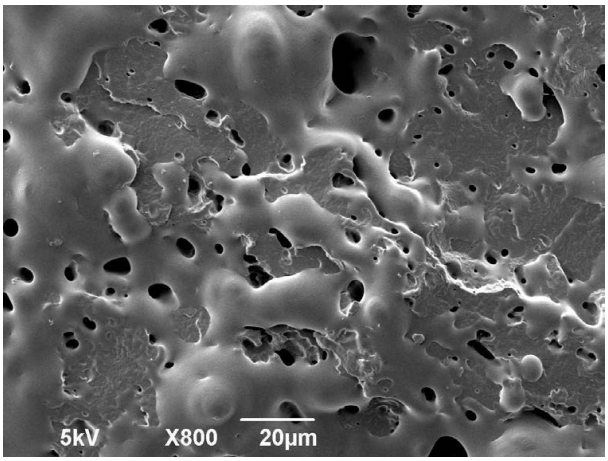

Figure 16 MEB image du mélange PBA/PLA (20/80) quand le tensioactif complexe –[1gBrij700 avec 2g PEGMEM] a été utilisé dans la préparation du latex PBA. dn=1.63 µm, dv=3.89 µm.

Par l'analyse de la distribution granulométrique des images au MEB, le tensioactif polymère PEGMEM n'a pas amélioré la dispersion des particules de PBA dans la matrice PLA. L'influence de PEGMEM pour assurer la compatibilité de ces deux polymères n'était pas aussi bonne que censé être.

En contrepartie de la PEGMEM dans le surfactant composite était seulement 2g pour la polymérisation en mini-émulsion et le produit a été lavé par de l'éthanol après la réaction, la quantité de PEGMEM laissé dans le produit ne peut pas être élevé. D'après les résultats actuels, on peut supposer que la quantité de PEGMEM collé aux particules PBA était trop faible et ne suffit pas à produire les meilleurs résultats possibles pour améliorer la compatibilité du mélange PBA/PLA. Comme perspective à ce travail, on peut considérer pour améliorer la quantité de tensioactif PEGMEM dans le complexe d'assurer les particules finales peut être entouré plus par des molécules PEGMEM, afin d'améliorer la distribution des particules d'élastomère dans la matrice PLA. De l'autre côté, l'existence de PEGMEM dans la matrice polymère, affaiblissent la résistance à la traction du mélange, l'addition de PEGMEM dans l'émulsion doit être ajustée dans une plage de trouver une valeur optimale.

3.7.3 Morphologie des mélanges des particules PBA-LRD-Si-3G ou PBA-LRD-Si-3A dans la matrice PLA

À partir de l'analyse de DLS, la taille des particules de latex PBA avec la 3A-LRD-Si

ou 3G-LRD-Si dans la polymérisation en mini-émulsion n'a pas changé après la réaction, qui a été encore maintenue autour de 100 nm.

Les latex PBA-LRD-Si-3A et PBA-LRD-Si-3G ont été coagulés par l'éthanol et lavés par de l'eau déminéralisée, puis séchés à 60 °C pendant 24 heures dans une étuve à vide avant de faire fondre le mélange. La concentration de PBA dans les mélanges a été fixée à 20 % en poids également.

De la figure 17 et la valeur du diamètre des cavités dans les MEB images, il est révélé que le remplacement de la LRD-Si par 3A-LRD-Si n'a pas donné une meilleure compatibilité pour les particules PBA avec PLA matrice. Bien que le diamètre moyen de la porosité est un peu plus petite, qui le pore éliminé par solvant indiquant ces particules PBA n'étaient pas fixés à la matrice de PLA telle sorte que le 3A-LRD-Si ne pas agir en tant que liaison pour les particules de PBA et de matrice PLA. En revanche, la figure 18, à l'aide de la 3G-LRD-Si, le mélange PBA-3%LRD-Si-3G/PLA (20/80) a presque pas de pores après extraction par le 2-butanol. Ceci pourrait être attribué à des groupes époxy de silane 2 (3G), faire réagir avec les groupes hydroxyles de la matrice de PLA qui aident les particules PBA à avoir la connexion avec le PLA par la 3G-LRD-Si et ne peut pas être dissoute par un solvant de PBA.

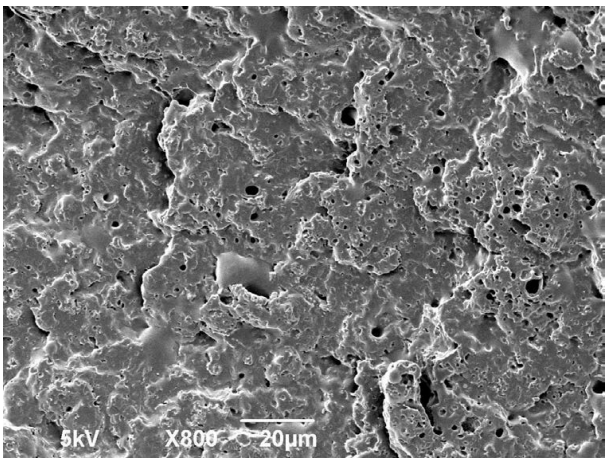

Figure 17 MEB image du mélange PBA-3%LRD-Si-3A/PLA (20/80). dn=0.78µm, dv=3.41 µm.

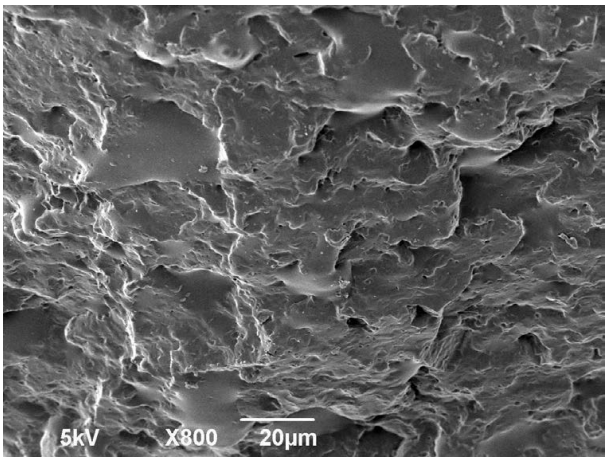

Figure 18 MEB image du mélange PBA-3%LRD-Si-3G/PLA (20/80).

Le test DSC (calorimétrie différentielle à balayage) pour le mélange PBA-3%LRD-Si-3G/PLA (20/80) démontré la température de transition vitreuse (T_g) du PLA était de 59 °C et la T_g du PBA -46 °C dans le mélange. Ils n'ont pas de grande différence avec la T_g du PLA pur ou celle de PBA dans les mélanges PBA-LRD-Si/PLA (20/80). Ces résultats impliquent l'ajout de Silane 2 (3G) n'ont aucune influence pour les propriétés thermiques du mélange PBA/PLA.

3.7.4 Morphologie des mélanges des (PBA/PMMA)/PLA

La figure 19 montre les images de MEB des mélanges (PBA/PMMA)/PLA (10/10/80), (PBA-3%LRD/PMMA)/PLA (10/10/80) et (PBA-3%LRD-Si/PMMA)/PLA (10/10/80). Leurs surfaces sont gravées avec le 2-butanol avant les analyses MEB. Des trous d'environ 350 nm de diamètre sont observés sur les surfaces des deux premiers mélanges tandis que le diamètre initial des particules PBA/PMMA est d'environ 125 nm après polymérisation en émulsion. Les trous sont beaucoup plus petits que ceux dans les mélanges PBA/PLA, ce qui indique que l'écorce en PMMA joue un rôle de compatibilisant entre PBA et PLA. Ceci améliore fortement la dispersion des nanoparticules dans la matrice PLA. Il n'ya pas de trous sur la surface du mélange (PBA-3%LRD-Si/PMMA)/PLA (10/10/80). C'est parce que dans ce mélange, le cœur PBA est réticulé par le silane greffé LRD (LRD-Si) et ne peut être attaqué par le 2-butanol.

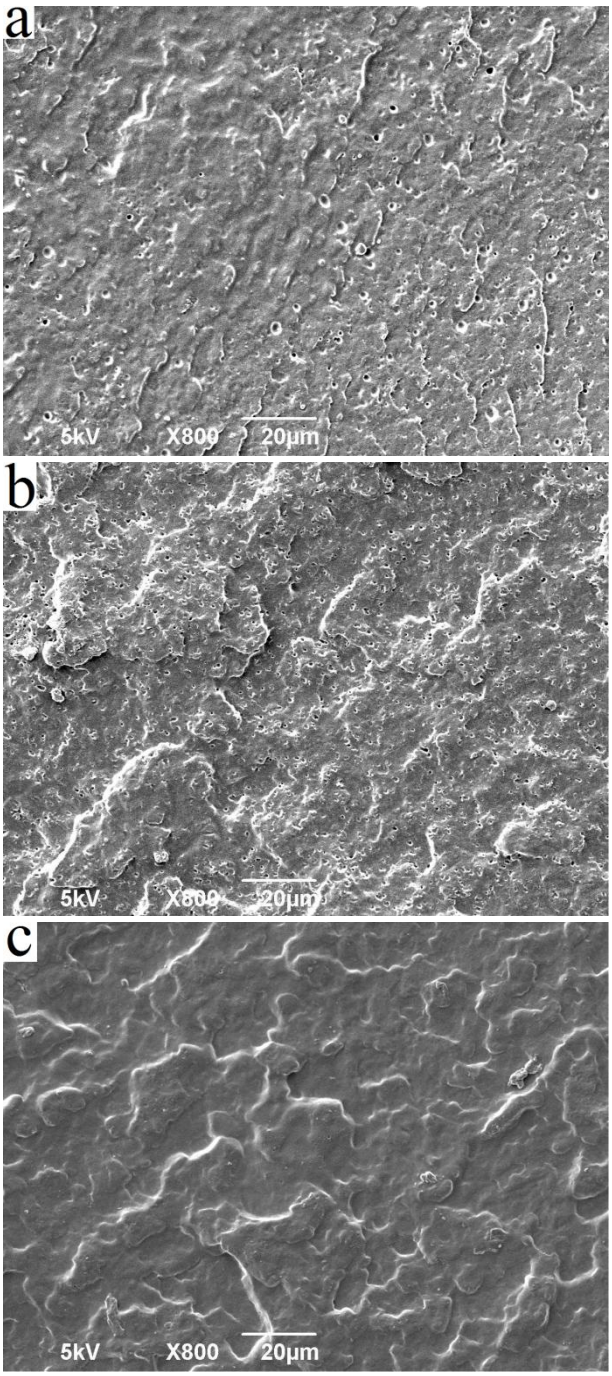

Figure 19 MEB images des surfaces fracturées des mélanges: (a) (PBA/PMMA)/PLA, (b) (PBA-3%LRD/PMMA)/PLA, et (c) (PBA-3%LRD-Si/PMMA)/PLA.

3.8 Propriétés mécaniques

3.8.1 Les mélanges PLA/LRD

La figure 20 montre l'augmentation du module d'Young du PLA contenant une charge de LRD croissante. Cependant, sa résistance à la traction diminue considérablement lorsque la teneur en argile augmente de 0 à 5% en poids. D'après la figure 21, la

résistance au choc des composites PLA/LRD est faible et essentiellement constante dans l'erreur expérimentale dans la gamme de contenu LRD de 0-5% en poids, ce qui signifie que la résistance aux chocs de PLA n'est pas affectée autant par l'incorporation de la LRD. Ainsi, lorsqu'il est soumis à des charges d'impact, les composites PLA et PLA/LRD échoué de manière fragile, d'où résulte dans les forces d'impact faibles.

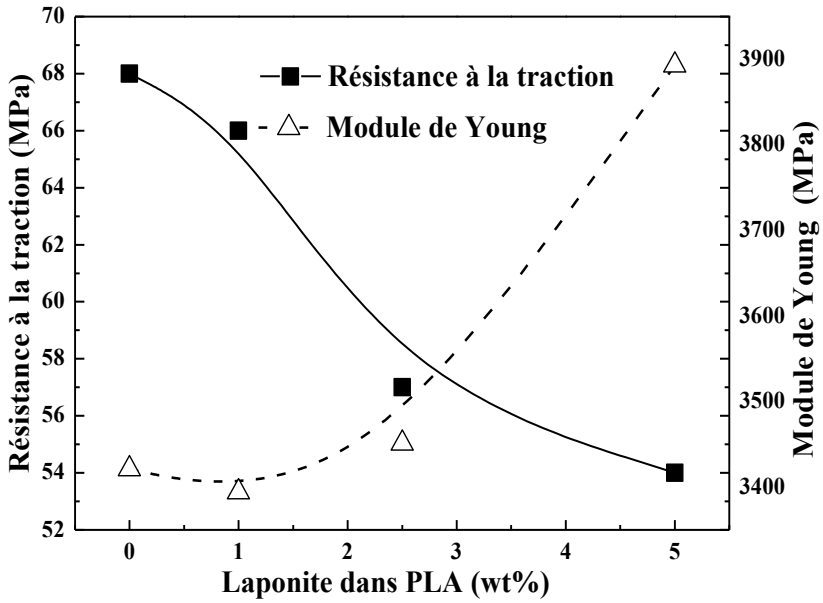

Figure 20 Résistance à la traction et le module d'Young des nanocomposites PLA/LRD avec des contenus différents de LRD.

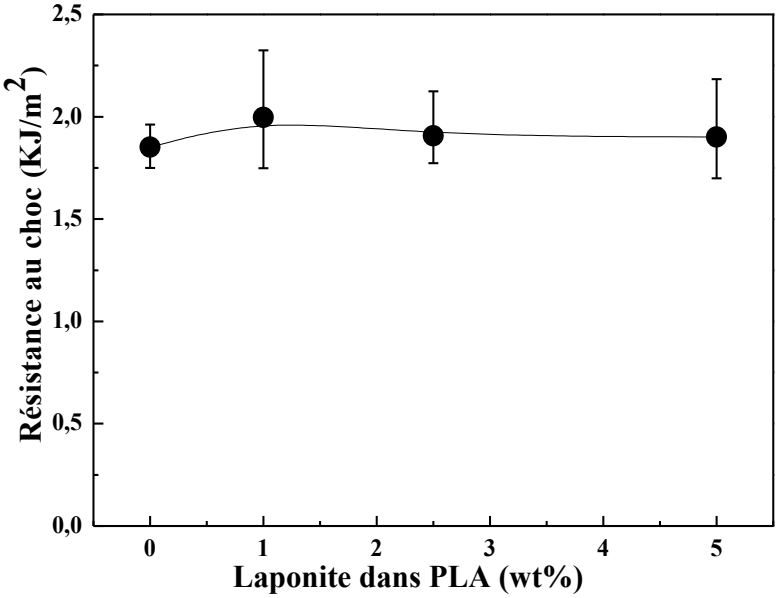

Figure 21 Résistance au choc sur les nanocomposites PLA/LRD ayant des teneurs différentes de LRD.

La baisse de la résistance à la traction des nanocomposites suggère que les couches de LRD ont agrégées pour agir en tant que défauts de matériaux, qui ont déclenché réponse cassante et rupture du matériau au début de l'essai de traction. Une étude précédente sur des nanocomposites de PLA [49] a également montré que la résistance à la flexion de PLA diminue lorsque les chargements en poids de MMT (montmorillonite) supérieur à 1%. Ceci est dû à la forte teneur en argile, ce qui conduit à l'agglomération dans le matériau polymère.

3.8.2 Mélanges PBA/PLA et (PBA/PMMA)/PLA

L'ajout de la PBA modifie considérablement le comportement en traction de PLA, comme le montre la figure 22 et tableau 5.

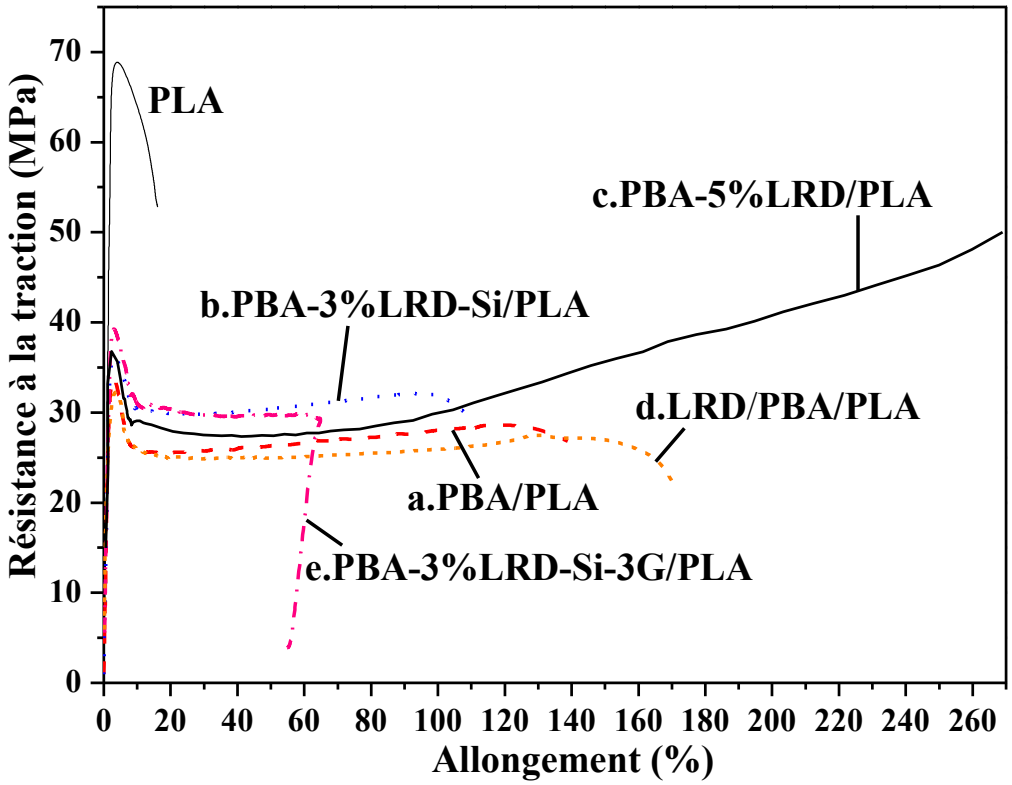

Figure 22 La résistance à la traction du mélange PBA/PLA avec des particules PBA ou des particules PBA-LRD-Si dans la matrice PLA par rapport à PLA pur: (a) mélange PBA/PLA (20/80), (b) mélange PBA-3%LRD-Si/PLA (20/80), (c) mélange PBA-5%LRD/PLA (20/80), (d) mélange LRD/PLA/PBA (1/79/20) et (e) mélange PBA-3%LRD-Si-3G/PLA (20/80).

Tableau 5 Résistance à la traction; le module d'Young et la résistance au choc du PLA pur, des mélanges PBA/PLA et (PBA/PMMA)/PLA.

Mélanges	*Résistance à la traction (MPa)*	*Modulus Young (MPa)*	*Résistance au choc (KJ/m^2)*
PLA pur	68	3421	1.85
PBA/PLA(20/80)	37	2061	2.39
PBA-2%LRD-Si/PLA(20/80)	33	2307	3.99
PBA-5%LRD-Si/PLA(20/80)	33	2105	4.50
PBA-3%LRD-Si-3G/PLA (20/80)	38	2073	4.10
LRD/PLA/PBA (1/79/20)	34	1969	3.71
(PBA/PMMA)/PLA (10/10/80)	51	2607	5.69
(PBA-2%LRD-Si/PMMA)/PLA (10/10/80)	52	2620	5.78
(PBA-5%LRD-Si/PMMA)/PLA (10/10/80)	47	2703	5.24
(PBA-5%LRD/PMMA)/PLA (10/10/80)	50	2565	5.51
LRD/PLA/(PBA/PMMA)(1/79/10/10)	54	2681	4.96

La rupture fragile du PLA est transformée en rupture ductile pour les mélanges PLA/PBA, sur eux étant soumis à des essais de traction. Le PLA pur est très rigide et cassant, avec une résistance autour de 68 MPa, alors que l'allongement à la rupture est seulement d'environ 15%. Tous les mélanges qui contiennent des particules PBA dans une matrice PLA ont une résistance au choc supérieur au PLA pur. Les échantillons ont été finalement rompus à un allongement sensiblement augmenté par rapport à celui du PLA.

Il est intéressant de constater que le mélange PBA-5%LRD/PLA (20/80) avait un allongement à la rupture très élevée de 268%, tandis que la résistance à la traction était 36MPa. La raison pour laquelle le résultat de ce mélange n'est pas clair, il est présumé que le exfoliée LRD autour de la surface de la particule PBA joue un rôle important pour sa plus grande élongation de l'essai de traction. En outre, pour le mélange LRD/PLA/PBA (1/79/20), même si ce mélange a la même quantité de LRD dans la masse, comme le mélange PBA-5%LRD/PLA (20/80), ni sa traction force ni son allongement est supérieur à celui du mélange PBA-5%LRD/PLA (20/80). Les agglomérats de LRD peuvent expliquer ce résultat d'essai de traction du mélange

LRD/PLA/PBA (1/79/20) plus affaiblie car l'exfoliation de LRD ne peut être formée par simple mélange de micro-compoundeur.

D'autre part, la résistance à la traction et le module d'élasticité diminue avec l'ajout d'élastomère PBA. En effet, le PBA a un plus faible module et une plus faible résistance mécanique que le PLA.

Les échantillons de mélanges PBA-LRD/PLA ont montré de plus grandes zones de déformation plastique à proximité de flanc de fracture par rapport aux mélanges PBA-LRD-Si/PLA. Comme les particules PBA-LRD-Si sont réticulés mais PBA-LRD composites ne sont pas, pour les particules PBA attachés avec LRD, la mobilité de la chaîne sont élevés par rapport aux les particules réticulés PBA-LRD-Si et l'on pense que l'allègement pour la traction d'un mélange PBA-LRD/PLA peut facilement se produire. L'existence de LRD permet à la cavitation aux particules PBA dans les conditions de contrainte de traction. Cette cavitation, à son tour, permet de contrainte d'écoulement plastique de la matrice avant de ligament le long de fissure fatale, ce qui entraîne des propriétés d'allongement élevées.

Ces propriétés des mélanges n'ont pas été significativement affectées par les différents types de particules PBA. Parce qu'il n'y avait pas de différence significative entre les échantillons de mélanges dans le module de traction et de résistance à la traction, il est estimé que la différence de l'allongement à la rupture a été causée par les secteurs de la zone de déformation plastique, où les matériaux ont montré un blanchiment.

La résistance à la traction du mélange PBA-3%LRD-Si-3G/PLA (20/80) est de 39 Mpa, qui est un peu plus élevé que l'autre mélange PBA/PLA tandis que son allongement à la rupture est plus courte en comparaison avec d'autres mélanges. Ces résultats sont liés à l'influence de la LRD-Si-3G plaquettaire. Il pourrait être due à des interactions accrues entre PLA et PBA qui sont reliés par le LRD-Si-3G a entraîné une diminution de la mobilité des chaînes.

La résistance au choc des mélanges PBA/PLA a également été mesurée pour différentes teneurs en argile, comme le montre dans tableau 5. Une addition du PBA a entraîné une augmentation spectaculaire de la ténacité. La résistance aux chocs a été significativement modifiée par rapport 1.851KJ/m^2 pour PLA pur à 2,391 KJ/m^2 pour

le mélange PBA/PLA (20/80) et 3,988 KJ/m^2 pour le mélange PBA-2%LRD-Si/PLA (20/80). Le mélange PBA-5%LRD-Si/PLA (20/80) a la plus grande force d'impact, soit 4,668 KJ/m^2, entre la PBA/PLA mélange.

L'amélioration de la résistance aux chocs du mélange PBA-LRD-Si/PLA (20/80) est vraisemblablement attribuable à une meilleure dispersion des particules réticulées PBA-LRD-Si dans la matrice PLA, car ils ne pouvaient pas avoir coalescence vaste comme les particules PBA dans la matrice PLA. La taille des particules réticulées PBA-LRD-Si dans la matrice doit être plus petite si l'on comparer avec les particules PBA pur mélangées avec PLA. La résistance au choc diminue de l'ordre de la taille des particules PBA augmente dans les mélanges. En fait, une telle corrélation a été fréquemment observée pour d'autres polymères de caoutchouc modifiés.

Les valeurs de T_α du PBA et du PLA sont présentées dans le tableau 6 dérivé de E" et tan δ courbes obtenues en DMTA (analyseur mécanique dynamique). Tous les mélanges montrent deux transitions vitreuses, l'une pour PBA moins environ -50 °C et l'autre pour PLA moins environ 78 °C, ce qui indique que les mélanges ne sont pas miscibles thermodynamiquement. Comme le montre le tableau 6, avec addition de LRD-Si dans la polymérisation en mini-émulsion, la T_α du PBA est légèrement augmenté et plus le chargement de l'argile plus la T_α supérieure. La T_α du PBA dans le mélange PBA-LRD-Si/PLA avec LRD-Si 5% en poids est de l'ordre de 3 °C de plus que dans le mélange pur PBA/PLA. Ces résultats indiquent qu'avec le LRD-Si dans le PBA, la structure de nanoparticules est différente de celle des particules PBA purs. Cela signifie que l'interaction entre le LRD-Si et PBA limite le mouvement segmentaire de la PBA.

Alors que la LRD est ajoutée dans la préparation du latex de PBA, la T_α du PBA n'a pas beaucoup changé ce qui implique que plus de LRD ne change pas la structure des particules PBA. En revanche, la T_α du PLA est croissante de ~ 3 ° C lorsque la LRD est introduit dans la polymérisation en mini-émulsion de PBA tandis que l'addition de LRD-Si dans PBA latex affecte la T_α du PLA légèrement. L'introduction de LRD autour des particules de la PBA peut former une dispersion exfoliée LRD dans la matrice PLA en mélangeant dans micro-compoundeur. La présence de plaquettes

LRD exfoliées eu un effet de renforcement de PLA en raison de sa capacité à inhiber le mouvement des chaînes PLA. Par conséquent, la T_α de PLA est augmenté. Bien que l'ajout direct de plaquettes LRD dans le mélange PLA/PBA en mélangeant dans micro-compoundeur, le degré de décollement pour les feuilles de LRD dans le mélange ne peut pas atteindre le même niveau que celui de LRD dans le mélange PBA-LRD/PLA. En conséquence, la T_α du PLA dans le composite LRD/PLA/PBA (1/79/20) seules hausses d'environ 1 °C. Ces résultats sont cohérents avec la valeur de E' et les résultats précédents essais de traction pour des mélanges PBA-5%LRD/PLA (20/80) et LRD/PLA/PBA (1/79/20).

Tableau 6 Les températures de relaxation (T_α) obtenues à partir des sommets des courbes du module de perte E" et des courbes de Tan δ (DMTA).

Mélanges	***T_α1 (°C)***	***T_α2* (°C)**
PLA pur	-	78
PBA/PLA (20/80)	-49	79
PBA-2%LRD-Si/PLA (20/80)	-49	78
PBA-5%LRD-Si/PLA (20/80)	-46	79
PBA-5%LRD/PLA (20/80)	-50	81
LRD/PLA/PBA (1/79/20)	-48	79
PBA-3%LRD-Si-3G/PLA (20/80)	-51	77

Par l'encapsulation de LRD-Si en particules PBA, l'espacement intercalaire d'argile augmente, même l'exfoliation aurait lieu. En outre, lorsque le cœur-écorce PBA-LRD-Si/PMMA a été obtenu, comme le PMMA est partiellement miscible avec PLA, l'interaction entre PBA et PLA pourrait être améliorée. Avec le grand espacement entre couches d'argile et de forte interaction PBA dans la matrice PLA, les propriétés correspondantes des nanocomposites obtenus ont été étudiées.

Il est à noter que le PLA modifié maintient module de traction et résistance à la traction élevée. En même temps, la résistance aux chocs de toute évidence augmenté. Ceci signifie que le matériau obtenu ayant une bonne rigidité ténacité équilibre. En outre, on peut s'attendre à ce que les mélanges présentent une résistance accrue à la chaleur par rapport aux PLA soignée en raison de l'augmentation de la température de transition vitreuse.

La liaison hydrogène forte entre les groupes ester-chaînes PMMA et de la matrice PLA fait disperser les nanoparticules dans la matrice et la ténacité des composites est accru considérablement en conséquence.

Le cœur caoutchouteux est constitué de PBA, qui a été légèrement réticulée par LRD-Si peut conserver sa morphologie sphérique et de taille au cours de la transformation et des mélanges de moulage. Dans le cas d'une bonne adhérence interfaciale, la force d'adhérence interfaciale est suffisamment solide pour supporter l'accumulation de contrainte suffisant autour des particules, ce qui induit fendillements de la matrice, en vidant les particules de caoutchouc ou de formation de cavité autour de l'interface à un certain niveau de contrainte critique.

T_α de PLA dans les mélanges avec particules cœur-écorce PBA/PMMA passé à des températures plus élevées. T_α de la phase PBA ou phase PMMA n'est pas clair à partir des courbes DMTA. T_α du PLA augmente avec l'ajout de PMMA qui améliore la compatibilité de mélange. Les mélanges PBA/PLA montrent que presque T_α mêmes correspondant à chacun des composants, ce qui indique la non-miscibilité thermodynamique entre PLA et PBA. L'ajout de PMMA modifie clairement les positions des pics de PLA. D'après le tableau 7, les T_α du PLA à se déplacer vers une température plus élevée, suggérant que les compatibilités entre le PLA et le PMMA.

Tableau 7 Les températures de relaxation (T_α) obtenues à partir des pics des courbes Tan δ (DMTA).

Mélanges	***T_α* (°C)**
PLA pur	78
(PBA/PMMA)/PLA (10/10/80)	92
(PBA-2%LRD-Si/PMMA)/PLA (10/10/80)	86
(PBA-5%LRD-Si/PMMA)/PLA (10/10/80)	85
(PBA-5%LRD/PMMA)/PLA (10/10/80)	91
LRD/PLA/(PBA/PMMA) (1/79/10/10)	89

Les résultats de DMTA sont cohérents avec ceux de MEB. Elle peut être expliquée sur la base du retard dans la relaxation des régions amorphes conférées par le renforcement de l'interaction physique avec la phase de renforcement et la matrice de PLA. L'augmentation de la T_α est associée avec la diminution de la mobilité des

chaînes de la matrice, ce qui indique une adhésion interfaciale améliorée entre le cœur PBA et la matrice PLA.

4. Conclusions

Ces travaux ont mis au point une méthode de polymérisation en miniémulsion et émulsion à synthétiser latex cœur-écorce PBA/PMMA qui sont ensuite incorporées dans le PLA, afin d'améliorer sa résistance au choc, sans réduire les propriétés de traction de manière significative. L'incorporation de PBA seul dans le PLA augmente sa résistance aux chocs tout en réduisant considérablement ses propriétés de traction. L'incorporation de l'argile (laponite) dans le PBA tente d'augmenter ses propriétés de traction. L'écorce en PMMA non seulement possède des propriétés de traction supérieures à celles mais aussi une meilleure compatibilité avec PLA. En tant que tel, l'incorporation de nanocomposites PBA-laponite/PMMA dans la matrice PLA permet d'améliorer de façon significative sa résistance aux chocs, tout en conservant, dans une large mesure, ses propriétés de traction.

Chapter 1. Literature review

Introduction

In the next two decades plastics are expected to gain important portion of the glass market and to substitute the traditional materials such as steel. However, the environmental impacts come from plastics are rather high compared to other materials. The manufacturing of biodegradable materials offers an interesting solution for the impact of plastic materials. Much of the increase in consumption is expected to come from polyesters such poly(lactic acid) (PLA) and its blends. PLA, a cost-effective biocompatible and biodegradable thermoplastic derived from lactic acid (2-hydroxy propionic acid) has attracted many attentions of polymer scientists during the past decade as a potential biopolymer to substitute the conventional petroleum based plastics because it is produced from renewable recourses such as starch. Its production consumes carbon dioxide and provides significant energy savings. Pure PLA can be degraded into carbon dioxide and water with long-term using, compared to other petroleum-based plastics. It is widely used for biomedical applications such as sutures and drug delivery devices because of its biodegradable and biocompatible nature. It provides good strength and easy process ability in most products. It can be easily processed into molded parts, film, or fiber, and so on. Unfortunately, PLA is a comparatively brittle and stiff polymer, its tensile strength and E modulus is around 60 MPa and 3.5 GPa, respectivley, with low deformation at break about 5-10%; with a glass transition temperature ranging from 55 to 65 °C, its toughness and heat resistance are not satisfactory for the practical application at room-temperature in many cases. Its low impact strength is comparable to non-plasticised PVC [1-11].

1. Poly(lactic acid) and reinforcement

The basic constitutional unit of PLA, lactic acid, can be manufactured by carbohydrate fermentation or chemical synthesis [12]. Lactic acid is the simplest hydroxyl acid with an asymmetric carbon atom and it exists in two optically active

configurations, the L (+) and D (-) isomers. Scheme 1.1 shows the chemical structure of the L and D lactic acids.

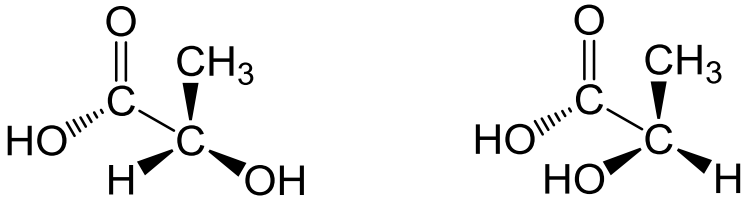

Scheme 1.1 Chemical structure of L and D-lactic acid (m.p. is melting point) [12].

Lactide, the cyclic dimer of lactic acid, is formed by the condensation of two lactic acid molecules as follows: L-lactide (two L-lactic acid molecules), D-lactide (two D-lactic acid molecules) and meso-lactide (a L-lactic acid and a D-lactic acid molecule) (see Scheme 1.2).

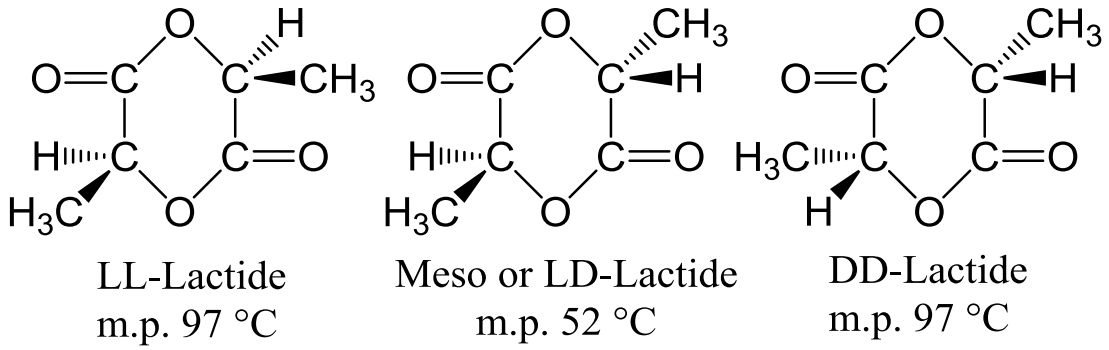

Scheme 1.2 Chemical structures of LL-, Meso- and DD-lactides (m.p. is melting point) [12].

The repeat units are either added as dimers during the lactide ring-opening polymerization or are added to the final polymer as lactic acid monomers via direct condensation polymerization, and a constitutional unit of –[OCH(CH_3)CO–O–CH(CH_3)–CO]– is formed. The repeat unit of PLA (72 g/mol) contains one stereocenter that is either L(S) or D(R) in configuration. Scheme 1.3 shows the constitutional unit of PLA polymers.

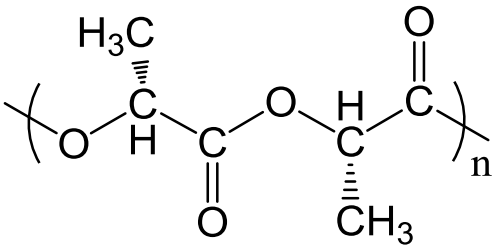

Polylactide, PLA

Scheme 1.3 Constitutional unit of polylactide [12].

Among these three possible isomeric forms, poly(L-lactic acid) and poly(D-lactic acid) are both semi-crystalline in nature, and poly(meso-lactic acid) or poly(d,l-lactic acid) is amorphous. Amorphous grades of PLA are transparent.

The physical and mechanical properties of PLA can be modified to a large extent through control of PLA chains and combination with any other relevant additives and/or fillers. Extensive efforts have been devoted to modifying the brittleness of PLA by copolymerization of lactides with other monomers; although copolymerization can be effective in improving the PLA toughness, commercializing a new copolymer is often to be a long and costly process, making them a less viable option for large-scale applications of PLA. Mineral fillers such as hydroxyapatite, calcium carbonate, calcium phosphate, calcium sulfate, bioceramics, bamboo fiber; some low molecular weight esters; plasticizer such as polyethylene glycol (PEG), glucosemonoesters and partial fatty acid esters or some second-phase polymers such as rubbers, polycaprolactone (PCL), poly(butylenes succinate) (PBSU), poly[(butylenes adipate)-co-terephthalate] have already been used in combination with PLA to improve the impact strength and toughness of PLA. Plasticizers are frequently used not only to increase the flexibility and ductility of glassy polymers, but also to improve the process ability or dispersion of fillers in filled systems. In relation to the processing properties, it is worth noting that addition of plasticizer into highly filled PLA can perform other functions, such as, assisting in viscosity control and lubrication of the compound or improving filler dispersion. More particularly,

plasticizers can reduce the melt viscosity of filled PLA composites, which is helpful in processing and extruding the polymer at lower temperatures, and can improve flexibility and reduce cracking tendencies of the finished products. The major drawback of plasticizers is that during long-term use of the material, they have a tendency to migrate to the surface of the material, causing brittleness of PLA. Blending PLA with a tough polymer may improve its toughness effectively, but this generally requires a relatively high amount of the tough polymer that can lead to a significant reduction in modulus and strength. Most of these PLA blends are immiscible and compatiblizers are needed to improve their compatibility. Meanwhile, their impact strength had increased, but normally the inherent stiffness of the material had sacrificed [1-3, 5, 7-10].

2. Toughening by elastomer or clay

2.1. Elastomeric toughening

Polymer toughening has attracted attention from both academia and industry. Some toughening is necessary in order to widen the possible applications of PLA. Blending PLA with other polymers presents a versatile and economic method to obtain toughened products. An effective method to toughen inherently brittle PLA is rubber toughening. Rubber has been used as a second-phase polymer for toughening brittle materials. While the incorporation of rubber particles improving the fracture toughness in PLA, it will also reduce the tensile modulus and tensile strength accordingly. Generally, the spherical rubber particles act as stress concentrators, initiating and terminating crazes in the brittle polymer matrices, which are responsible for the enhanced fracture energy absorption [1] [5] [13] [14].

It was reported that the interfacial interaction affects the mechanical properties of the composite [4]. The main reason of the worse mechanical properties for PBA/PLA blends is PBA has poor compatibility with PLA. PBA cannot be dispersed well and

stacked in the PLA matrix which generated the poor interfacial adhesion.

Avella et all. [15] have tried to improve toughness of PLA by reactively blending technologies (R type) and non-reactive blending technologies (NR type) with poly(butyl acrylate) (PBA). In their study, for the blending by reactive technique (R type), a reacted interface between the rubber and PLA has been achieved but the multiphase system failed to produce the desired toughening. The impact resistance and flexural modulus of the PLA matrix severely worsen by the presence of PBA. The values recorded for blending by non-reactive technique (NR type) were even worse than those for R type. The mechanical properties of the blends are indicated in Table 1.1. The unsuccessful improvement for toughness of PLA was due to the poor interfacial adhesion between PBA and PLA.

Table 1.1 Impact data and flexural modulus of blends and homopolymers [15].

Code	G_c (KJ/m^2)	K_c (MN/4 m$^{2/3}$)	E (MPa)
PLA	3.14	2740	2920
PLA/PBA 80/20	0.87	1070	2050
PLA/PBA 70/30	0.83	969	1461
PLA/PBA 70/30[a]	0.70	930	1450

[a] Non-reactive blend.

To achieve an improved toughness for PLA matrix, it should treat the poor compatibility of PBA with PLA firstly. Furthermore, from an application view point, one would naturally prefer to have materials that are tough and with the tensile properties maintained. The natural choice would be the incorporation of rigid fillers (such as inorganic particulates or glass fibers) and soft elastomeric inclusions simultaneously.

2.2. Clay toughening

In recent years, polymer/nanometer-sized inorganic particles nanocomposites have received significant attentions from both academic and industrial area because they exhibit remarkable enhancement of mechanical, thermal, optical, electrical, and magnetic properties compared to the pure material or conventional composites and

potential application in areas of plastics and rubber reinforcement, coatings, electronics, catalysis, and diagnostics. These improvements can include high modulus, increased strength and heat resistance, decreased thermal expansion coefficients, decreased gas permeability and flammability, enhanced ionic conductivity. Polymer/clay nanocomposites are of interest because they combine the structure, physical and chemical properties of both inorganic and organic materials [16-21].

The properties of the polymer/layered silicate nanocomposites depend on the distribution and dispersion of the layered silicate in the polymer matrix. Since the optical, thermal, rheological, and mechanical properties of these materials strongly depend on the techniques used for their elaboration, considerable effort has been made to develop synthetic methods with the aim to control dispersions of the inorganic filler within the host polymer. There are three main preparations of polymer/layered silicate nanocomposites, which can be summarized as polymer/pre-polymer intercalation from solution, melt intercalation, and in-situ polymerization, which includes bulk, solution, and suspension polymerization, emulsion polymerization, and miniemulsion polymerization.

Although nanocomposites can be prepared by simply blending of nanoparticles with base polymers via high shear stirring or ball milling, the dispersing degree of nano-particles and the interfacial adhesion were obviously insufficient to obtain desirable material properties [9][18]. Poly(L-lactide)-clay blends made from a solvent-cast blend showed a poor dispersion of clay in the mix. However, the Young's modulus of the blend increased with a small amount of clay [12].

There has been a great number of reports on the synthesis of nanocomposites by in-situ intercalative polymerization. However, these processes mainly produce polymeric solutions of exfoliated clay sheets and do not acheive exfoliation of clay particles. Among the approaches mentioned above, the product in aqueous form has distinct advantages, because of the facility of manipulation, low cost, and absence of environmental concerns. Furthermore, in the last years, the in-situ polymerization method that mainly includes emulsion polymerization, has gained a lot of interests because this heterophase polymerization process offers many advantages compared to

solution or bulk polymerizations such as a low viscosity of the suspension medium, high polymer molecular weights, the simplicity of the polymerization and the possibility to control particles morphology.

For the production of waterborne nanocomposites for coating and adhesive applications, in-situ emulsion polymerization is the best suited alternative, especially when hydrophilic pristine Na-MMT is employed. In most cases, unmodified clay prefers to stay in the water phase or at the oil-water interface but not in the oil phase. The unmodifed clay which was simply mixed into the aqueous phase or added in a emulsion polymerization step made the final products obtained were not a thermodynamically stable latex but were apt to form aggregates. Other works have also shown that it is possible to synthesize waterborne nanocomposites using clay platelets as the only stabilizing agent, which so-called pickering emulsions. However, the stability of these clay dispersions in pickering emulsions is very weak and they are very sensitive to the type of initiators employed during the polymerization. Furthermore, if organophilic clays (where the naturally occurring cations on pristine clays have been substituted by cationic exchange with long alkyl ammoniumsalts) are employed, emulsion polymerization is not the best alternative because the clay will not be incorporated into the polymer particles. By emulsion polymerization, the nanocomposite particles with core-shell, raspberry-like, daisy-shape, and multipod-like morphology were obtained depending on the surface chemistry and the size of the inorganic particles. The emulsion polymerization is also not available as a result of the contradiction between the nucleation mechanism of this approach and the location of clay to be encapsulated, even though it has been a powerful tool in manipulating a wide range of latex products. If clay particles must be kept separate within a droplet, they should withstand coalescence and coagulation caused by the collision of droplets under high shear. There should be no transfer of oligomeric radicals from the swollen micelles in the aqueous phase into the oil phase, where the clay exists, for this will unavoidably cause coagulation, if the nucleation mechanism in a normal emulsion polymerization process is followed. In a conventional emulsion polymerization procedure, the organophilic clay cannot be incorporated into the

polymer particles because diffusion of organophilic clay through the water phase is not favoured.

A promising approach for synthesizing polymer/clay nanocomposite particles (in the submicron range) using organically modified clays is miniemulsion polymerization, where the monomer droplets might contain the hydrophobic clay stacks that upon polymerization (the nucleation and polymerization occurs in the miniemulsion droplets) might lead to exfoliated nanostructures. Meanwhile, miniemulsion polymerization has many advantages for synthesizing polymer encapsulated inorganic nanocomposite because of its excellent stability both before and after polymerization, the submicron droplet size between 50 and 500 nm, and its unique droplet nucleation mechanism during polymerization. The miniemulsion is a relatively stable oil-in-water dispersion, which is typically obtained by shearing a system that containing monomer(s), water, surfactant and a costabilizer. Miniemulsion enables the formation of nanoparticles or 'nanoreactors' dispersed in a continuous medium, such as water. Because of their small size, the large overall surface area of the droplets can effectively compete for radical capture. As a result, monomer droplets in a miniemulsion become the dominant site for particle nucleation. The concept of nanoreactors is based on the proposal that inside each miniemulsion droplet, generally in the order of 50-500 nm, a hypothetical bulk polymerization would take place. Nanoclay particles have a platy morphology with a broad size distribution (aspect ratio varing severely), resulting in more difficulties in the dispersion and the encapsulation of these platelets in monomer droplets and polymer latex in miniemulsion polymerization. By introducing coupling agents or reactive groups onto the surface of nanoparticles, a good interfacial adhesion between inorganic and organic components can also be achieved. If the inorganic particles could be well dispersed in the monomer phase followed by minemulsification, each submicron droplet could indeed act as a nanoreactor, which produces nanocomposite particles with great encapsulation efficiencies of inorganic particles. Meanwhile, the size of nanocomposite particles can be adjusted by varying the surfactant concentration and the shear intensity during the miniemulsification. Therefore, miniemulsion

polymerization is a powerful tool in preparing nanocomposite particles [20-22, 25, 50-54].

It is difficult to disperse the clay filler in the polymer matrix because of the tendency for face to face stacking and their inherent hydrophilic properties. Morgan and Harris [25] found that the properties of nanocomposites are greatly influenced by both the dispersing degree of nano-particles in the polymers matrix and the interfacial adhesion between the inorganic and organic components. The degree of nanoclay dispersion generally depends on the interaction between the nanoclays and the base polymer. However, it is not known what level of clay dispersion (exfoliated, intercalated) is necessary for a particular property of required. It is generally assumed that exfoliation of the clay is preferred for the greatest increases in nanocomposite properties, but that may not always be correct. For example, it appears that in certain systems, exfoliation is desired for mechanical properties, but not necessarily for flammability properties.

It was found that the particle size, the size distribution and the surface properties of nanoclay play remarkable roles in encapsulation and exfoliation as well as the final product stability in a miniemulsion polymerization process. All strategies usually require pretreatment of the clay mineral in order to improve its compatibility with the polymer matrix and achieve a good dispersion.

On the other hand, the nanoparticles morphology and the latex properties were also affected by the nature of the interaction between the surfactant and the clay surface both. According to the morphology of clay particles in composites, two distinct types of structure can be obtained, namely intercalated nano-composites where the polymer chains are sandwiched in between silicate layers and exfoliated or delaminated nano-composites where separated silicate layers are more or less uniformly dispersed in polymer matrix.

The surface hydrophobicity of the clay particles is important in miniemulsion polymerization. A hydrophobic clay, compared to its intrinsic hydrophilicity, is therefore required to favor its stay within the oil phase before polymerization. This hydrophobicity will aid the entry of monomer into the interlayer galleries of the clay

and exfoliate the clay from a face to face stacking to an individually dispersed platelet form after polymerization. It is well-known that the basal surfaces of clays are hydrophobic and their edge surfaces are hydrophilic. The hydrophobicity of the basal surfaces dues to the fact that the atoms exposed on the surface are linked together by siloxane (Si-O-Si) bonds and, hence, do not form strong hydrogen bonds with water. Furthermore, the hydrophobicity of the basal surfaces is also important for the intercalation of clay particles because the hydrophobic basal surfaces aid the entry of the monomer into the inner galleries of the clay. The edge surfaces, on the other hand, are composed of hydroxyl ions, magnesium, silicon, and substituted cations, all of which undergo hydrolysis. As a result, the edges are hydrophilic and can form strong hydrogen bonds with water. It is often needed to render the naturally hydrophilic clay filler in order to increase its compatibility with organic polymeric material [21] [22]. However, to the best of our knowledge, there exist only few reports dealing with the incorporation of ion-exchanged clays into emulsion polymers.

Organic compounds can be incorporated into the interlayer galleries through an ion exchange process. Ion exchange reactions with cationic surfactants including primary, tertiary, and quaternary ammonium ions render the silicate surface hydrophobic, which makes possible the subsequent intercalation of a variety of monomers and/or polymers. In addition, Norma et al. [20] have incorporated clay with the alkylammonium cations which can provide functional reactive groups (e.g., monomers, initiators, catalysts, etc.) that can participate in the polymerization and promote exfoliation of the clay layers.

It was reported that delaminated polymer-layered silicate (PLS) nano-composites is more effective in improving the strength of polymer matrix than intercalated PLS nano-composites. The concentration of clay in the composites is very important, as clays will re-aggregate back to larger agglomerate above 2-3 wt% solids content. Take it into consideration, the final nanocomposite must not have more than 2-3 wt% clay content to obtain a truly exfoliated clay in the polymer matrix. However, when the strength of polymer matrix is remarkably enhanced, its impact strength decreased. Furthermore, the greater extent the silicate layers are exfoliated or delaminated in

polymer matrix, the better the effect of strengthening is, nevertheless, the worse the impact strength is [23-25].

3. Emulsion and miniemulsion polymerization

3.1. Emulsion polymerization

Emulsion polymerization is a well-known technique for preparing latex polymers with defined structures. Several researchers [24, 26-28] have used conventional emulsion polymerization in the presence of face-modified clay platelets to prepare polymer-clay composite latex particles.

Emulsion polymerization is the most common way of forming polymer latexes; in the simplest system, the ingredients comprise water, a monomer of low water solubility (e.g. styrene), water-soluble initiator (e.g. persulfate) and surfactant (latexes can also be synthesized without added surfactant and/or initiator, but this is not common). A new phase is quickly formed: a polymer colloid, comprising a discrete phase of colloidally stable latex particles, dispersed in an aqueous continuous phase. Virtually all polymerization occurs within these colloids. By the end of the reaction, each colloid contains many polymer chains. Colloidal stabilizers may be electrostatic (e.g. with an ionic surfactant such as sodium dodecyl sulfate), steric (with a steric, or polymeric, stabilizer such as poly (ethylene oxide) nonylphenyl ether), or electrosteric. Polymer latexes are used in the production of a wide range of specialty polymers including adhesives, paints, binders for nonwoven fabrics, additives for paper, textiles and construction materials, impact modifiers for plastic matrices, diagnostic tests, and drug-delivery systems [55-58]. The development of this industry arises from the possibility of producing polymers with unique properties, the environmental concerns and governmental regulations to substitute solvent-based systems by waterborne products.

Commonly, the products mentioned above are produced by means of emulsion polymerization. Batch emulsion polymerization is commonly used in the laboratory to study reaction mechanisms, develop new latex products and obtain kinetic data for

process development and reactor scale-up. In this process, monomer is dispersed in an aqueous solution of surfactant with a concentration exceeding the critical micelle concentration (CMC) and polymerization is started by means of an (most often water-soluble) initiator system. In principle, polymer particles can be formed by entry of radicals into the micelles (heterogeneous nucleation), precipitation of growing oligomers in the aqueous phase (homogeneous nucleation), and radical entry in monomer droplets. However, monomer droplets are relatively large (1-10μm) compared to the size of monomer-swollen micelles (10-20 nm), and hence the surface area of the micelles is several orders of magnitude greater than that of the monomer droplets. Consequently, the probability for a radical to enter into the monomer droplets is relatively low, and most particles are formed by either homogeneous or heterogeneous nucleation. Once they are nucleated, the polymer particles undergo substantial growth by polymerization. The monomer required for the polymerization must be transported from the monomer droplets by diffusion through the aqueous phase. In some cases, this represents a severe limitation of the emulsion polymerization. Thus, water resistance of coatings prepared from dispersed polymers is significantly improved if very hydrophobic monomers, e.g. lauryl and stearyl methacrylates, are incorporated into the polymer backbone. However, mass transfer of these monomers from monomer droplets to polymer particles through the aqueous phase is diffusional-controlled, and hence they cannot be readily incorporated into the polymer in emulsion polymerization.

Emulsion polymerization is a complex process. The literature contains extensive reviews of emulsion polymerization theory [59-63]. The earliest qualitative theory of emulsion polymerization was developed by Harkins [64] and was quickly quantified by Smith and Ewart (SE) [65]. Although this theory only holds for the special case of water-insoluble monomers, it is the typical starting point for most other theories. This theory is based on the batch emulsion polymerization of styrene. It includes three intervals, as depicted in the Figure 1.1. The first interval begins with the initiation of the reaction and continues until all micelles become nucleated or are used up as surface stabilizing agents. At this point, particle formation ceases. During interval II,

the particles grow at a constant rate in the presence of monomer droplets. Once the monomer droplets disappear, interval III begins. The monomer concentration in the particle decreases and the reaction within the particles becomes diffusion-limited throughout the remainder of the polymerization.

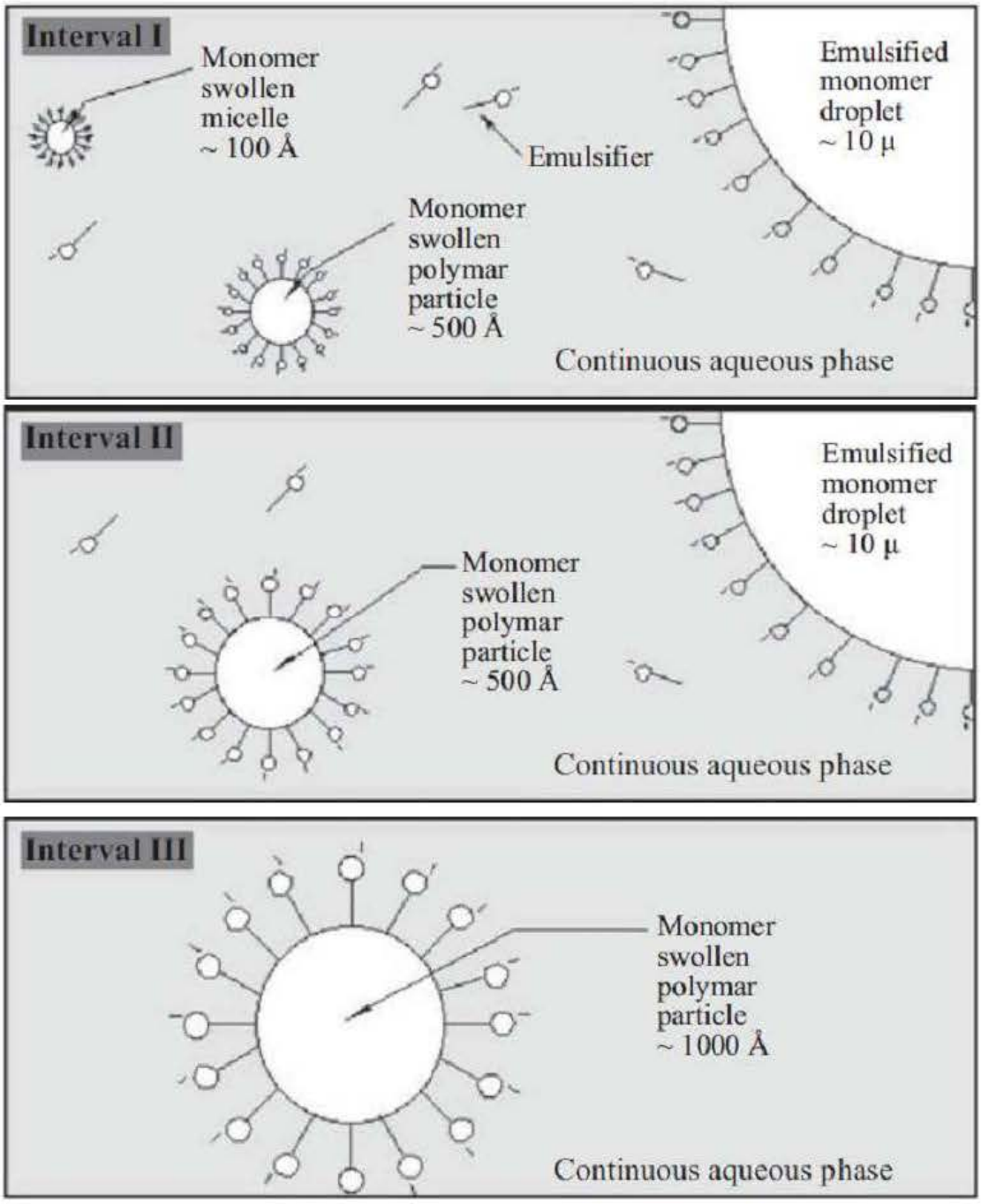

(a) Emulsion polymerization

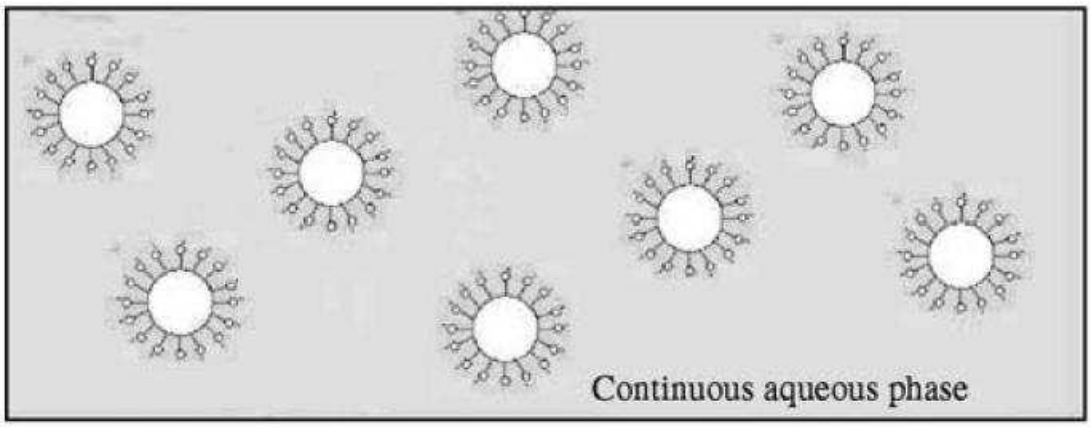

(b) Miniemulsion polymerization

Figure 1.1 Emulsion polymerization versus miniemulsion polymerization

Interval I - Particle Nucleation

Nucleation mechanisms are generally divided into three types: micellar, homogeneous and droplet. Statistically, all three types can occur simultaneously in every reaction. However, it is the preponderance of one mechanism with respect to the others in a given system that causes authors to consider only one in their studies. Numerous extensions have been made to the SE [65] micellar nucleation theory in an effort to furnish explanations for experimental results observed for monomers with slight water solubility.

Detailed reviews of these extensions are readily available [63] [64] [66] [67]. Monomer droplet nucleation is normally neglected, except when considering mini- and micro- emulsions, due to its insignificant contribution to the particle number and the size distribution.

1. Micellar Nucleation

All quantitative theories based on micellar nucleation can be developed from balances of the number concentrations of particles and of the concentrations of aqueous radicals. Smith and Ewart [65] solved these balances for two limiting cases:

(i) all free radicals generated in the aqueous phase assumed to be absorbed by surfactant micelles,

(ii) micelles and existing particles competing or compete for aqueous phase radicals.

In both cases, the number of particles at the end of Interval I in a batch emulsion polymerization is predicted to be proportional to the aqueous phase radical flux to the power of 0.4, and to the initial surfactant concentration to the power of 0.6. The Smith Ewart model predicts particle numbers accurately for styrene and other water-insoluble monomers. Deviations from the SE theory occur when there are substantial amounts of radical desorption, aqueous phase termination, or when the calculation of absorbance efficiency is in error. Deviations with respect to order from the SE theory increase as the monomer water solubility increases.

2. Homogeneous Nucleation

Although the SE [65] micellar nucleation theory explains data for certain systems, it fails for others. This has led some authors to propose a different mechanism for nucleation. In the homogeneous nucleation theory, aqueous phase radicals polymerize to form oligomers. These latter continue to grow until they reach a critical chain length, the size of a primary particle, and then precipitate. Throughout the growth process, the oligomers may also flocculate or coagulate. This theory is typically employed for relatively water-soluble monomers. Slight variations of this theory have also been postulated.

Prior to 1952, little evidence for homogeneous nucleation existed [68] [69]. In 1952, Priest [70] studied the polymerization of vinyl acetate and presented a qualitative theory for homogeneous nucleation. He concluded from experimental work that aqueous phase nucleation is important in systems with monomers that have relatively high water solubility. Primary particle formation occurs throughout the course of the reaction. During later periods of the reaction, large monomer-swollen polymer particles act as sinks for these primary particles, encouraging coagulation.

In 1968, Roe [71] developed the SE limiting case equations for particle number from the homogeneous nucleation theory. He showed that the SE equation for particle nucleation is not unique to micellar nucleation, but results from the SE assumptions. By assuming that (i) the nucleation stops upon depletion of micelles, (ii) the volumetric growth rate is constant, and (iii) the radical absorption is strictly a function of radical generation, he showed that the SE dependency on radical flux and

surfactant concentration could be generated from homogeneous nucleation theory.

Fitch and Tsai [72] developed a quantitative theory for homogeneous nucleation. By using the collision theory for radical capture, Fitch [73] showed that the rate of radical capture is a function of radical production, particle number, particle size, and diffusion distance. Primary particles may coagulate with each other because of their small size and lower surface charge. As particles coagulate, the surface to volume ratio decreases, which causes an increase in surface potential. When particles become sufficiently large, coagulation ceases due to insufficient kinetic energy to overcome the biparticle surface repulsion. Fitch and Tsai have provided experimental support for this theory by polymerizing MMA with different initiators.

Ugelstad and Hansen [63] proposed that free radicals in the aqueous phase propagate with dissolved monomer. Primary particles form by precipitation when a critical chain length is reached. During growth from a monomer radical to a primary particle, each oligomer can (i) terminate with other radicals, (ii) precipitate if its length exceeds the critical chain length, or (iii) be captured by particle.

A fundamental extension to the homogeneous nucleation theory was proposed [74] [75]. Their theory is based on the positive skewness of the particle size distribution (PSD) as a function of volume during Interval II. This implies that the rate of nucleation during Interval I increase with time until it eventually drops of at the end of nucleation. Lichti et al. [74] and Feeney et al. [75] claim that micellar nucleation or one step homogeneous nucleation incorrectly predict either decreasing or constant nucleation rates.

This theory has been given the name coagulative nucleation. According to Lichti and Feeney's mechanism, precipitated 'precursor particles' undergo coagulation to form 'true' or 'mature' latex particles. A precursor particle is unstable and said to be formed in either a micelle or the aqueous phase. Due to their small size and hydrophilic nature, the precursors have low swelling capacity and high radical desorption rates. Consequently, the propagation rate is low and these precursors tend to coagulate with other precursors or mature latex particles. These conclusions then rule out micellar nucleation as a possible mechanism for precursor formation.

Maxwell et al. [76] suggested that the values to be used for the critical chain length are much smaller than originally thought. They also suggested that oligomeric radical capture is independent of particle size and limited by the rate of propagation of the radical in the aqueous phase. However, this theory does not consider variations in other parameters with particle size.

3. Droplet Nucleation

Nucleation of monomer droplets has typically been neglected in emulsion polymerization. The large diameter (1-10 μm) and small number (10^{13} versus 10^{21} micelles) of droplets in emulsions usually makes their consideration of no importance. Regardless of this, all droplets do get nucleated, because of their large size. These droplets show up in TEM photographs as abnormally large particles in very low concentrations. In 1973, Ugelstad et al. [77] showed how submicron styrene monomer drops can be made stable enough to become numerically significant in nucleation when a co-stabilizer is used to enhance the stability of the smaller droplets. Chamberlain et al. [78] have presented experimental evidence that the efficiency of radical capture by droplets is much lower than that for micelles or particles. Ugelstad et al. [79] [80] have shown how nucleation of monomer droplets can lead to latexes with large monodisperse particles. However, if insufficient shear or co-stabilizer is used, the potential for production of bimodal PSDs exists [81] [82]. This could be desirable in certain instances.

The distinguishing feature of droplet nucleation as opposed to micellar or homogeneous nucleation is the nature of the particle at 'birth'. Droplets, which are nucleated into particles, begin as nearly 100% monomer. Micellar or homogeneous nucleated particles start out with much lower monomer concentrations and eventually swell to around 60% (for MMA) in the presence of monomer droplets. This fundamental difference may lead to large differences between miniemulsion and emulsion polymerizations in radical desorption and/or intra-particle termination during Intervals I and II.

4. Competition for Radicals

As pointed out above, particle nucleation includes all three mechanisms - micellar,

homogeneous, and droplet, since these mechanisms may compete and coexist in the same system. Often one will dominate. Therefore, any general model of emulsion polymerization should include all three mechanisms. Hansen and Ugelstad [83] have presented probabilities for each of these mechanisms in the presence of all three. The competition for oligomeric radicals also includes particles that have been created with emulsions, since both micellar and homogeneous nucleation result in a large shift in the surface area from micelles to particles as the particles are created and grow.

Interval II - Particle Growth

SE Interval II begins at the cessation of nucleation, or in light of the nucleation theory just reviewed, when the particle number becomes relatively constant. Most theories developed for this interval assume a constant particle number and use the quasi-steady-state approximation (QSSA) for average number of radicals per particle. The kinetics and mechanisms of Interval II have been some of the most studied aspects of emulsion polymerization. SE Interval II ends when the monomer droplets disappear and the monomer concentration in the particles begins to decrease.

The rate of polymerization during Interval II is usually considered constant for two reasons. The monomer concentration within the particle, as defined by equilibrium thermodynamics, is approximately constant in the presence of excess monomer. Mass transfer is assumed to be fast and particle size has little effect on this concentration. Secondly, emulsion polymerization kinetics tend to give a constant radical concentration within the particles during Interval II. Therefore, the rate of polymerization is approximately constant until the end of Interval II, where $[M]_p$, $\bar{n}$, and k_p begin to change. These two assumptions have been substantiated by experimental observations and are considered reasonable. The challenge for Interval II is to determine the average number of radicals per particle. Particle monomer concentration can be determined as a function of particle radius by an equilibrium relationship equation [84] that considers both surface energy and mixing energy. Propagation rate coefficients have been widely studied and are readily available [85]. The particle number concentration is assumed constant.

Smith and Ewart developed three limiting cases for Interval II. Each of these cases can be generated through a balance of N_{pi} (the number of particles containing i radicals), where the number of particles is considered constant (no nucleation). For Case 1, Smith and Ewart assume $N_{p0} >> N_{p1} >> N_{p2} >>$ .... For this case, $\bar{n}$ will be significantly less than 0.5. This case occurs when significant monomeric radical desorption occurs, and is more common with monomers of significant water solubility.

Case 2 assumes instantaneous termination of the existing radical with an entering radical. In this case, each particle will contain either zero or one radical, and $\bar{n}$ becomes 0.5. Styrene generally follows Case 2 kinetics. Smith and Ewart Case 3 assumes that both desorption from particles and aqueous phase termination may be neglected, and so $\bar{n}$ >> 1.0. This occurs with large particles, and in the limit results in bulk kinetics.

Coagulation of latex particles during Interval II is often neglected. If surfactant is available in great enough proportion, the particles will remain stable throughout the reaction.

Interval III - Gel and Glass Effects

Interval III begins when all monomer droplets have vanished and/or the aqueous phase becomes unsaturated. Since each droplet in an emulsion actually absorbs radicals, they cannot disappear but rather shrink to a point where they have no excess monomer. The monomer in the aqueous phase decreases corresponding to the decrease in the particles. The conversion at which Interval III begins varies for different monomers and systems, but is typically around 40 to 50%. However, it may not be as distinguishable in miniemulsion due to early initiation of the gel effect.

As the monomer within the particles is consumed by polymerization, the viscosity rises within the particles and the diffusion rate of the polymeric radicals decreases. This causes a reduction in the rate of termination, which corresponds to a dramatic increase in the radical concentration. A higher radical number within the particle results in an 'auto acceleration' of the rate of polymerization. Common practice is to

model this auto acceleration or gel effect by decreasing the termination rate constant by several orders of magnitude as a function of percent monomer in the particle. A free volume approach has been used by Sundberg et al. [86]. Buback et al. [87] suggest a completely empirical approach from precise experimental data. Empirical correlations used in modeling the gel effect in bulk or solution polymerization have also been modified for use in emulsion processes [88-91].

The problem when applying correlations derived from other systems to emulsion polymerization is twofold. First, normal emulsion particles are said to be created with 30 to 40% monomer in them and so the unbiased (zero conversion) termination rate is unknown. Secondly, the diffusion limitations in particles might be quite different from those observed in bulk or suspension polymerizations. For these reasons, an empirical approach is suggested.

If the reaction temperature is below the polymer glass transition temperature and the amount of monomer in the particle decreases far enough, the glass effect may become important. The polymerization rate virtually goes to zero because the particle becomes so internally viscous, essentially glasslike, that the diffusion of monomer to the radicals is limited. The glass transition point varies for different polymers. This effect has also been studied by several researchers [86, 92-94].

3.2. Miniemulsion polymerization

In the previous discussion of emulsion polymerization, all three forms of particle nucleation were discussed. Micellar and homogenous nucleation dominate in emulsion polymerization. This is because the large sizes of the monomer droplets, and their consequent low interfacial area, make them ineffective in competing for water-borne free radicals. Droplet nucleation undoubtedly takes place in emulsion polymerization, but it is generally considered to be insignificant. If the monomer droplet size can be reduced to below 0.5 μm, two phenomena will occur. First, the droplets will be able to compete successfully for water-borne free radicals with any remaining micelles. Secondly, the huge increase in interfacial area caused by the reduction in droplet size will require a monolayer of surfactant to remain stable. The

surfactant necessary to support this large interfacial area will come from the break-up of surfactant micelles.

The existence of droplet nucleation had been previously suggested by Ugelstad et al. [81] for the emulsion polymerization of vinyl chloride stabilized with a combination of anionic surfactants and fatty alcohols.

Ugelstad et al. [77] was the first to demonstrate that under conditions in which the droplet size is small enough, nucleation of monomer droplets could account for an important part of the particles formed. The need of mass transport of monomer through the aqueous phase would be greatly diminished if all (or at least a large fraction) monomer droplets were nucleated. Prevalent droplet nucleation can only occur if the surface area of the monomer droplets is large compared with that of the micelles, and this requires submicron droplet size. The word miniemulsion was coined by Chou et al. [29] to describe submicron oil-in-water dispersions that are stable for a period ranging from hours to months.

Miniemulsion polymerization is an effective approach for obtaining thermodynamically stable water dispersions. They are specially formulated as heterophase systems in which stable nanodroplets are dispersed in a continuous phase. The miniemulsions are usually more stable than similar conventional emulsions.

Early work also reported on the key role of both formulation and emulsification process on droplet size and stability. Ugelstad et al. [95] prepared styrene miniemulsions by stirring sodium hexadecyl sulfate/hexadecanol mixtures with water at 70°C, then the system was cooled to 60°C and monomer added under stirring at 600 rpm. It was found that the droplet size decreased and the stability increased as the surfactant/fatty alcohol ratio increased from 1 to 3. Miniemulsions degrade with time, the degradation being faster at higher temperature. A mechanism for emulsification was proposed. In the first stage, a temporary complex surfactant/fatty alcohol layer is formed which helps to emulsify the monomer. Later, the fatty alcohol diffuses towards the interior of the droplets reducing the stability of the droplets. According to this mechanism, a minimum amount of fatty alcohol is needed to saturate the droplets and have enough fatty alcohol to form the complex at the interface. This idea was

supported by experiments in which the fatty alcohol was dissolved in styrene prior emulsification and only coarse unstable systems were obtained. However, the mechanism is based on the idea that the only role of the fatty alcohol is to modify the droplet surface, and it has been proved that this is not the case. Polymerization of the styrene miniemulsions yielded bimodal particle size distributions (PSD), the large particles being produced through droplet nucleation. Only large fatty alcohol/surfactant ratios led to a generalized droplet nucleation. Because the fatty alcohols led to the reduction of the interfacial energy and to the formation of ordered structures, these compounds were called cosurfactants.

Fitch [96] found that the longer the fatty alcohol, the more stable the miniemulsion. Inspired by the works of some researchers [97-100] who had found that the stability of light petroleum, benzene and hexane emulsions was strongly improved by small amounts of hexadecane (HD: water solubility estimated at $1x10^{-9}$ [101]), they decided to use this compound instead of a fatty alcohol to stabilize the monomer miniemulsion.

It was found that with ordinary stirring equipment, addition of hexadecane did not give the rapid emulsification that could be obtained with the long chain fatty alcohols. Therefore, a more efficient homogenization system was used. It was found that when the hexadecane containing emulsions were homogenized with a Manton-Gualin high pressure laboratory homogenizer, extremely stable monomer miniemulsions were obtained. The use of Mantton-Gaulin homogenizer did not lead to any improvement in the stability of fatty alcohol containing miniemulsions, but in this case, the stability of the miniemulsion was independent of the order in which the components of the formula were mixed.

Durbin et al. [31] applied different degrees of emulsification (no emulsification, hand shaking, homogenization with a hand-homogenizer (Fisher Scientific), and ultrasonication) to a styrene-anionic surfactant-water system. It was found that in the absence of cetyl alcohol or hexadecane, droplet nucleation was negligible. This early work established the basis for the miniemulsion polymerization process, namely, that energetic homogenization should be applied to reduce the size of the monomer

droplets, and that these droplets should be protected against both diffusional degradation and droplet coagulation by suing a water-insoluble compound and an efficient surfactant.

Monomer diffused from small to large droplets leading to larger droplets and emulsion destabilization. To create a stable miniemulsion, the droplets must be stabilized against molecular diffusion degradation (Ostwald ripening or τ_1 mechanism) as well as against coalescence by collisions (τ_2 mechanism). However, droplet coalescence plays an important role in destabilizing monomer miniemulsion. The instability of the miniemulsion affects the number of monomer droplets and, therefore, the rate of polymerization, the particle size and the molecular weight of the final product. The formation of small droplets is a requirement for the enhancement in both droplet nucleation and the polymerization rate. If Ostwald ripening is allowed to continue unchecked, creaming of the monomer will occur as the droplet sizes become large enough for Stokes law creaming to occur. This will occur in a matter of seconds to minutes. If the system is initiated, bulk polymerization of the monomer layer will occur. If the emulsion is stirred, an emulsion of large monomer droplets (of the order of those of an emulsion) will result, and if the stirred emulsion is initiated, emulsion polymerization will take place. Smith [100] suggested that the effect of the addition of small amount of hexadecane might be due to the prevention of miniemulsion degradation by molecular diffusion (Ostwald ripening effect). This approach to emulsion stability was first presented by Higuchi and Misra [30], and it was based on the fact that due to the surface energy, the chemical potential of the monomer in small droplets is higher than in large droplets or plane surfaces. Higuchi and Misra [30] predicted that the addition of a small amount of a water-insoluble compound would retard the emulsion degradation by molecular diffusion because the slow rate of diffusion of the water-insoluble compound would permit the monomer to remain essentially equilibrated among the droplets.

The early work also influenced nomenclature. Thus, the water-insoluble low-molecular weight compound is often referred to as a co-surfactant in miniemulsion polymerization publications. However, with the exception of the long

chain alcohols, this is a misnamed because compounds like hexadecane have no surface activity. In addition, the main stabilizing effect of these compounds (including cetyl alcohol (CA: water solubility estimated at $6x10^{-8}$ [101]) is not a surface effect but a bulk effect. The compound responsible for stabilizing the monomer droplets against Ostwald ripening has also been called a hydrophobe to account for its water-insolubility. However, although any water-insoluble compound may retard diffusion degradation, its efficiency strongly depends on the molecular weight. Thus low-molecular weight water-insoluble compounds are much more efficient than high-molecular weight water-insoluble compounds. Therefore, the term co-stabilizer is used in this thesis to refer to low-molecular weight water-insoluble compounds, which are highly efficient in stabilizing monomer droplets against diffusion degradation.

According to all the previous researches, it can be concluded that miniemulsions are one kind of aqueous dispersions with droplet sizes between 50 and 500 nm and are opaque and of milky appearance. A miniemulsion is a relatively stable submicron dispersion of oil-in-water containing oil, water, a surfactant and a co-stabilizer and is typically obtained by shearing system. Generally, miniemulsions are prepared by subjecting the monomer/water mixture to high shear stress in the presence of suitable surfactant and co-stabilizer. The stability of these droplets arises from the use of an ionic or nonionic surfactant coupled with a co-stabilizer which is a highly monomer soluble, highly water insoluble material (typically long-chain alkane and alcohol), which is added to limiting degradation by retarding the diffusion of monomer from small droplets to large ones (Ostwald ripening). If Ostwald ripening is retarded by using a co-stabilizer, predominant droplet nucleation can be achieved. This is the basis of miniemulsion polymerization. One of the first comprehensive studies of miniemulsion polymerization was done on styrene by Choi et al. [102].

In a properly formulated miniemulsion, all micelles will be sacrificed to support the droplet interfacial area. Therefore, not only do the small droplets compete effectively for micelles, their presence causes the destruction of the micelles, leaving droplet nucleation (monomer phase initiation) as the dominant particle nucleation process and

homogeneous nucleation (water phase initiation) has been considered to act as a minor nucleation mechanism as well. The particle number per unit aqueous phase before and after polymerization provides important information about the nucleation mechanism of miniemulsion polymerization. Generally speaking, the particle number per unit aqueous phase after polymerization increases if both droplet nucleation and homogeneous nucleation exist simultaneously. The droplet nucleation predominates in miniemulsion polymerization as most of the surfactant is absorbed to droplet surface with little surfactant available to form micelles or stabilize aqueous homogeneous nucleation. Hence, in an ideal miniemulsion polymerization, no monomer transport is involved and the latex particles obtained from it have about the same size as the initial droplets [50][103].

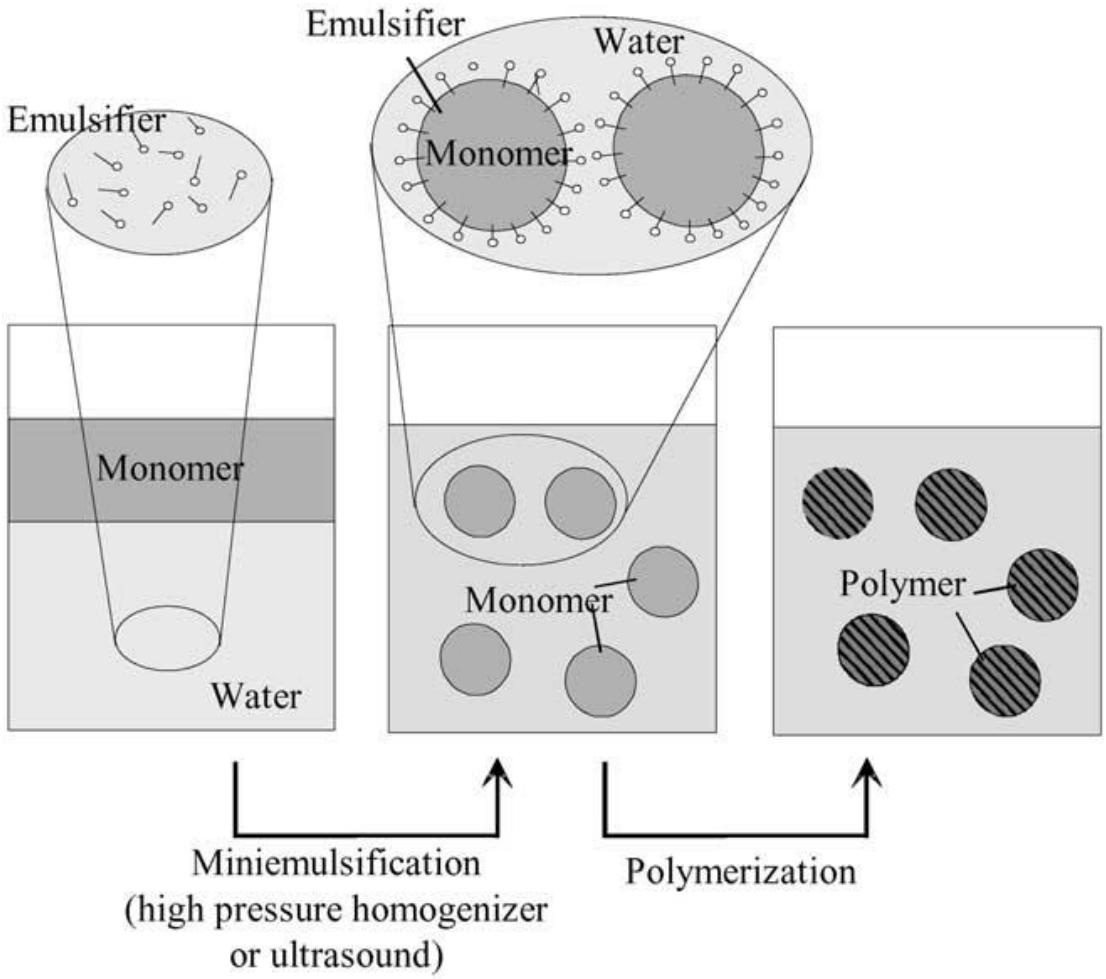

Figure 1.2 The principle of miniemulsion polymerization [104].

The Figure 1.2 shows the principle of ideal miniemulsion polymerization. In an ideal

miniemulsion polymerization with 1:1 copy of droplets, the smaller the monomer particle, the smaller the particle size of the final product; however, practically it is difficult to obtain 1:1 copy during miniemulsion polymerization.

Asua [32] figured out that the droplet size also decreases with the agitation time, the sonication power, the sonication time and the amount of surfactant used, and increases with the volume fraction of the dispersed phase.

When a liquid emulsion is subjected to high shear, small droplets will result. There will still be a statistical distribution of droplet sizes. If the monomer is even slightly soluble in the continuous aqueous phase (and most are, as evidenced by the fact that Interval II of emulsion polymerization takes place), the monomer will, over time, diffuse from the smaller monomer droplets into the larger ones. This results in a lower interfacial area (and interfacial energy), since the loss in interfacial area of the smaller droplets is larger than the gain in interfacial area of the larger ones. The reduction in interfacial energy is the driving force for degradation of the small droplets. Figure 1.3 indicates the particle size region for miniemulsion polymerization.

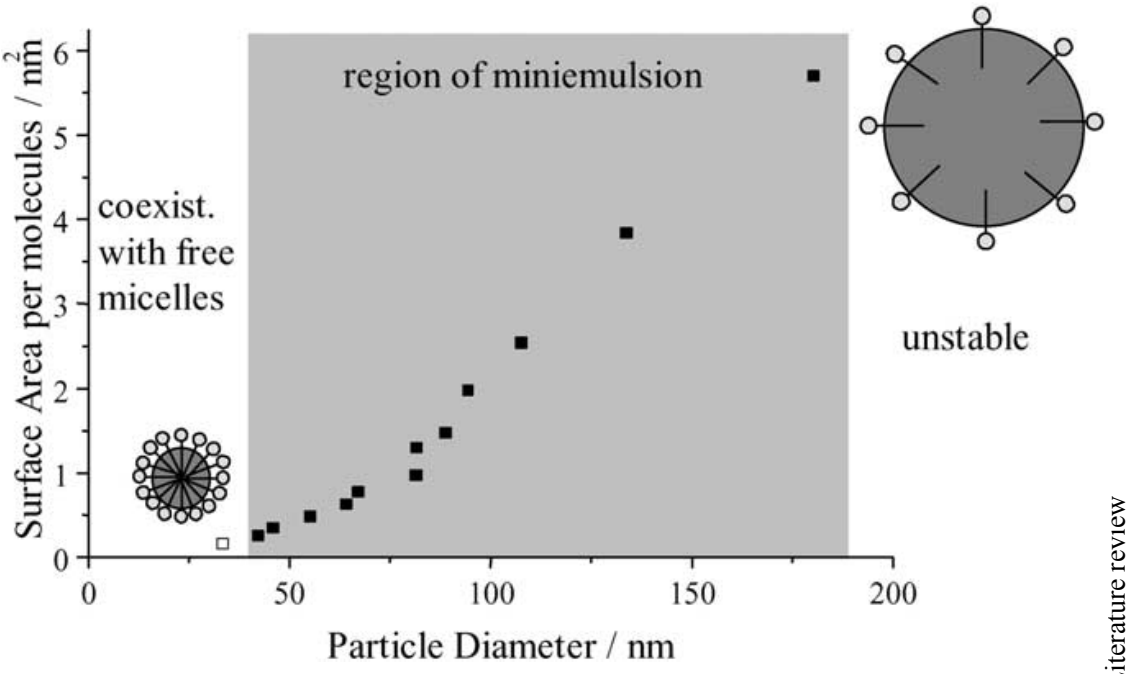

Figure 1.3 Surface tension versus the diameter of the particles [104].

Prior to 1962, droplets below 1 mm were considered too unstable to participate in the nucleation process. In 1962, Higuchi and Misra [30] proposed that the addition of a

water insoluble compound to the monomer will enhance the stability of small droplets by prohibiting diffusion. In 1973, Ugelstad et al. [77] showed how submicron styrene droplets could be made stable enough to participate in the nucleation processes by adding small amounts of cetyl alcohol. Later, Ugelstad [105] used Eq. (1.1) to explain these experimental observations.

Monomer droplet stability can be understood in terms of free energy. The partial molar free energy of adding a second component to a droplet is composed of two terms, the partial molar free energy of mixing and the interfacial partial molar free energy. The partial molar free energy of mixing [106] expression can be combined with the interfacial partial molar free energy to give:

$$\frac{\Delta\overline{G}_i}{RT} = \ln\varphi_i = \left(1 + m_{ij}\right)\varphi_j + \chi_{ij}\varphi_j^2 + \frac{2\overline{V}_i\gamma}{RTr} \qquad \textbf{(1.1)}$$

Ugelstad and Mork [107] applied this equation to various monomers and surfactants. It is clear from this equation that the free energy increases as the phase diameter decreases. The smaller the monomer droplet, the less stable it is. Therefore, a driving force exists for the monomer to diffuse from a small droplet to a larger one. Over time, non-monodisperse systems of droplets of pure monomer will decrease in number as the smaller droplets swell the larger ones and then disappear. Jansson et al. [108] has shown that this occurs in unagitated systems, and that the timescale for diffusional instability can be of the order of seconds.

It can be shown for two phases in equilibrium that the partial molar free energies must be equal. In an emulsion (or miniemulsion), there are three phases: monomer droplets, the aqueous phase and polymer particles. Since monomer is soluble in all these phases, the equilibrium condition requires that the three phases have equal partial molar free energies.

In the presence of monomer droplets, emulsion polymer particles contain 30-80% monomer in them. Therefore, co-stabilizers are said to be 'swollen' with monomer. Ugelstad [65] and Fitch [96] have shown that the addition of a third water-insoluble component to a swollen polymer particle can increase the monomer to polymer ratio. It is well known that co-stabilizers such as hexadecane and high molecular weight

alcohol act as osmotic agents to block monomer ripening. They have shown that an optimum chain size for the additive exists since the solubility of the additive increases as the chain size decreases. They found that the optimum hydrocarbon stabilizer is hexadecane (HD). Others have found that if a fatty alcohol is used as the stabilizer, the minimum chain length required is 12 carbon atoms [109]. In their original discovery of miniemulsion polymerization, Ugelstad et al. [77] used either CA or HD to retard monomer diffusion from submicron monomer droplets. Both CA and HD are the co-stabilizers most often used in publications. Polymers have also been used to reduce Ostwald ripening. It is worth pointing out that polymers are not true co-stabilizers but hydrophobes. Reimers and Schork used poly (methyl methacrylate) to stabilize MMA miniemulsions finding that miniemulsion stability depends on polymer content and polymer molecular weight. The droplet size decreased with the concentration of polymeric hydrophobes. Fitch [96] have shown how this theory may be used to devise a method to prepare large monodisperse particles of predetermined size. By using the appropriate amount of co-stabilizer, polymer particles can be swollen with monomer to the desired size. Polymerization in conditions that prevent additional nucleation results in large monodisperse polymer particles of size 1-100 μm. This method has been criticized by other groups as being in error due to measurement selectivity.

However, these co-stabilizers remain in the polymer particles and may have deleterious effects on the properties of the product and are therefore not entirely desirable in the final product.

3.3. Differences between emulsion polymerization and miniemulsion polymerization

Figure 1.4 demonstrates the difference between the processes of emulsion polymerization and miniemulsion polymerization.

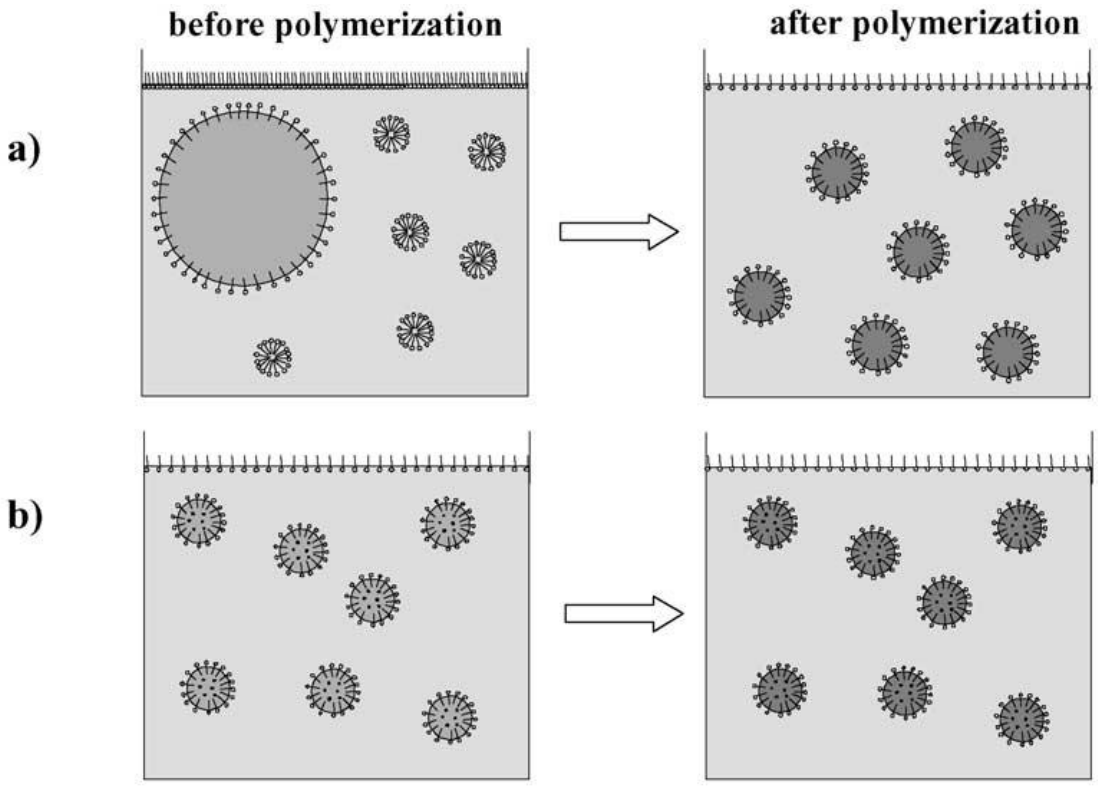

Figure 1.4 Comparison of different heterophase polymerization processes: (a) emulsion polymerization; (b) miniemulsion polymerization [104].

Below a threshold of surfactant amount, which also depends on temperature, monomer concentration and the properties of the emulsifier, no miniemulsion but kinetically stabilized emulsions are formed. Therefore, large monomer droplets (1-10 μm in diameter), which are stabilized by surfactant, and empty or monomer-swollen surfactant micelles coexist in the initial state. For polymerization, one starts from large monomer droplets and surfactant micelles in the water phase. The water soluble initiator forms oligo radicals from slightly water soluble monomer units. These oligo radicals then enter the micelles and start to form particles. During polymerization, monomer diffuses through the water phase to the micelles in order to sustain polymer particle growth. Particles with a diameter of usually more than 100 nm are formed. Due to the increase of the interfacial area, the surface tension of a latex increases with polymerization. In the literature, the term emulsion polymerization is used for this process [110]. The differences between emulsion polymerization and miniemulsion polymerizations are obvious. In emulsion polymerization, the latex particle does not

correspond to the primary emulsion droplet, and the size is established by kinetic processes where kinetic parameters, such as temperature or the amount of initiator, play a predominant role. These factors remain unseen in miniemulsion polymerization where the latexes are essentially a polymerized copy of the original droplets, the size of which is essentially given by dispersion process and droplet stability, but not by polymerization parameters.

4. PMMA and PLA

The properties of polymer blends depend not only on the chemical composition of the blend but also on the compatibility or miscibility of the components. However, most polymer blend systems are immiscible. The impact strength of a two-phase polymer system is generally influenced by several morphological parameters, such as the particle size, particle size distribution, particle volume fraction, particle configuration in the matrix and matrix ligament thickness (surface-to-surface interparticle distance). However, some of the morphological parameters are interrelated. Consequently, considering the PBA and PLA are immiscible; the blend of PBA/PLA could not achieve the desired toughening by solvent-cast mixing. The large amount of PBA in the PLA matrix improved the impact resistance of the blend but had the drawback of the diminution of its elastic modulus. Poly(methyl methacrylate) (PMMA) is used in various field of our daily life, i.e., in the building industries and medical aspects. Meanwhile, PMMA has been found partially miscible with PLA, and the presence of PMMA has improved the Young's modulus of blends PLA/PMMA [5] [14] [15] [33] [34] [111].

Avella et al. [14] had shown the use of PMMA as dispersed phase in blend with PLA. The blends are prepared in reactive (R-type blends) as well as non-reactive (NR-type blends) methodologies, according to the preparation of the blends either by polymerizing the acrylic monomer in the presence of PLA or by melt mixing the two polymers (PLA and PMMA) in bulk, respectively. It is interesting to note the influence of the addition of PMMA on the thermal property of PLA. DMTA analysis of pure PLA and PMMA/PLA blends indicates that T_g values of PLA in blends

increase from 67°C (in homo-PLA) to 76°C (in NR-type PLA/PMMA 70/30 mechanical blend). The increase of T_g of PLA is the indication of interactions between PLA and PMMA. Fracture surfaces of PLA and blends reveal the surface of the NR PLA/PMMA 70/30 blend is very homogeneous and distinct PMMA dispersed particles are not seen. Flexural and impact properties of blends have been analyzed and the Young's modulus were improved for PLA/PMMA blends. The explanation of the above can be found in the extensive reaction occurred at the interface of the blends.

5. PMMA and PBA

Core/shell polymerization is probably the most versatile and industrially important technique when looking at the synthesis of structured particles. Due to the distinct geometry of core/shell particles, numerous applications have evolved which include impact modifiers and toughening agents, gloss enhancers for paper coatings, polymeric nanocapsules for controlled and sustained drug delivery and encapsulation of volatile solvents or toxic substances. Core-shell nanoparticles comes to be used in a wide variety of polymer renforcement: they can evidently increase the polymer's wear ability, abrasion resistance, anti-water property, weather fastness, UV-resistance, tensile strength, impact strength and interfacial interaction, improve the transparency, decrease the minimum film-forming temperatures and improve the process ability [36] [37].

The performances of polymers formed by core-shell emulsion strongly depend on the morphology of the latex particles. The structure of latexes particles depends, e.g.,on the choice of the monomers or comonomers, the synthesis parameters such as temperature, type of initiator and surfactant, the crosslinking density, and other variables. The synthesis of core-shell latexes usually does not lead to an ideal core-shell morphology with a complete phase separation. In most cases, the resulting particle morphology cannot be described simply as a core/shell type. This is due to an interplay of thermodynamic as well as kinetic parameters during the polymerization process. Figure 1.5 displays possible substructures of such core-shell latexes with

different interfaces.

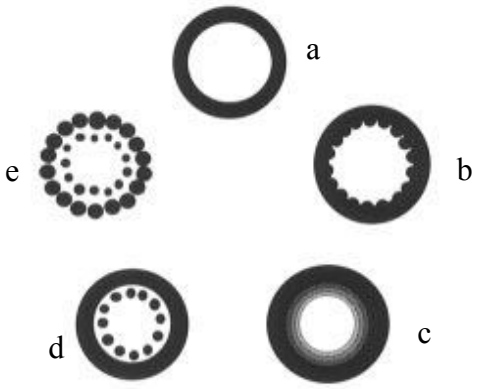

Figure 1.5 Morphologies deviating from the (a) ideal coreshell: (b) interface with a wavy structure; (c) interface with a gradient of both components; (d) interface with microdomains; (e) microdomains in the interface and an island structure as shell [36].

These interfaces consist of mixed phases which are composed of the core and the shell component. Depending on the compatibility of the two polymers and the reaction conditions, the components can be mixed on a molecular level in the interface where a continuous concentration gradient of microdomains can be formed [36, 38-41].

Core/shell particles can be prepared via various routes such as a two-stage seeded emulsion polymerization process, suspension crosslinking, coacervation, interfacial polymerization, solvent evaporation and vesicle polymerization and even combining mini- and microemulsion polymerization with the above mentioned techniques to create polymeric nanocontainers and nanocapsules.

The seeded emulsion polymerization gradually becomes the most widely-used way and the most common process to prepare core-shell polymer nanocomposite particles, because through it we can obtain composite particles with different morphologies and properties. This technique allows one to create particles in a well defined way regarding the resulting particle size. Using different monomer compositions at different stages in a seeded emulsion polymerization, it is possible to achieve complex particle morphologies by different phase distributions within a particle [45] [39]. With the increasing amount of second stage, a core-shell type is more favorable. The

coverage by second stage hard phase material is increased by increasing the amount of second stage materials, other reaction parameters kept constant.

The compatibility of the components used in particle synthesis also plays an important role. A disadvantage of incompatible polymers is often the weak bonding of one phase to another. This can lead to poor stress transfer across the interface resulting in inferior mechanical properties of the material. To increase the mechanical compatibility between the polymer phases, an improvement in the interfacial adhesion is required. This can be achieved by the addition of compatibilizing agents such as block or graft copolymers possessing segments that are miscible with those of the polymers being blended.

In most cases, we need to choose a monomer with lower hydrophilicity as the core monomer and a monomer with higher hydrophilicity as the shell monomer, so that well-defined core-shell structure particles will form. In the opposite case the core monomer or polymer with higher hydrophilicity will migrate to the water phase and form abnormal structure particles. Many researches proved that incompatible polymer chains moved from the position in which they were formed, and migrated toward the equilibrium morphology to minimize the free energy of the system. For example, if one choose butyl acrylate as the core monomer and styrene as the shell monomer, as the hydrophilicity of the former is obviously higher than that of the latter, the composition structure of core-shell particles prepared will be inverted after a year's storage, poly (butyl acrylate) (PBA) will gradually migrate to the outer part, while PS will migrate to the core part. The solubility parameters of PBA ($8.8[cal/cm^3]^{1/2}$) and PMMA ($9.25[cal/cm^3]^{1/2}$). The PMMA shell is more hydrophilic than PBA, a particle with core-shell structure is expected [36] [38] [40] [42].

Poly(butyl acrylate) / poly(methyl methacrylate) (PBA/PMMA) core-shell latexes are widely used in various industrial applications as impact modifiers as well as for applications requiring improved properties such as water resistance, tensile strength, spoil resistance, radiation resistance and adhesive strength. With the addition of a certain amount of core-shell particles to a PVC homopolymer increases the impact strength of the resulting product by a factor of 5 with respect to that of the

untoughened PVC. In the specific case of impact modifiers, the core needs to be made of highly elastics material such as poly(butyl acrylate) (PBA) to provide resistance to shock. It is generally accepted that strong interfacial adhesion is essential for the superior mechanical properties of toughened polymer alloys, whereas a fine PMMA shell enhances the compatibility with the matrix and the toughness of the material. The dynamic mechanical property improvements of an impact modifier directly depend on the properties of the rubbery core, the thickness of the PMMA shell (as thin as practical) and the particle size distribution of the latex (as well-defined as possible, and preferably no bigger than 200nm). However, the reason of existing optimum particle size has not been clearly explained. If the shell is too thick, a hard core (high modulus) of these core/shell particles results, and the rubbery nature required for an impact modifier is lost. On the other hand, when the shell is too thin, the shell layer is simply unable to fully protect and cover the inner rubbery core during powerful processing conditions [43] [44].

The rubbery core consisting of PBA was slightly cross-linked in order to maintain its shape and size during melt blending. The PBA core particles were first formed and sequentially grown to the desired size. To obtain the expected core-shell structure by seeded emulsion polymerization, the addition speed of MMA monomer should be slower than its polymerization rate (drop-wise to the reaction system to keep it in a starved condition). Monomer 2 (MMA) was added in a starved process and some new initiator was added at the same time. With the existence of the new initiator, the tertiary carbon of the PBA chain will be initiated to produce terminal free radicals, which is stabilized by the conjugated structure of the side group, as shown in scheme 1.4. In this way, grafting at the surface of the seed particles occurred. Therefore, core-shell blends are expected to have stronger interfacial adhesion than core/matrix blends, whereas the interfacial adhesion between PBA particles and matrix is only due to van der Waals attraction, and the core-shell particles have primary chemical bonding between the PBA core and the PMMA shell. Under starved condition, the product obtained showed a narrow size distribution (polydispersity index-PDI was small) and a well-defined core-shell structure. They deduced that the seed latex would

have enough time to capture monomer 2 only when the feed speed of monomer 2 is slow enough so that monomer 2 would enter the seed particle to form well-defined core-shell particles. If monomer 2 is added in a non-starved state, some monomer 2 would still enter the seed particles and polymerize at the surface of seed particles, while the others would absorb surfactant to form micelles, and finally polymerize to form homo-polymer, which leads to a broader sized distribution and the abnormal core-shell structure. It made no difference in final conversion and gel efficiency to increase the amount of the surfactant, but the size distribution broadened obviously. The surfactant formed empty micelles when increasing the amount of the surfactant and the large amount of empty micelles gave the opportunity of monomer 2 to enter the micelles, which led to the formation of homo-polymer particles with different size, so that the size distribution broadened evidently. In this system a stage ratio of 50/50 is required to achieve PBA core-PMMA shell particles. For the latexes with a shell content below 35%, the shell structure is still incomplete [38] [43] [45] [46].

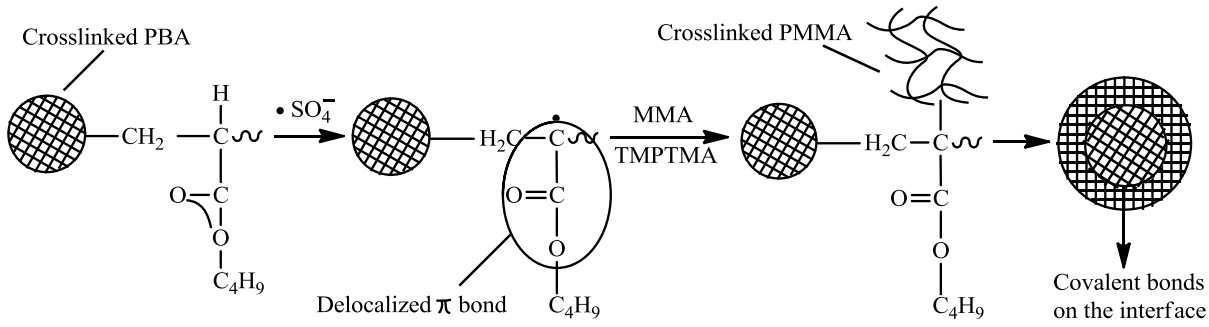

Scheme 1.4 Reaction mechanism of monomer 2 [38].

Wang et al. [23] had prepared core-shell structure complex poly(n-butyl acrylate) (PBA)/OMMT core and PS outer shell by radiation seed emulsion polymerization to reinforce PS matrix. Figure 1.6 shows the conception of the preparation of core (PBA/OMMT)–shell (PS) structured.

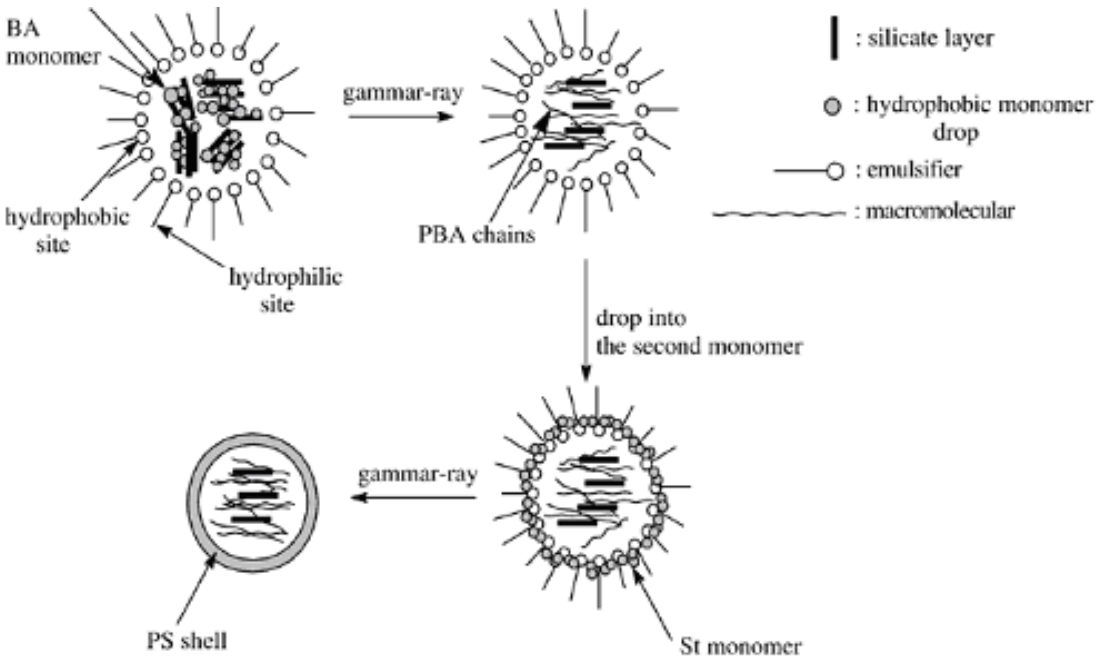

Figure 1.6 Schematic illustration of the preparation of core (PBA/OMMT)-shell (PS) structured complex via radiation seeded emulsion polymerization [23].

After Na-MMT was organophilic modified by CTAB, the surface of the silicate layers of MMT is hydrophobic. So the OMMT and the BA monomers mixed to form the latex. Some BA monomers can disperse into the galleries of the silicate layers of OMMT so that the OMMT was intercalated or delaminated by PBA via in situ radiation emulsion polymerization. Thus a common PBA/layered silicate nanocomposite was prepared. Since the polarity of PBA is different from that of PS, a PS shell was synthesized via radiation seeded emulsion polymerization to improve the miscibility of PBA/layered silicate nanocomposites with PS matrix.

When such a core-shell structured complex was blended with bulk PS matrix to obtain PS/layered silicate nanocomposite, combines the advantage of the strengthening of silicate layers and the toughening of elastomer in plastic matrix, the impact strength of blend was improved and the tensile strength of PS remains as well.

6. Conclusion

PBA has been used as a toughening agent for many plastic matrixes. Although it was mentioned that PBA could improve the toughness of PS, several researchers have

showed the blend of PBA/PLA did not have a superior mechanical property and the morphological analysis were reported to prove this blend is not miscible. It is expected that addition of PBA could increase the impact strength with little sacrificing of the modulus and tensile strength. To achieve the goal of reinforcement for impact resistance of PLA by PBA particles, the immiscibility of these two polymers should be solved. And the compatibility of PBA and PLA might be improved by introducing some compatibilizers. On the other hand, rigid clay particle is also a very popular choice to reinforce polymer in many reports. Meanwhile, the combination of clay particles with elastomer at the same time to improve the performance of polymer complex has not been researched widely. In our study, the preparation methods of PBA composite nanoparticles, the parameters of miniemulsion polymerization, the miscibility and the mechanical or thermal properties of the PLA/PBA blends have been investigated. The influence of the addition of clay and compatibilizer for the properties of the PLA/PBA blends has also been studied.

Chapter 2. Instruments and experimental techniques

1. Materials used

1.1. Monomers

The monomer used in the preparation of toughening agents by miniemulsion polymerization or emulsion polymerization are listed in the Table 2.1.

Table 2.1 Monomers used in the synthesis of latexes.

	Butyl acrylate	***Methyl methacrylate***
Abbreviation	BA	MMA
Formula	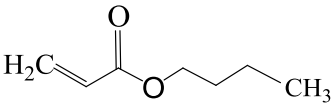	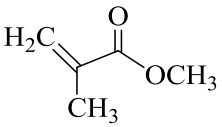
Molecular weight (g/mol)	128.17	100.12
Purity	≥99%	≥99%
Volumic mass (g/ml)	0.894	0.936
Boiling point °C	145	100
Refractive index of polymer	1.474	1.49
Glass transition temperature (T_g) of polymer °C	-55	105
Supplier	Aldrich (France)	Fluka (France)

1.2. Surfactants

The anionic surfactant SDS, non-ionic surfactants Brij 78 and Brij 700, and polymer surfactant poly (ethylene glycol) methyl ether methacrylate (PEGMEM) were tested in our study. The appropriate addition of surfactants in the miniemulsion polymerization is desirable to obtain final product with narrow size distribution. All the surfactants were purchased from Aldrich in France.

Table 2.2 Surfactants employed for the synthesis of latexes with narrow particle distribution.

Name	*Formula*	*Purity*	*Description*
Sodium dodecyl sulfate (SDS)	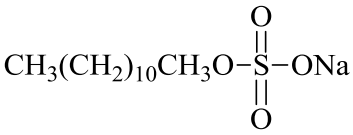	≥98.5%	Anionic Surfactant
Brij 700®	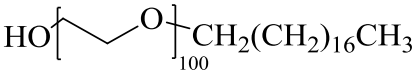	≤1% water	Non-ionic Surfactant
Brij 78®	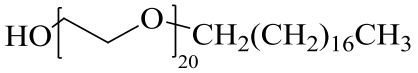	100%	Non-ionic Surfactant
Poly (ethylene glycol) methyl ether methacrylate (PEGMEM)	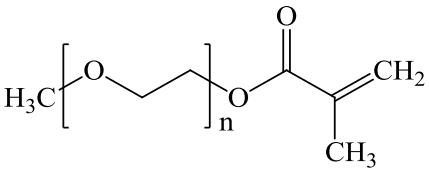 Average Mn ~950	100 ppm MEHQ and 300 ppm BHT as inhibitor	Polymer surfactant

1.3. Initiators, buffers and inhibitor

Two kinds of initiators, water soluble potassium persulfate (KPS) and oil soluble 2,2'-azobis (2-methylbutyronitrile) (AMBN) were used in the polymerizations. The variation of pH existed in the reactions which was caused by the decompositions of KPS. The buffering agents ($NaHCO_3/Na_2CO_3$) were needed to preserve the stability of the latexes. After the polymerization, the reaction was stopped by the addtion of hydroquinone.

Table 2.3 The initiators used for the polymerizations and the buffering agents.

Name	*Formula*	*Purity*	*Molecular weight*	*Supplier*
2,2'-Azobis (2-methylbutyronitrile) (AMBN)	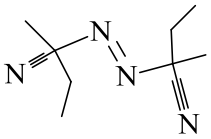	≥98%	192.26	Fluka
Potassium persulfate (KPS)	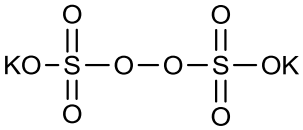	≥99%	270.32	Aldrich
Sodium bicarbonate (NaHCO3)	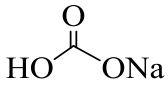	≥99%	84.01	Fluka
Sodium carbonate (Na2CO3)	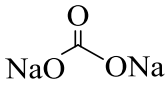	≥99%	105.99	Aldrich
Hydroquinone	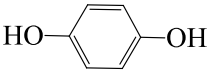	≥99%	110.11	Aldrich

1.4. Co-stabilizers

Co-stabilizers were added in the miniemulsion polymerization to retard the miniemulsion degradation by preventing molecular diffusion and improve the stability of miniemulsion by against droplet coagulation. Three kinds of co-stabilizers were used in our studies which were hexadecane (HD), dodecane and n-Decane.

Table 2.4 Co-stabilizers used for improve the stability of miniemulsion.

Name	*Linear Formula*	*Molecular weight*	*Purity*
Hexadecane (HD)	$CH_3(CH_2)_{14}CH_3$	226.44	anhydrous, ≥99%
Dodecane	$CH_3(CH_2)_{10}CH_3$	170.33	≥99%
N-Decane	$CH_3(CH_2)_8CH_3$	142.28	≥99%

1.5. Clays

Sodium montmorillonite (MMT) , OMMT-Cloisite® 20A and Laponite RD were all bought from Southern Clay Products, inc. Rockwood additives limited.

MMT is reported to have an approximate aspect ratio of 250:1, and is a 2:1 tetrahedral/octahedral aluminum silicate smectite mineral with an idealized chemical formula of $Na_{0.33}[Mg_{0.33}Al_{11.67}Si_4O_{10}](OH)_2$ and a cation exchange capacity of 0.95 mequiv/g. Cloisite® 20A is a natural montmorillonite modified with a quaternary

ammonium salt. Its organic modifier is dimethyldioctadecylammonium chloride. The moisture of Cloisite® 20A is <2% and it's density is 1770 kg/m^3.

Laponite RD is a synthetic trioctahedric hectorite clay, a charge deficiency of 0.7 per unit cell. It is composed of two tetrahedral silica sheets and a central octahedral magnesia sheet. It contains 59.5% SiO_2, 27.5% MgO, 0.8% Li_2O, and 2.8% Na_2O. It has a specific surface area of 370 m^2/g. A cationic exchange capacity (CEC) of 7.3x10^{-4}mol/g. Its chemical formula can be expressed as $Na^{+0.7}[(Si_8Mg_{5.5}Li_{0.3})O_{20}(OH)_4]^{-0.7}$ with a cation exchange capacity of 0.95 mequiv/g and it has a density of 2570 kg/m^3. The disks have an overall negative charge with the rim being amphoteric. These layers are stacked together by weak ionic and van der Waals forces. In water Laponite RD can be dispersed as individual disk-shaped colloids with a lateral diameter of ca. 25-35 nm and ~1 nm in thickness and form stable colloidal systems (informations which were listed in supplier's website and comfirmed by our in house lab analyses). The moisture of LRD is ≤2%.

1.6. Modified agents

Three types of silanes purchased from ABCR (Germany) have been introduced to modify the clay as coupling agent in the study. All three kinds of silanes are in the form of liquid.

Table 2.5 The modified agents for clay.

Name	*Formula*	*Purity*	*Density*
3-Methacryloxypropyltrimethoxysilane (MPTMS)	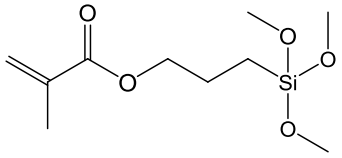	>98%	1.045
3-Aminopropyltriethoxy silane (3A)	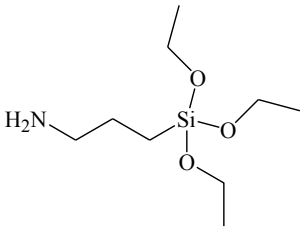	>98%	0.943
(3-Glycidoxypropyl)trimethoxy silane (3G)	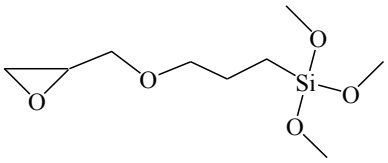	>98%	1.07

1.7. Cationic surfactants

Three kinds of cationic surfactants were added in the miniemulsion polymerization with Laponite in order to facilitate the dispersion of Laponite into monomer. The cationic surfactants were supplied by Aldrich are white powder.

Table 2.6 Cationic surfactants added in the miniemulsion polymerization with Laponite.

Name	*Formula*	*Molecular Weight*	*Purity*
Hexadecyltrimethylammonium bromide (CTAB)	$H_3C(H_2C)_{15}-\overset{\overset{CH_3}{\vert}}{\underset{\underset{CH_3}{\vert}}{N^+}}-CH_3\ \ Br^-$	364.45	≥99%
Octadecyltrimethylammonium bromide (OTAB)	$H_3C(H_2C)_{15}CH_2-\overset{\overset{CH_3}{\vert}}{\underset{\underset{CH_3}{\vert}}{N^+}}-CH_3\ \ Br^-$	392.50	≥98%
Dimethyldioctadecylammonium chloride (DDAC)	$H_3C-\overset{\overset{CH_2(CH_2)_{16}CH_3}{\vert}}{\underset{\underset{CH_2(CH_2)_{16}CH_3}{\vert}}{N^+}}-CH_3\ \ Cl^-$	586.5	≥97%

1.8. Solvents

Toluene was used as solvent for preparation of Laponite modification. 2-Butanol was the solvent for pre-treating SEM samples in order to dissolve PBA. They are both supplied by Aldrich.

Table 2.7 Principle physical and chimical caracteristics for the used solvents.

Material	*Formula*	*Purity*	*Molecular Weight*	*Density at 25°C (g/L)*	*Boiling point °C*
Toluene	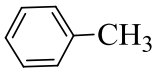	≥99.8%	92.14	0.808	110.6
2-Butanol	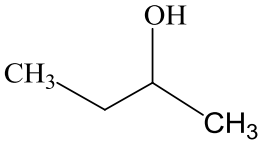	≥99.5%	74.12	0.865	98

1.9. PLA

The poly (lactic acid) denoted as PLA was provided by Natureplast under the trade name of PLE 005. It contains 95% of L-isomer and 5% of D-isomer. The physical properties of PLA (provided by the supplier) are summarized in Table 2.8.

Table 2.8 Physical properties of PLA

Physical properties		**ASTM**
Density	1.25	D-792
Melt Index, g/10 mn (190°C/2.16 K)	2~5	D-1238
Optical properties	Transparent	
Melting temperature (°C)	145-155	
Glass transition temperature (°C)	55-60	

Mechanical properties		**ASTM**
Tensile elastic limit, MPa	55-58	D-882
Tensile modulus, GPa	1.9-2.1	D-882
Tensile strain, %	5-6	D-882
Impact resistance, J/m	2-2.9	D-256

Polylactides are soluble in dioxane, acetonitrile, chloroform, methylene chloride, 1,1,2-trichloroethane and dichloroacetic acid. Ethyl benzene, toluene, acetone and tetrahydrofuran only partly dissolve polylactides when cold, though they are readily

soluble in these solvents when heated to boiling temperatures. Crystalline poly(L-lactide) is not soluble in acetone, ethyl acetate or tetrahydrofuran. All polylactides are insoluble in water, some alcohols and alkanes. Solubility parameters were measured and reported to be around 10.3 $cal^{1/2}/cm^{1.5}$ for amorphous poly(D, L-lactide).

2. Miniemulsion or emulsion polymerization

Reactor and system of mixing

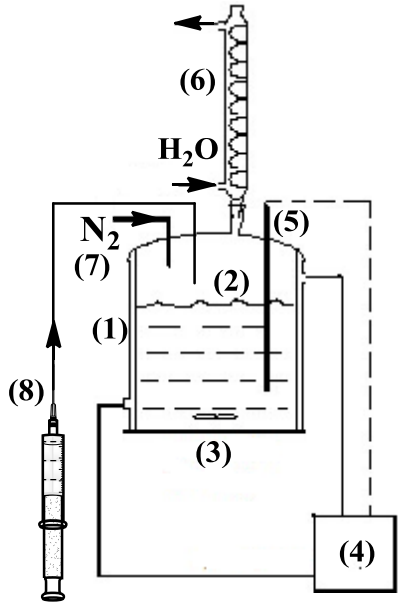

(1) 250 ml jacketed reactor
(2) pre-emulsion
(3) magnetic stirrer
(4) thermostat
(5) temperature sensor
(6) condenser
(7) nitrogen sparge
(8)syringe for feeding of second monomer

Figure 2.1 System schematic of reactor using for miniemulsion and emulsion polymerization.

Figure 2.1 shows a schematic description for the reactor which was used in our study. The temperature of the reactor was controlled by a thermostat. The part of syringe was not used for miniemulsion polymerization and only used for the feeding of the second monomer when preparing the core-shell particle by the emulsion polymerization.

The homogenization was conducted by ultrasonification on a sonicator (Hielscher) with pre-emulsion being cooled by an ice bath, with 0.5s of cycle time, 70% of amplitude.

3. Machines for the blends of latex and PLA

3.1. Microcompounder

The preparation of mixtures of PLA and elastomer or mixtures of PLA and clay were made of a plastic microcompounder (DSM Xplore) (Figure 2.2). It consists of a chamber in which there are two corotating conical screws. The useful volume can be set at 5, 10 or 15 ml. The introduction of polymeric materials is by means of a piston guide. A recirculation channel, placed at the output profile, allows reducing continuously the mixture in the screw head. Emptying the contents of the mixing chamber is initiated by a valve which prevents access to the recirculation channel and directs flow to an outlet channel. After leaving the mixture, it can be shaped (films, fibers and specimens) from other equipment attached (mini-injection molding, calendering, thus stretching films). Figure 2.2 shows a picture of microcompounder and a cross-section of the mixing chamber. The particles were added by piston, then mixed and pushed by the twin screws. The mixing was recirculated by going through the recirculation channel. After mixing for several minutes, the mixture came out from the outlet channel by opening the valve.

The blends were prepared with the microcompounder-DSM Xplore with a twin screw at a rotation speed of 60 rpm at 180°C for 10 min.

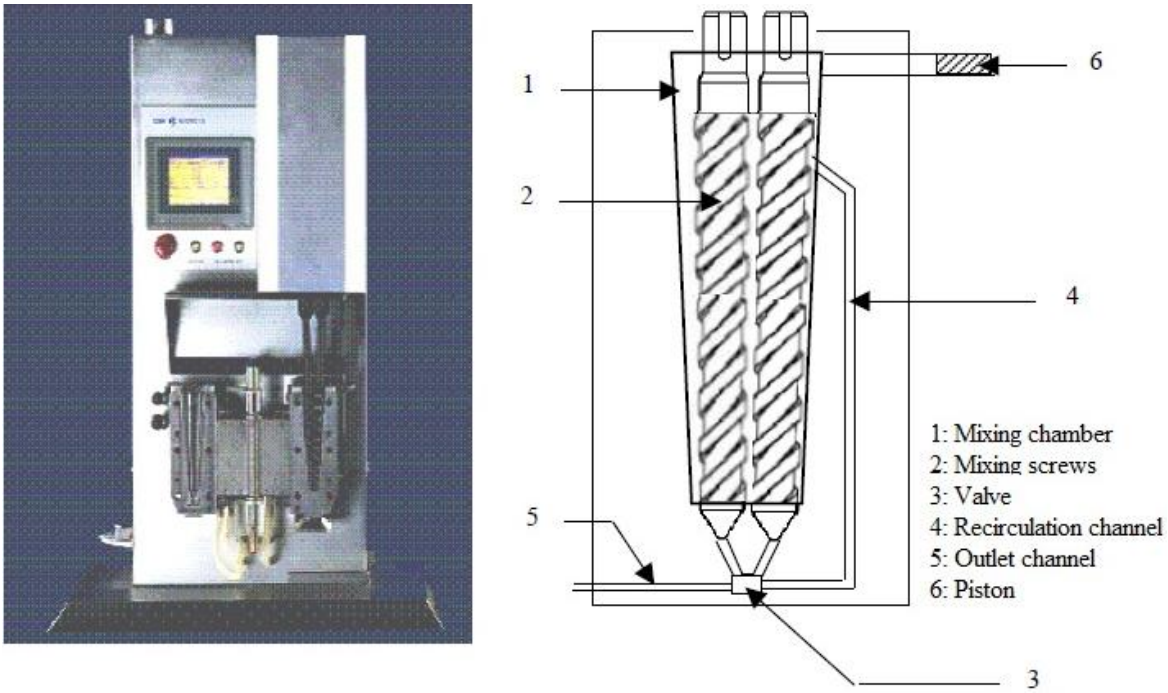

Figure 2.2 Microcompounder DSM Xplore and its mixing chamber.

3.2. Injection molding

The mini-injection molding DSM (Figure 2.3) is dedicated to the injection of small amounts of polymers. It allows accelerating the development of new polymers to achieve quickly specimens. The polymer in the hot state is pushed into a mold where it is cooled to the desired shape. The sleeve of the injection molding machine can be fed directly from the microcompounder DSM to inject specimens from molten polymer.

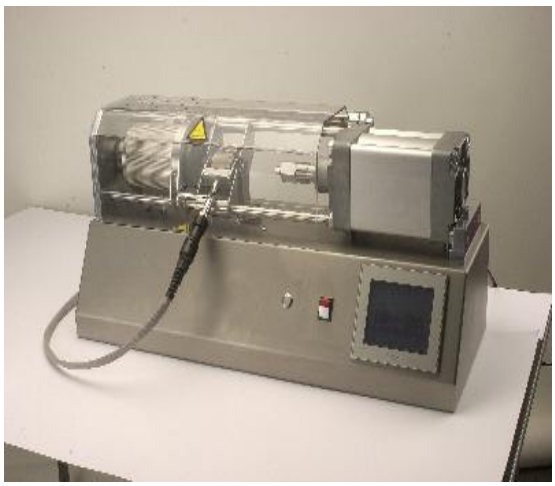

Figure 2.3 Mini-injection molding

Principle of operation: after opening the valve on the die, the molten polymer exited continuously from microcompounder and filled a cylinder thermostat with a piston. This cylinder filled with material was then placed on a metal support in the mini-injection molding machine. A piston with compressed-air pushed the molten polymer into the mold to form a thermostated specimen. It was possible to set the pressure and the injection time, but also the temperature and the duration of maintaining the material in the mold. Thus, a complete injection cycle could be set. The pressure used in this work is 6 bar and a holding time of 10 seconds to well prepare the specimens. The cylinder temperature thermostat was set to the same temperature as that of the microcompounder. The mold temperature was 55 °C for mixtures of PLA-clay and 50 °C for the PLA/elastomer-clay.

4. Characterization of the latex, clay-modified and the blends

4.1. Solid content by gravimetry technique

Principle and utilization

Gravimetry determines the overall conversion by measuring the solids content of the sample taken from the reactor. This dry extract ES is defined by the ratio between the mass of the dried residual solids content and the gross mass of the sample started.

The equipment used to perform this measurement is a thermobalance HG53 Halogen Moisture Analyzer. About 1 g of latex is placed on an aluminum dish. Evaporation of the volatile species is carried out at 175 ° C. The weighing is carried out continuously during the drying of the sample and, when the decrease in weight per unit time is less than a criterion fixed in advance, drying will stops automatically and the residual solids content is listed in the screen of the device.

The solids will then be used to determine the conversion X.

$$X = \frac{M_{total} \times ES - m_{sol}}{m_{mono}} \quad \textbf{(2.1)}$$

Where M_{total} = the total quantity of the sample at time t;

m_{sol} = the quantity of the various solid residues (initiator, surfactants, co-stabilizer ...);

m_{mono} = the quantity of monomer;

ES = the ratio between the quantity of the dried residual solids content and the total quantity of the sample started;

X = the conversion of monomer to polymer.

4.2. Malvern mastersizer 2000

Measure the size of the latex by Mastersizer

The size of particles obtained by the miniemulsions or emulsion polymerization was measured directly by using the light diffraction with a Mastersizer 2000 from Malvern Instruments. This device is responsive to the volume of the particles and can determine the size distribution of particles between 0.02 microns to 2000 microns. The calculation method of the device is based on the outcome of Mie theory equations of electromagnetism of Maxwell. Mie theory provides how-Helium Neon laser light (electromagnetic wave) will be diffracted or scattered by the spherical particle and takes into account the way light passes through the particle or is absorbed by the particle. The laser light is not only diffracted or scattered but it is also reflected or refracted and absorbed by the particle (see Figure 2.4).

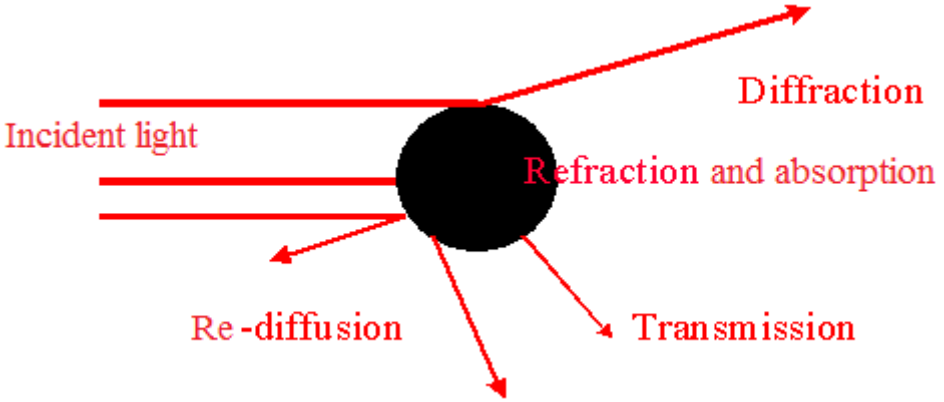

Figure 2.4 Interaction of laser light with a particle (source: Malvern Instrument).

It was assumed that in our case the particles do not absorb light. This theory also takes into account the shape of the particle, which introduces a form factor P (θ). The form

factor can interpret the direction in which light is scattered or diffracted. Diffraction by the particles due to rapid fluctuations of the diffracted light intensity around a mean value, because of the imposed stirring, and which for a given angle θ. The laser beam passing through the cell filled with water which circulates the sample will spread without deflection until it encounters a particle whose refractive index is different from the index of the medium. And to make the measurements of size of particles that we obtained, it is necessary to know the refractive indices of the particles and that of the dispersion medium in which the analysis is performed in order to estimate the size correctly. The angle at which the light is deflected by a droplet is inversely proportional to the size of the droplets. The amount of light I (θ) is proportional to the particle size, in our case: large particles scatter large amounts of light at small angles while smaller particles scatter very small amounts of light at large angles (see Figure 2.5).

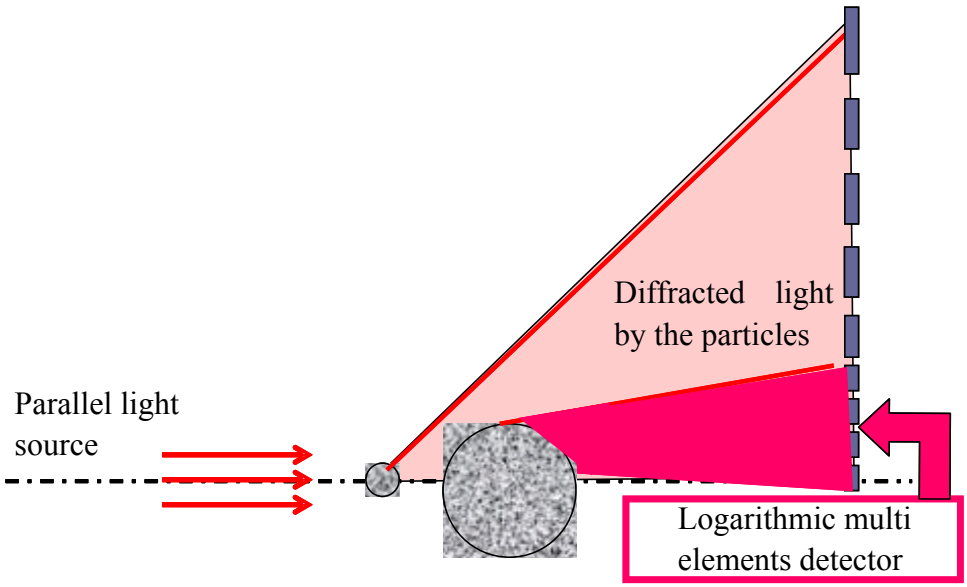

Figure 2.5 Principle of light scattering by particles with different sizes. (Source: Malvern Instrument)

Procedure

The analysis of the diameter of the latexes is carried out as follows:

A few drops of latexes were introduced into the dispersing unit containing a solution of NaCl in Milli-Q water at a concentration of 10^{-3} mol / L. The mixture was stirred at

a speed of 1300 rpm to dilute the emulsion at room temperature and to allow the passage of the liquid in the optical cell. Each sample was analyzed at least three times and the data were presented in the form of a distribution curve or number.

We could express the average diameter of the particles as a function of the volume fraction of dispersed hexadecane by the Sauter diameter or surface diameter $D_{[3,2]}$ and the volume diameter $D_{[4,3]}$. The Sauter diameter is the diameter which a spherical particle from an isometric sample whose surface identical to that of covered by the sample would have. It is defined as follows:

$$D_{[3,2]} = \frac{\sum_{i}^{n} n_i \, d_i^3}{\sum_{i}^{n} n_i \, d_i^2} \ (\mu m) \qquad \textbf{(2.2)}$$

The volume average diameter is the diameter which a spherical particle from an isometric sample whose volume identical to the volume occupied by the particles would have. It is defined as follows:

$$D_{[4,3]} = \frac{\sum_{i}^{n} n_i \, d_i^4}{\sum_{i}^{n} n_i \, d_i^3} \ (\mu m) \qquad \textbf{(2.3)}$$

where n_i *is* the number of particles of diameter d_i.

4.3. Fourier transform infrared spectroscopy (FTIR)

Infrared spectra were recorded by transmission from the pellets of the samples which were prepared by using a hydraulic press and KBr powder, with a Bruker Tensor 27 with 64 scans between 600cm^{-1} and 4000cm^{-1}. The treatment of the spectra is made with the software OPUS 4.0.

4.4. Thermogravimetric analysis (TGA)

The thermogravimetric analysis-TGA can track the degradation of a product according to the variation of temperature in a given atmosphere. The TGA is to measure the mass loss of a sample over time when the sample is subjected to a

defined program of changed temperature. A nacelle containing the sample is placed in an oven that can be maintained under vacuum or be swept away by a carrier gas and control the total flow rate. From the measurements of weight of the sample at each instant the thermograms are plotted:

$$\frac{m}{m_0} = f(T) \tag{2.4}$$

where m is the weight of the sample at time t

m_0 is the initial weight of the sample

T(°C) is the temperature at time t

The general appearance of such a thermogram is shown schematically in Figure 2.6. Before the start of the degradation, the weight of the sample is constant. After that, when the product beginning to degrade, the weight of sample decreases slowly or quickly. Finally, it stabilizes around a value when no further mass loss of the product can be tested.

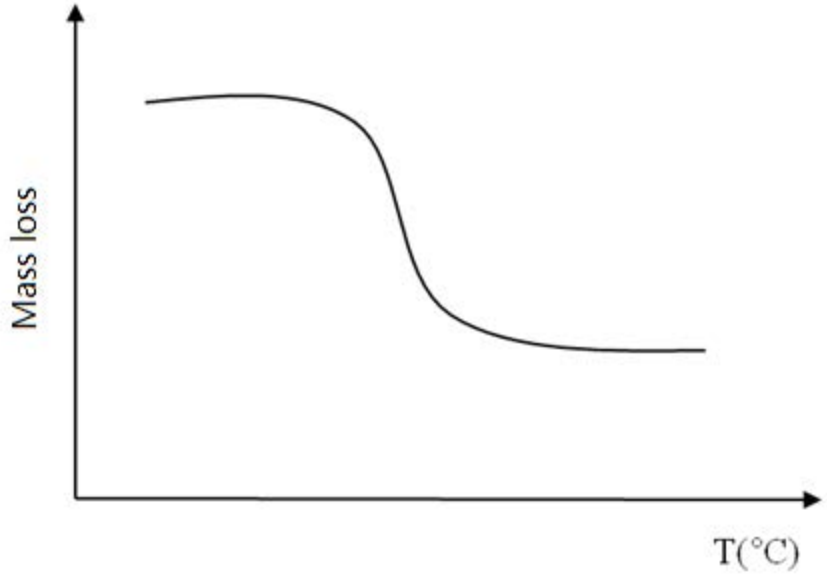

Figure 2.6 General appearance of a thermogram TGA

4.5. Differential scanning calorimetry analysis (DSC)

The thermal transitions of the thermoplastic PLA and those of mixtures elastomer and PLA are detected by using DSC. The principle of DSC is based on the measurement

of the difference between the thermal energy supplied by the sample and that of from a vacuum capsule (reference) when the sample are holding in a capsule also and it keeps in the same temperature with the reference capsule. This difference in behavior induced by the thermal properties of the sample, can determine the melting temperature (T_m), glass transition temperature (T_g) and crystallization (T_c), and enthalpy of fusion (ΔH_f) and crystallization (ΔH_{cr}) of the compound. The apparatus used in this work is a differential scanning calorimeter (DSC Pyris1, Perkin Elmer).

A sample ~10mg in an aluminum pan was heated from -80 to 250 °C at a heating rate of 5 °C/min (the first heating scan). The melting temperature was taken as the peak top of the DSC endotherm. The samples were melted in the DSC apparatus at 150 °C for 2 min, quenched to -80°C with liquid nitrogen, and then reheated up to 250 °C at a heating rate of 5 °C/min (the second heating scan). The glass-transition temperature was taken as the inflection point in the jump of the heat capacity in the second heating scan as the summit of the peak of the differentiated DSC curve.

4.6. Dynamic mechanical thermal analysis (DMTA)

Polymeric materials have a viscoelastic behavior over a wide temperature range. It means that their response to a mechanical stress is intermediate between a perfect elastic solid or perfect viscous solid. The Dynamic Mechanical Thermal Analysis (DMTA) of a polymer intended to determine the elastic and viscous components of the material when it subjected to a sinusoidal strain at a given frequency and temperature.

Principe of the method: Principle of the method: The samples are subjected to a sinusoidal stress (σ^*) of low amplitude. The resulting strain (ε^*) is also sinusoidal but has a phase shift (δ) with the constraint. The phase shift δ, between stress and strain, characterized precisely the importance of the viscous character of the material. Its value lies between 0 and $\pi/2$: For a pure elastic material $\delta = 0$, and when the material is perfectly viscous $\delta = \pi/2$.

Following Hooke's law, we can write:

$$\sigma^* = E^* \varepsilon^* \quad \textbf{(2.5)}$$

where E^* is complex elastic modulus (By convention : $E^* = E' + iE''$)

The storage modulus E' characterizes the fraction of energy stored as elastic and therefore refundable. In contrast, the loss modulus E'' characterizes the energy dissipated by internal friction due to the viscous component of the material.

The occurrence of molecular mobility in the material (depending on the frequency of stress and the temperature) occurs by a process of absorption qualified mechanical relaxation. Storage of energy is accompanied by an increase of the phase shift δ between stress and strain.

$$\tan\delta = E''/E' \quad \textbf{(2.6)}$$

Two major types of mechanical relaxations related to the intrinsic structure of macromolecular chains are mainly highlighted in polymer materials:

- The secondary relaxation termed sub-vitreous corresponding to simple movements and localized segments of the macromolecular chains.
- The main relaxation associated with the glass transition of the polymer and the movements involving long segments of the macromolecular chains. When the polymer is semi-crystalline, the transition is followed by another relaxation which corresponds to the fusion of segments.

Equipment: The analysis is performed with the device DMTA V 902-50010 from Rheometric Scientific. This device is connected to a computer with a software Orchestrator. It works well at low and high temperature.

Sample preparation and method: Sample preparation and method: rectangular samples with 20 mm long, 13 mm wide and 2 mm thick were made using a manual hydraulic press. The test conditions are as follows:

DMTA tests were taken in the three point bending mode. The dynamic loss was determined at a frequency of 10 Hz and a heating rate of 2°C/min as a function of temperature from -90°C to 210°C, the constant strain is 0.1%.

4.7. Nuclear magnetic resonance (NMR)

To determine the chemical structure of the core-shell latexes, analysis of nuclear magnetic resonance were performed on the PBA/PMMA latexes. NMR is a spectroscopic method that allows a structural analysis and a quantitative analysis of molecules.

Like all the spectroscopic methods, NMR based on the transitions between different energy levels. To induce these transitions, a magnetic field $\vec{B}$ is applied, associated with an electromagnetic wave of frequency ν. This field is perpendicular to an external field $\vec{B}_0$ fixed. When the frequency of the field $\vec{B}_0$ is that it allows the transition between two energy levels, resonance occurs, which causes the reversal of the nuclear spin. After being excited, the nuclei relax and return to their original spin state. For the resonance, there is a continual phenomenon of excitation and relaxation. The spin flip induces an electric current which is measured by the apparatus. The resulting graph shows the current as a function of the chemical shift which is proportional to the frequency of excitation (ν). Different frequencies where resonances occur are characteristic of the type of resonant atom (hydrogen, carbon ...) in a given environment. The multiplicity of a peak is also characteristic of the environment of the atom considered. The peak integration, in turn, provides information on the amount of resonant atoms which are analyzed.

NMR spectra were recorded on a Bruker Avance 300 spectrometer equipped at 300 MHz using deuterated chloroform ($CDCl_3$) as a solvent. The spectra were then processed by the software XWINNMR 3.0.

4.8. Microscopy

4.8.1. Scanning electron microscopy (SEM)

The scanning electron microscopy to visualize the surface of the polymer blends and to assess the distribution of the incorporated particles and their sizes. The image of the sample is formed by the secondary electrons (low energy electrons) generated by the

interaction of the superficial layer of the sample with the electrons emitted by a tungsten filament of the device.

Equipment and procedure: The samples are placed on pads with double faced adhesive tape. Before the observation of the surface of the samples, all the samples were covered with a thin layer of gold in advance. Firstly, the vacuum is performed on the samples for 5 minutes. Then, they are sputtered by the gold (the voltage of 1.2 kV and the current of 5 mA for 5 min).

The scanning electron microscope comprises a vacuum chamber, an optical column of a set of sensors and a sample holder device. The microscope used is a model JEOL 6490LV. Once the pads are placed in the SEM, the vacuum is created. During the experiment, the acceleration voltage of electrons is 8kV.

Sample preparation: To perform analysis which reflects the morphology of the mixture produced veritably, it is necessary to note that during its preparation, the surface of sample has not been subjected stress that may cause a change in morphology. This is why the freeze-fracture technique is widely used when the samples are prepared for analysis by scanning electron microscopy (SEM).

The material coming from the outlet channel of microcompounder was in form of a cylinder with a diameter of 2 to 3 mm. The cylinder was immersed in liquid nitrogen for a few minutes, and then a sharp blow was applied to fracture it in two pieces. The surface for analysis was created. The freeze-fracture was necessary because the PLA and elastomer mixtures might have a glass transition temperature (T_g) near to room temperature. The liquid nitrogen cooled the sample from surface to the heart, making the temperature of sample to be enough low and so that the glass state was obtained. Meanwhile, morphology was not affected by the freeze-fracture.

Extraction of the dispersed phase PBA: Extraction of PBA: the sample was stirred for 24 h in 2-Butanol and washed with 2-Butanol to remove surface deposits. After the extraction, the samples were washed by deionized water and dried by a vacuum oven for 12 h at 60°C.

4.8.2. Transmission electron microscopy (TEM)

The cross-sectional morphology of latexes was observed by transmission electron microscopy (TEM) of type Philips CM20 at an acceleration voltage of 200 KV. The analysis was carried out in the Service Commun de Microscopies Electroniques et de Microanalyses X (ECMEM) à la faculté des sciences de Nancy with the help from MR. J. Ghanbaja.

Sample preparation: The latexes prepared by miniemulsion polymerization or emulsion polymerization were centrifigated to get rid of precipitation and diluted 20 times before the TEM. The pre-prepared dye solution (uranyl acetate) to 2% was put in ultrasound device and turned on the sonication for 2 min. Place 10 µL of the sample on the carbon grid. After 2 min, added a little of the dye solution on the sample grid and waited the staining for 30 seconds. Removed the left dye solution on the grid by filter paper and leave the grid with stained sample drying in air for 5 min.

4.9. Mechanical properties

4.9.1. Tensile properties

It is a standard test for all polymers, which determines the stress-strain behavior in a given direction. The usual features that we deduce are the Young's modulus, the stress and elongation.

Equipment: Tensile properties of the blend sample were investigated by tensile testing machine universal hydraulic MTS 810. The device is a variation of the tensile testing system developed by Vidéo Traction TM Gsell et al. [112]. The test specimens used have a thickness of 4 mm, a width of 6 mm and 30 mm in length as shown in Figure 2.7. The evolution of seven spots carried by the specimen is monitored in real time by a camera (Figure 2.8a). A data processing system treats the data. The image analysis software identifies spots by the coordinates of their centroids. The variation of distance between the spots can give useful information to calculate the real deformations. Volumetric strain is obtained by summing the strains in the three

directions. The crosshead speed was 10 mm/min, at 25°C. Five specimens were tested for each set of samples, and the mean value and the standard deviation were calculated.

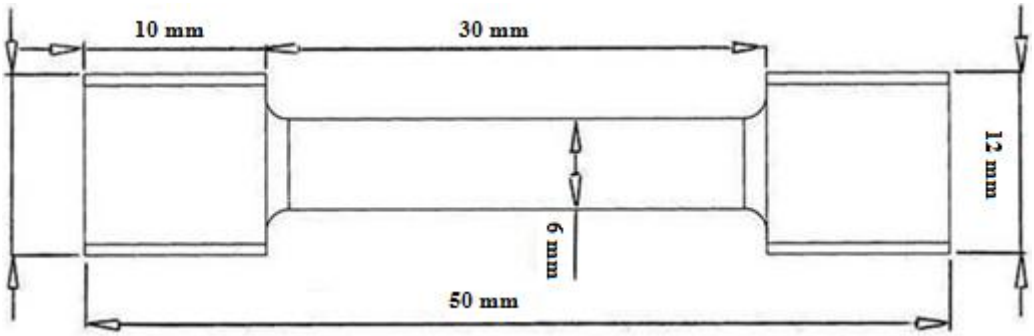

Figure 2.7 Dimensions of the specimens used.

A programmable function generator is used to control the testing machine to maintain the constant strain rate during the test. The device is shown schematically in Figure 2.8 (b). The software is capable of handling more than 50 frames per second with an accuracy of about 10^{-3} on the variation of volume.

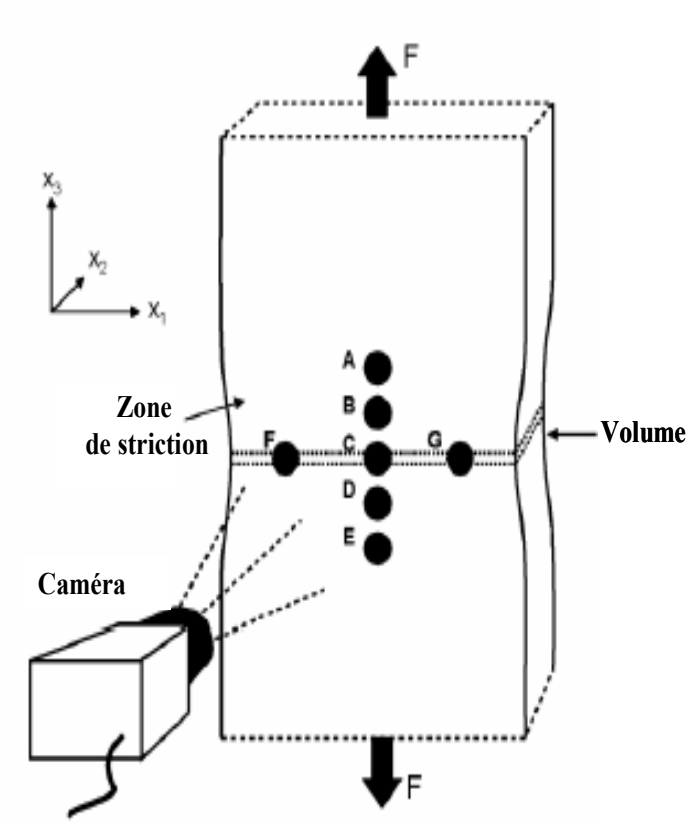

(a)

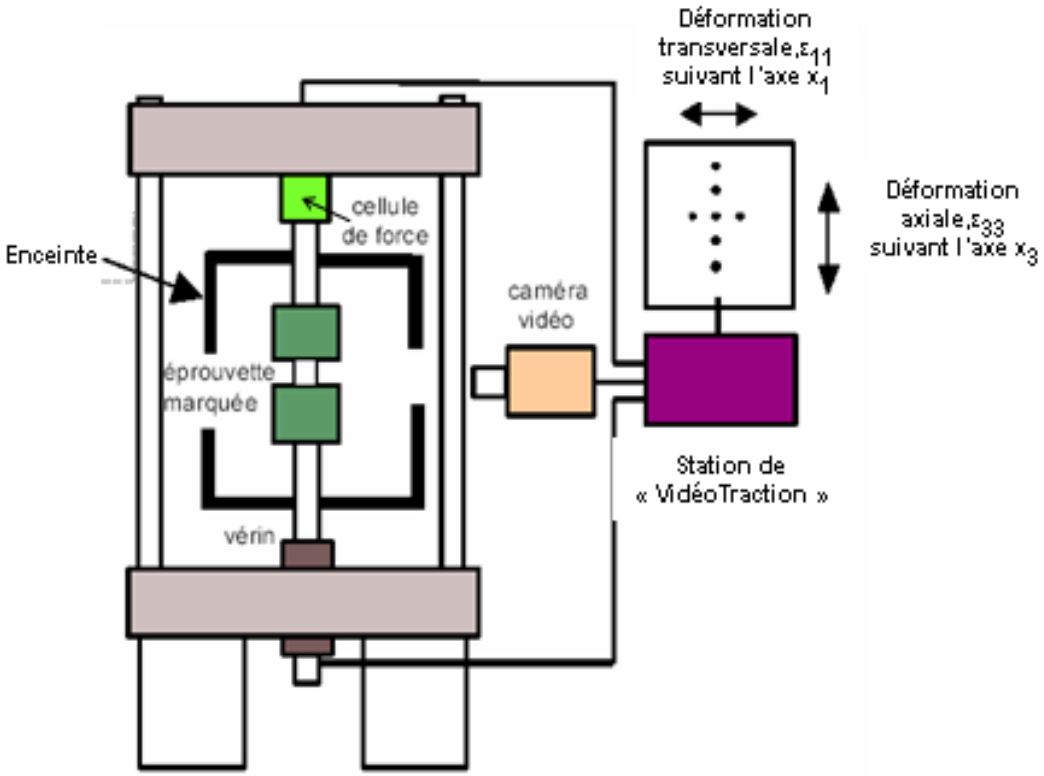

(b)

Figure 2.8 a) Tensile test samples with seven spots marked; b) Experimental device.

Sample preparation and method: The samples are obtained by injection with the injection molding of DSM. The surfaces of the samples were treated by polish and milling in the middle part is made in order to locate the center of the sample exactly and avoid the risk of the formation of macroscopic shear bands during the traction.

Seven fluorescent spots are applied to the larger face of the specimen. Five of these spots are aligned in the axial direction of the test piece x_3, the other two being aligned with the precedent central spot in the transverse direction x_1. Figure 2.9 demonstrates after the test, the rupture sample still locked by the machine.

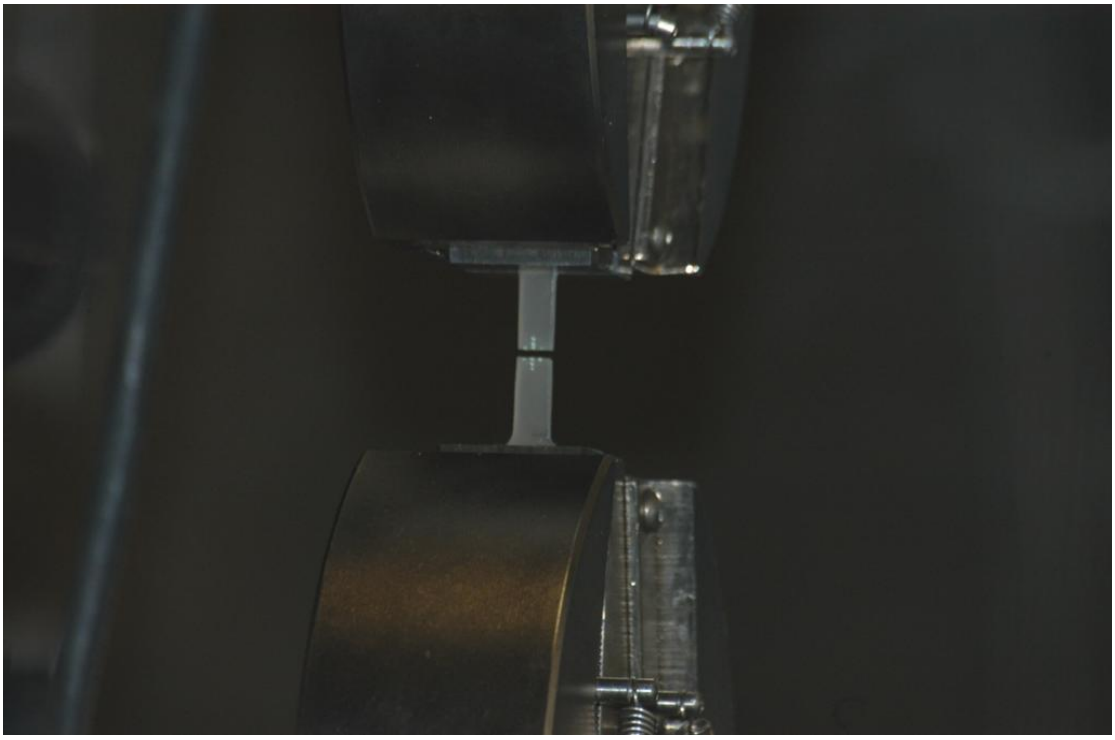

Figure 2.9 A photo of tensile test sample after rupture.

Principe of the method: Figure 2.10 (a) and (b) shows a series of images from a mechanical tensile test, and the curve which the evolution of force versus time.

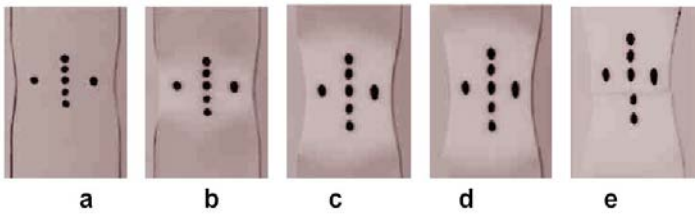

(a)

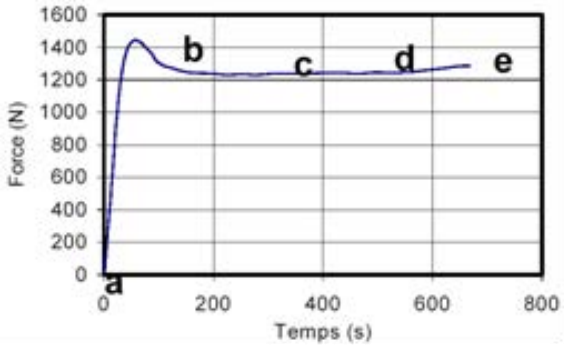

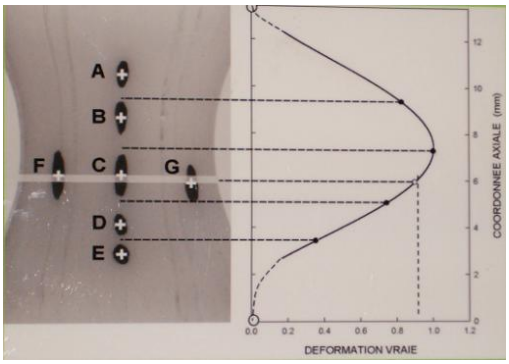

(b) **(c)**

Figure 2.10 (a) Corresponding axial images/time; (b) force/time curve; (c) Schematic interpretation of the method of seven spots.

Software for data analysis and treatment also processing continuous records:

- the axial force applied to the test piece,
- duration,
- the distance between the central position of the two adjacent vertical spots (AB, BC, CD, DE) and the mean position of centroids of the three spots cross (FC and CG) (Figure 2.10 (c)),
- the axial deformations relative to the zones AB, BC, CD, DE.

Local values of the axial deformation can be written according to the updated lagrangian formalism:

$$\varepsilon_{33}^{AB} = \ln\left(\frac{AB}{A_0B_0}\right) \quad \varepsilon_{33}^{BC} = \ln\left(\frac{BC}{B_0C_0}\right) \quad \varepsilon_{33}^{CD} = \ln\left(\frac{CD}{C_0D_0}\right) \quad \varepsilon_{33}^{DE} = \ln\left(\frac{DE}{D_0E_0}\right) \quad \textbf{(2.7)}$$

Where A, B, C, D, E are the positions of spots after stretching of the initial points A_0, B_0, C_0, D_0, E_0.

- The axial deformation at FCG zone which located near the center of the working portion of the sample (Figure 2.10 (c)) calculated from the previous data (by polynomial interpolation of degree 5, two additional points of zero strain supposed to infinity, are added to the four measured points), we obtain the axial strain at the FCG area, then this will be called true deformation,

$$\varepsilon_{33} = \left[\text{interpolation de } 0, \varepsilon_{33}^{AB}, \varepsilon_{33}^{BC}, \varepsilon_{33}^{CD}, \varepsilon_{33}^{DE}, 0\right]_{x_3(FCG)} \quad \textbf{(2.8)}$$

- The transverse deformation in the area FCG. Assuming the transverse isotropy, two true transverse deformations are determined in FCG zone by:

$$\varepsilon_{11} = \varepsilon_{22} = \frac{1}{2}\left(\ln\left(\frac{FC}{F_0C_0}\right) + \ln\left(\frac{CG}{C_0G_0}\right)\right) \quad \textbf{(2.9)}$$

- The volumetric deformation in the slice FCG is deduced from the three components of the deformation: $\varepsilon_v = \varepsilon_{11}+\varepsilon_{22}+\varepsilon_{33}$. From the definitions of lagrangian deformation, volumetric deformation ε_v is connected to the expansion of a piece of material as a result of the deformation applied:

$\varepsilon_v = \ln(V/V_0)$ where V and V_0 are the values of the current and initial volumes of the material element considered.

From the previous information the true axial stress can be obtained easily (Cauchy stress) by the relation:

$$\sigma_{33} = \left(F/S_0\right)\exp(-\varepsilon_{11})\exp(-\varepsilon_{22}) \qquad \textbf{(2.10)}$$

where S_0 is the initial section of the specimen, measured before the start of the tensile test.

4.9.2. Izod impact

Izod impact tests were performed at room temperature with an instrument CEAST Resil Impactor 6967. The specimens (80.5 mm long, 10.5 mm thick and 4.0 mm wide) were prepared in a hot press at 180°C for 15 min under load by using a manual hydraulic press. At least five specimens were tested for each sample to get an average value.

Chapter 3. Synthesis of PBA nanoparticles

This chapter was divided into two sections. The first section was focus on the study of synthesis of PBA nanoparticles by miniemulsion polymerization as well as the influences of all the parameters of miniemulsion polymerization. The second section was mainly tried to achieve an encapsulation of clay within the PBA nanoparticles. This part also included the modification of clay.

In this chapter, the description of experiment was presented. After that, the results of examinations for the obtained PBA nanoparticles were also indicated.

1. Miniemulsion polymerization

The mechanical property improvements of an impact modifier depend on the properties of the toughening particles, and the particle size distribution of the latex (as preferably no bigger than 200nm). With respect to particle size, the miniemulsion polymerzaiton has been chosen to synthesize the PBA particles.

1.1. Synthesis of the PBA latex particles

All the PBA latex nanoparticles were synthesized by miniemulsion polymerization. Table 3.1 and Figure 3.1 show the basic recipes and the conceptual reactor for polymerization, respectively. The synthesis was composed of two consecutive steps: preparation and polymerization for the miniemulsion.

Table 3.1 Recipe used for the preparation of PBA latex particles by miniemulsions polymerization.

Mixtures	***Components***	***Amount(g)***	***Concentration***
Oil phase	BA	20	20 wt%[a]
	HD	0.8	4 wt%[b]
Water phase	H_2O	78-79	78-79%[a]
	SDS	0.05-0.75	2-35 mmol[c]
	KPS	0.2	8.87 mmol[c]
	$NaHCO_3/Na_2CO_3$	0.2750/0.0932	4.09/11 mmol[c]

[a] Based on total recipe. [b] Based on monomer. [c] Based on aqueous

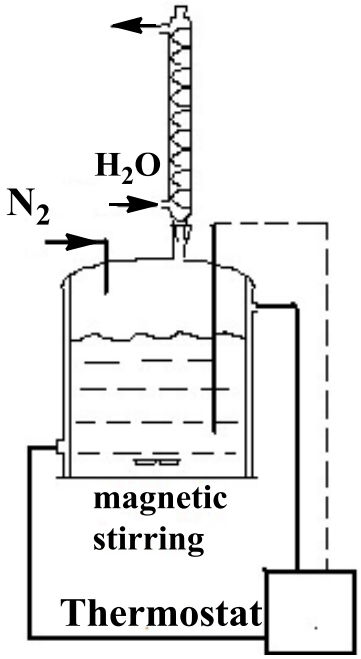

Figure 3.1 Reactor for miniemulsion polymerization to obtain PBA latexes.

Preparation of the miniemulsion

The PBA particles were prepared according to the following procedure using a typical recipe illustrated in Table 3.1. The oil phase consisting of 20g BA and 0.8g hexadecane (HD) in glass beaker was subjected to magnetic stirring for 1h and cooled in an ice bath. Following that, the oil phase was poured into the water phase which containing 79g water and 0.375g SDS. The mixture of oil phase and water phase was then under a vigorous mechanical stirring also in an ice bath for 1h. After that, the mixture was immediately subjected to ultrasonication for 3 min using a sonicator of type Hielscher (the sonic horn was placed in the mixture about 0.5 cm above the magnetic stir bar, and activated at 0.5s of cycle time, 70% of amplitude; samples being cooled by an ice bath to avoid polymerization in the sonication due to heating and to facilitate homogeneous sonication) to realize the homogenization. The resulting mixture was ready for the subsequent polymerization.

Miniemulsion polymerization

The as-prepared miniemulsion was transferred to a 250ml stainless steel reactor and first purged with pure nitrogen for 30 min under magnetic stirring within the reactor at 20°C. The reactor was double envelope which connected to a thermostat to control its

temperature and equipped with a reflux condenser also. The temperature of the reactor was thereafter raised to 60 °C. Upon reaching the reaction temperature, the polymerization was achieved by injecting the aqueous solutions of KPS initiator and buffering agents $NaHCO_3/Na_2CO_3$ at 60 °C while continuously purging with nitrogen. The reaction was undertaken at given temperature for more than 1.5h with continuous stirring and terminated by directly adding hydroquinone to the system. After polymerization, the final product was passed through centrifugation to separate the latex and the aggregate. Polymer yields were determined by gravimetry. The droplet sizes of the latexes were determined by dynamic light scattering (DLS).

1.2. Characterization of the latex PBA

After the 1.5h of miniemulsion polymerization, there was few aggregate neither within the reactor nor around the stirrer. By analyzing with the gravimetry and consequent calculations, it could be found that the mean yield of the PBA latexes reached 90%. Furthermore, from the Figure 3.2, it is well demonstrated that the distribution of particle size is in a narrow range and the particle size is around 100 nm.

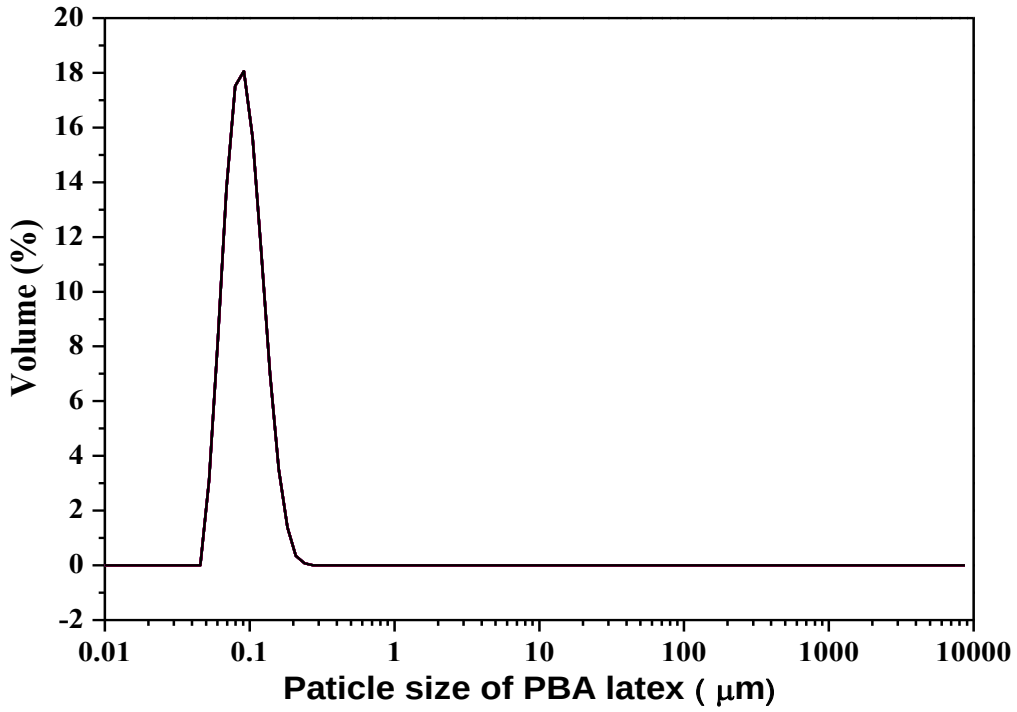

Figure 3.2 The particle size distribution of PBA latex by miniemulsion polymerization.

The image of TEM Figure 3.3 also confirms the particle size distribution from DLS result.

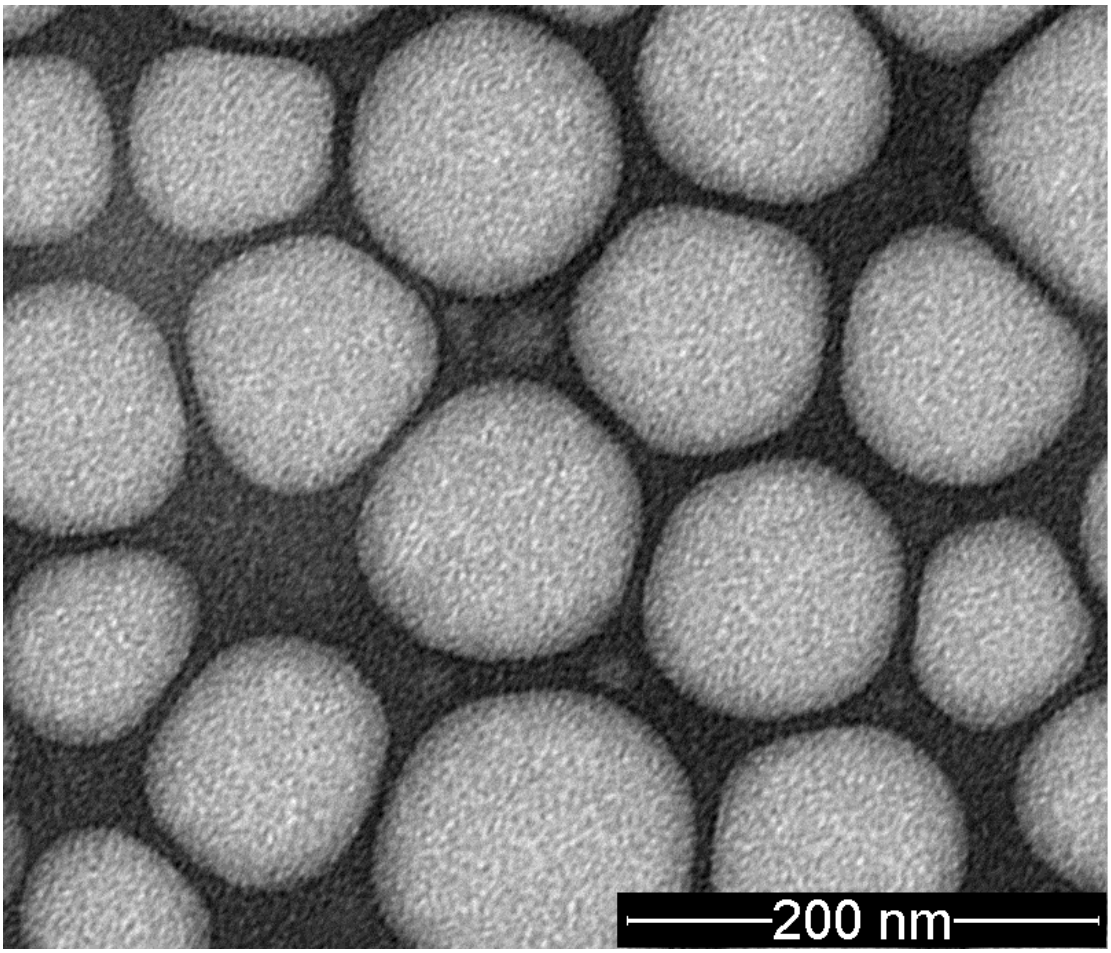

Figure 3.3 The TEM image of PBA particles from miniemulsion polymerization latex.

The solids content in the study was only kept at 20wt%. In the condition of higher solids content, more amount of surfactant should be added in the system to obtain the required nanosize particle. While the high solids content would give rise to significantly increased viscosity of the aqueous phase and the stability of the latex during the polymerization is difficult to sustain in the presence of next step-clay encapsulation.

1.3. Influence of surfactants

To produce a properly nanosize PBA particles by miniemulsion polymerization,

relatively high levels of surfactant may be necessary to reduce the interfacial tension and enhance the colloidal stability of the small monomer droplets. Accordingly, a series of miniemulsion polymerization were tested in order to examine the efficiency of surfactant. Colloidal stability is usually influenced by type and amount of the employed surfactant. In miniemulsion process, the fusion-fission rate equilibrates during sonication and therefore the size of the droplets after primary equilibration directly depends on the amount of surfactant. The amount of surfactant was systematically varied over a range in order to control the particle size in nano range. In order to achieve the incorporation of clay into the latex, it is necessary to find the adequate type and amount of surfactant to yield latex particles which have the appropriate size and surface charge to allow encapsulation.

PBA miniemulsion with sodium dodecylsulfate (SDS) as surfactant, the co-stabilizer (hexadecane, HD) level was kept in constant at 4wt% based on monomer. By varying SDS concentration, the final particle sizes between 120 nm to 95 nm can be obtained by DLS test.

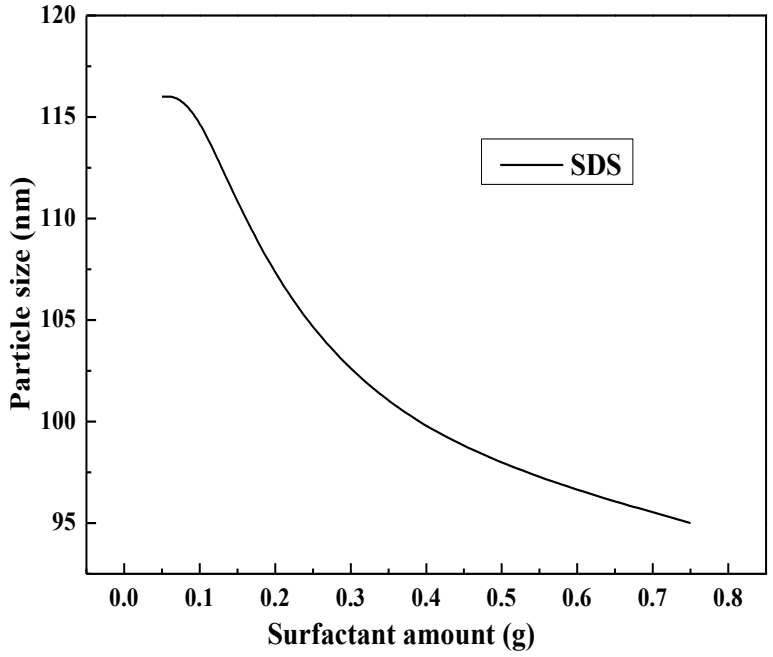

Figure 3.4 Average diameters of final PBA nanoparticles as a function of the amount of SDS in the feed. The initial amount of BA monomer is 20 g.

Surfactant molecules were partitioned between the aqueous phase and the surface of the miniemulsion droplets according to an adsorption isotherm. The particle diameter

decreased with the total SDS concentration increasing (Figure 3.4). Smaller droplets require lower interfacial tensions (i.e., greater amounts of surfactant in the miniemulsion) to form during emulsification. In any case, the surface charge density must be sufficient to maintain colloidal stability.

The non-ionic surfactants such as Brij 78 and Brij 700, their polar head groups containing poly(ethylene oxide) moieties were miscible with PLA. As a result, the latex particles obtained with these two surfactants might possess improved compatibility with PLA base.

The data of the PBA mini-emulsion polymerization with different amounts of Brij 78 are summarized in Table 3.2. All the processes in the miniemulsion polymerization with the surfactant of Brij 78 are the same as the previous descriptions for the polymerization with SDS.

Table 3.2 The results of the conversion, the particle size and the amount of the deposits after the miniemulsion polymerization by using Brij 78 as surfactant.

BA (g)	***HD (g)***	***Brij78 (g)***	***KPS (g)***	***H_2O (g)***	***Na_2CO_3/$NaHCO_3$ (g)***	***Conversion (%)***	***Size (nm)***	***Deposit (g)***
20	0.8	1.0	0.2	78	0.2760/0.0930	86	118	0.77
20	0.8	0.8	0.2	78	0.2750/0.0939	84	147	0.75
20	0.8	0.4	0.2	78	0.2748/0.0960	67	176 (two peaks)	3.40
20	0.8	0.2	0.2	78	0.2748/0.0943	43	186 (two peaks)	8.20
20	0.8	0.1	0.2	79	0.2750/0.0932	5	2246 (three peaks)	11.22

It can be speculated from the Table 3.2, when the amount of Brij 78 is less than 0.4g (2wt% of monomer), the distributions of PBA particle size are not homogeneous anymore and there are two or three peaks exist in the DLS results which well demonstrated in the Figures 3.5-3.8. From these four Figures, they indicated that the quantities of surfactant-Brij 78 used in the miniemulsion were very important for the stability of the latex obtained. This means for the amount of Brij 78 in the PBA miniemulsion polymerization less than 0.8g, the PBA latex is not stable anymore. And

in the tests of DLS, as showed in Figures 3.6-3.8, the less amount of surfactant made the curves of particle size have at least two peaks. When the quantity of Brij 78 was only 0.1g in the system, even though its concentration was more than the CMC of Brij 78 (4.0×10^{-5} mol/L or 0.046 g/L), is was not sufficient for maintaining the stability of the products of miniemulsion polymerization. When PBA latex was added in the chamber of DLS test, after the increasing chance of collision causing by the DLS test, the particles of PBA coalesced to form some larger particles of PBA so that the peaks of particle size in DLS curve moved to higher values, which was demonstrated in Figure 3.8. Furthermore, the yield of the PBA latex is also decreasing when the amount of Brij 78 changes from 1g to 0.1g.

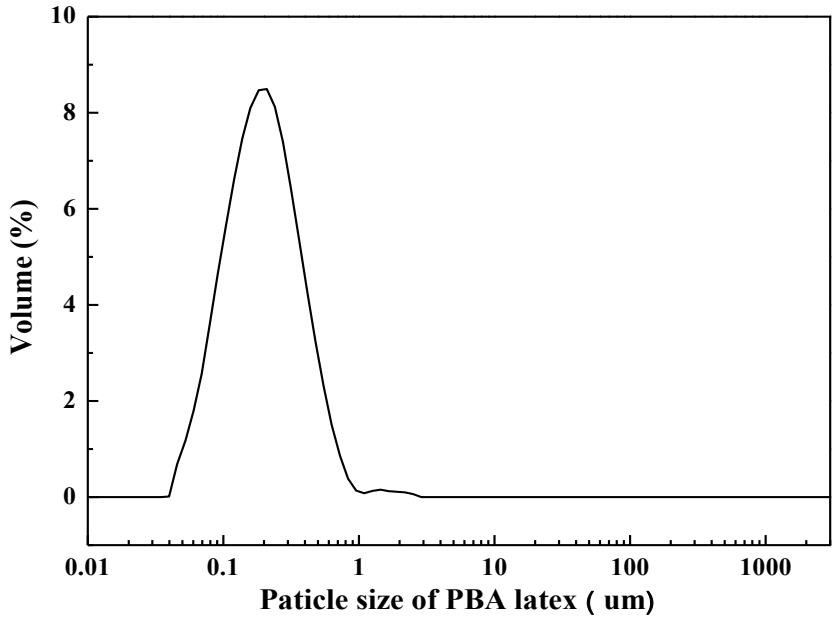

Figure 3.5 The size distribution of PBA particles (Brij 78= 0.8g).

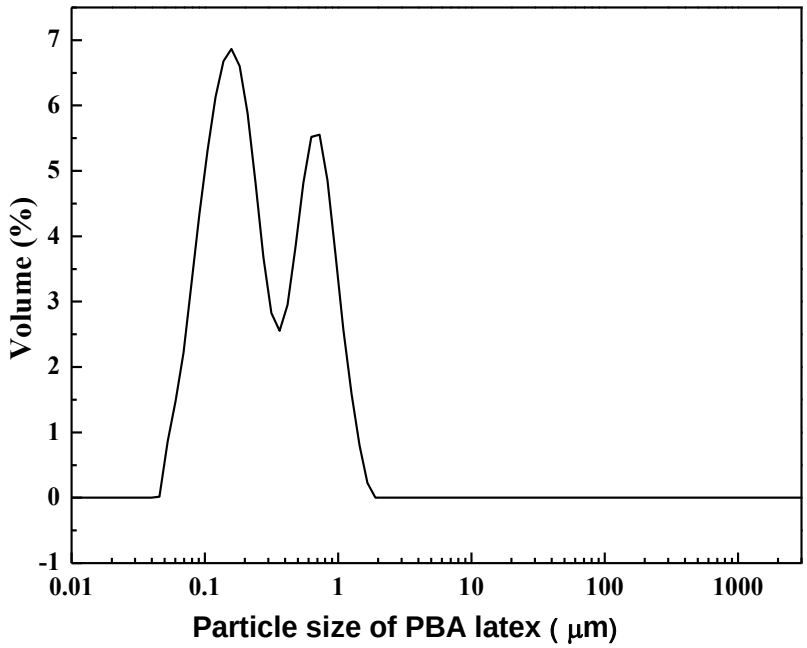

Figure 3.6 The size distribution of PBA particles (Brij 78= 0.4g).

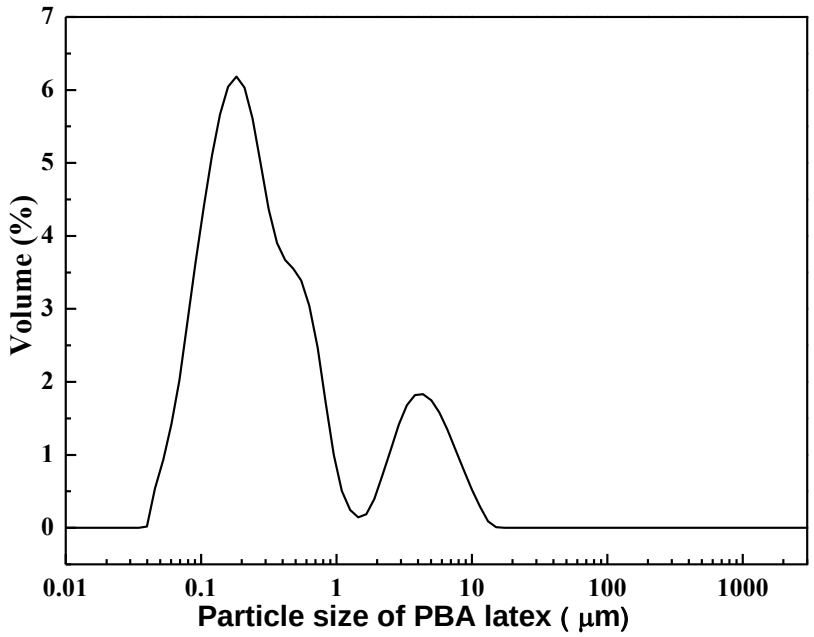

Figure 3.7 The size distribution of PBA particles (Brij 78= 0.2g).

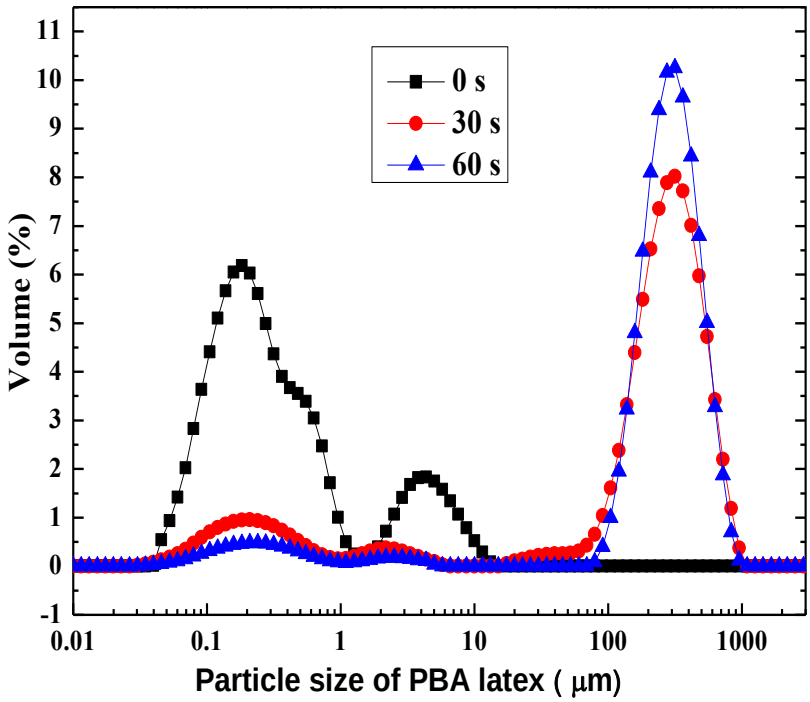

Figure 3.8 The size distribution of PBA particles (Brij 78= 0.1g).

Comparing the particle size of PBA latex after polymerization with same amount of these two different surfactants-SDS or Brij78, PBA latex using SDS has smaller particle size. Furthermore, the quantity of aggregate within the reactor after miniemulsion polymerization with surfactants SDS and Brij78 is presented in the Figure 3.9. It can be concluded from Figures 3.4 and 3.9, that Brij78 is not a surfactant as efficacious as SDS in the miniemulsion polymerization because when achieving the same particle size and small quantity of deposit, the amount of Brij 78 used in the miniemulsion polymerization was much higher than that of SDS.

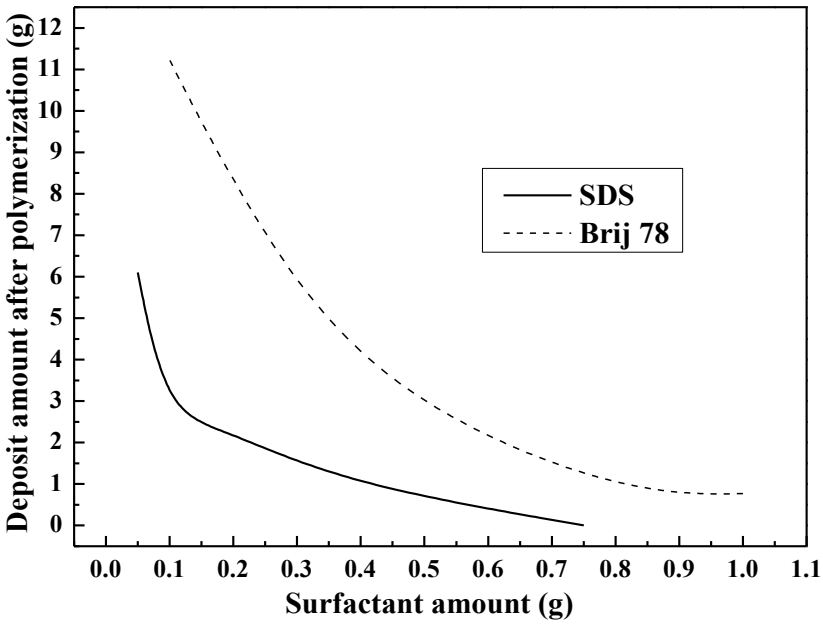

Figure 3.9 Evolution of deposit amount of PBA latex after miniemulsion polymerization with different quantity of SDS or Brij78.

The structure of Brij700 ($C_{18}H_{37}(OCH_2CH_2)_nOH$, n=100) is similar as that of Brij78, the only difference is the hydrophilic part of Brij700 is longer than that of Brij78.

Table 3.3 Characters of PBA latex with Brij 700 as surfactant.

BA (g)	*HD* (g)	*Brij700* (g)	*AMBN* (g)	*H_2O* (g)	*Conversion* (%)	*Size* (nm)	*Deposit* (g)
20	0.8	2.0	0.4	77	78	108	5.86
20	0.8	3.0	0.4	76	80	100	2.45
20	0.8	4.0	0.4	75	80	98	0.45
20	0.8	6.0	0.4	73	82	98	~0

Figures 3.10 and 3.11 show the evolution of PBA particle size and the corresponding amount of precipitates after miniemulsion polymerization, respectively, as a function of Brij 700 or Brij 78 content. From Figure 3.10, the diameter of PBA particles is around 100 nm and the efficiency of the two surfactants is similar. The two figures suggest that both surfactants are effective when their concentrations exceed 4 wt% (weight fraction in the system) and the latexes are stable after polymerization.

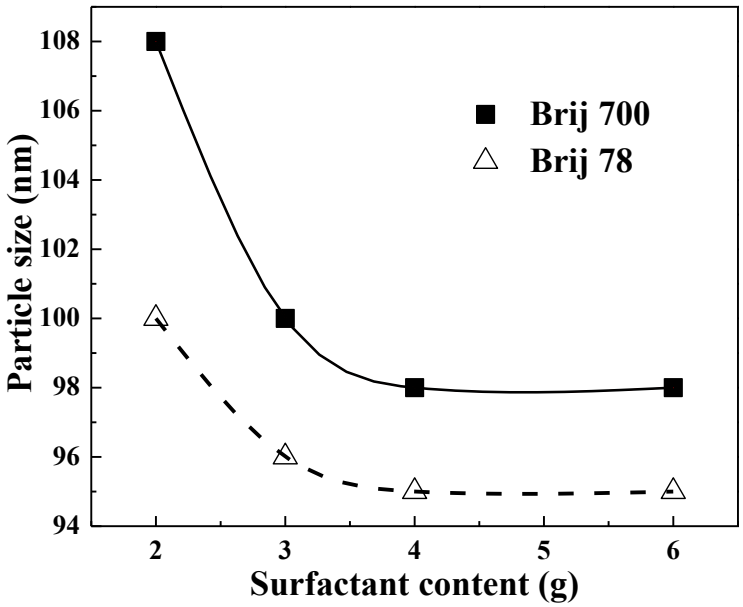

Figure 3.10 Average diameter of final PBA nanoparticles as a function of the amount of Brij 700 or Brij 78 in the feed. The initial amount of BA monomer is 20 g.

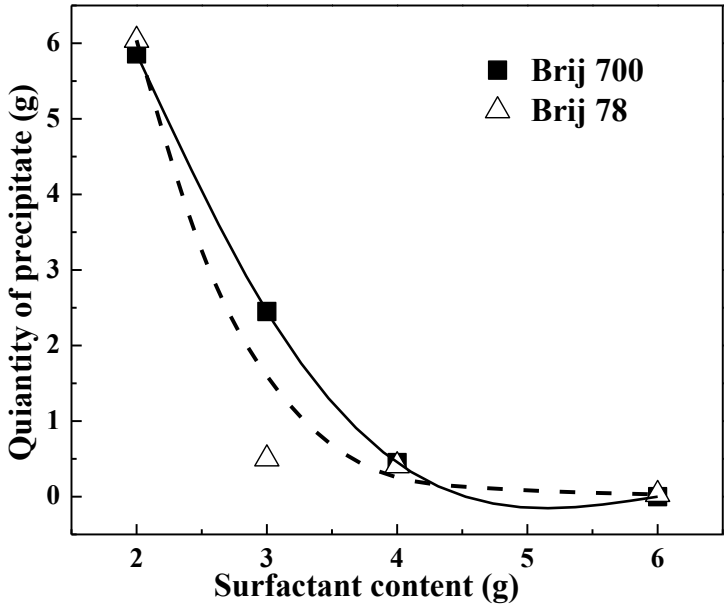

Figure 3.11 Amount of recovered precipitate after miniemulsion polymerization as a function of the surfactant amount (Brij 700 or Brij 78) in the feed. The amount of BA monomer in the feed is 20 g.

The results for particle size show that the PBA particle size is essentially controlled by a limit of the surfactant coverage on the latex particles. The two surfactants Brij700 and Brij 78 are somewhat less efficient with regarding the results of SDS.

1.4. Choice of initiator

It is well know that the addition of nanoclay will significantly increase the monomer viscosity even can form a gel at high concentration of nanoclay. Because of the increase of viscosity inside the monomer droplet in the presence of nanoclay, the molecular diffusion of both initiator and monomer from the reaction sites (oil droplet) to water phase could be significantly reduced and, consequently, water phase nucleation be prohibited.

For the consideration of preparing PBA/clay particle, the oil-soluble initiator AMBN (2,2'-Azobis (2-methylbutyronitrile) $C_{10}H_{16}N_4$) would take the place of water-soluble initiator KPS. The PBA latex with AMBN as initiator has been tested before PBA/clay composites preparation. The temperature for starting reaction with initiator AMBN has been chosen at 75°C. After same reaction time of 1.5h for miniemulsion polymerization, the yield of PBA latex initiated by AMBN is only around 75%, which is slightly lower than that of KPS (with KPS, after 1.5h of polymerization, the conversion was 85%-90%). Thus, the reaction time should be prolonged to reach a desirable conversion with AMBN. When we prolonged the reaction time from 1.5h to 3h, the conversion of BA to PBA could reach around 85%. Meanwhile, we also find the different initiators had influence for the stability of miniemulison. By comparing the curve of Brij 78 in Figure 3.9 and Figure 3.11, when the KPS was using, the Brij 78 was more efficient than that was with AMBN. Furthermore, during polymerization, the buffering agents were not needed in order to maintain the pH=7 with the oil soluble initiator AMBN.

1.5. Influence of ultrasound

It is well-known that a vigorous mechanical homogenization is an indispensable step for the preparation of stable emulsions or miniemulsions. Ultrasonication is commonly used to make stable emulsions or miniemulsions also. In our miniemulsion study, an ultrasonication treatment before polymerization is a very important factor for obtaining a stable state. However, because a quantitative study of the

ultrasonication effect requires well-defined equipment and experimental setup and is beyond the goal of this research, only a qualitative study was conducted.

It was found that the droplet size was acting as a function of the amount of ultrasound used. The size of droplets change rapidly throughout sonication as it approach a pseudo-steady state, when a required minimum of energy for reaching this state is used. Once this state is reached, the size of the droplet does not change any more.

At our experimental conditions, the results obtained indicated that, the relatively high energy introduction at short ultrasonic time (3 min) benefited the formation of stable and uniform miniemulsion droplets. Ultrasonication times beyond 5 min caused the coalescence of the miniemulsion particles. It was also found in our study that the stability of the final nanoclay composite depended strongly on the stability of pre-polymerization miniemulsion. A largely precipitated clay/polymer solid mixture was observed when an unstable miniemulsion was used in the polymerization.

After stopping sonication, a rather rapid and minor equilibration process has been occurred where the chemical potential in each droplet was equilibrating. For this reason, the reaction of miniemulsion polymerization after the sonication should be initiated as soon as possible to maintain the droplet size and to minimize the phenomenon of droplet coalescence.

The power and the duration time that the ultrasound was effected for the miniemulsion was changed as listed in the Table 3.4.

Table 3.4 The results of PBA particles after miniemulsion polymerization with different setting of ultrasound before the reaction.

Power	*Conversion (%)*	*Size (nm)*	*Time (s)*	*Deposit (g)*
80%	90	102	180	0.977
50%	91	102	180	0.76
20%	90	108	180	0.255
20%	85	105	30	0.828

From the results in Table 3.4, the particle size after polymerization was in the same range and was not affected significantly by the ultrasound's intensity. The most important difference is the amount of precipitate after polymerization. A stronger

power of ultrasound treatment did not give a better result for the PBA latex preparation. Only the appropriate energy from ultrasound could make PBA latex which has a high conversion and few deposits after reaction.

The conclusion to be drawn might be that there is indeed no significant difference in particle size when the energy from sonication is enough for the mini-emulsion approach a pseudo-steady state.

1.6. Influence of co-stabilizer

It is known that a small amount of co-stabilizer builds up an osmotic pressure in miniemulsion droplets and provides stability against Oswald ripening. The required minimum molar ratio of co-stabilizer to monomer is about 1:250 for creating enough osmotic pressure in the droplets.

The miniemulsions were made from the same recipe as Table 3.1, but with different co-stabilizers or no co-stabilizer for miniemulsion polymerization.

Table 3.5 The characters of PBA latex with different types of co-stablizers in the miniemulsion polymerization or without co-stabilizer in the miniemulsion polymerization.

Co-stabilizer	*Conversion (%)*	*Size (nm)*	*Deposit (g)*
Hexadecane 0.8g	90	103	0.95
N-decane 0.8g	92	105	1.16
Dodecane 0.8g	76	105	1.15
No co-stabilizer	94	99	1.20

Comparing the results in Table 3.5, the efficency of hexadecane (HD) is better than that of n-decane or dodecane. There was less deposit after reaction when HD was added in the miniemulsion which means the miniemulsion with HD is a little bit more stable than the others.

Furthermore, the particle size of miniemulsion droplets rapidly polymerized after sonication either do not depend on the amount of the co-stabilizer, or are very weak functions of the amount of co-stabilizer. It was found that miniemulsion without the co-stabilizer does not increase the radius of particle; it is presumed that the effective

pressure have to be the same in every droplet, a stabilizing mechanism, which in principle does not depend on the amount of co-stabilizer.

For the case of clay encapsulation, the co-stabilizer HD not only acts as the osmotic swelling agent for the miniemulsification process to suppress Ostwald ripening, but also hope it can partially adsorbs onto the clay particles to prevent the formation of clay aggregates in PBA particles.

1.7. Conclusion

It can be concluded from the previous part that PBA miniemulsions are critically stable systems, which can be polymerized directly after the miniemulsification in a nearly 1:1 copying process under retention of the critically stabilized state. A post-stabilization with an adequate amount of surfactant allows one to create a stable state where the osmotic pressure and the Laplace pressure are balanced.

To try the experiments of encapsulation of clay, the amount of surfactant - 4 g of Brij 78 or Brij 700 was used. Meanwhile, oil-soluble initiator AMBN was chosen and co-stabilizer HD was added also in the further studies.

2. Encapsulation of clays

Since the synthesized Polyamide 6/clay nanocomposites were first demonstrated by a group at the Toyota research center in Japan, many researchers have explored the improvement in mechanical performance when a few weight percent of nano-silicate was added to polymer. For the past few years, the field of PLA nanocomposites based on layered silicates, such as montmorillonite (MMT), has gained its popularity among scientist and industrials. The nanoscale distribution of such high aspect ratio (~250:1) fillers brings up some large improvements to the polymer matrix in terms of mechanical, fire retardant, rheological, gas barrier and optical properties, especially at low clay content (as small as 1 wt.%) in comparison with conventional microcomposites. A large aspect ratio of the silicate layers results in a high interfacial area minimizes the chain mobility, and creating a reinforcement effect. In addition, this interface facilitates stress transfer to the reinforcement phase, thus leads to

improvement of the properties for polymers.

In order to reach this nanoscale distribution, the naturally hydrophilic clay filler has to be organically modified to be more compatible with the organic polymer matrix. One often-employed strategy to modify inorganic clay is the exchange of stabilizing alkali by organic cations such as alkyl ammonium, making the clay organophilic and compatible with polymers.

For a given concentration of montmorillonite, the mechanical properties of the polymer/clay nanocomposites are best when the clay platelets are completely exfoliated in the polymer matrix. Polymer/clay nanocomposites in which the clay is partially exfoliated or a modest amount of polymer is intercalated between the clay layers showed lower performance. Therefore, the goal is to completely exfoliate the clay in the polymer matrix.

There are four known ways to prepare an exfoliated nanocomposite based upon what has been written in the open literature. These include melt compounding, in situ polymerization, emulsion/suspension polymerization, and solution blending. The first, melt compounding, is a procedure that is widely used today to generate polymer nanocomposites, but it has only generated well exfoliated polymer nanocomposites with very polar polymers, such as Nylon-6. The second, in situ polymerization has had a great deal of success in the open literature. Examples include the original Toyota Nylon-6 nanocomposite work as well as more recent polystyrene work. In situ polymerization very often involves clay organic treatments that have functional groups which the polymer monomer can either co-polymerize with the organic treatment, or begin polymerization initiation at the organic treatment site. Emulsion polymerization has shown success in styrenic polymers, but the stability of the resulting nanocomposites to additional thermal processing is unknown. Solution blending has been a widely used technique, and it is one of the approaches that consistently give exfoliated materials, provided the clay organic treatment, solvent, and blending conditions are considered.

Melt intercalation and in situ polymerizations in the presence of organically modified clays have been used to produce polymer-clay nanocomposites with improved

mechanical and thermal properties of the polymer. Emulsion polymerization in the presence of clays was employed to prepared polymer/clay hybrid particles, but only armored particles (clay being located at the particle surface) were obtained [26] [27] [113]. Encapsulation of clays by polymer appears to be very challenging.

Emulsion polymerization with Na-MMT suggested that the clay platelets were preferentially located in the aqueous phase. Partially exfoliated poly(methyl methacrylate-co-butyl acrylate)/MMT nanocomposites had been obtained by seeded semi-continuous emulsion polymerization when the clay was incorporated during the in situ polymerization whereas existed aggregates of clay platelets, and hence after a physical blend with polymer matrix, a poor dispersion of the clay in the polymer matrix were observed [114].

2.1. Montmorillonite (MMT)

To achieve the goal of encapsulating clay particles in PBA particles, the organically modified montmorillontie (OMMT) - Cloisite® 20A which is montmorillonite modified with dimethyl chloride was used in the miniemulsion polymerization.

OMMT was dried in a vacuum oven at 80 °C for 3 hours before added in the miniemulsion polymerization. The co-stabilizer (hexadecane) was dissolved with monomers and they were mixed with OMMT by magnetic stirring for at least 30 minutes. After a passage of ultrasonication for 3 min (the mixture in the beaker was cooled by ice), it was mixed with the surfactant solution and subjected a further magnetic stirring for 30 minutes then the pre-emulsion was subjected to another passage of ultrasonication for 3 min (cooled by ice as well). The following steps were the same as the previous synthesis process mentioned for the PBA latex.

It was found that when PBA/OMMT latex obtained was not passed a centrifugation, the particle size mesured by DLS (Mastersizer 2000) was not consistent. The particle size distribution envolved is shown in Figure 3.12. The distribution has two peaks in which the first is around 100 nm and the second peak is around 100 µm. It was likely due to the clay particles were not located in the center of PBA particles but just sitting around the surface of the PBA particles. When the latex was tested in DLS, OMMT

and PBA particles had collided and coalesced so that larger polymer particles were formed in the DLS chamber by stirring. Thus, limited flocculation took place in the test process and the size of the particle increased. That explained in the Figure 3.12, when the testing time of the DLS was increasing, the curve of particle size was changed and peaks moved to the larger values.

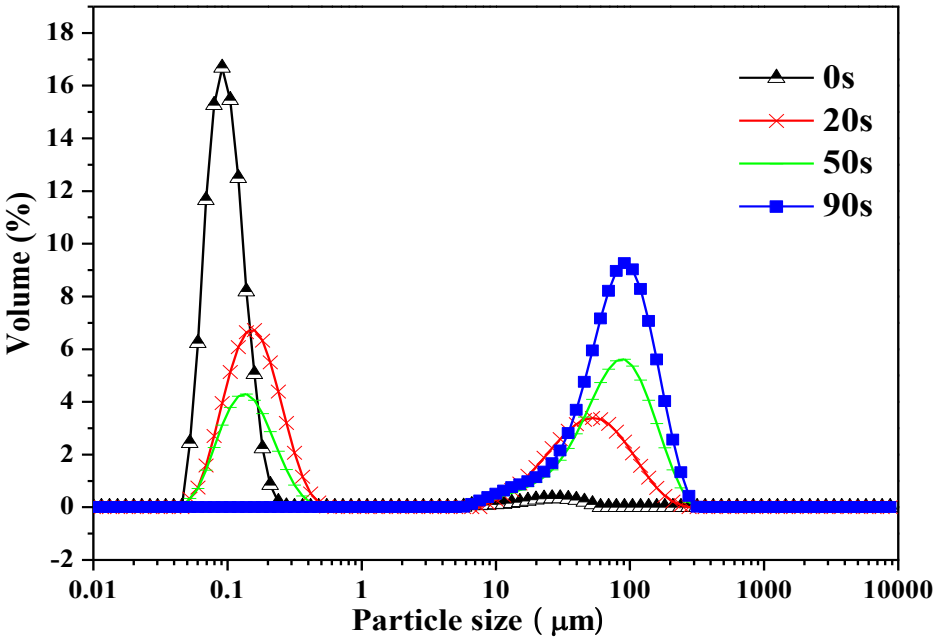

Figure 3.12 The particle size distribution of PBA/OMMT latex before centrifugation with difference duration time in the DLS test machine-Mastersize 2000.

However, as shown in Figure 3.13, when a centrifugation was passed for the latex obtained, even though DLS test for the latex was taken for a long time (the same time was used as in Figure 3.12), the particle size did not change with time in DLS mesurement. The layer of OMMT which could not remain in the polymer particles was removed by centrifugation. The association of clay platelets to the polymer particle surfaces-armored particles (as in the pickering emulsions) seemed to be proven.

The particle size of clay influenced the morphology of final latex, the efficiency of encapsulation of clay by polymer, and the stability of final latex particles. As our initial goal was incorporating the hydrophobic OMMT platelets (~300 nm in length) within the monomer droplets, slightly larger droplets were needed to assure their

complete incorporation in the droplets. However, the lower surfactant concentration is adequate to produce droplet sizes above 300 nm (as to fully engulf clay platelets ~300 nm wide in the droplets) yielded unstable miniemulsions. Therefore in the miniemulsions prepared as described above, the large clay particles can only be suspended in the final latex system by adhering to the latex particle surface.

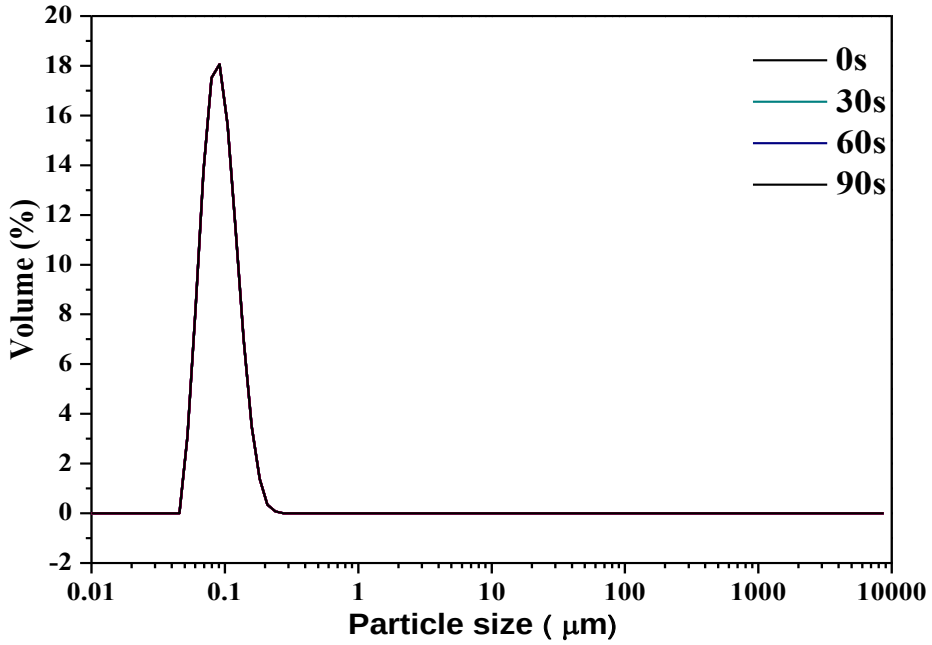

Figure 3.13 The particle size distribution of PBA/OMMT latex after the centrifugation.

The aggregate amounts after reaction have no regularity when changing amount of OMMT from 0.2 g to 0.6 g (1wt% ~3wt% of monomer). The final yield of PBA latex decreased when 3wt% of OMMT has been added in the BA monomer.

Table 3.6 Characters for PBA latex after centrifugation for the miniemulsion containing OMMT or without OMMT.

OMMT (g)	*Conversion (%)*	*Size (nm)*	*Deposit (g)*
0.2	91	105	2.16
0.4	89	104	2.60
0.6	86	104	3.51
-	91	105	1.04
0.4 (in water phase)	90	104	1.06

The conversion gradually decreases as the weight percent of OMMT increases. The

introduction of OMMT particles would change the physical properties of dispersed phase. It can be seen that the viscosity of system increases as more OMMT incorporated in monomer phase. As a result, the monomer phase became more difficult to be dispersed to small droplets during the mini-emulsification process. On the other hand, the rigid OMMT particles would absorb more ultrasonic energy than acrylate monomers, which would cause the decrease of the effective ultrasonic power acted on the formation of droplets.

Generally speaking, the addition of inorganic particles, such as SiO_2, TiO_2, $CaCO_3$, will reduce both the monomer conversion and the reaction rate in emulsion and suspension polymerizations. Similar results were also observed in our study. The final conversions after 3 h of polymerization with and without 3wt% clay achieved 86% and 91%, respectively. The increasing viscosity of system and the lower monomer concentration lead to a decrease of polymerization rate. Under the same conditions, due to the restricted movement of monomer and the inhibition of the propagating chain radicals in the OMMT galleries, the polymerization rate of monomer was decreased. Therefore, the conversion of monomer in the OMMT system was lower than in the pure system.

This can be attributed to the instability of miniemulsion in the presence of large MMT particles. The large MMT particles could only attach to the surface of the monomer droplets, resulting in a remarkable decrease for the miniemulsion stability. From our study, the miniemulsion in the presence of MMT was unstable and high-viscosity gel-like monomer phase was observed before emulsification. The partial phase separation was also shown during the emulsification process. The encapsulation of large clay particles in PBA particles could only obtain a suspension of OMMT clusters in the final latex system, or OMMT particles were adhering to the latex particle surface.

2.2. Laponite RD (LRD)

Laponite clay-polymer nanocomposites are of great interest, as the inorganic fillers-by addition of relatively low quantities in percentages is known to enhance for example

the mechanical and thermal properties of polymeric materials. Preparation of such composites via emulsion/suspension polymerization systems include heterocoagulation of the clay minerals onto the polymer particles, complexation of monomers/surfactants or covalent modification of the Laponite to facilitate dispersion into the polymer matrix, and use laponite as pickering stabilizer in conjunction with ordinary surfactant stabilization. Norma et al. [20] have synthesized a series of composite latexes poly(Styrene-co-BA)/laponite by seeded emulsion polymerization of styrene and butyl acrylate with laponite clay particles which previously functionalized by cation exchange of the sodium ions with a free radical initiator-AIBA. This synthesis resulted in the formation of composite latexes which surface was recovered by the clay platelets. A direct encapsulation of covalently modified clay platelets via surfactant-free, starved-feed emulsion polymerization has been succeeded by Voorn et al. [47].

2.2.1. Properties of LRD

Laponite is a trioctahedral 2:1 layered silicate structurally related to the naturally occurring hectorite but free from the extraneous elements which are normally present in samples of that mineral. Laponite RD can be dispersed in water as individual disk-shaped colloids with a lateral diameter of 25-35 nm and ~1 nm in thickness and form stable colloidal systems.

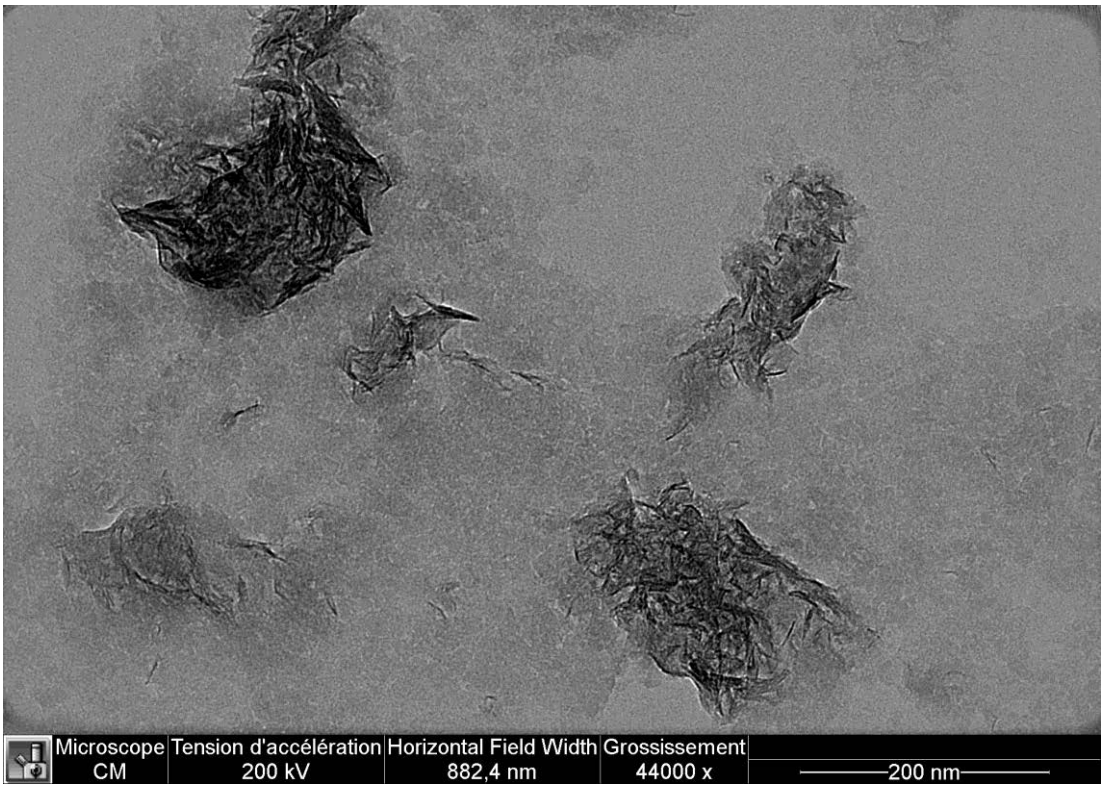

Figure 3.14 The TEM image of LRD.

Figure 3.14 shows the TEM image for LRD dispersed in deionized water. The image demonstrates the typical length and thickness of a LRD is around 25nm and 1nm, respectively.

2.2.2. Modification of LRD

3-Methacryloxypropyltrimethoxysilane (MPTMS) is regarded as a suitable coupling agent for the laponite particles since trimethoxylsilyl groups can be hydrolyzed and be condensed with the silanol groups at the surface of laponite particles and the alkylate chain of MPTMS is hydrophobic. The coupling reaction of MPTMS from laponite particles surface is shown in Schema 3.1 as follows:

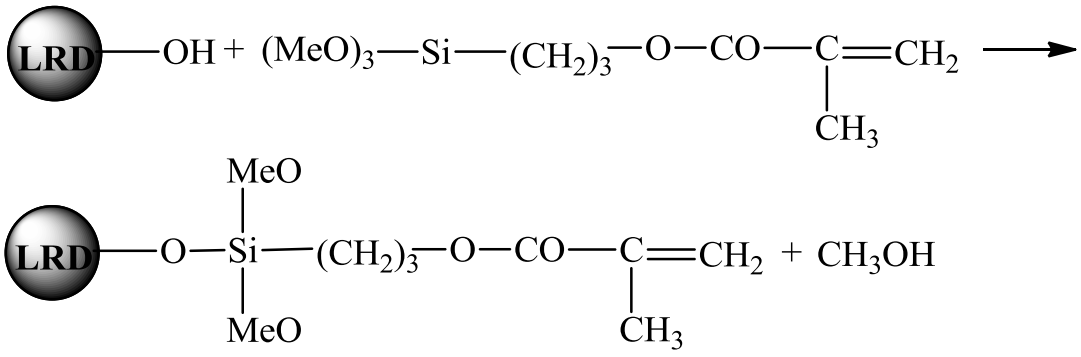

Schema 3.1 Modification of laponite by MPTMS.

It should be pointed out that when MPTMS is introduced in the clay suspension, a sudden increase in the ionic strength and the rapid neutralization of the surface charges of laponite promote the formation of small tactoids made of three or four clay sheets stacked together. Therefore, it can be assumed that in the very first seconds after the addition of MPTMS, aggregation takes place in such a way that the MPTMS molecules can no longer have access to the clay interlayer region and only substituted at the edges of the laponite. The absorption between LRD particles and silane occurred because of the electrostatic attraction between them, and the amount of net charge on the LRD surface gradually decreased as more and more silane was absorbed. When the added amount of silane was close to a critical value, the net charge of the LRD particles was close to zero; thus, the electrostatic repulsive force between the LRD particles was not great enough to resist the centrifugal force. Inevitably, aggregation of the LRD particles occurred.

The dispersion of the laponite in the BA monomer prior to the miniemulsion polymerization required hydrophobic modification of its surface. This step was carried out using silylation reaction in toluene.

Functionalization of LRD:

The silylation of the LRD was carried out in toluene. The LRD (6g) dried at 60°C for 12 hours in a vacuum oven was introduced in a flask containing 200mL of anhydrous toluene. The silylation agent, MPTMS (4.4g), was introduced in the reaction flask and stirred for 10 days at 60°C. The resulting LRD (LRD-Si) was extensively washed with toluene in order to remove the non-grafted silane and dried at 40°C in a vacuum oven

overnight for subsequent use.

After extensive washing with toluene to eliminate the non-reacted MPTMS coupling agent and drying at 40°C in a vacuum oven overnight, the LRD and LRD-Si powders were characterized by FTIR and TGA.

Figure 3.15 shows the FTIR spectrum of the bare LRD and that of MPTMS grafted LRD denoted as LRD-Si. The bare LRD spectrum exhibits a band at around 3453 cm^{-1}, indicating the presence of physisorbed water. This is corroborated by the presence of a band at 1640 cm^{-1} characteristic of the υOH and δOH deformations. A small shoulder at around 3680 cm^{-1} is due to hydroxyls on the LRD surfaces.

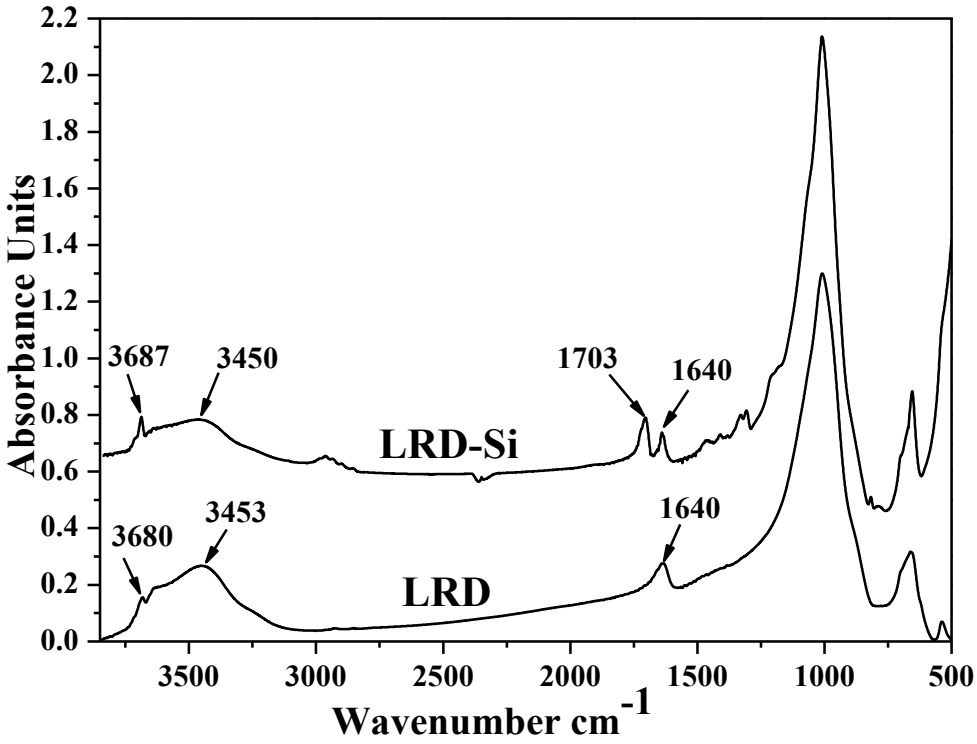

Figure 3.15 FTIR spectra of the bar LRD and MPTMS grafted LRD (LRD-Si).

After the grafting of MPTMS onto the LRD, the spectra shows a characteristic vibration of the carbonyl (υC=O, 1703 cm^{-1}); the small shoulder at around 3680 cm^{-1} corresponding to the hydroxyl moieties on the LRD surfaces (Mg_s-OH) is shifted to 3687 cm^{-1}. Moreover, it becomes sharper and increases in intensity. At the same time, the area under the broad band at 3450 cm^{-1} decreases. The existence of residual Mg_s-OH in the LRD-Si FTIR spectra indicates that they are not accessible to the

MPTMS silane coupling molecules. The increase in the Mg_s-OH band intensity results from a decrease in the amount of physisorbed water after the MPTMS grafting. TGA is used to evaluate the amount of the silane molecules chemically bonded on the clay edges. Figure 3.16 shows the TGA curves before and after the grafting of the MPTMS onto the LRD. The region between 200 and 600°C corresponds to the thermal decomposition of the silane moiety [47]. From the TGA curves, the LRD-Si contains approximately 15 wt% MPTMS grafted onto the LRD. For comparison, the reaction feed contained 42 wt% MPTMS. Therefore approximately 24 % of MPTMS had reacted.

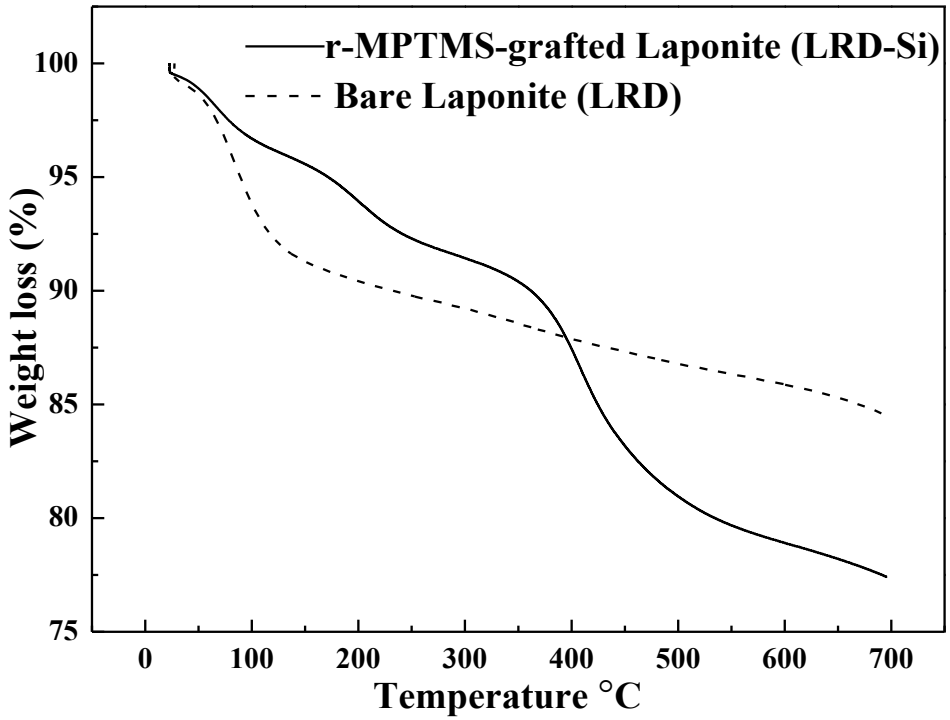

Figure 3.16 TGA traces of the bare LRD and MPTMS-grafted LRD.

With the unsaturated double bond, the LRD-Si can easily graft on the PBA chains after the miniemulsion polymerization.

2.2.3. Encapsulation of LRD-Si in PBA particles

The pristine LRD is hydrophilic and requires pre-modification to be dispersed in the monomer. The concentration of clay in the composites is very important, as clays will re-aggregate back to larger tactoids above 2-3 wt% solids content. With this in mind,

it is better for the final nanocomposite not have more than 2-3 wt% inorganic content if it is to be truly exfoliated in the latex particles. A large inclusion of nanoclay within the latex particles causes destabilization of the droplets. Meanwhile, a highly viscous solution was formed if the amount of the modified LRD in the monomer was higher than 5 wt% because well dispersed nanoclay in the monomer significantly increased the oil phase viscosity, resulting in an unstable miniemulsion. For this reason, the content of nanoclay is not higher than 5 wt% in our research in order to prepare a stable composite suspension.

SDS is an anionic surfactant which is very common and efficient for emulsion as well as miniemulsion polymerization reactions. Nevertheless, in our experiments showed that SDS was not suitable for miniemulsion polymerization in the presence of LRD or LRD-Si when their solid content exceed 3wt%. When it was added to the miniemulsion of BA with 5%LRD or 5%LRD-Si, the latex became unstable and exhibited high content sediments (> 80 wt% of the initial monomer) after the polymerization. These might be due to the higher concentration of laponite in the monomer droplets made the laponite have more opportunities to contact with SDS molecular and the repellency between laponite and SDS had been displayed more significant in comparison with that of monomer droplets with smaller concentration of laponite.

Unlike poor performance of SDS in miniemulsion polymerization in conjunction with LRD, non-ionic surfactants Brij 78 and Brij 700 efficiently stabilized miniemulsions. In addition, their polar head groups containing poly (ethylene oxide) moieties were miscible with PLA. As a result, the latex particles obtained with these two surfactants might have better compatibility with PLA. For all the previous reasons, Brij 78 and Brij 700 were chosen as surfactants for the miniemulsion polymerization of PBA-clay composites.

The hydrophilic clay themselves require a hydrophobic surface so that they can be dispersed into the hydrophobic monomer phase. The surface properties of the clay play a critical role in the dispersibility of intercalated clay in the monomer. Untreated clay particles are organophobic and are not easily dispersible in organic media. In the

case of LRD, the nanoparticles were modified with a silane prior to dispersing the clays into the oil phase. Up to 5wt% of LRD based on monomer has been tried to be dispersed into PBA particles.

In terms of preparation of the PBA-clay miniemulsion, two principal steps should be well executed: In a first step, the already hydrophobized clay ready for incorporation has to be dispersed in the monomer phase. Thereafter, the miniemulsification under vigorous stirring has to be carried out.

Table 3.7 and Figure 3.17 show the basic recipes and the miniemulsion polymerization procedure, respectively. The latter was composed of two consecutive steps: preparation of the miniemulsion and polymerization.

Table 3.7 Basic recipe for the preparation of PBA latex particles.

	Mixture A						Mixture B	
Latex PBA	BA (g)	LRD (g)	LRD-Si (g)	CTAB (g)	HD (g)	AMBN (g)	Brij700 or Brij78(g)	H_2O (g)
PBA	20	-	-	-	0.8	0.4	4	74
PBA-LRD	20	0.4 - 1	-	0.8	0.8	0.4	4	74
PBA-LRD-Si	20	-	0.4 - 1	0.8	0.8	0.4	4	74

Preparation of the miniemulsion:

Mixtures A and B were charged to two glass beakers, respectively, under the action of a magnetic bar. After 1h of magnetic stirring in an ice bath, mixture A was immediately subjected to ultrasonication for 3 min using a sonicator of type Hielscher (0.5s of cycle time, 70% of amplitude; samples being cooled by an ice bath). Mixture B was prepared with magnetic stirring at room temperature for 1 h, and then cooled in an ice bath. At last, mixtures A and B were mixed together in a glass beaker with magnetic stirring in the ice bath for 30 min and further homogenized with the sonicator in the ice bath for another 3 min. The resulting mixture was ready for the subsequent polymerization.

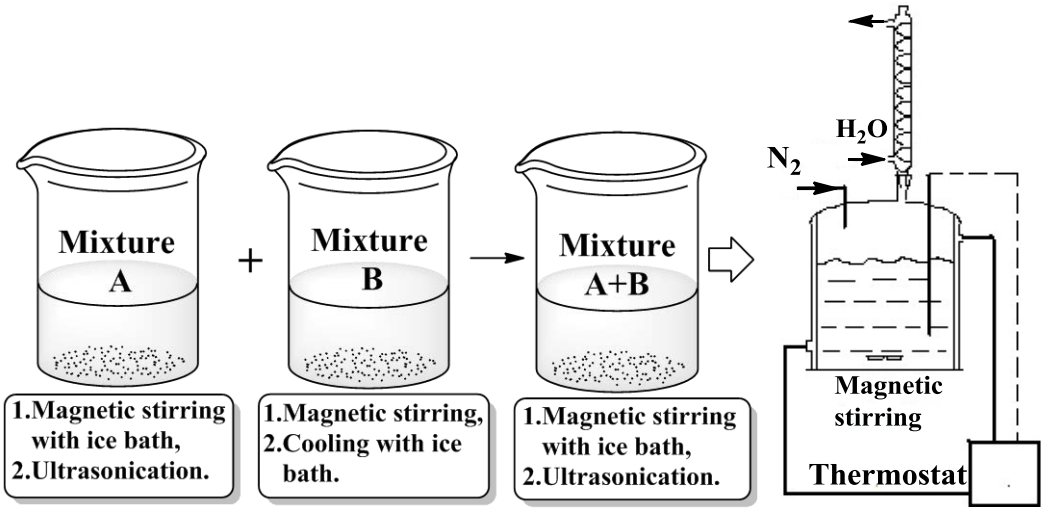

Figure 3.17 Procedure for the preparation of the miniemulsion and its polymerization to obtain PBA latexes.

Polymerization:

The as-prepared miniemulsion was first degassed by bubbling with pure nitrogen for 30 min under magnetic stirring in a stainless steel reactor at 20°C. The temperature of the reactor was then raised to 75°C. The polymerization was undertaken at that temperature for more than 3h with continuous stirring and was terminated by adding hydroquinone to the system. Polymer yields were determined by gravimetry.

The monomer solids content in our study is always maintain no more than 20%. There are two main difficulties to increase the solids content of a polymeric nanocomposite dispersion containing clay: i) increasing the solids content, while maintaining the ratio clay/monomer, means increasing significantly the clay/water ratio, and this implies a significant increase in the viscosity of the aqueous phase; ii) maintaining the stability of the latex during the polymerization is also more difficult because platelet to platelet interaction is enhanced (which increases the effective volume fraction of the particles in the dispersion) and hence coagulation risk is higher.

2.2.4. Influence of the cationic surfactant

Contribution of cationic surfactants to dispersion of the laponite in BA:

More than 95wt% of the LRD-grafted (LRD-Si) was precipitated out after the polymerization in the absence of CTAB, OTAB or DDAC. This is because in the

as-prepared mixture prior to miniemulsion polymerization, the suspension of LRD-Si was not stable without those cationic surfactants. Table 3.8 shows that among those three cationic surfactants, CTAB was the most effective at promoting the dispersion of LRD-Si in BA monomer and avoiding massive sedimentation during miniemulsion polymerization.

Table 3.8 Amounts of precipitates after the polymerization without or with a cationic surfactant in the miniemulsion of PBA-3%LRD-Si. Initial amounts of BA: 20g).

Cationic surfactant (0.8 g)	Without	DDAC	OTAB	CTAB
Amount of precipitates (g)	18.3	2.2	2.1	0.5

The cationic surfactant added in the miniemulsions, contains hydroxyl groups, which may offer a higher compatibility with the acrylic monomer, thus leading to intercalation or even exfoliation of clay platelets due to a better penetration of the monomer in the interlayer space. The stable dispersion of laponite particles in the miniemulsion droplets is the key step to promote the formation of PBA/LRD nanocomposite with high encapsulation efficiency of laponite particles.

2.2.5. Characterization of PBA/LRD-Si latexes

Thermogravimetric analysis (TGA):

It is not easy to directly detect the incorporated LRD-Si content via transmission electron microscopy since the polymer particles were too thick to be penetrated by the electron beam, but it is possible to calculate the presence of free, non encapsulated clay quantities by TGA.

The TGA thermograms of PBA, LRD, LRD-Si, PBA/LRD and PBA/LRD-Si nanocomposites are presented in Figure 3.18 and 3.19. The thermal degradation profile of PBA exhibits one main decomposition stage with starting at around 300 °C. The stage is attributed to the degradation of the whole material. Evidently, LRD is inorganic material with high thermal stability and PBA has very little ash after thermal degradation.

After the miniemulsion polymerization, aggregates were collected from the reactor

and the deposit after centrifugation. TGA was used to investigate the contents of LRD or LRD-Si consisting in the precipitates. As shown in Table 3.7, the initial amount of BA monomer is 20 g and that of LRD or LRD-Si added is 0.6 g for the preparation of PBA nanocomposite latex. Figures 3.18 and 3.19 show the TGA of the PBA latex and that of the precipitates, respectively. According to Figure 3.18, the amount of the LRD in the precipitate after the miniemulsion polymerization is about 0.3g. This means that only 50% of the LRD is incorporated in the PBA latex, even though CTAB is used as a surfactant. On the other hand, according to Figure 3.19, 85% of LRD-Si is incorporated in the PBA latex.

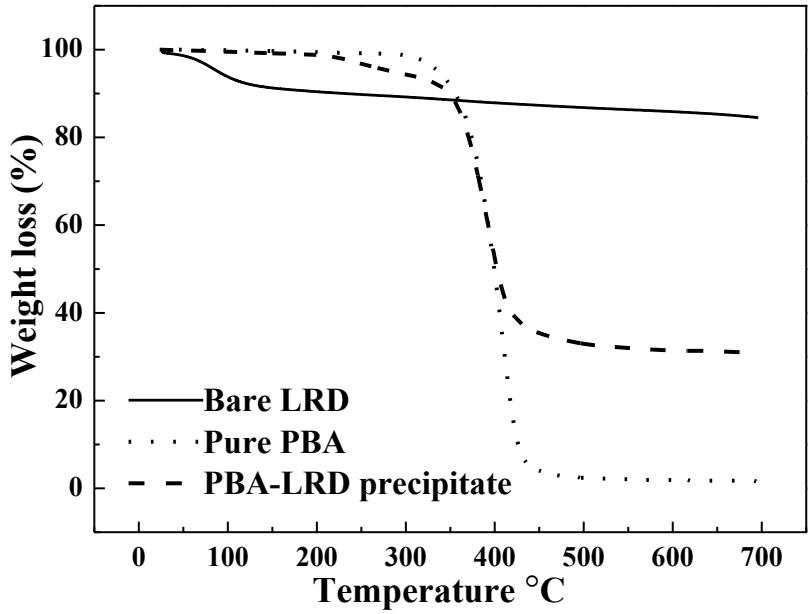

Figure 3.18 TGA traces of the bare LRD, pure PBA and PBA-3%LRD precipitate obtained from the miniemulsion polymerization. The initial amount of LRD is 0.6g and the amount of the precipitate after the polymerization is 0.9g.

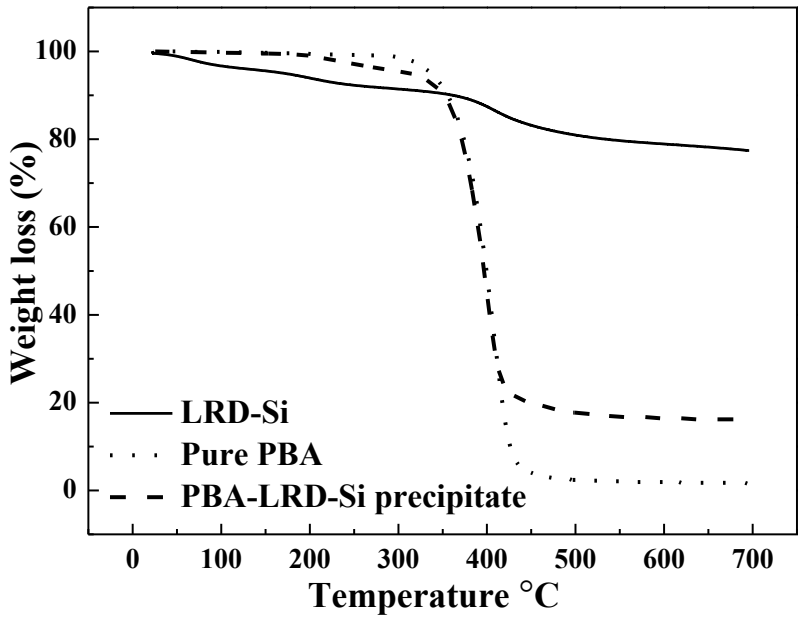

Figure 3.19 TGA traces of the bare LRD-Si, pure PBA and PBA-3%LRD-Si precipitate after miniemulsion polymerization. The initial amount of LRD-Si is 0.6g and that of the precipitate after polymerization is 0.5g.

The above results show that the employ of a cationic surfactant such as CTAB allows obtaining PBA-LRD and PBA-LRD-Si latexes. As a matter of fact, the silane grafted LRD-Si nanoparticles are well suspended in the miniemulsion of BA monomer and a high percentage of clay are incorporated in the PBA latex particles after polymerization. The MPTMS silane molecules coupling on the LRD-Si nanoparticles had reacted with the BA monomer during the polymerization could account for the succeeded encapsulation of clay in PBA particles.

Transmission electron microscopy (TEM):

The particle sizes were determined by TEM and dynamic light scattering (DLS). All the PBA particles remain spherical after the polymerization and their diameter is around 100 nm which is consistent with the average diameters determined by dynamic light scattering.

A direct representation of sample structure can be depicted by TEM. The limitation of this method lies in the fact that often a distinction of different phases is only possible after staining the sample. TEM suffers from difficulties in sample preparation.

To prevent the latex particles from beam damage, the samples were also negatively

stained with UAc. TEM was used to examine the particle morphology in the wet state. The results depend strongly on the ability to induce a contrast between different structures; through different electron densities in the particle. Figure 3.20 shows representative TEM images of PBA latex particles containing LRD-Si. Dark "filaments" are observed on the surface of some particles, they correspond to laponite crystallites seen edge-on with respect to the observation direction and exhibiting a strong diffraction contrast. Laponite sheets with a different orientation do not generate much contrast and can hardly be detected in the images. The black line the Figure 3.20b is a LRD-Si platelet with its basal plane parallel to the electron beam. The individual LRD platelet is disk-shaped, with a lateral diameter of 13~30nm and a thickness of ~1nm.

Some of the spherical particles are free of clay platelets (nonetheless, the spherical shape without black line or disk does not necessarily imply there is no clay platelet inside). The basal plane orientation of LRD-Si which was more perpendicular to the electron beam had reduced the diffraction contrast of the platelet, effectively making it invisible.

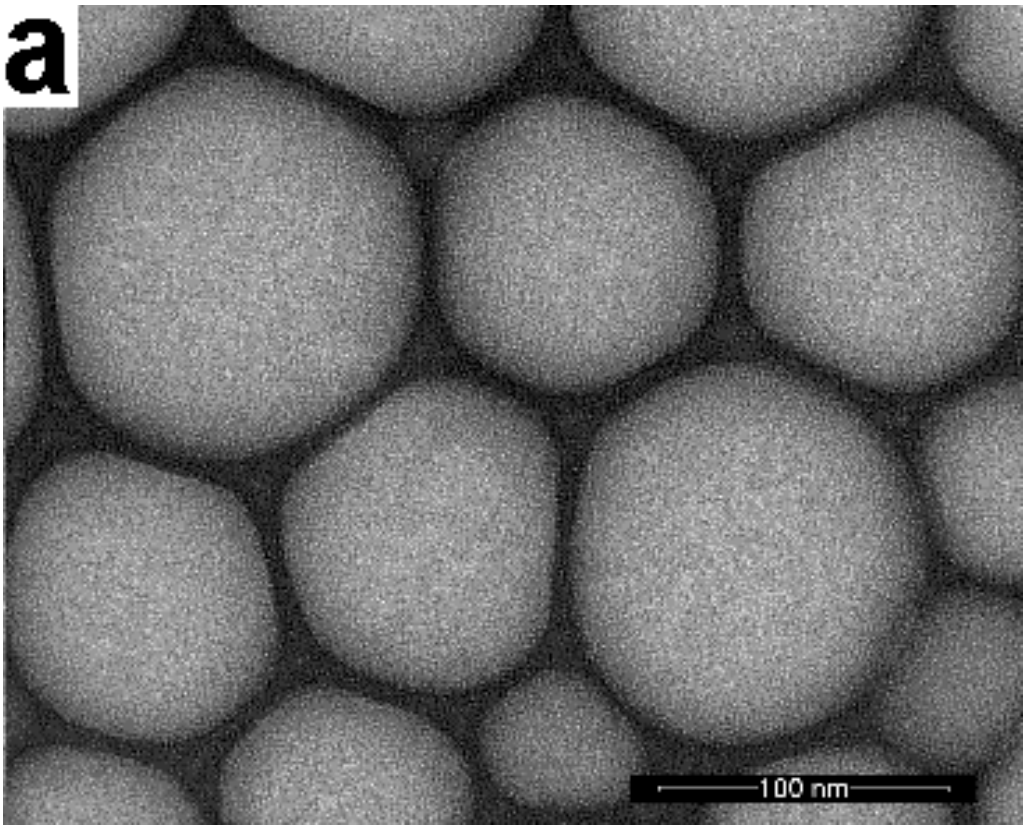

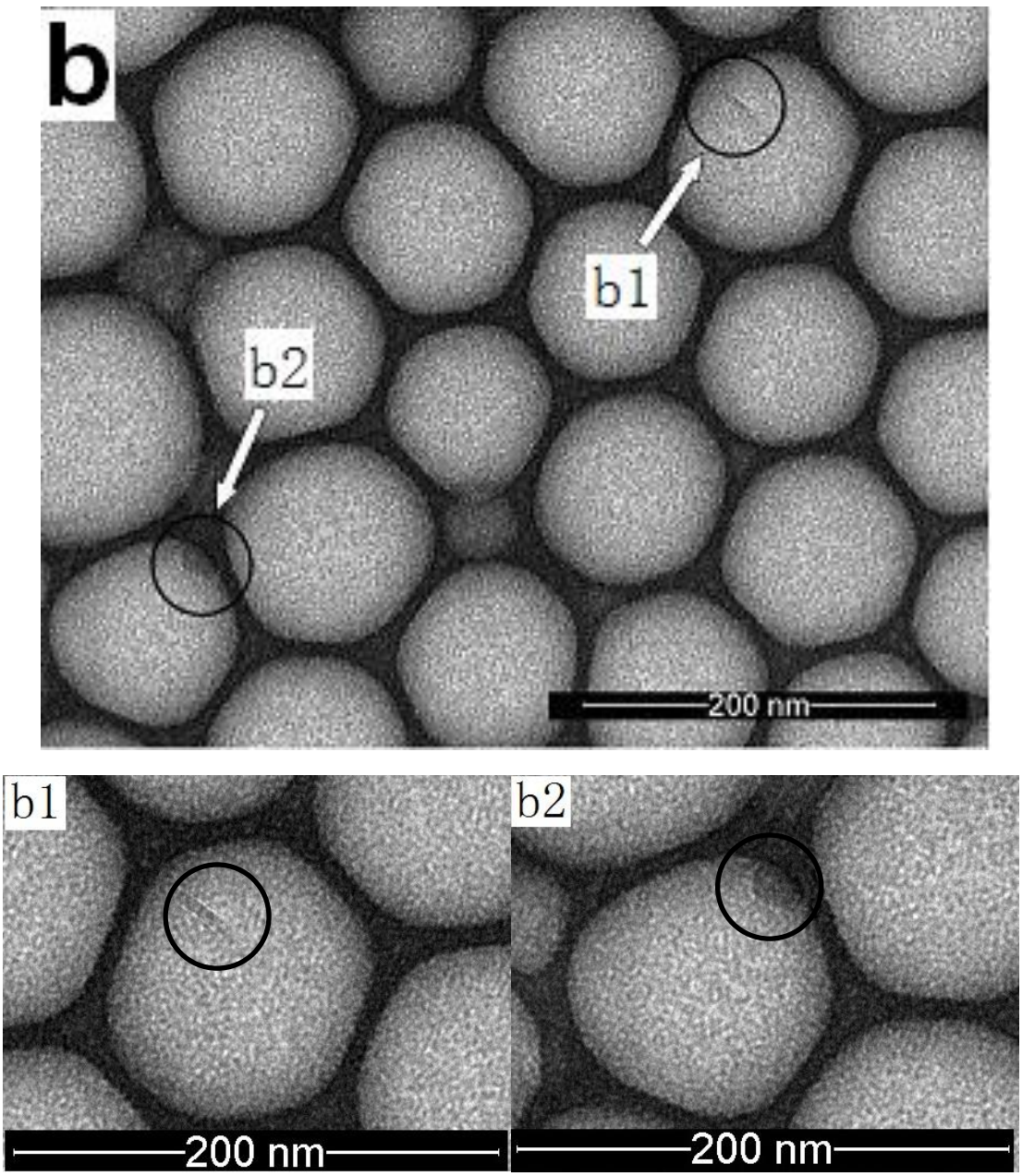

Figure 3.20 TEM images of (a) PBA-3%LRD latexes, (b) PBA-3%LRD-Si latexes and two enlarged images of b. The laponite content in the latexes is 3 wt%.

Figure 3.20b1 and 3.20b2 shows TEM images of individual PBA-LRD-Si spherical nanoparticles, with a diameter ranging from 70 to 130 nm indicating a relatively narrow particle size distribution.

Soxhelt extraction:

The degree of crosslinking was tried to be determined by Soxhelt extraction in which the free chains of PBA is dissolved in solvent and removed. All the PBA/LRD-Si

composites with different content of LRD-Si have been explored by Soxhelt extraction.

After drying in the vacuum oven at 60 °C over night, the dried PBA/LRD-Si was extracted with 2-butanol for 48h by Soxhelt extraction. Then, after the Soxhelt extraction, it can be discovered that the PBA/LRD-Si composites were swelling. The solvent left in PBA/LRD-Si composite was eliminated by drying it in vacuum oven at 60 °C over night again and the PBA/LRD-Si composite did not change its weight by comparing with the weight of initial dry PBA/LRD-Si composite before the Soxhelt extraction. This indicates the crosslinking degree cannot be found out by Soxhelt extraction.

Furthermore, no sediment was appeared when the PBA/LRD-Si composite was put in its solvent after 2 days, indicating the formation of a heavy crosslinked polymer network in the composite particles. This phenomenon is accordance with the result of Soxhelt extraction.

The LRD particles with grafted MPTMS in which exhibited many alkyl groups and acted as a crosslinking agent in the copolymerization. When the concentration of allyl groups exceeded a critical value as the weight fraction of LRD-Si and the average number of grafted MPTMS molecules per PBA particle increased, a crosslinked polymer network would be formed, in which the LRD-Si particles acted as the 'crosslinking sites'.

3. Conclusion

The PBA mini-emulsions by using surfactant SDS, Brij78 and Brij700 with co-stabilizer hexadecane are critically stable systems, with the particle size around 100 nm.

The trial of OMMT encapsulation in the PBA latex particles could not succeed because of the large size of OMMT particles and it is impossible to achieve an encapsulation of OMMT in the nanosize miniemulsion. Laponite RD could be a better choice for the clay encapsulation when the length of this clay is only around 25 nm.

The modification of laponite by coupling agent MPTMS is confirmed and is very

useful for clay encapsulation within polymer particles because the double bonds of MPTMS are helpful for the combination of laponite with PBA particles through copolymerization. The LRD particles with grafted MPTMS exhibiting many alkyl groups acted as a crosslinking agent in the copolymerization. Cationic surfactant is indispensable for obtaining a well dispersion of laponite in the BA monomer.

By the examination of TEM, due to there is no small patches of LRD agglomerates existing in the TEM images, it is assumed that laponite in PBA particle is not forming small tactoids but well exfoliated.

Chapter 4. Blending of PLA and its properties' improvement

This chapter was divided into three sections. The first one described the dispersion of PBA particles blended with PLA matrix. The second section indicated the efforts we did to improve the dispersion of PBA particles in matrix with some additions. The last section contained the preparation of PBA-PMMA core-shell particles, the examinations for core-shell particles and the morphologies of the blending of core-shell particles with PLA matrix.

1. PBA particles and PLA blends

1.1. PBA/PLA blends

PBA latexes were demulsified by ethanol and washed by deionized water, then dried at 60°C for 24h in a vacuum oven before melt blending in microcompounder. To study the effect on mechanical properties and morphologies for PLA blending with various PBA components, it was necessary to make the comparisons at a constant PBA content. The concentration of the PBA in the PLA blends was fixed at 10 or 20 wt%.

The blends of PLA and dried latexes were prepared in a microcompounder (DSM Xplore) at a screw speed of 60 rpm for 10 min at 180°C. The neat PLA was subjected to the same mixing treatment so as to have the same thermo-mechanical history as the blends. The samples were immersed and kept in liquid nitrogen for 10 min and then broken cryogenically.

The morphology of pure PLA and PLA/PBA blends was investigated with scanning electron microscope (SEM). Prior to the SEM analyses, the surfaces of these materials are etched with 2-butanol, a good solvent of PBA and a non-solvent for the PLA.

The SEM micrographs of cryofractured surfaces showed a particle-dispersed morphology caused by phase separation. That is, PBA particles in the PLA matrix

with smooth, distinct particle interfaces, indicating poor interfacial adhesion, were observed.

The average volume diameter dv of the PBA particles can be calculated by the equation 4.1:

$$dv = \frac{\sum di^4}{\sum di^3} \tag{4.1}$$

Different temperatures for PBA/PLA blended in the microcompounder were also carried out prior to our sample preparations for mechanical tests. The results in Figure 4.1 reveal that within these three different operational temperatures, temperature at 180°C could be a suitable choice for the PBA/PLA blends preparation when a higher might increasing the opportunity of collision between the PBA particles and would also cause a degradation problem for PLA matrix.

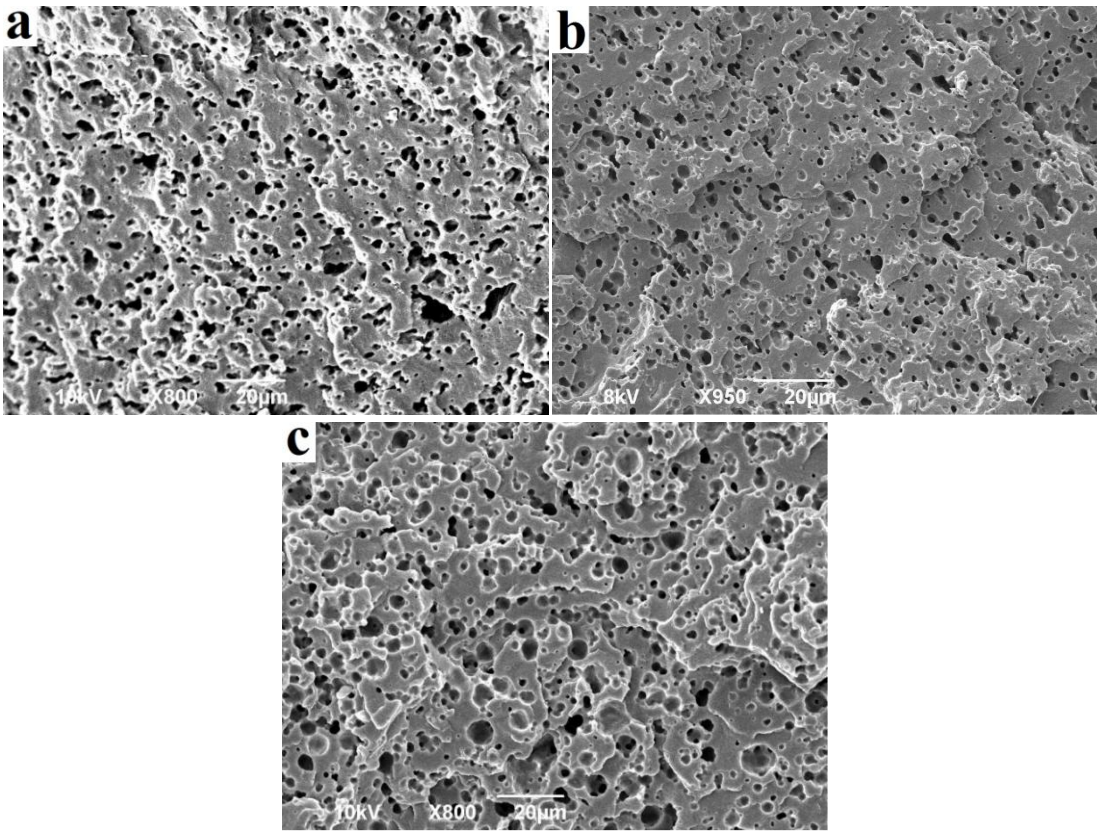

Figure 4.1 The PBA particle distributions of PBA/PLA (20/80) blends after melting blended in microcompounder at the same rotational speed of screw (60rpm) with different temperatures: (a) 170°C, dn=1.35 µm, dv=1.84 µm; (b) 180°C, dn=1.12 µm, dv=1.58 µm; (c) 200°C, dn=2.25 µm, dv=2.10 µm.

Considering the influence of the shear rate in the microcompounder, theoretically, if only the failure mechanisms are considered, the particle diameter of the dispersed phase should decrease as the shear rate increases [115]. Experimentally, several authors have observed that the particle size of the dispersed phase passes through a minimum when the shear rate increases [116-118]. Thus increasing the rotational speed of the screw changes the failure and coalescence mechanism in mixtures. Comparison of morphologies of the blends prepared with different speeds for exploring the mechanism of failure and coalescence were not performed in detail and we only tested two different speeds for the twin screws in our research. From the Figure 4.2, with the different rotational speed of screw in microcompounder, the values of dn and dv indicate with a higher screw speed would not offer a better influence for the PBA particle dispersion in our study. Therefore we only chose a medium rotational speed at 60rpm for the screw in the operations of blending.

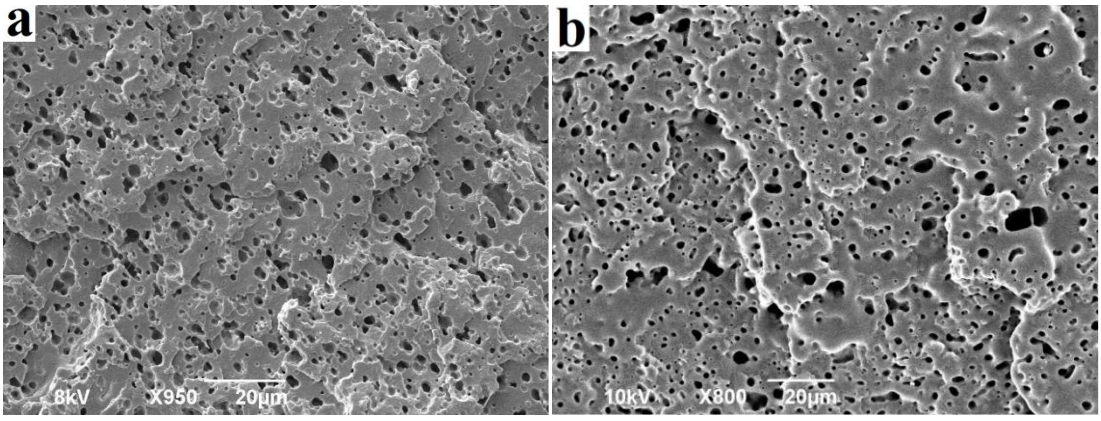

Figure 4.2 The PBA particle distributions of PBA/PLA (20/80) blends after melting blended in microcompounder at the same temperatures (180°C) with different rotational speed of screw: (a) 60rpm, dn=1.12 µm, dv=1.58 µm; (b) 75rpm, dn=1.03 µm, dv=2.11 µm.

Meanwhile, from Figure 4.3, it can be seen that there is no change in the morphology when the mixing time in the microcomponder is increased from 10 to 15 minutes to a mixture of PBA/PLA (20/80).

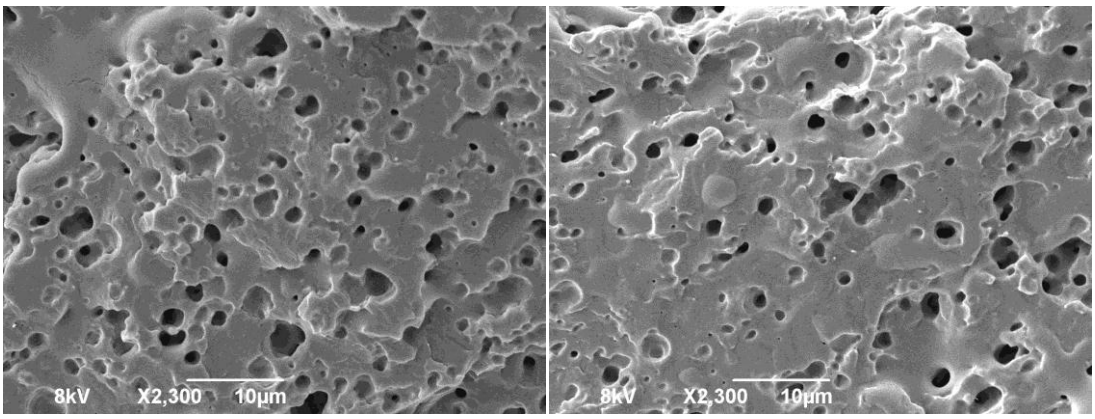

Figure 4.3 Influence of the time on extrusion of mixtures PBA/PLA (20/80). 10 mins of mixing (left photo) and 15 mins of mixing (right photo).

According to Favis [119], morphology is stabilized during the first minutes of the extrusion. We also observed that the morphology does not change by increasing the time of the extrusion. However, an increase in the time of extrusion may affect the molecular weight of the PLA matrix by degradation so that we used 10 mins of extrusion for all PLA blends in our studies.

For the PBA/PLA (20/80) blend, diameters of PBA domain range from 0.2 to 3 µm in Figure 4.6. The mean particle size dn of PBA was around 1.2-1.8 µm. The domain size is very large due to the immiscibility between the two components. It is seen that the interface between the two phases is very weak, indicating a totally incompatible polymer blend.

To address the reason that the blend morphology was so different between the PBA/PLA (10/90) blend (in Figure 4.5) and PBA/PLA (20/80) blend (in Figure 4.6), we have to consider the coalescent effect. There are some reports about the composition effect on the final particle size in immiscible polymer blend system. Sundararaj and Macosko [118] reported that the particle size distribution broadens at higher concentrations because breakup and coalescence are occurring concurrently during blending at higher concentrations. This fact can partially account for the morphology difference of these two blends. Thus, the PBA/PLA (20/80) blend had a broader filler particle size distribution, and as its composition was twice than that of the PBA/PLA (10/90) blend, many large cavities could be observed in SEM image.

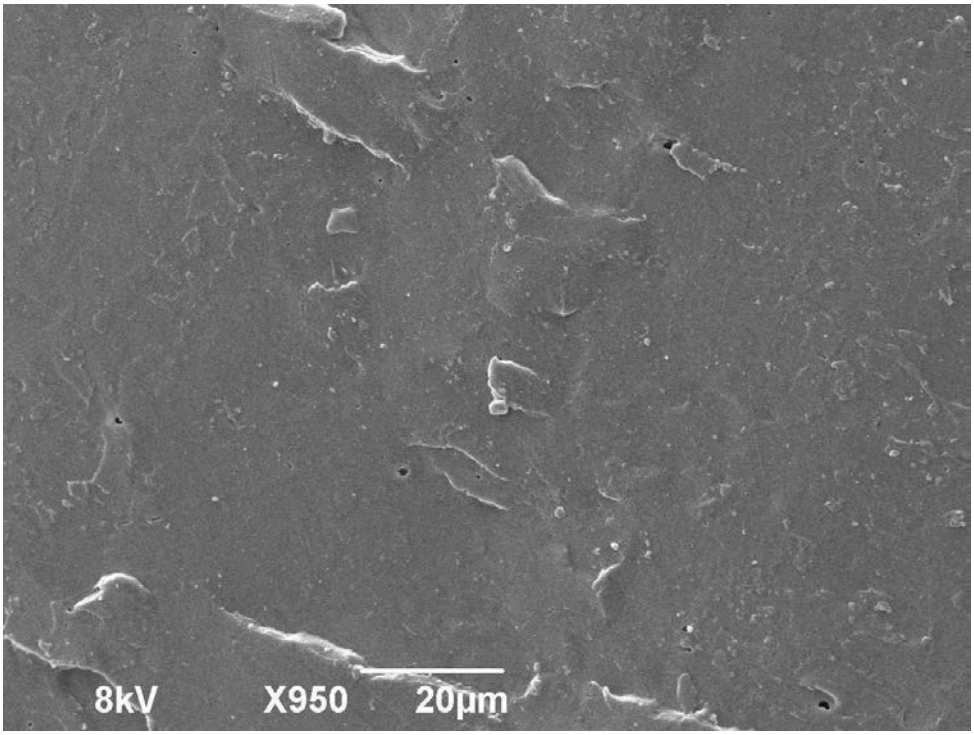

Figure 4.4 SEM images of pure PLA.

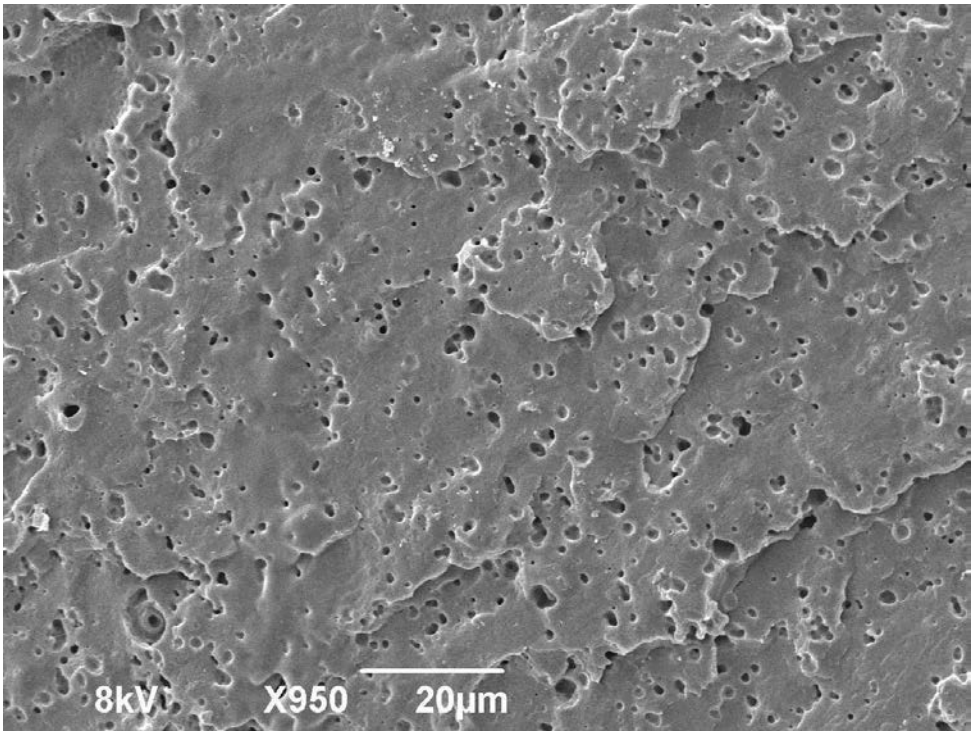

Figure 4.5 SEM images of PBA/PLA (10/90) blend. dn=0.78 µm, dv=1.56 µm.

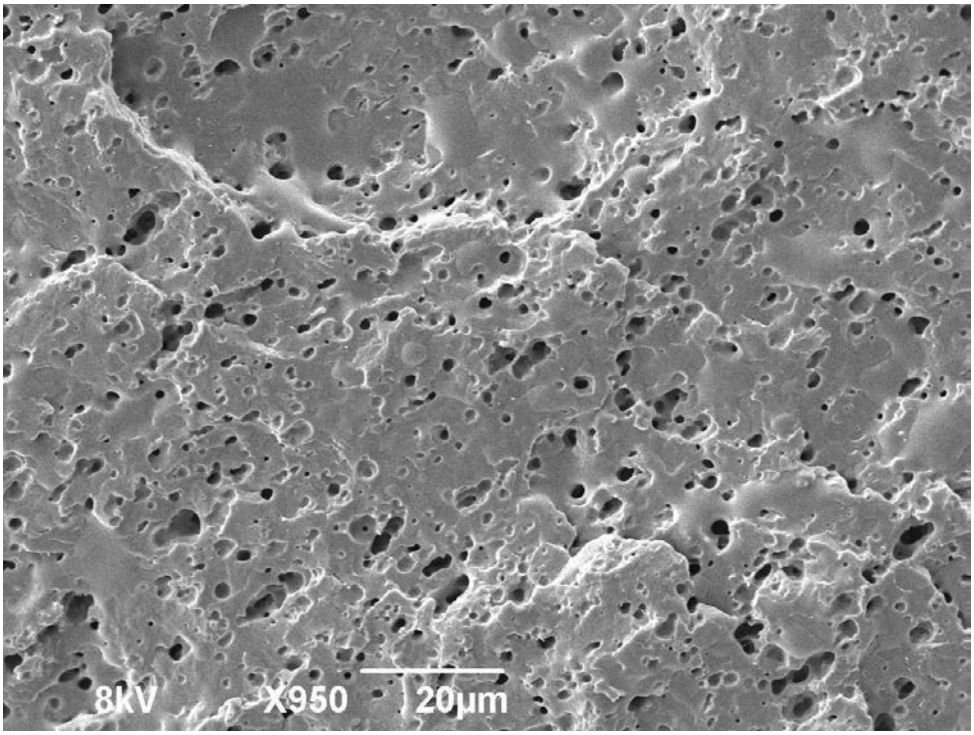

Figure 4.6 SEM images of PBA/PLA (20/80) blend. dn=1.12 µm, dv=1.78 µm.

As demonstrated in Figure 4.7 and Figure 4.8, when the surfactant such as SDS or Brij 78 was not eliminated and washed out by ethanol, the pore size of PBA/PLA blend blends did not decrease but turn to be a little bigger than that of pure PBA/PLA blend. It means the miscibility of Brij78 and PLA did not minimize the occurring of PBA coalescence when PBA particles were blended with PLA matrix. The surfactant Brij78 could not stick to the PBA particles might account for the phenomenon and the existence of Brij78 reduce the viscosity of PBA/PLA mixture and facilitate the movement of PBA particles which make the coalescence of PBA become more easier and the final size of PBA particle in the blends were bigger. This means the surfactant of Brij 78 can not act as a compatibilizer for PBA/PLA blends.

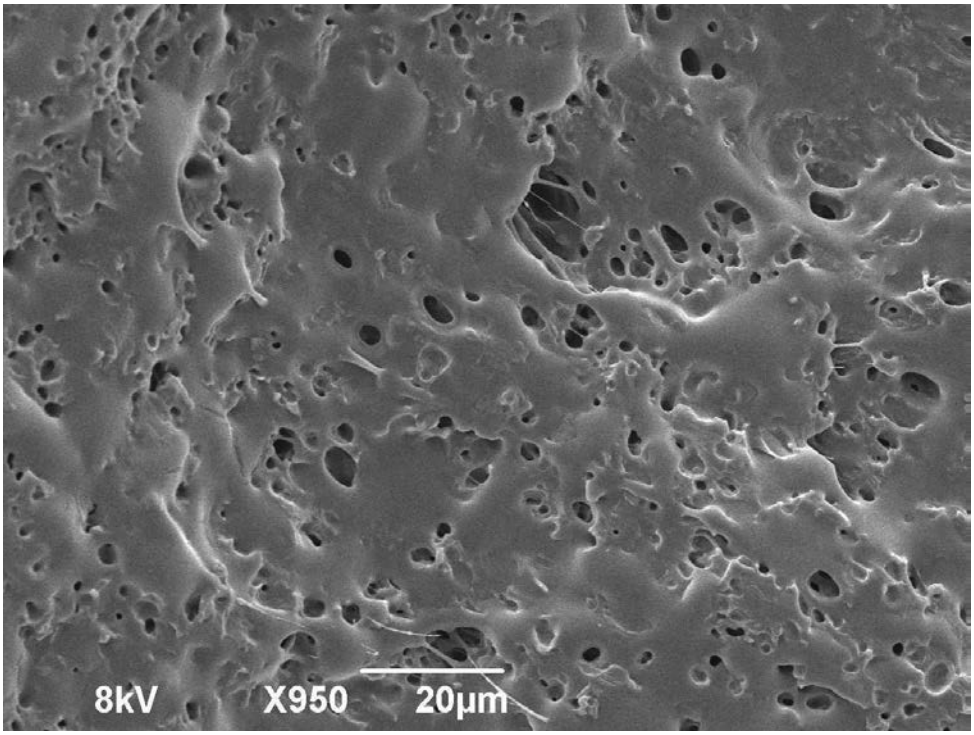

Figure 4.7 SEM images of PBA/PLA (20/80) blend with surfactant SDS. dn=1.5 µm, dv=2.7 µm.

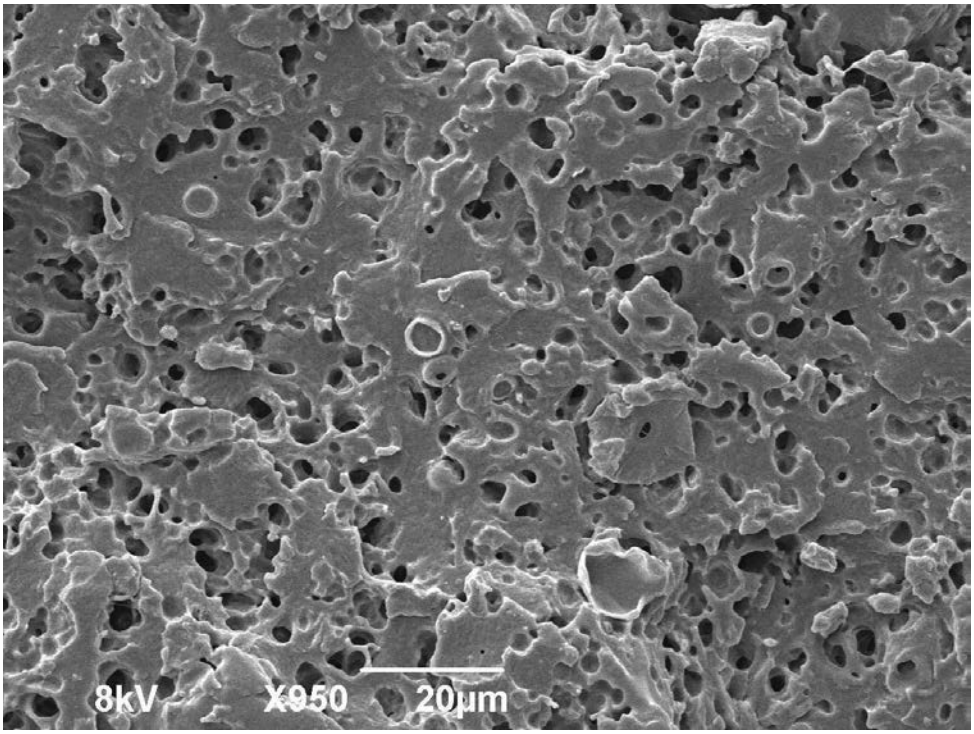

Figure 4.8 SEM images of PBA/PLA (20/80) blend with surfactant Brij78. dn=2.03 µm, dv=2.95 µm.

1.2. PBA-LRD-Si/PLA blends

PBA-LRD or PBA-LRD-Si composite latexes were also demulsified by ethanol and washed by deionized water, then dried at 60°C for 24h in a vacuum oven before melt blending. The concentration of PBA in the blends was fixed at 20 wt%. The blends of PLA and dried latexes were prepared in a microcompounder (DSM Xplore) at a screw speed of 60 rpm for 10 min at 180°C.

Figure 4.9 shows the SEM images of the PBA/PLA (10/90), PBA/PLA (20/80), PBA-5%LRD/PLA (20/80), PBA-2%LRD-Si/PLA (20/80), PBA-3%LRD-Si/PLA (20/80) and PBA-5%LRD-Si/PLA (20/80) blends together with that of the pure PLA. The surfaces of the PBA/PLA (10/90), PBA/PLA (20/80) and PBA-3%LRD/PLA (20/80) blends exhibit holes while the surfaces of the three PBA-LRD-Si/PLA (20/80) blends (d) to (f) trend to be smooth. Concerning the average diameter of the holes in these blends which corresponds to the etched PBA domains, it is about 0.8, 1.1, 2.7, 1.9 and 1.4 μm for blends (a), (b), (c), (d) and (e), respectively. As for blend (f) which contains 5%LRD-Si, there are almost no holes in the surface after etching, confirming that the PBA-LRD-Si particles are crosslinked during the miniemulsion polymerization by the MPTMS grafted laponite (LRD-Si). The degree of crosslinking is enhanced with increasing the LRD-Si content. Meanwhile, the values of these holes in the blends are significantly higher than the average diameter of the PBA nanoparticles recovered from miniemulsion polymerization (~100nm). This implies that they are likely agglomerated during the drying stage of the latexes before blending with the PLA. Agglomeration during the melt blending could also be possible.

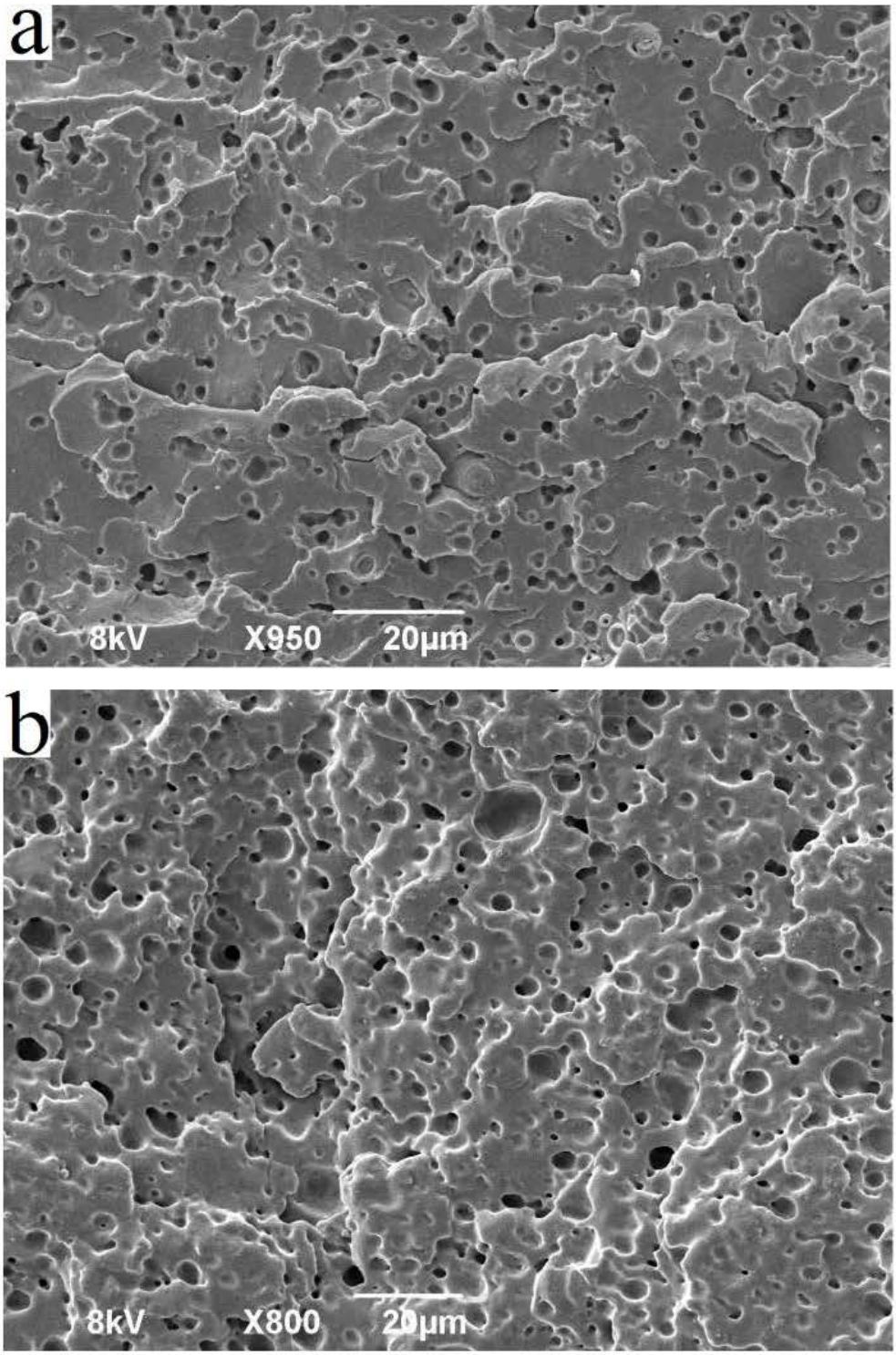
a
8kV X950 20µm
b
8kV X800 20µm

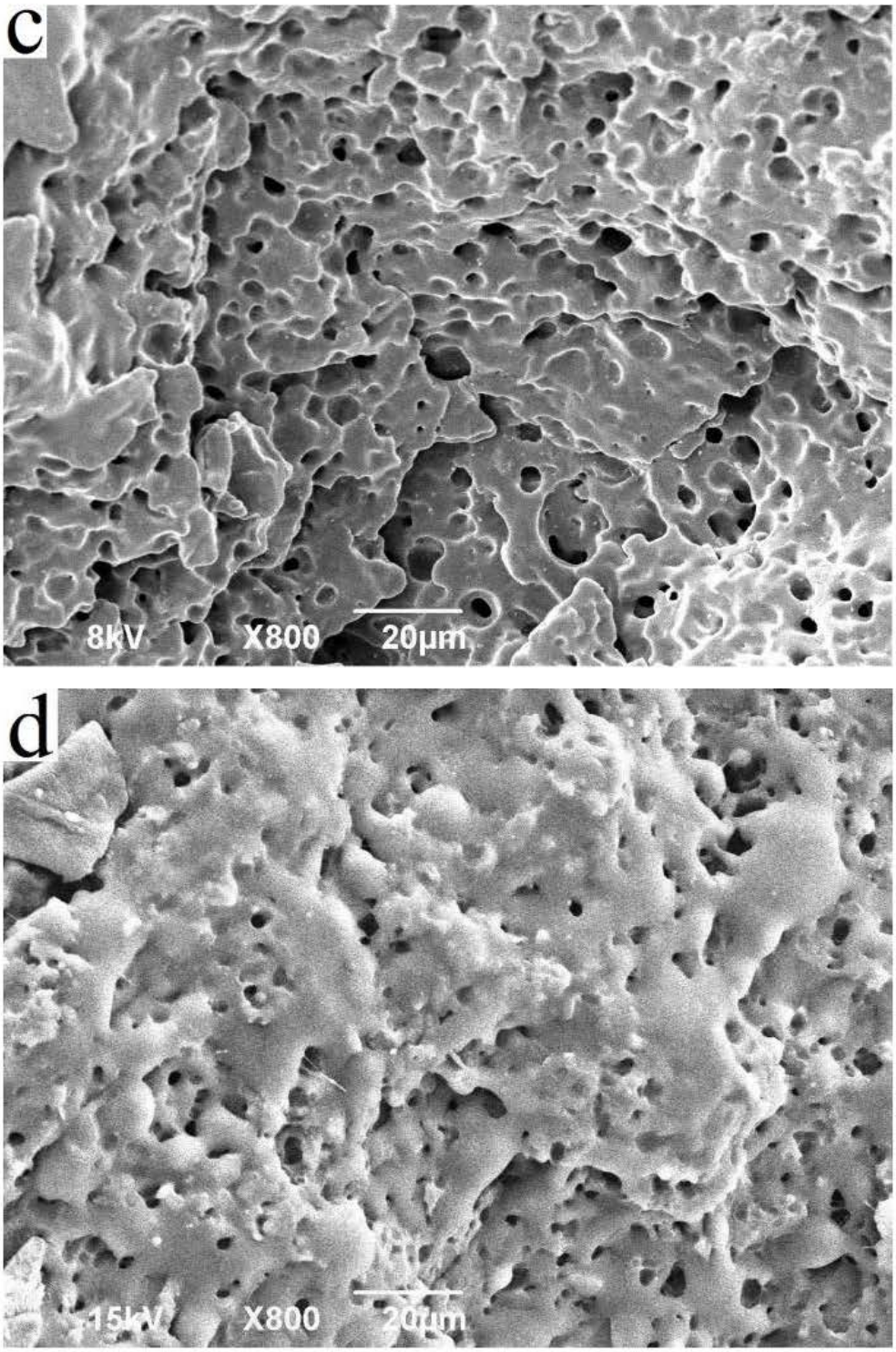
c
8kV X800 20μm
d
15kV X800 20μm

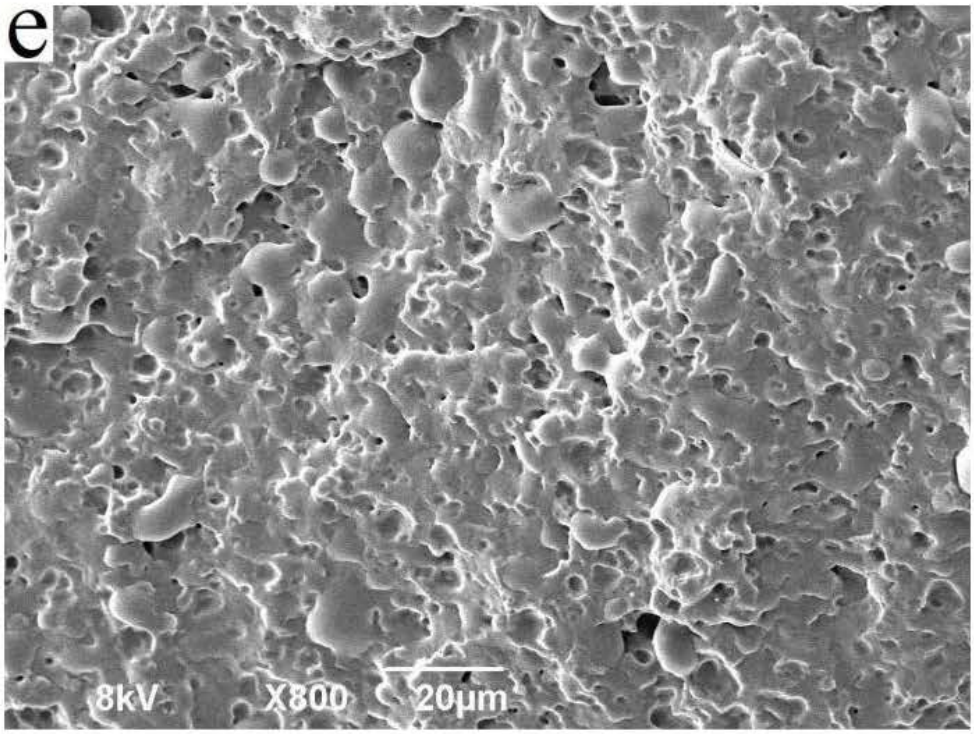
e
8kV
X800
20μm

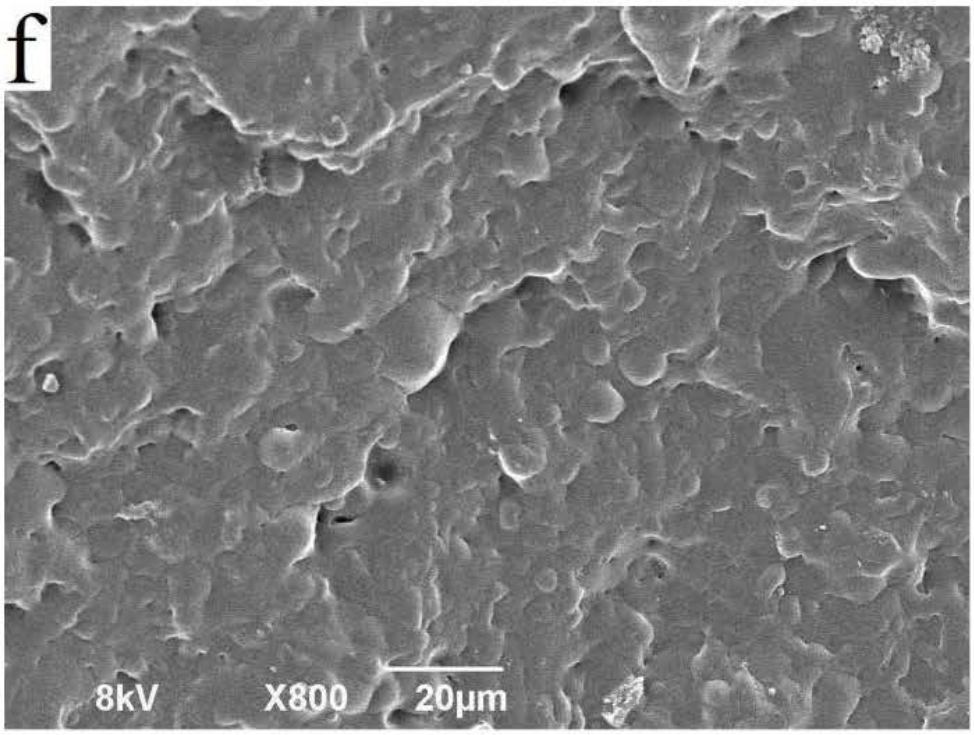
f
8kV
X800
20μm

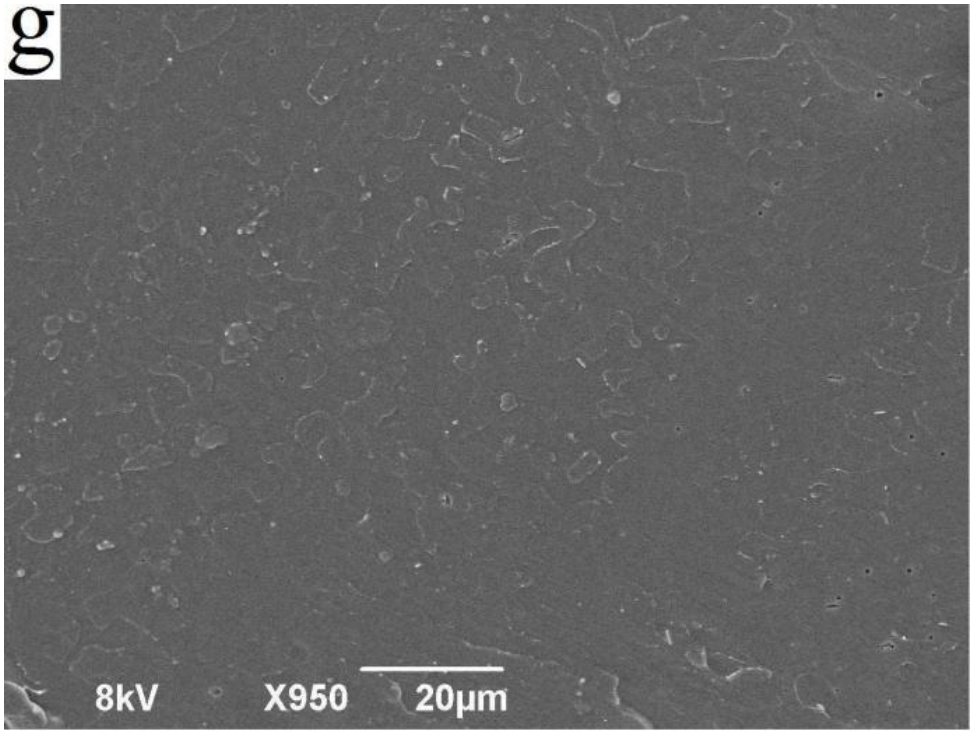

Figure 4.9 SEM images of (a) PBA/PLA (10/90) blend, dn=0.78 µm, dv=1.56 µm (b) PBA/PLA (20/80) blend, dn=1.12 µm, dv=1.78 µm (c) PBA-5%LRD/PLA (20/80) blend, dn=2.74µm, dv=4.08µm (d) PBA-2%LRD-Si/PLA (20/80) blend, dn=1.95µm,dv=3.57µm (e) PBA-3%LRD-Si/PLA (20/80) blend, dn=1.44µm,dv=2.41µm (f) PBA-5%LRD-Si/PLA (20/80) blend, and (g) pure PLA.

The thermal properties of PLA and PBA/PLA blends were investigated using DSC. The data obtained from the first heating cycle provide the thermal history of the injection-molded samples, while the data obtained from the second heating cycle allows for a direct comparison of different materials after erasing the thermal history through the first heating cycle.

Table 4.1 shows the DSC results of neat PLA and the PBA/PLA blends with or without laponite. The T_g of PBA increased slightly with the addition of LRD-Si, which is consistent with the DMTA results (Table 5.1). The results can be attributed to molecular interactions between the PBA chains and the crosslinking agent LRD-Si. However, the T_g value of PLA obtained from DSC was lower than the T_α value obtained from DMTA, which can be attributed to the different measuring mechanisms for DMTA and DSC.

Table 4.1 DSC data of the PLA, PBA and several PBA/PLA blends.

Samples	*T_g1 (°C)*	*T_g2 (°C)*
Pure PLA	-	59
Pure PBA	-48	-
PBA/PLA (20/80) blend	-48	59
PBA-2%LRD-Si/PLA (20/80) blend	-46	59
PBA-3%LRD-Si/PLA (20/80) blend	-46	59
PBA-5%LRD-Si/PLA (20/80) blend	-46	59
PBA-5%LRD/PLA (20/80) blend	-47	61
PBA/PLA/LRD (20/79/1) blend	-48	57

For the PBA particles containing LRD-Si, the T_g of PBA was a little bit higher than that of the pure PBA (around 2°C). The T_g of PLA was not affected by the existence of PBA particles, which means the miscibility between the two materials is very poor. When the LRD was directly added in the mixture of PBA/PLA, the T_g of PLA was lower. However, with the unmodified LRD added in PBA miniemulsion polymerization, the T_g of PBA was not increased but the T_g of PLA was higher. These could because that the unmodified LRD was located at the surface of PBA particles and when they were blended with PLA, the unmodified LRD was exfoliated in the PLA matrix, which lead the thermal stability of PLA increasing.

2. Reactive particles and PLA blends

2.1. Particles with polymer surfactant and their PLA blends

Li and Shimizu [7] investigated the miscibility and mechanical properties of PLA/poly(ethylene oxide) (PEO) blends. They demonstrated that PLA/PEO was a miscible blend and the elongation at break of the blend showed a marked increase with PEO concentration.

Poly(ethylene glycol) methyl ether methacrylate (PEGMEM, Mn = 950) is a polymer surfactant with double bond. The part poly(ethylene oxide) is hydrophilic group and miscible with the PLA. Another part with the double bond is the hydrophobic group

which could react with the monomer droplet surface. After miniemulsion polymerization, the polymer surfactant may not only simply adhere to the surface of PBA particles but can have chemical bond connecting with the PBA particles. When the PBA particles surrounded by PEGMEM chain are mixed with PLA matrix, the compatibility between PBA and PLA was supposed to be improved.

2.1.1. Particles preparation

Poly (ethylene glycol) methyl ether methacrylate (PEGMEM, Mn=950) was added as a surfactant in the miniemulsion polymerization to prepare PBA latexes.

Table 4.2 Recipe used for the preparation of PBA latex particles by miniemulsions polymerization with the surfactant PEGMEM.

Mixtures	***Components***	***Amount(g)***	***Concentration***
Oil phase	BA	20	20 wt%[a]
	AMBN	0.4	2 wt%[b]
	HD	0.8	4 wt%[b]
Water phase	H_2O	70-77	70-77%[a]
	PEGMEM	2-8	0.03-0.12mmol[c]

[a] Based on total recipe. [b] Based on monomer. [c] Based on aqueous

The efficiency of the surfactant PEGMEM was not as well as Brij78 or Brij700. Even though the concentration of PEGMEM in the system has reached 8wt% (8g PEGMEM was added), the viscosity of the miniemulsion before polymerization was high, while the final product obtained was still a bunch of polymer agglomeration and was not forming a stable system at all.

Owing to the poor efficiency of the surfactant PEGMEM, thus, PEGMEM was mixed with Brij 700 or Brij 78 to form a complex surfactant before added in PBA miniemulsion polymerization. Within the complex surfactant, the amount of PEGMEM was fixed at 2g and the quantity of Brij 700 or Brij 78 was varied from 0.25g to 2g.

When the amount of Brij 700 or Brij 78 was less than 0.5g in the complex surfactant, the emulsion was not stable and more than 70wt% of the PBA would precipitate after reaction. While the amount of Brij 700 or Brij 78 was higher than 0.5g in the complex

surfactant, the precipitation after miniemulsion polymerization was less than 1g (5wt% of the PBA). As listed in chapter 3, with only 2g of Brij 700 or Brij 78 in the miniemulsion polymerization, that would have 6g of precipitation after the polymerization. These results means the complex surfactants had a better influence for stability of PBA latex and is more efficient as a surfactant in comparison with the efficiency of pure PEGMEM or Brij78 and Brij700 for miniemulsion polymerization.

2.1.2. Blend with PLA and the morphologies

With the addition of PEGMEM, even though the PBA latex has been washed by ethanol after reaction, the PBA latex did not precipitate obviously after washing which means some of the PEGMEM was sticking to the surface of PBA particles and do act like a surfactant even if its efficiency was not as effective as SDS or Brij78.

After washing by ethanol, particle size was examined by DLS. The size of PBA particles was between 170 nm to 661 nm by using complex surfactant-[0.5g Brij700 with 2g PEGMEM]. When the complex surfactant [1g Brij700 with 2g PEGMEM] was used, the particle size was between 81nm to 193 nm.

All the PBA latexes were demulsified by ethanol and heavily washed by deionized water to diminish the free surfactant in the latex, then dried at 60°C for 24h in a vacuum oven before melt blending. The concentration of PBA in the blends was fixed at 20 wt% also. The blends of PLA and dried PBA latexes were prepared in a microcompounder at a screw speed of 60 rpm for 10 min at 180°C.

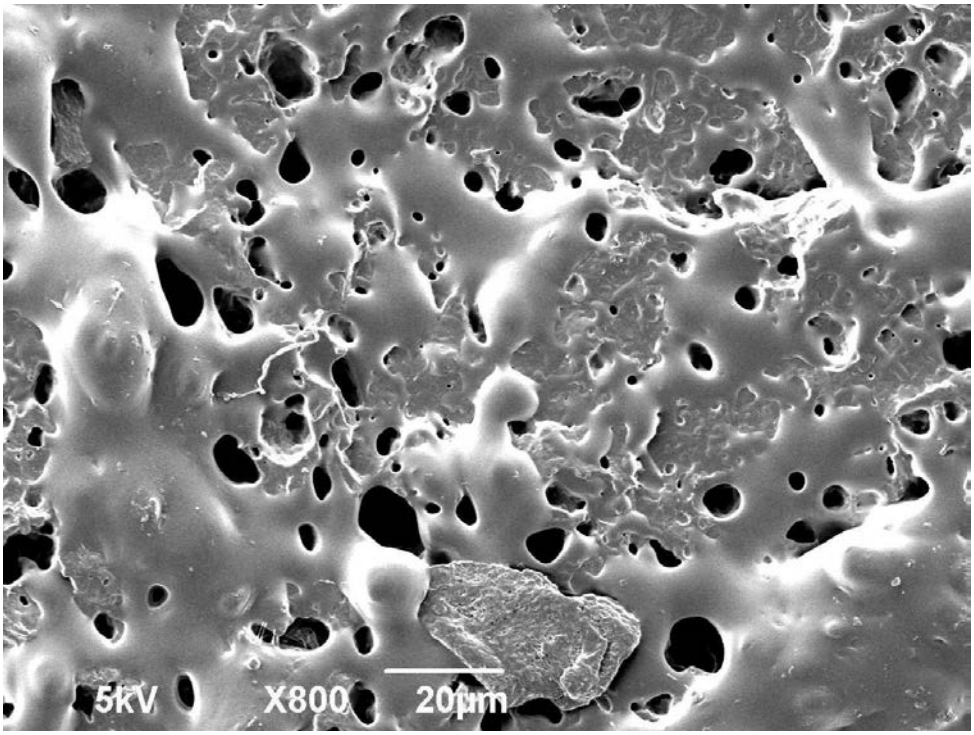

Figure 4.10 SEM images of PBA/PLA (20/80) blend while composite surfactant-0.5gBrij700 with 2g PEGMEM was used in the preparation of PBA latex. dn=1.57 µm, dv=5.05 µm.

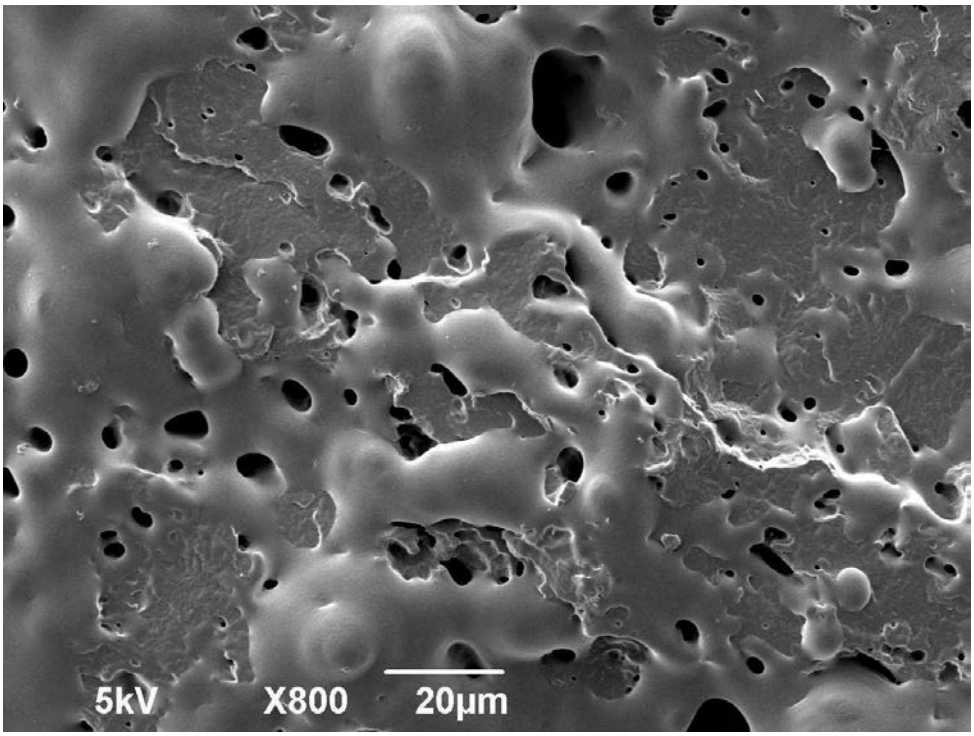

Figure 4.11 SEM images of PBA/PLA (20/80) blend while composite surfactant-1 gBrij700 with 2g PEGMEM was used in the preparation of PBA latex. dn=1.63 µm, dv=3.89 µm.

By analyzing the pore distribution from SEM images in Figure 4.10 and Figure 4.11, the polymer surfactant PEGMEM did not improve the dispersion of PBA particles in PLA matrix. The influence of PEGMEM for compatibility of these two polymers was not as good as supposed to be.

In consideration of the PEGMEM in the composite surfactant was only 2g for the miniemulsion polymerization and the product was washed by ethanol after the reaction, the amount of PEGMEM left in the product could not be high. From the present results, it can be presumed that the quantity of PEGMEM sticking to the PBA particles was too low and was not enough to produce the best possible results for improving compatibility of the PBA/PLA blend. For the further study, we can consider to enhance the amount of PEGMEM in the complex surfactant to insure the final latex particles can be surrounded by more PEGMEM molecules in order to improve the distribution of the elastomer particles in the PLA matrix. On the other side, as the existence of PEGMEM in the polymer matrix will weaken the tensile strength of the blend, the addition of PEGMEM in the emulsion should be adjusted in a range to find an optimal value.

2.2. Reactive PBA-LRD

Silane treatment:

3-Aminopropyltriethoxy silane (silane 1) and 3-Glycidoxypropyltrimethoxy silane (silane 2) were used as coupling agents to modify the surface of LRD. The reaction taking place in surface treatment was shown as Scheme 4.1.

Silane 1 (3A): 3-Aminopropyltriethoxy silane

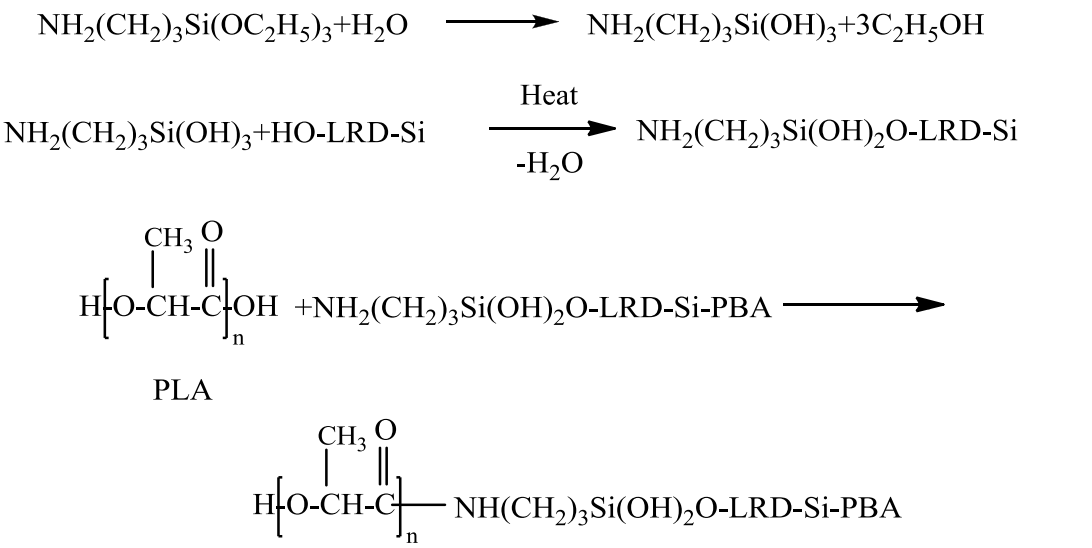

silane 2 (3G): (3-Glycidoxypropyl)trimethoxysilane

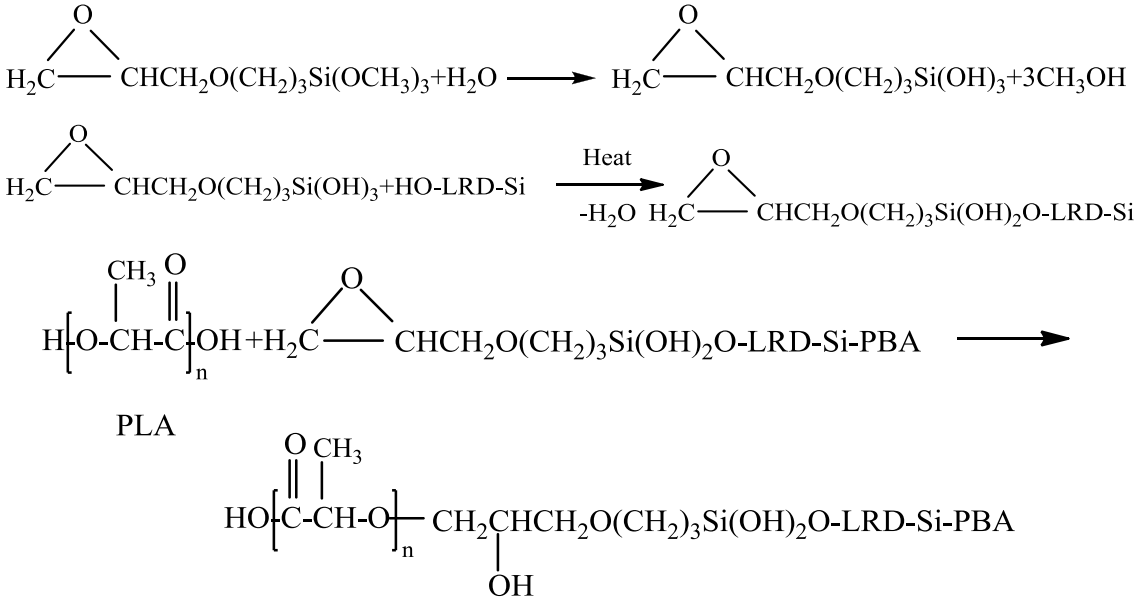

Scheme 4.1 Reactions of surface treatment.

For the silane treatment, silane 1 (3A) and silane 2 (3G) react with water to form silanol and alcohol. Then silanol reacts with the hydroxyl groups on LRD-Si units, thereby bonding itself to LRD layer and connecting to PBA later. When combining with PLA matrix, another functional groups on the silane molecule, such as NH_2 for silane 1 and epoxy groups for silane 2, would react with hydroxyl groups of the PLA resin. Thus, chemical bonding could be established between the LRD-PBA and the PLA matrix. Interfacial properties could thus be improved.

2.2.1. Modification of LRD particles and the preparation of PBA-LRD-Si-3G or PBA-LRD-Si-3A particles

Silane 1 (3A) and silane 2 (3G) were diluted to a 6% concentration in acetone before use. Two portions of modified LRD-Si were separately immersed into these two silane solutions for 24 h and then washed by acetone and dried in the vacuum oven at 60 °C for 4 h to remove the residual solvent. The 3A-LRD-Si and 3G-LRD-Si were obtained by the modification of LRD-Si. Then, 3A-LRD-Si or 3G-LRD-Si was used in miniemulsion polymerization with BA monomer to take the place of LRD-Si in the preparation of PBA-clay composite latex. All the experimental processes were the same as the descriptions in chapter 3 for the PBA-LRD-Si. The concentration of 3A-LRD-Si or 3G-LRD-Si in the BA monomer was setting at 3wt% (compared to monomer quantity).

2.2.2. Blend with PLA and the morphologies

From analysis of DLS, the particle size of PBA latex with the 3A-LRD-Si or 3G-LRD-Si in the miniemulsion polymerization did not change after reaction which was still kept around 100 nm.

PBA-LRD-Si-3A or PBA-LRD-Si-3G latexes were demulsified by ethanol and washed by deionized water, then dried at 60°C for 24h in a vacuum oven before melt blending. The concentration of the PBA in the blends was fixed at 20 wt% also. The blends of PLA and dried latexes were prepared in the microcompounder at a screw speed of 60 rpm for 10 min at 180°C also.

From the Figure 4.12 and the diameter value of the cavities in the SEM images, it is revealed that the replacement of the LRD-Si by 3A-LRD-Si did not give a better compatibility for PBA particles with PLA matrix. Although the mean diameter of the pore was a little smaller, the pore which eliminated by solvent indicating these PBA particles were not attached to the PLA matrix so that the 3A-LRD-Si do not act as a connection for PBA particles and PLA matrix. Therefore, we did not use it for further study. By contrast, in Figure 4.13, with the aid of 3G-LRD-Si, the PBA-3%LRD-Si-3G/PLA (20/80) blend has nearly no pore after the extraction by

2-butanol. This could be ascribed to the epoxy groups of silane 2 (3G), do react with hydroxyl groups of the PLA matrix which assist the PBA particles connecting with PLA by the 3G-LRD-Si and cannot be dissolved by solvent of PBA.

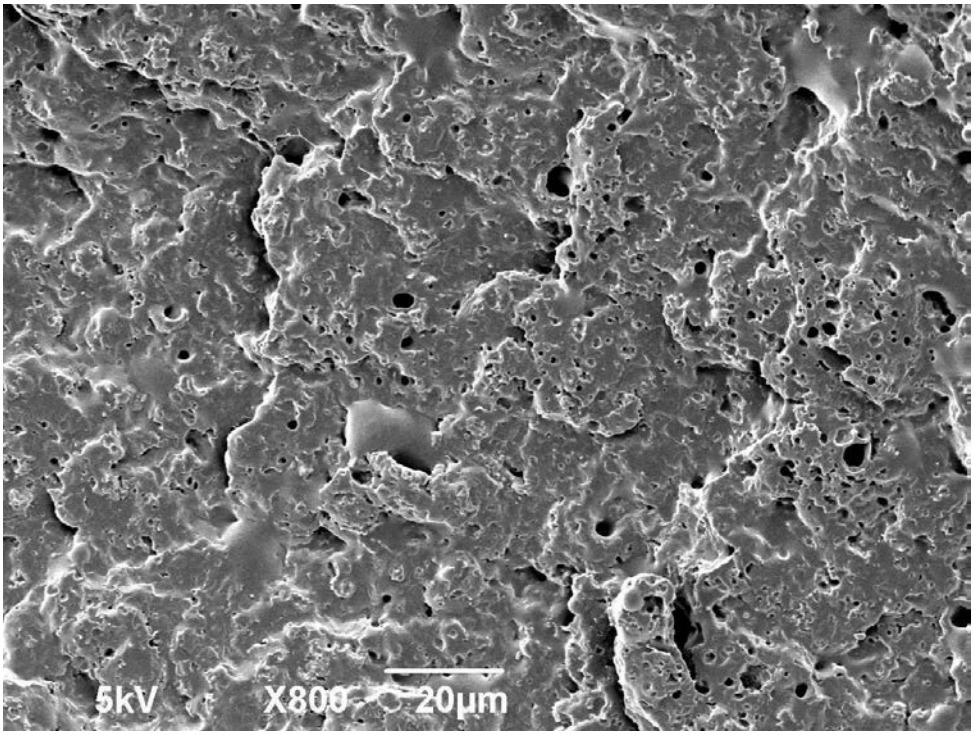

Figure 4.12 SEM images of PBA-3%LRD-Si-3A/PLA (20/80) blend. dn=0.78μm, dv=3.41 μm.

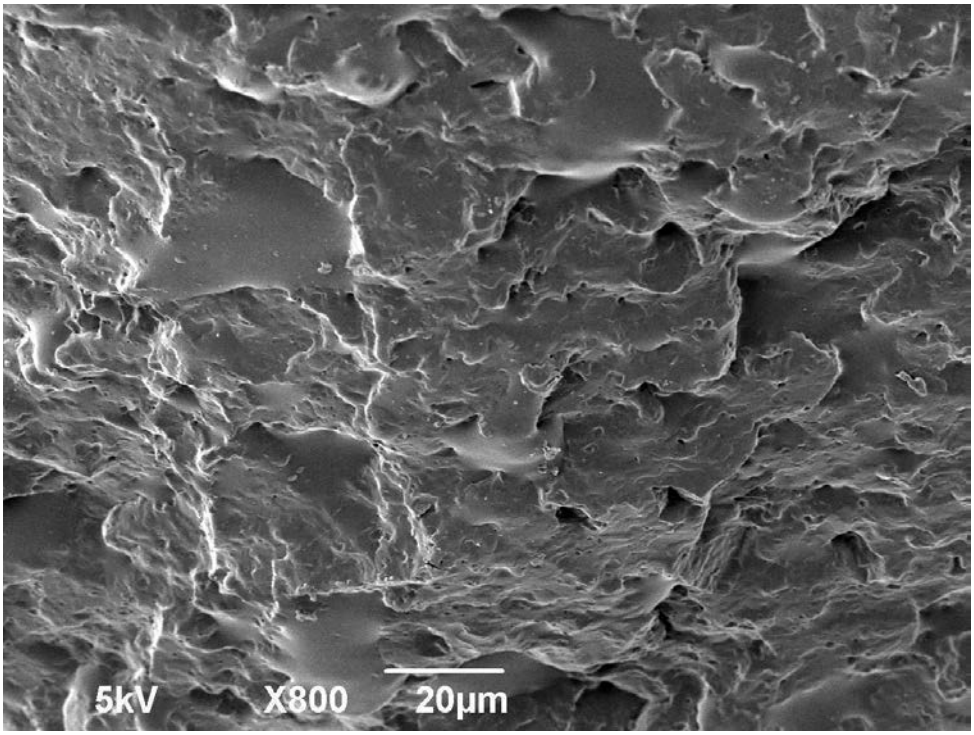

Figure 4.13 SEM images of PBA-3%LRD-Si-3G/PLA (20/80) blend.

The DSC test for PBA-3%LRD-Si-3G/PLA (20/80) blend demonstrated the T_g of PLA was 59 °C and -46.5°C for the T_g of PBA in the blend. They have no big difference with the T_g of pure PLA or that of PBA in PBA-LRD-Si/PLA (20/80) blend. These results imply the addition of Silane 2 (3G) have no influence for the thermal property of PBA/PLA blend.

3. Core-shell particles and PLA blends

It is generally accepted that phase size and interface between blend components take the key role in determining the mechanical performance of a polymer blend. Take into consider that PBA and PLA are immiscible; incorporation of PBA in PLA matrix by simple mixing may not likely be able to improve the toughness of the latter. To decrease the PBA domain size and strengthen the interface between PLA and PBA, poly(methyl methacrylate) (PMMA) has been used as the compatibilizer. On the other hand, it is reported that PMMA is partially miscible with PLA and has a higher Young's modulus than PLA, and thus the presence of PMMA in PLA improves the Young's modulus of the latter.

PBA/MMA core-shell latexes with or without LRD (or LRD-Si) were prepared by seeded emulsion polymerization in order to improve compatibility between nanoparticles and matrix (The PMMA shell, is miscible with PLA matrix). PBA latexes with or without LRD (or LRD-Si) were used as seeds (see experimental part). MMA was polymerized in the presence of these seeds in order to obtain PBA/PMMA core-shell particles. The feed rate of MMA monomer was sustained constant and under starved conditions so that the seed PBA latex particles had enough time to polymerize with MMA, thus preventing the second generation of PMMA particles. The BA/MMA ratio was about 50/50 w/w in order to obtain well-defined core-shell structures.

3.1. Synthesis of PBA latex particles by miniemulsion polymerization

The PBA/PMMA core-shell latex particles were prepared by a conventional two-stage

seeded emulsion polymerization process. The PBA, PBA-LRD and PBA-LRD-Si latex particles were prepared by miniemulsion polymerization. The synthesis process of the preparation was the same as that of in the chapter 3 (2.2.3). The PBA elastomer core was synthesized according to the recipe shown in Table 3.7 of chapter3. The only difference was after the 3h of miniemulsion polymerization, hydroquinone was not needed for the system to terminate the reaction.

3.2. Synthesis of the PBA/PMMA core-shell latex particles by emulsion polymerization

The PMMA rigid shell was synthesized by using LRD-PBA latexes or (LRD-Si)-PBA latexes as seeds. Table 4.3 shows the recipes for preparing the core-shell composite particles. Figure 2.1 in chapter 2 demonstrates the conceptual reactor for emulsion polymerization of shell PMMA. The feed rate of MMA was controlled by a syringe.

Table 4.3 Recipes in weight for the preparation of PBA/PMMA latexes

Latex core-shell	*Seed*	*MMA (g)*	*MMA/PBA (w/w)*	*AMBN (g)*	*Brij700 (g)*	*H_2O (g)*
PBA/PMMA	Latex PBA	20	1 : 1	0.2	0.9	10
PBA-LRD/PMMA	Latex PBA-LRD	20	1 : 1	0.2	0.9	10
PBA-LRD-Si/PMMA	Latex PBA-LRD-Si	20	1 : 1	0.2	0.9	10

The PBA cores prepared by miniemulsion polymerization were further purged with pure nitrogen and under stirring in the stainless steel reactor at 60°C. A mixture of MMA, deionized water, surfactant and AMBN was added to the reactor under starved conditions (0.25 ml/min). After the addition of the monomer mixture, the temperature was raised to 85°C. The reaction proceeded for 3h under continuous stirring and terminated by the addition of hydroquinone. Polymer yields were determined by gravimetry.

3.3. Characterization of the core-shell particles

Core-shell nanoparticles were characterized by ^{1}H NMR, DLS and TEM.

3.3.1. Chemical structures of particles

Figure 4.14 shows the ^{1}H NMR spectra of PBA-PMMA latexes. The peak at 3.6ppm (c) and multiple peaks at 4.0 ppm (3) correspond to the O-CH_2 of the PBA and O-CH_3 of the PMMA, respectively. The peaks between 0.8 and 2.0ppm can be ascribed to the overlapping between protons.

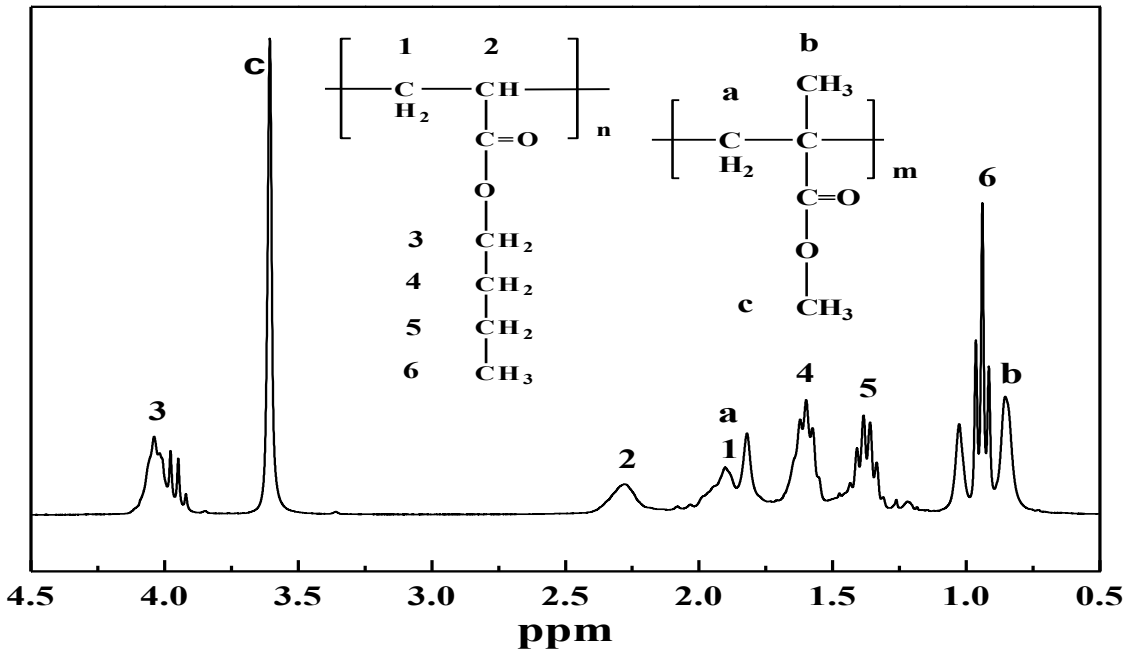

Figure 4.14 ^{1}H NMR spectrum of PBA-PMMA core-shell particles.

By comparing the OCH_2 protons in PBA (3) and the OCH_3 protons in PMMA (c), the composition of each fraction was determined by integration. Percentages of PMMA and PBA [48] were calculated by:

$$\%PBA = [(n/2)/(n/2+m/3)] \times 100$$

$$\%PMMA = [(m/2)/(n/2+m/3)] \times 100$$

Where n is the area under the peak at 4.0ppm and m is the area under the peak at 3.6ppm.

From data in Figure 4.14, it can be calculated that for the nearly 100% conversion core-shell PBA/PMMA, the latex composition is PBA: PMMA=51:49.

3.3.2. Size and morphologies of particles

The particle sizes were determined by TEM and dynamic light scattering (DLS).

The core-shell samples were also stained with UAc. TEM was used to examine the particle morphology in the wet state. For all cases the shells are a little thinner than calculated from the molar mass ratio of the components introduced during the synthesis.

The diameters of the PBA-LRD-Si and PBA-LRD-Si/PMMA composite particles determined by DLS are represented in Figure 4.15 where the diameter of PBA-LRD-Si latex is around 100 nm, and the particle size of PBA-LRD-Si/PMMA latex is around 120 nm.

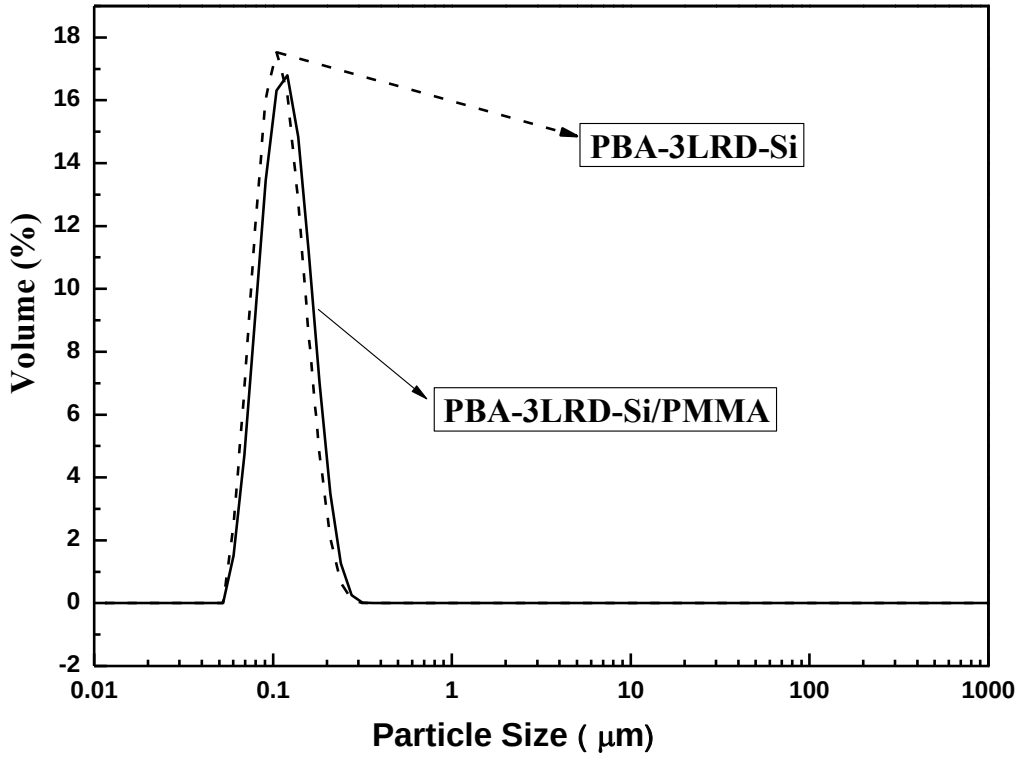

Figure 4.15 The particle size distribution of PBA-3%LRD-Si and PBA-3%LRD-Si/PMMA.

In addition, presuming the number of composite particles to be constant, the diameter of PBA-LRD-Si/PMMA latex (D_2) can be calculated from the weight change of the composite particles by this equation 4.2:

$$\frac{D_2}{D_1} = \left(\frac{V_2}{V_1}\right)^{1/3} \approx \left(\frac{W2}{W1}\right)^{1/3} \quad \textbf{(4.2)}$$

where the diameter of PBA-LRD-Si latex (D_1) is 100 nm, measured by DLS, W_2/W_1

is the weight ratio of PBA-LRD-Si/PMMA to PBA-LRD-Si composite particles, which can be determined by MNR analysis. From the above comparison, it can be seen that the diameter of PBA-LRD-Si/PMMA latex particles obtained from direct observation was close to the theoretical calculation, supporting that MMA polymerization mainly occurred on the surface of the PBA/LRD-Si particles.

Figure 4.16 shows the TEM images of the PBA-PMMA core-shell particles. The soft core in PBA and the hard shell in PMMA are clearly seen. The former covers the latter sufficiently well and uniformly. The thickness of the shell and the diameter of the core are 10-20 and 90~130nm, respectively.

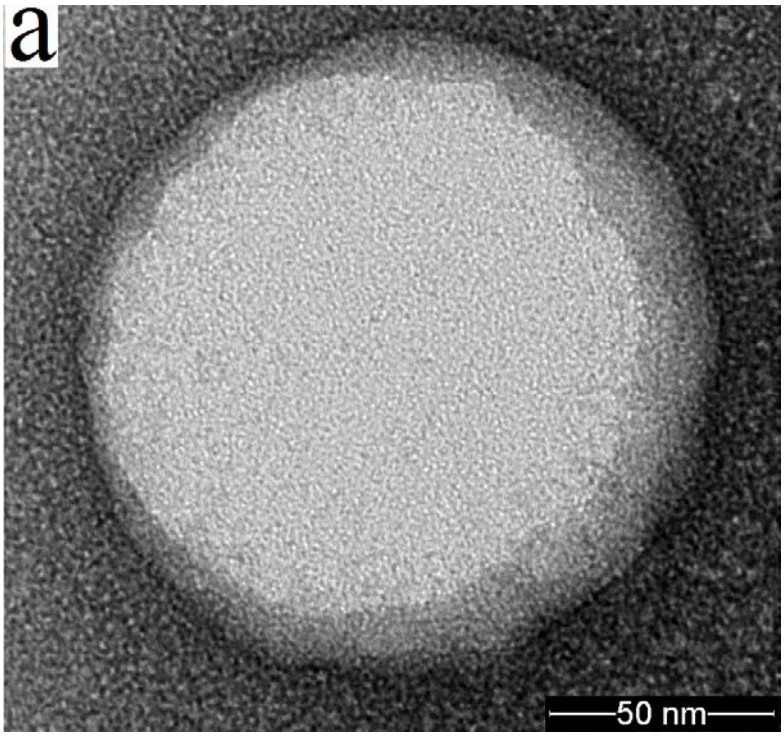

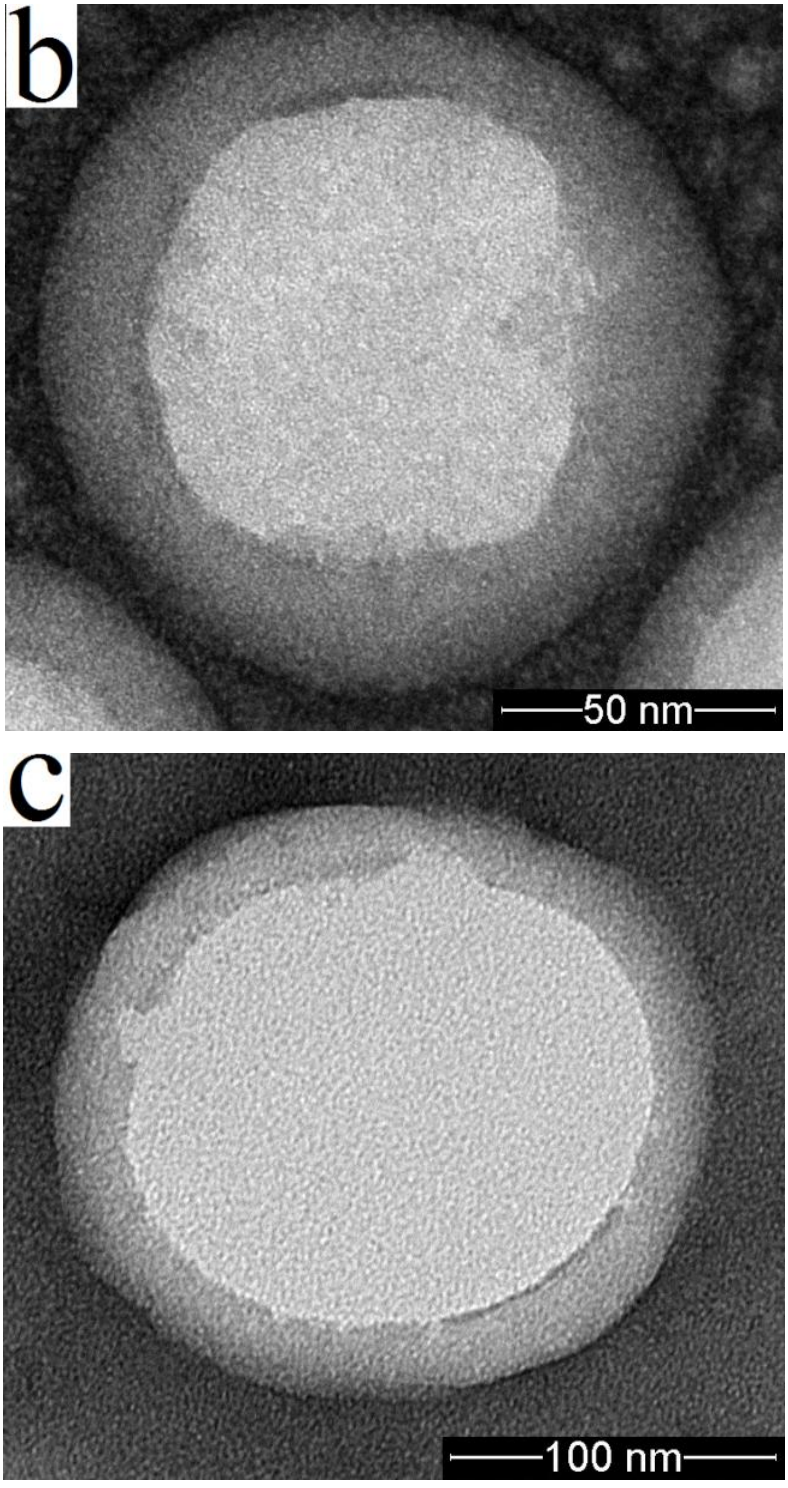

Figure 4.16 TEM images of PBA-PMMA core-shell particles. (a) PBA-PMMA, (b) (PBA-3%LRD)-PMMA, and (c) (PBA-3%LRD-Si)-PMMA.

3.4. Core-shell particles blend with PLA

The addition of PMMA results in a decreased PBA domain size and a narrow size

distribution in PLA matrix, as shown in Figure 4.17.

Figure 4.17 shows the SEM images of (PBA/PMMA)/PLA (10/10/80), (PBA-3%LRD/PMMA)/PLA (10/10/80) and (PBA-3%LRD-Si/PMMA)/PLA (10/10/80) blends. Their surfaces are etched with 2-butanol prior to the SEM analyses. Holes of about 350 nm in diameter are observed on the surfaces of the first two blends, keeping in mind that the diameter of the original PBA-PMMA core-shell particles is around 125 nm after the emulsion polymerization. The fact that these holes are much smaller than those in the PBA/PLA blends implies that the PMMA shell does play a role of compatibilization between PBA and PLA. This strongly improves the dispersion of nanoparticles in the PLA matrix. There are no holes on the surface of the (PBA-3%LRD-Si/PMMA)/PLA (10/10/80) blend. This is because in this blend, the PBA core is crosslinked by the silane grafted LRD (LRD-Si) and cannot be etched by 2-butanol.

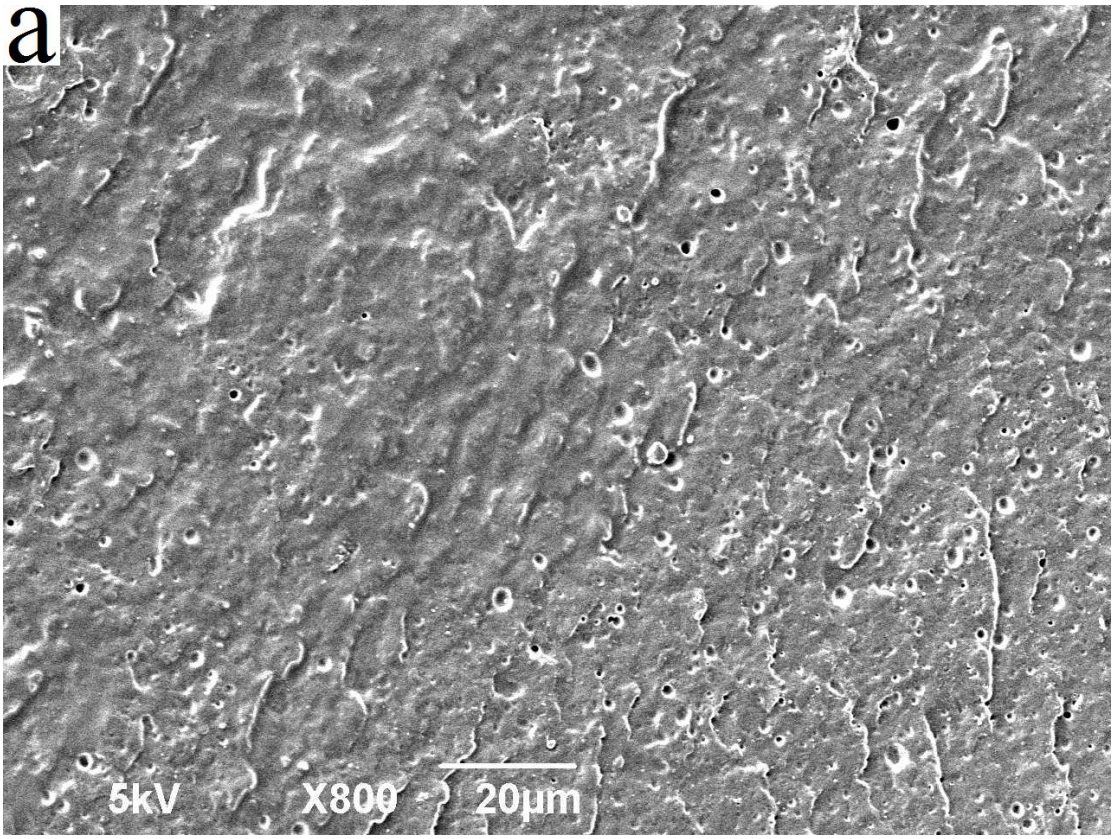

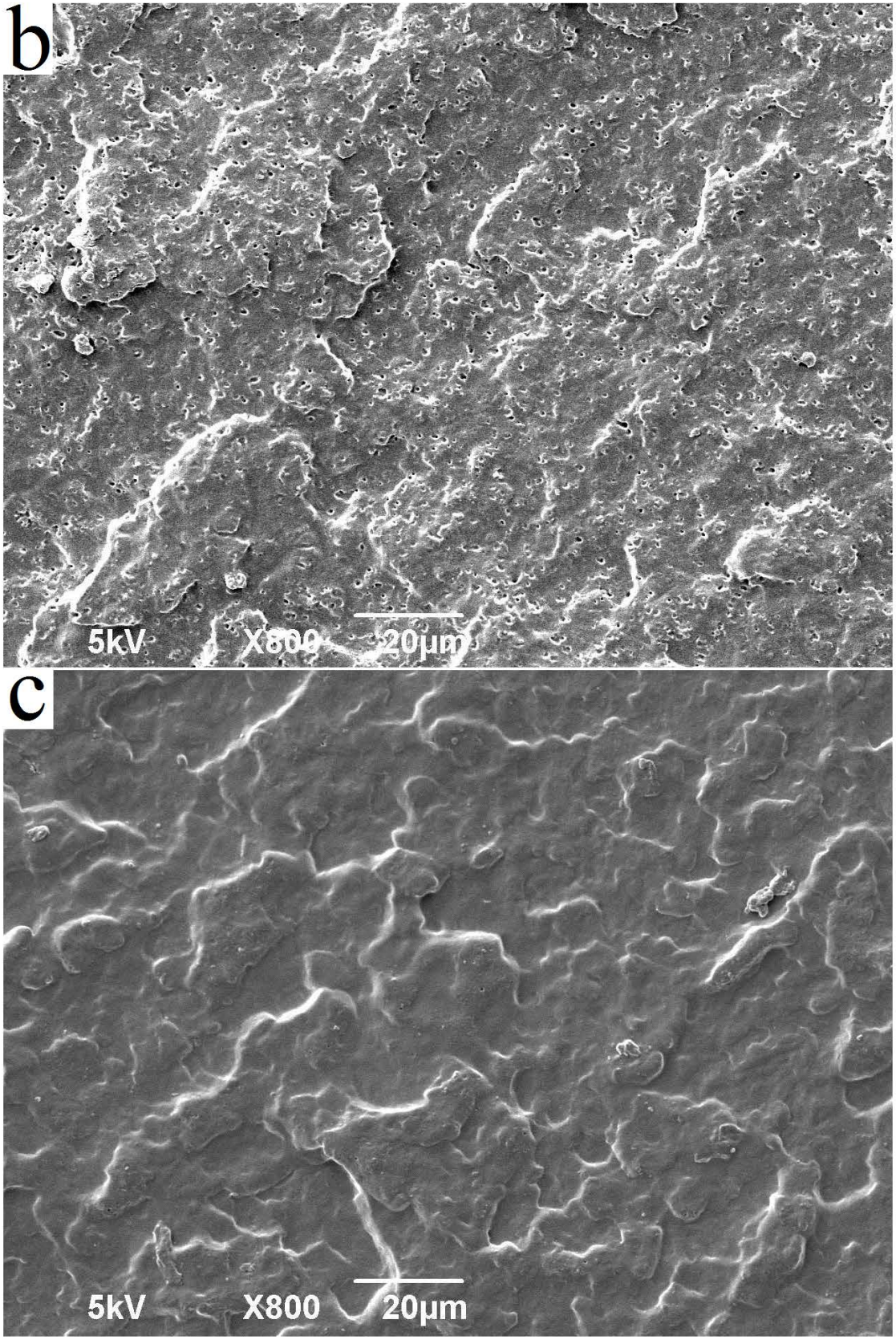

Figure 4.17 SEM micrographs of freeze-fractured surfaces of (a) (PBA/PMMA)/PLA, (b) (PBA-3%LRD/PMMA)/PLA, and (c) (PBA-3%LRD-Si/PMMA)/PLA blends.

4. Conclusion

The pore of PBA in the PBA/PLA blends was significantly higher than the average diameter of the PBA nanoparticles recovered from miniemulsion polymerization. This implied that they were coalescence during the stages of drying latexes and melt blending with the PLA. The PBA particles in PLA matrix had smooth, distinct particle interfaces, indicating poor interfacial adhesion. It is seen that the interface between the two phases is very weak, indicating a totally incompatible polymer blend.

PBA-LRD-Si particles were crosslinked during the miniemulsion polymerization by the grafted LRD-Si. The degree of crosslinking was enhanced with increasing the LRD-Si content.

Polymer surfactant poly(ethylene glycol) methyl ether methacrylate (PEGMEM, Mn=950) which has a double bond has been tried in the miniemulsion polymerization with the aim to improve the compatibility between PBA particle and PLA matrix. The hydrophilic group poly(ethylene oxide) is miscible with the PLA. The part with the double bond is the hydrophobic group which could react with the monomer droplet surface. After the miniemulsion polymerization, the polymer surfactant was linked with the PBA particles. But the compatibility of PBA and PLA was not improved with such small amount of PEGMEM.

Furthermore, in order to improve interfacial properties of PBA particles and PLA matrix, two kinds of silanes were used to modify LRD-Si. The functional groups on the silane molecule, such as NH_2 for 3-Aminopropyltriethoxy silane (silane 1) and epoxy groups for 3-Glycidoxypropyltrimethoxy silane (silane 2) would react with hydroxyl groups of the PLA. 3A-LRD-Si or 3G-LRD-Si took the place of LRD-Si in the preparation of PBA-clay composite latex. From the SEM images, silane 2 has a better influence for improving the interfacial properties of PBA particles and PLA matrix.

Poly(methyl methacrylate) (PMMA) is partially miscible with PLA. PBA/PMMA core-shell latexes with or without LRD (or LRD-Si) were prepared by seeded emulsion polymerization in order to improve compatibility between PBA

nanoparticles and PLA matrix. PMMA shell did play a role of compatibilizer between PBA and PLA. It strongly improved the dispersion of PBA nanoparticles in the PLA matrix.

Chapter 5. Reinforcement of PLA

Introduction

Many materials, when in service, are subjected to forces or loads. In such situation it is necessary to know the characteristics of the material and to design the member from which it is made such that any resulting deformation will not be excessive and fracture will not occur. The mechanical behavior of a material reflects the relationship between its response or deformation to an applied load or force. Important mechanical properties are strength, hardness, ductility, and stiffness.

If a load is static or changes relatively slowly with time and is applied uniformly over a cross section or surface of a member, the mechanical behavior may be ascertained by a simple stress-strain test; these are most commonly conducted at room temperature.

One of the most common mechanical stress-strain tests is performed in tension. The tension test can be used to ascertain several mechanical properties of materials that are important in design. A specimen is deformed, usually to fracture, with a gradually increasing tensile load that is applied uniaxially along the long axis of a specimen. A standard tensile specimen is shown in Figure 2.7. This 'dogbone' specimen configuration was chosen so that, during testing, deformation is confined to the narrow center region (which has a uniform cross section along its length), and, also, to reduce the likelihood of fracture at the ends of the specimen.

The tensile strength is the stress at the maximum on the stress-strain curve. This corresponds to the maximum stress that can be sustained by a structure in tension; if this stress is applied and maintained, fracture will result. However, at this maximum stress, a small constriction or neck begins to form at some point, and all subsequent deformation is confined at this neck, and fracture ultimately occurs at the neck.

Ductility is another important mechanical property. It is a measure of the degree of plastic deformation that has been sustained at fracture. A material that experiences very little or no plastic deformation upon fracture is termed brittle. Ductility may be

expressed quantitatively as percent elongation. Brittle materials are approximately considered to be those having a fracture strain of less than about 5%.

Toughness is a mechanical term that is used in several contexts; loosely speaking, it is a measure of the ability of a material to absorb energy up to fracture. For dynamic (high strain rate) loading conditions and when a notch is present, notch toughness is assessed by using an impact test. For the static (low strain rate) situation, toughness may be ascertained from the results of a tensile stress-strain test. It is the area under the σ-ε curve up to the point of fracture. For a materials to be tough, it mist display both strength and ductility; often, ductile materials are tougher than brittle ones. The typical room-temperature values of tensile strength and ductility are sensitive to any prior deformation, the presence of impurities, and/or any heat treatment to which the material has been subjected. The modulus of elasticity is one mechanical parameter that is insensitive to these treatments.

Any fracture process involves two steps-crack formation and propagation-in response to an imposed stress. The mode of fracture is highly dependent on the mechanism of crack propagation. Ductile fracture is characterized by extensive plastic deformation in the vicinity of an advancing crack. Furthermore, the process proceeds relatively slowly as the crack length is extended. Such a crack is often said to be stable. That is, it resists any further extension unless there is an increase in the applied stress. On the other hand, for brittle fracture, cracks may spread extremely rapidly, with very little accompanying plastic deformation. Such cracks may be said to be unstable, and crack propagation, once started, will continue spontaneously without an increase in magnitude of the applied stress. Ductile fracture is almost always preferred for two reasons. First, brittle fracture occurs suddenly and catastrophically without any warning; this is a consequence of the spontaneous and rapid crack propagation. On the other hand, for ductile fracture, the presence of plastic deformation gives warning that fracture is imminent, allowing preventive measures to be taken. Second, more strain energy is required to induce ductile fracture inasmuch as ductile materials are generally tougher.

The blends of the PLA were prepared by melt compounding for 10 min at 180°C with

a screw speed of 60 rpm in a microcompounder-DSM Xplore and compression molding for 30 seconds at 180°C under 12 bar. The samples were then cooled to room temperature with air. PLA was treated as all the blends experienced to get the same treatment history.

Tensile test were carried out according to the JIS K7113 test method using dogbone-shaped samples. The tests were performed using a tensile testing machine MTS 810.

1. Mechanical properties of PLA/LRD blends

Figure 5.1 shows that the Young's modulus of the PLA increases with increasing LRD load. However its tensile strength decreases significantly when the clay content increased from 0 to 5 wt%. From Figure 5.2, the notched Izod impact strength of the PLA/LRD composites is low and basically constant within the experimental error in the LRD content range of 0-5 wt%, which means the impact strength of PLA is not affected much by the incorporation of the LRD. Thus, when subjected to impact loading, PLA and PLA/LRD composites failed in a brittle manner, hence resulting in lower impact strengths.

Meanwhile, with the addition of 5wt% LRD-3G particles in the PLA matrix did not increase substantially the impact strength of the blend (increased by 12%). And its increasing for Young's modulus of the PLA (increased from 3421MPa to 3702MPa) did not exceed the incensement for the PLA blended with 5wt%LRD. These indicate the influence of silane 3G for the LRD layers and PLA matrix is insignificant. This result implies the connection between LRD-3G and PLA matrix do not perform well.

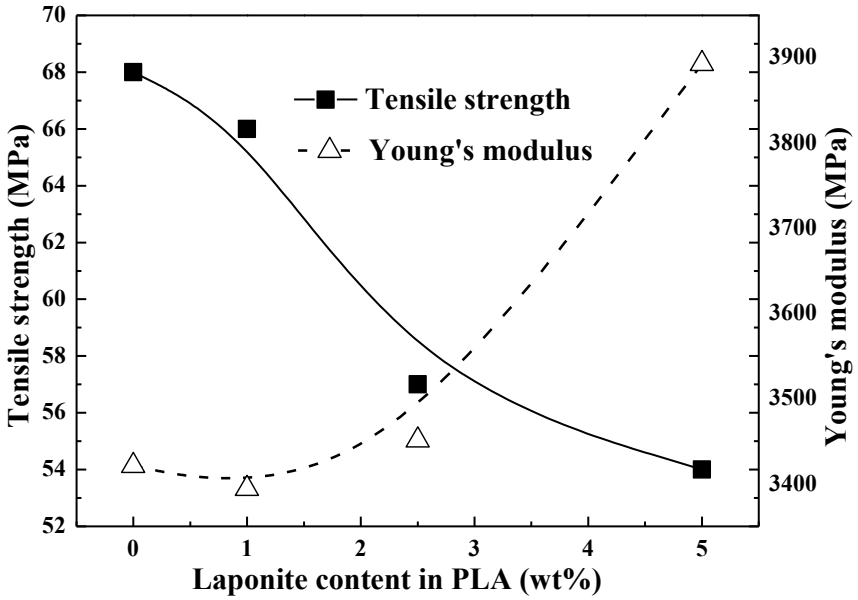

Figure 5.1 Effect of the incorporation of the LRD on the tensile strength and Young's modulus of the PLA.

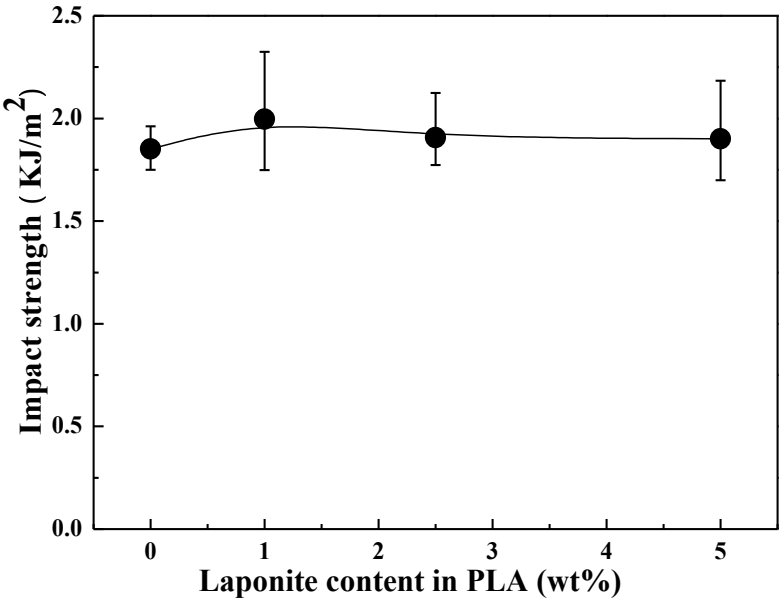

Figure 5.2 Effect of the incorporation of the LRD on the impact strength of the PLA.

The addition of silicate layers in matrix leads to improved modulus. The stiffness of the silicate layers contributes to the presence of immobilized or partially immobilized polymer phases. Thus the improvement in stiffness was due to the reinforcement effect of the rigid inorganic LRD which constrains the molecular motion of PLA chains. In addition, the existence of hydrogen–bonding interactions between PLA hydroxyl end groups and the LRD platelets surfaces resulting in enhanced interaction

between PLA and LRD with improved rigidity. The PLA's chain movement was also suppressed by LRD tethering and gallery confinement.

The improvement in the modulus of PLA/LRD composites may also be caused by the intercalation and exfoliation of LRD layers in PLA. When the clay particles are dispersed in intercalated and/or exfoliated form, it could lead to a higher aspect ratio of the silicate layer, and a larger interfacial area. Both of the higher aspect ratio and interfacial area will make stress transfer to the silicate layers more effective, and subsequently improve the mechanical properties of the formed nanocomposites. The dramatic improvement of modulus provided by the exfoliated nanocomposites structures on PLA/Clay nanocomposites had also been reported by previous researchers.

The drop in tensile strength of the nanocomposites suggests that the LRD layers had aggregated to act as material flaws, which triggered brittle response and early material failure in the tensile testing. Previous study on PLA nanocomposites by Shyang and Kuen [49] also showed that the flexural strength of PLA decreased when the MMT loadings more than 1 wt%. This was due to the high clay content, which leads to agglomeration in the polymeric material.

From Figure 5.3, the fracture surface of pure PLA is smooth. It can be noted from Figure 5.4 and 5.5 that at higher LRD concentration (5phr), more agglomerates of LRD were visible in the nanocomposites. This is due to the filler–filler interactions of the LRD sheets, resulting in agglomerates, which restricted delamination of the LRD and eventually decreased the degree of exfoliation. The agglomeration of LRD had acted as stress concentrator leading to poor mechanical properties in terms of impact strength, tensile strength. It was also stated that disc–disc interaction in LRD plays an important role in determining the stability of the clay particles and as a result enhancing the mechanical properties of such nanocomposites.

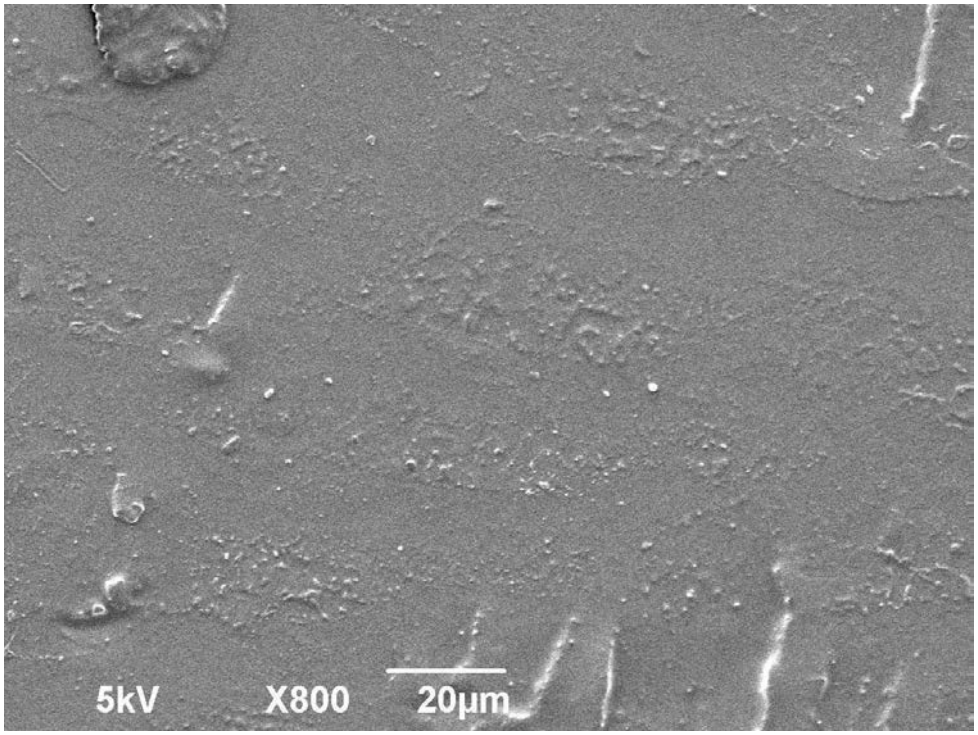

Figure 5.3 SEM image of PLA fracture surface.

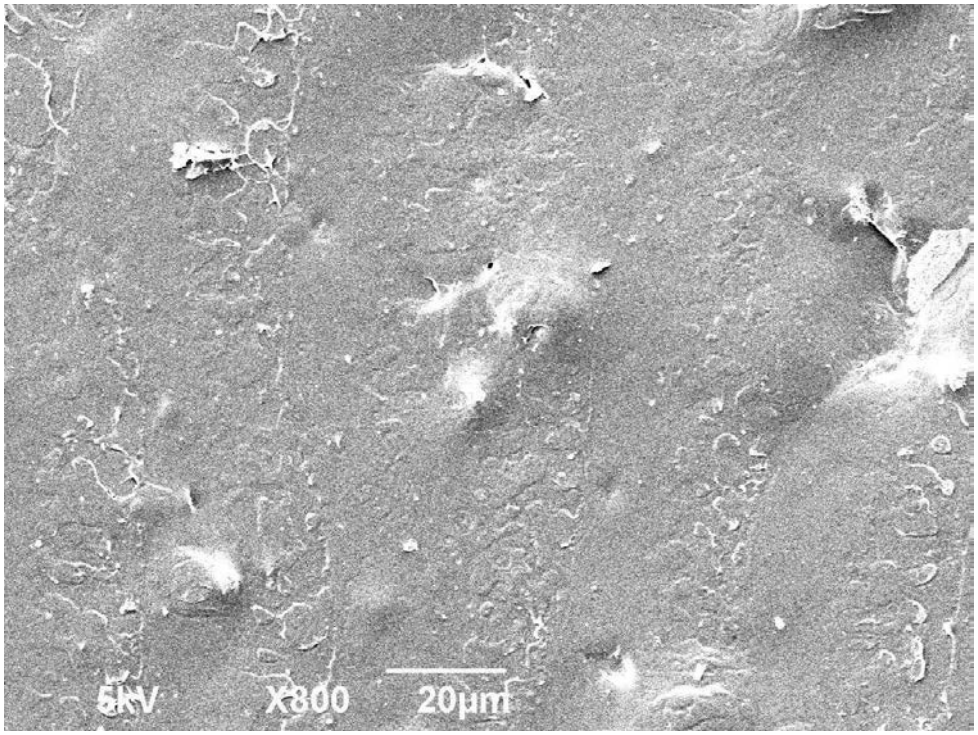

Figure 5.4 SEM image of 5%LRD-PLA fracture surface.

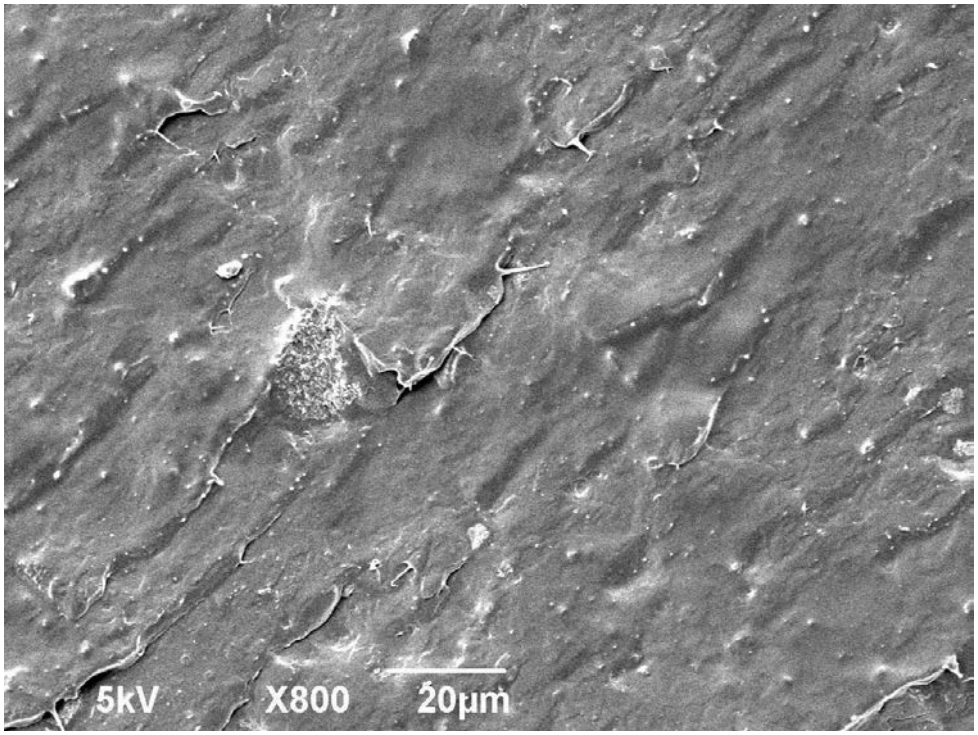

Figure 5.5 SEM image of 5%LRD-3G-PLA fracture surface.

2. PLA and PBA/LRD blends

2.1. Tensile strength

The addition of PBA significantly changes the tensile behavior of the PLA, as shown in Figure 5.6 and 5.7. Fracture toughness, which is the energy-to-fracture per unit volume of the specimen, is obtained by integrating the area under the stress–strain curve.

The brittle fracture of the neat PLA transformed into ductile fracture for the PLA/PBA blends, upon them being subjected to tensile testing. Neat PLA is very rigid and brittle, with tensile strength around 68 MPa; whereas the elongation at break is only about 15%. Neat PLA shows a distinct yield point with subsequent failure immediately upon the tensile load. In contrast, all of the blends which contain PBA particles show clear yielding behavior upon stretching and have higher impact strength than pure PLA. After yielding occurred the strain developed continuously, while the stress remained almost constant. The samples were finally broken at a significantly increased

elongation, compared with that for the neat PLA.

It was very interesting to find that the PBA-5%LRD/PLA (20/80) blend had a very high elongation at break of 268%, while the tensile strength was 36MPa. The reason for the result of this blend is not clear; it is presumed that the exfoliated LRD around the surface of PBA particle is playing an important role for its longest elongation of the tensile test. Furthermore, for the LRD/PLA/PBA (1/79/20) blend, even though this blend has the same amount of LRD in the mass as the PBA-5%LRD/PLA (20/80) blend, neither its tensile strength nor its elongation is higher than that of PBA-5%LRD/PLA (20/80) blend. The agglomerates of LRD can account for this more weakened tensile test result of LRD/PLA/PBA (1/79/20) blend because the exfoliation of LRD cannot be formed by simple mixing in micro-compound.

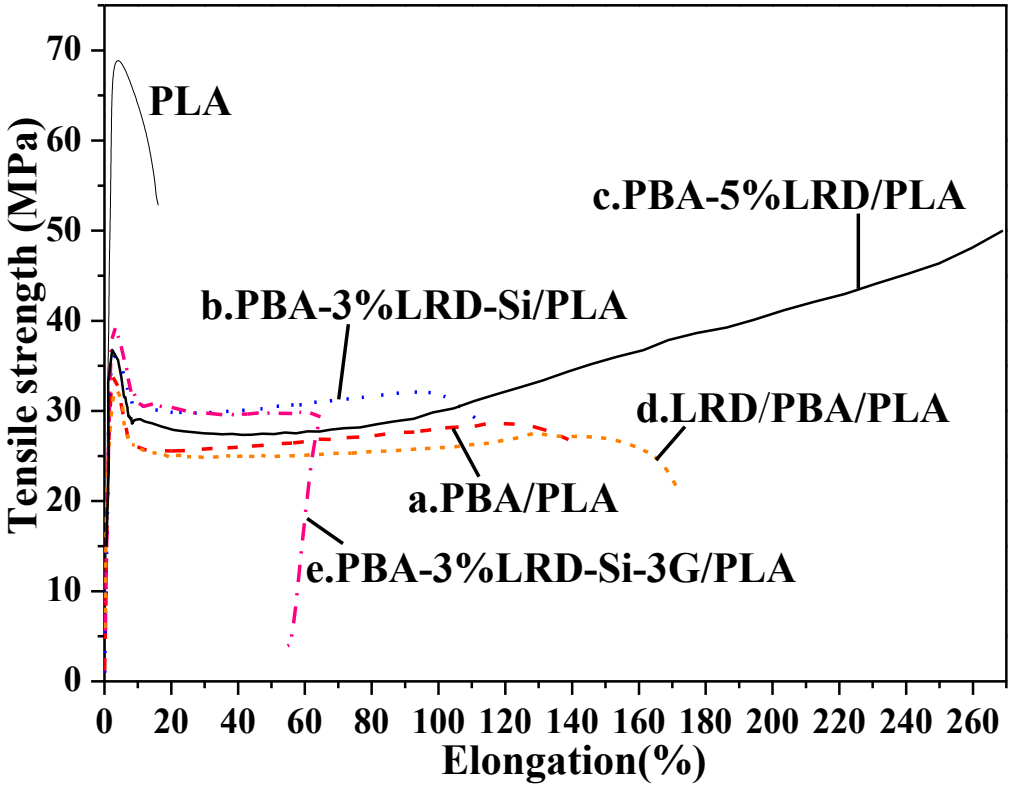

Figure 5.6 The tensile strength of PBA/PLA blends with PBA particles or PBA-LRD-Si particles in PLA matrix compared with pure PLA: (a) PBA/PLA (20/80) blend, (b) PBA-3%LRD-Si/PLA (20/80) blend, (c) PBA-5%LRD/PLA (20/80) blend, (d) LRD/PLA/PBA (1/79/20) blend, and (e) PBA-3%LRD-Si-3G/PLA (20/80) blend.

The tensile strength of PBA-3%LRD-Si-3G/PLA (20/80) blend is 39 MPa which is a

little higher than the other PBA/PLA blends while its elongation at break is shorter in comparison with other blends. These results are associated with the influence of LRD-Si-3G platelet. It might be due to the enhanced interactions between PLA and PBA which are connected by LRD-Si-3G resulting in a decrease of chain mobility.

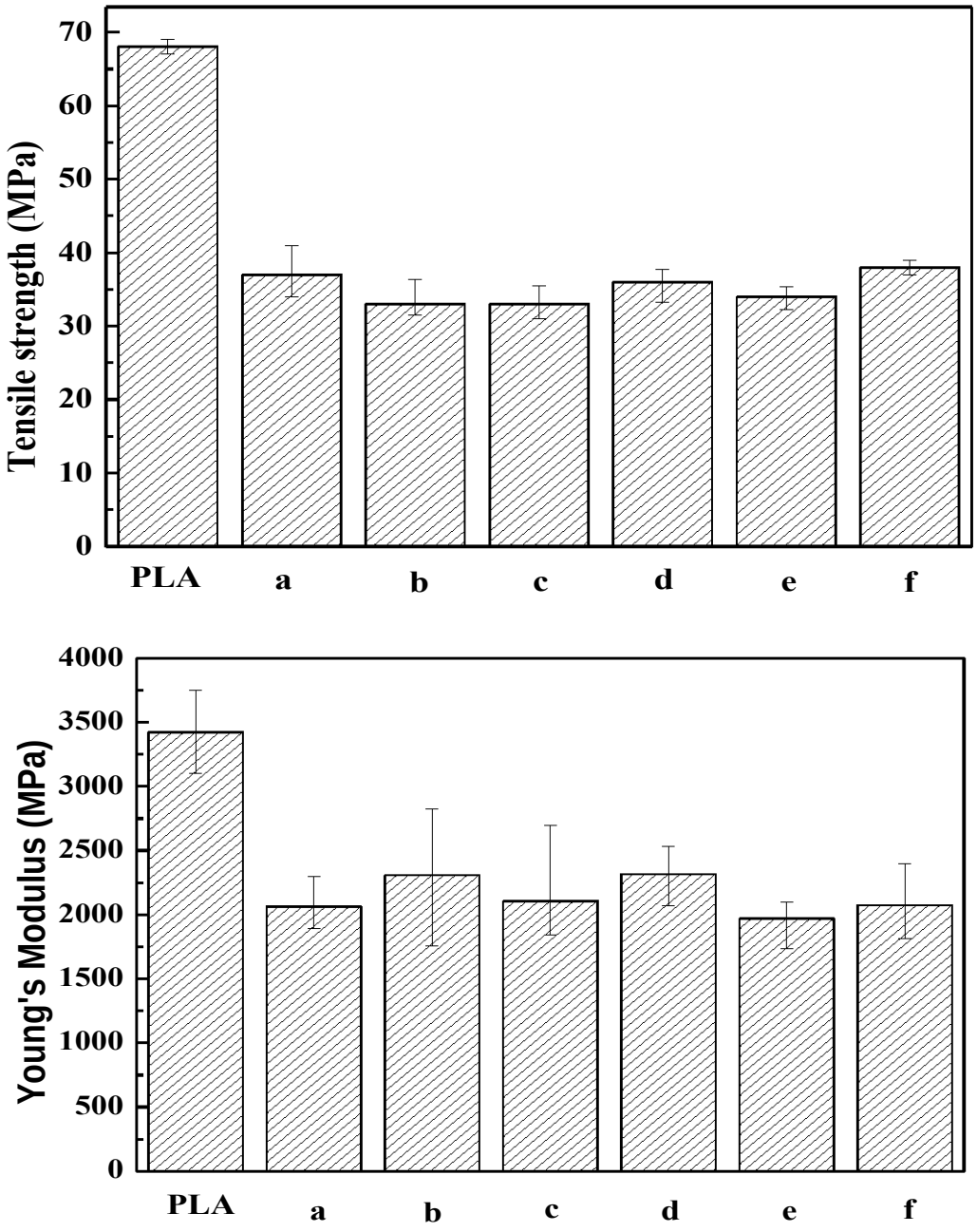

Figure 5.7 Tensile strength and Young's modulus of pure PLA, PBA/PLA blends: (a) PBA/PLA (20/80) blend, (b) PBA-2%LRD-Si/PLA (20/80) blend, (c) PBA-5%LRD-Si/PLA (20/80) blend, (d) PBA-5%LRD/PLA (20/80) blend, (e) LRD/PLA/PBA (1/79/20) blend, and (f) PBA-3%LRD-Si-3G/PLA (20/80) blend.

On the other hand, the tensile strength and the modulus decreased with the addition of PBA elastomer, which was due to PBA elastomer has a lower modulus and tensile strength than PLA.

The PBA-LRD/PLA blend samples showed larger plastic deformation zones near the fracture flank in comparison with the PBA-LRD-Si/PLA blends. As the PBA-LRD-Si particles are crosslinked but PBA-LRD composites are not, for the PBA particles attached with LRD, the mobility of the chain are high compared to the crosslinked PBA-LRD-Si particles and it is thought that the relief for tensile stress of PBA-LRD/PLA blend can easily occur. The existence of LRD allows the PBA particles to cavitate under the tensile stress conditions. This cavitation, in turn, allows unconstrained plastic flow of the matrix ligament before the fatal crack run, resulting in the high elongation properties.

These properties of the blends were not significantly affected by the different type of PBA particles. Because there was no significant difference among the blends samples in the tensile modulus and tensile strength, it is believed that the difference in elongation at break was caused by the areas of the plastic deformation zone, where the materials showed whitening.

2.2. Impact strength

The Izod impact strength of the PBA/PLA blends was also measured for various clay contents, as shown in Figure 5.8. An addition of the PBA resulted in a dramatically increase in toughness. The impact strength was significantly changed from 1.851KJ/m^2 for neat PLA to 2.391 KJ/m^2 for the PBA/PLA (20/80) blend and 3.988 KJ/m^2 for PBA-2%LRD-Si/PLA (20/80) blend. PBA-5%LRD-Si/PLA (20/80) blend has the highest impact strength 4.668 KJ/m^2 among the PBA/PLA blends.

The improvement in the impact strength of PBA-LRD-Si/PLA (20/80) blend is most likely attributable to a better dispersion of crosslinked PBA-LRD-Si particle in the PLA matrix, as they could not have extensive coalescence like the PBA particles in the PLA matrix. The particle size of crosslinked PBA-LRD-Si particle in the matrix should be smaller when comparing with the pure PBA particle blended with PLA. The

impact strength decreased in the order of increasing PBA particle size in the blends. In fact, such a correlation has been frequently observed for other rubber-modified polymers.

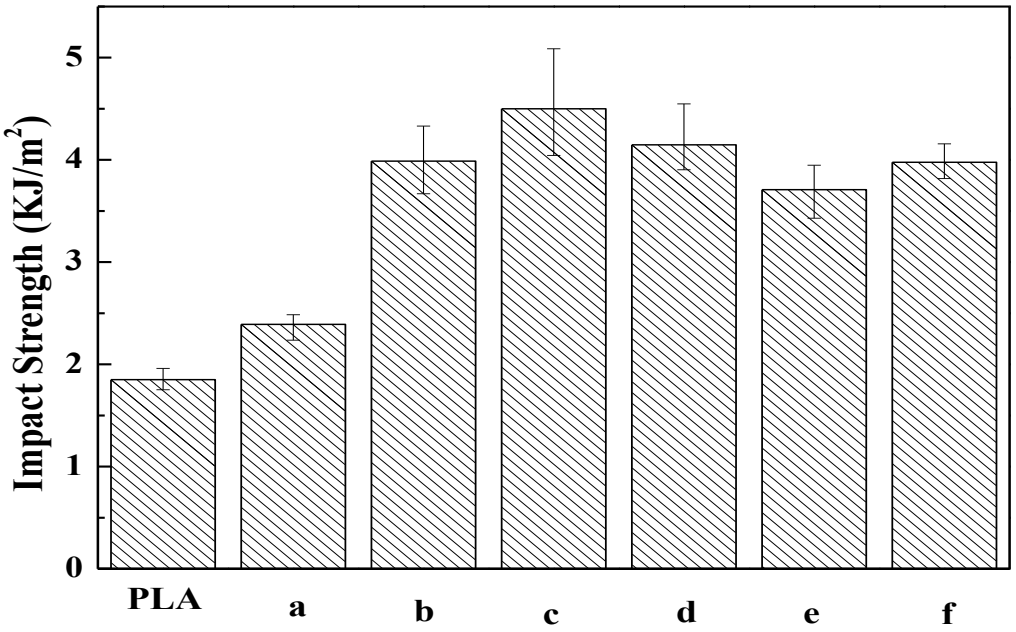

Figure 5.8 Impact strength of pure PLA, PBA/PLA blends: (a) PBA/PLA (20/80) blend, (b) PBA-2%LRD-Si/PLA (20/80) blend, (c) PBA-5%LRD-Si/PLA (20/80) blend, (d) PBA-5%LRD/PLA (20/80) blend, (e) LRD/PLA/PBA (1/79/20) blend, and (f) PBA-3%LRD-Si-3G/PLA (20/80) blend.

2.3. Dynamic mechanical properties

Figure 5.9 depicts the dynamic mechanical spectra (dynamic storage modulus E', dynamic loss modulus E'', and loss factor tan δ) as a function of temperature for PLA and PBA/PLA blends. In the present work, the study is focused on the temperature range from around T_g of PBA (about -50°C) up to below the T_m of PLA.

The storage modulus E' is closely related to the load bearing capacity of the material. From Figure 5.9A the storage modulus of all the materials drop rapidly after ~ 60°C due to the glass transition of PLA and reach their minimal value around 78°C. The storage modulus E' for PBA/PLA based composites is lower than that of pure PLA from 0°C until the T_g of PLA (~ 60°C). This might be due to decrease in the stiffness of the reinforcement imparted by the elastomer. These results show clearly that the

addition of PBA into PLA matrix results in a decrease of stiffness. With the addition of PBA, The E' curves display a rubbery plateau.

The PBA/PLA based blends exhibited an enhanced E' below the glass transition temperature of PBA in comparison with that of pure PLA. The PBA nanocomposites with laponite did not show an increase in E', and in fact the E' of PBA/PLA based blends decreased below the glass transition temperature of PBA for PBA containing LRD or LRD-Si or LRD-Si-3G platelets. The higher concentration of LRD-Si in the PBA particles, the lower E' in the PBA-LRD-Si/PLA blends. A similar phenomenon was also observed in the tensile testing results (Figure 5.7). This may be explained as follows: the introduction of LRD-Si or LRD-Si-3G can form many cross-linking points which strengthen the interaction of the LRD sheets and PBA chains; when the concentration of LRD-Si is higher, some LRD forms clusters in the composites and these clusters may act as stress concentrating points resulting in a decrease in E'.

The loss modulus E'' for these blends is shown in Figure 5.9B. It indicates a broad peak around -50°C and a narrow peak around 78°C. The former peak may correspond to the relaxation temperature (T_α) of PBA. The second peak is due to the relaxation temperature of PLA. With the increase of LRD-Si concentration in the PBA nanocomposites, the peaks of PBA are shifted to higher temperature.

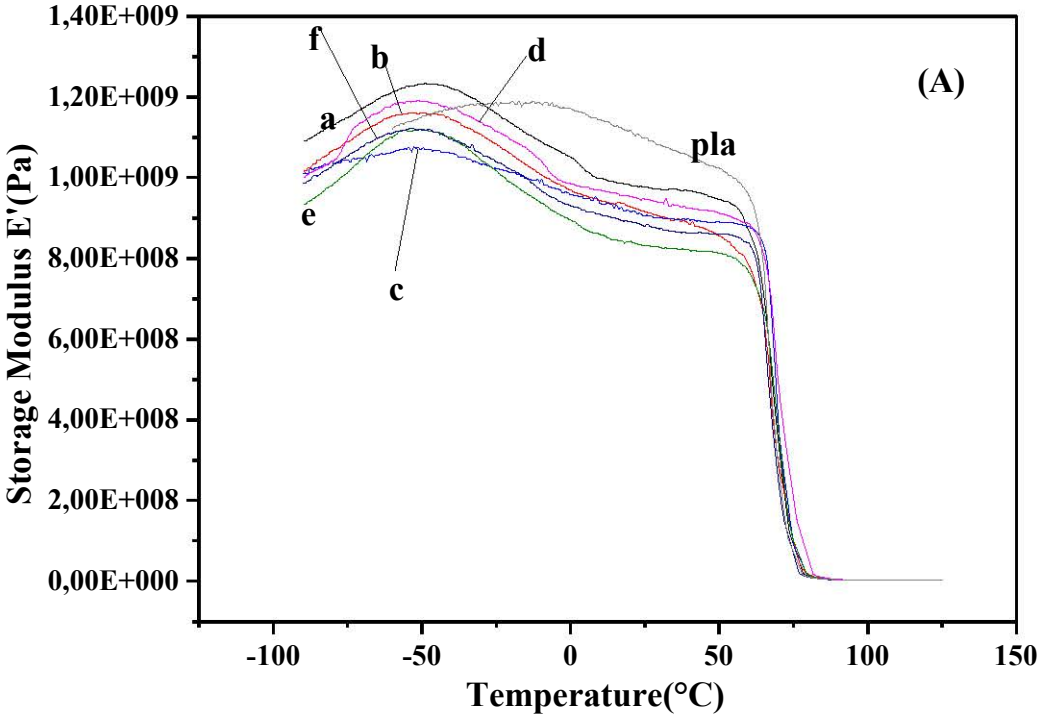
(A)
Storage Modulus E'(Pa)
Temperature(°C)
1,40E+009
1,20E+009
1,00E+009
8,00E+008
6,00E+008
4,00E+008
2,00E+008
0,00E+000
-100
-50
0
50
100
150
a
b
c
d
e
f
pla

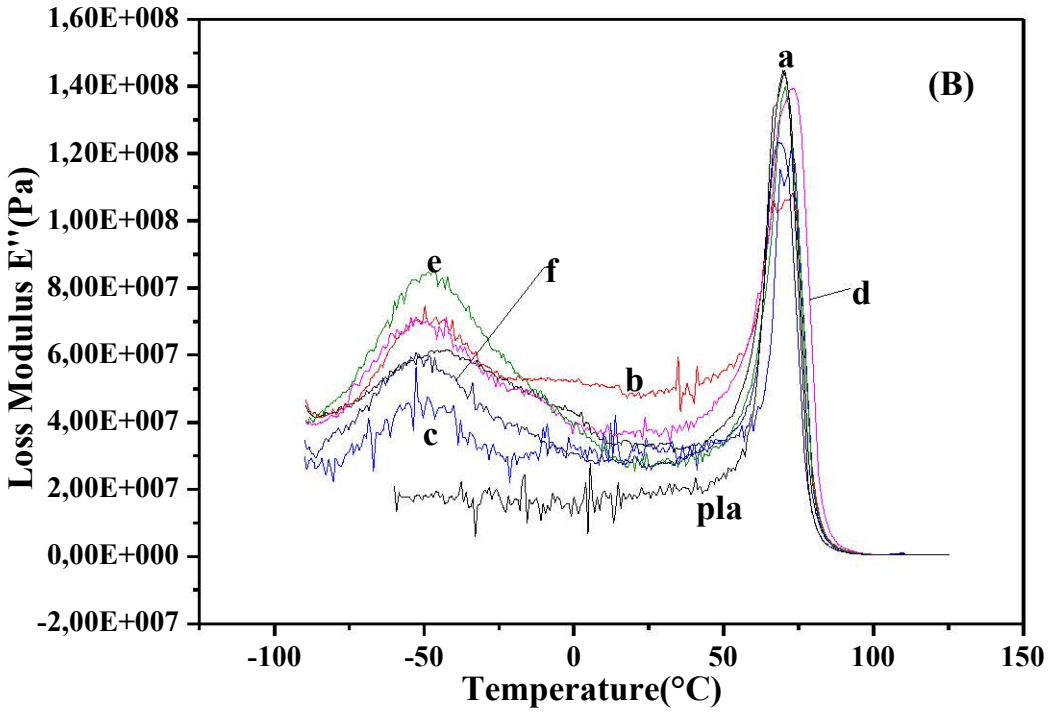
(B)
Loss Modulus E''(Pa)
Temperature(°C)
1,60E+008
1,40E+008
1,20E+008
1,00E+008
8,00E+007
6,00E+007
4,00E+007
2,00E+007
0,00E+000
-2,00E+007
-100
-50
0
50
100
150
a
b
c
d
e
f
pla

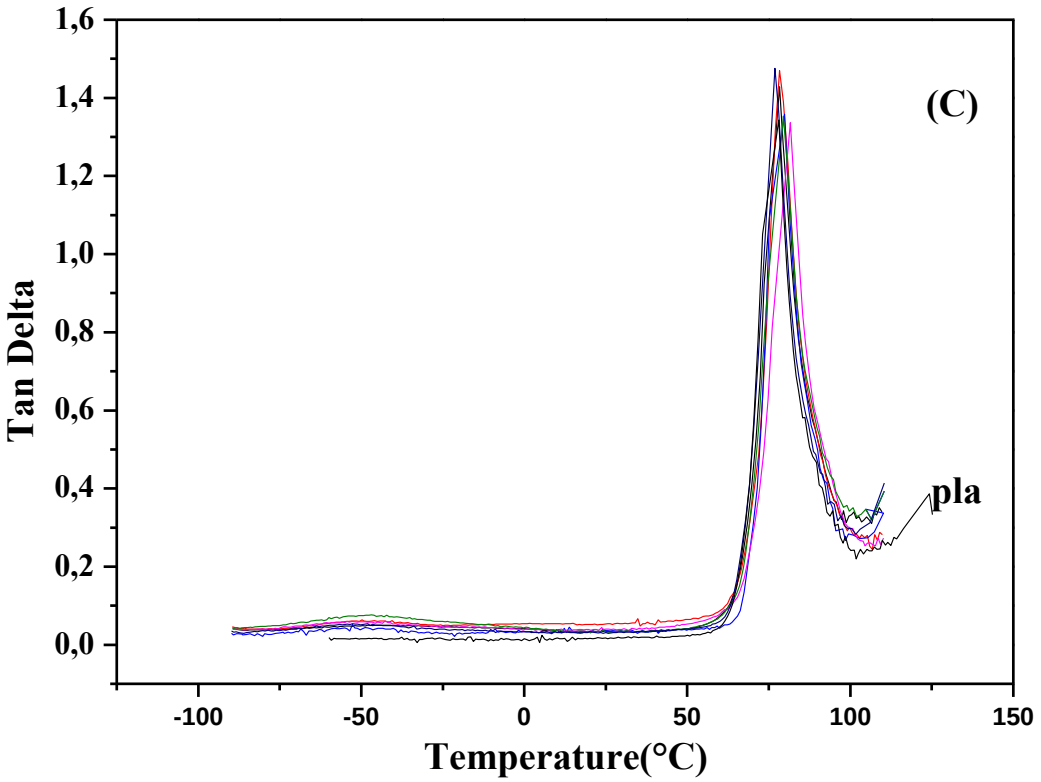

Figure 5.9 Temperature dependence of (A) storage modulus, (B) loss modulus and (C) tangent delta of pure PLA and PBA-LRD/PLA or PBA-LRD-Si/PLA composites: (a) PBA/PLA (20/80) blend, (b) PBA-2%LRD-Si/PLA (20/80) blend, (c) PBA-5%LRD-Si/PLA (20/80) blend, (d) PBA-5%LRD/PLA (20/80) blend, (e) LRD/PLA/PBA (1/79/20) blend, and (f) PBA-3%LRD-Si-3G/PLA (20/80) blend.

Loss modulus of PLA and PBA/PLA based composites are shown in Figure 5.9B. The maximum heat dissipation occurs at the temperature where loss modulus is maximum indication the relaxation temperature (T_α) of the system. The values of T_α of PBA and PLA are presented in Table 5.1 derived from E'' and tan δ curves. As observed from the E'' curves, all of the blends show two relaxation temperature, one for PBA at about -50°C and the other for PLA at about 78°C, indicating that the blends are not thermodynamically miscible. As shown in Table 5.1, with the addition of LRD-Si in the miniemulsion polymerization, the T_α of PBA is increased slightly and more clay loading the T_α higher further. The T_α of PBA in the PBA-LRD-Si/PLA blend with 5wt% LRD-Si is about 3°C more than that in the pure PBA/PLA blend. These results indicate with the LRD-Si in the PBA particle, the structure of nanoparticles is different from that of the pure PBA particles. It means the interaction between the LRD-Si and PBA limits the segmental movement of the PBA.

While LRD is added in the PBA latex preparation, the T_α of PBA has not changed a lot which implies LRD addition does not change the structure of PBA particles. In contrast, T_α of PLA is increasing for ~3°C when the LRD is introduced in the PBA miniemulsion polymerization while the addition of LRD-Si in PBA latex affects the T_α of PLA slightly. The introduction of LRD around PBA particles may form exfoliated dispersion of LRD in PLA matrix by mixing in microcompounder. The presences of exfoliated LRD platelets had reinforcement effect on PLA due to its ability to inhibit the movement of PLA chains. Hence, the transition temperature of PLA is increased. While the direct addition of LRD platelets in the PLA and PBA mixture by blending in microcompounder, the degree of delamination for LRD sheets in the blend cannot reach the same level as that of in the PBA-LRD/PLA blend. As a result, T_α of PLA in the LRD/PLA/PBA (1/79/20) composite only increases ~1°C. These results are consistent with the value of E' and the previous tensile test results for PBA-5%LRD/PLA (20/80) and LRD/PLA/PBA (1/79/20) blends. The variation tendency of T_α results from DMTA is also according with the results of DSC in chapter 4.

Table 5.1 The relaxation temperatures (T_α) obtained from the peaks of the loss modulus E'' curves and that of Tan δ curves.

Blends	***T_α1 (°C)***	***T_α2* (°C)**
Pure PLA	-	78
PBA/PLA (20/80)	-49	79
PBA-2%LRD-Si/PLA (20/80)	-49	78
PBA-5%LRD-Si/PLA (20/80)	-46	79
PBA-5%LRD/PLA (20/80)	-50	81
LRD/PLA/PBA (1/79/20)	-48	79
PBA-3%LRD-Si-3G/PLA (20/80)	-51	77

2.4. Morphology of specimens

To investigate the mechanism of the markedly increased elongation at break caused by the addition of PBA elastomer and the fracture mechanism of the blends, the morphologies of different necking regions of the tensile tested specimens was

investigated using SEM after etched by solvent. The fracture process normally occurs in several stages. First, after necking begins, small cavities, or microvoids, form in the interior of the cross section. Next, as deformation continues, these microvoids enlarge, come together, and coalesce to form a crack, which has its long axis perpendicular to the stress direction. Finally, fracture ensues by the rapid propagation of a crack around the outer perimeter of the neck, by shear deformation at an angle of about 45° with the tensile axis-this is the angle at which the shear stress is a maximum. In this type of fracture specimen (Figure 5.10 and 5.11), the central interior region of the surface has an irregular and fibrous appearance, which indicative of plastic deformation.

Note that neat PLA exhibited no necking phenomenon during the tensile test and broke with small elongation (<20%). The fracture surface for the tensile-tested specimens was almost the same as for neat PLA and no plastic deformation in the stress direction could be observed (not shown here).

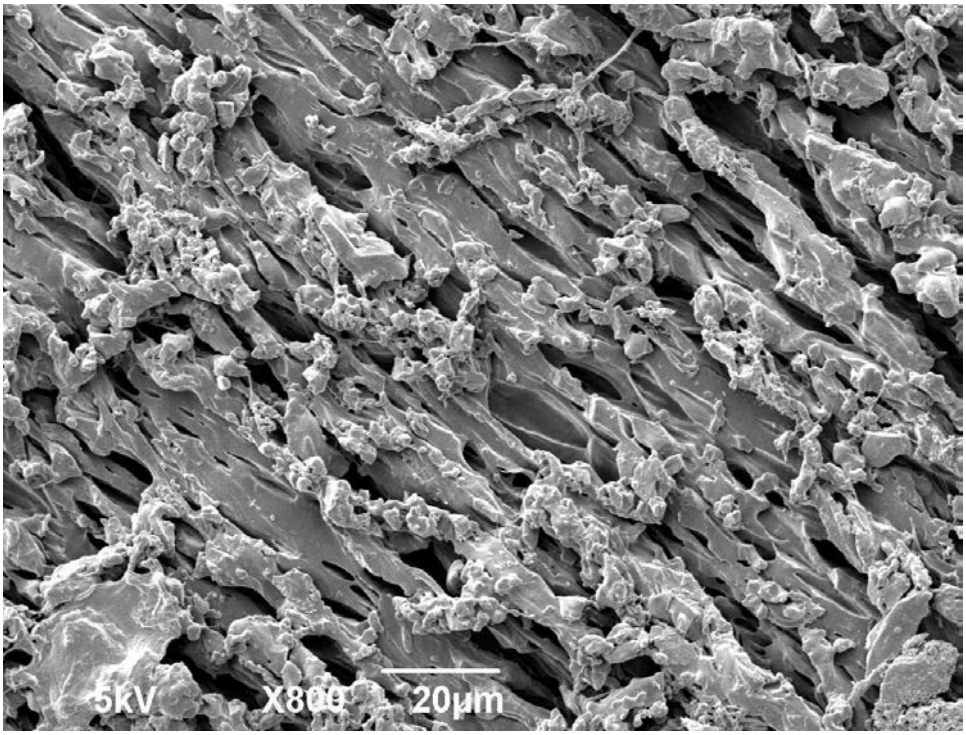

Figure 5.10 SEM fractograph showing fibrous characteristic of specimen PBA/PLA (20/80) after the tensile test. It is the surface chosen in the necking part within the specimen and the surface is parallel to the stress direction.

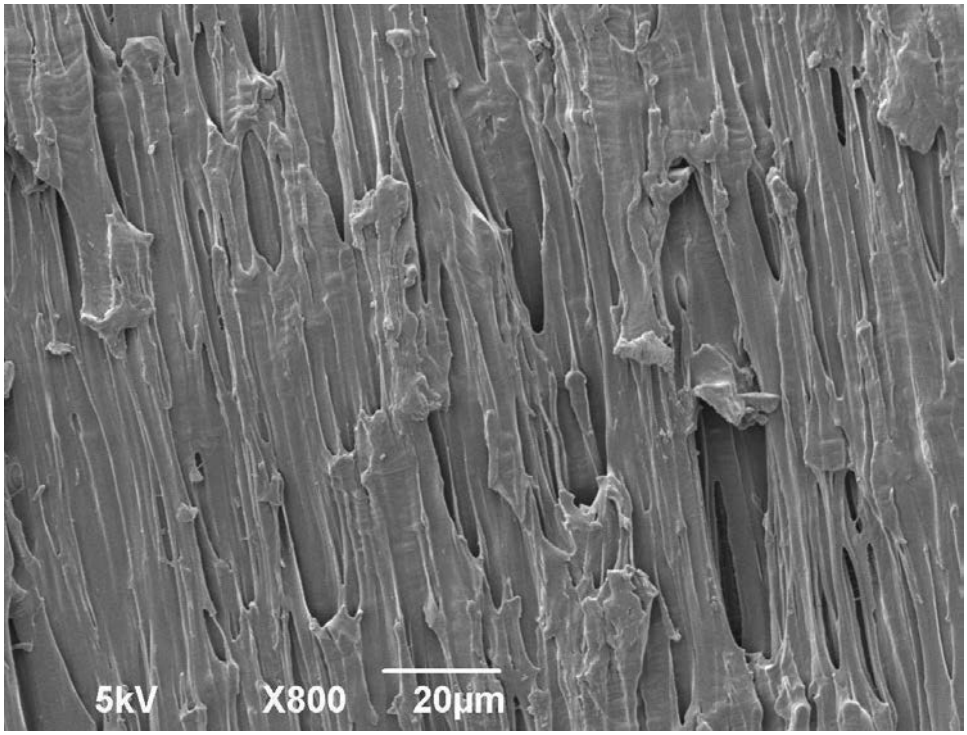

Figure 5.11 SEM fractograph showing fibrous characteristic of specimen PBA/PLA (20/80) after the tensile test. It is the outside surface of the specimen chosen in the necking part and the surface is parallel to the stress direction.

For a rubber-toughened plastic system, two types of cavitations induced by impact or tensile testing have been discriminated: internal cavitations in the rubber domains for the blends with strong interfacial adhesion, and debonding cavitations between the interfaces, when the interfacial adhesion was not sufficient. For the PBA/PLA blends, it is considered that the PBA domains act as stress concentrators upon being subjected to the tensile test in the initial state, because they have an elastic property that differs from the PLA matrix. This stress concentration leads to the development of a triaxial stress in the PBA particles and debonding occurs at the particle-matrix interface due to insufficient interfacial adhesion. Once the debonding occurs, the triaxial tension is locally released in the surrounding voids and the yield strength is lowered. Therefore, yielding occurs and the stress is then applied to the PBA domains. At this stage, the PBA domains are elongated along the stress direction and their shape becomes an ellipsoid, as shown the shape of pores in Figure 5.10. As the debonding progresses, the PLA matrix between the PBA particles deforms more easily and therefore shear yielding occurs. By this mechanism, orientation of both the matrix (Figure 5.11) and

the domains occurs (Figure 5.10). This debonding-induced shear yielding can also be confirmed by the large matrix deformation on impact testing (Figure 5.13), which will be discussed below.

The fracture surfaces of the neat PLA, the PBA/PLA (20/80) blends, and the PBA-2%LRD-Si/PLA (20/80) blends after the impact testing are shown in Figure 5.12, 5.13 and 5.14. The fracture surfaces are examined with the scanning electron microscope.

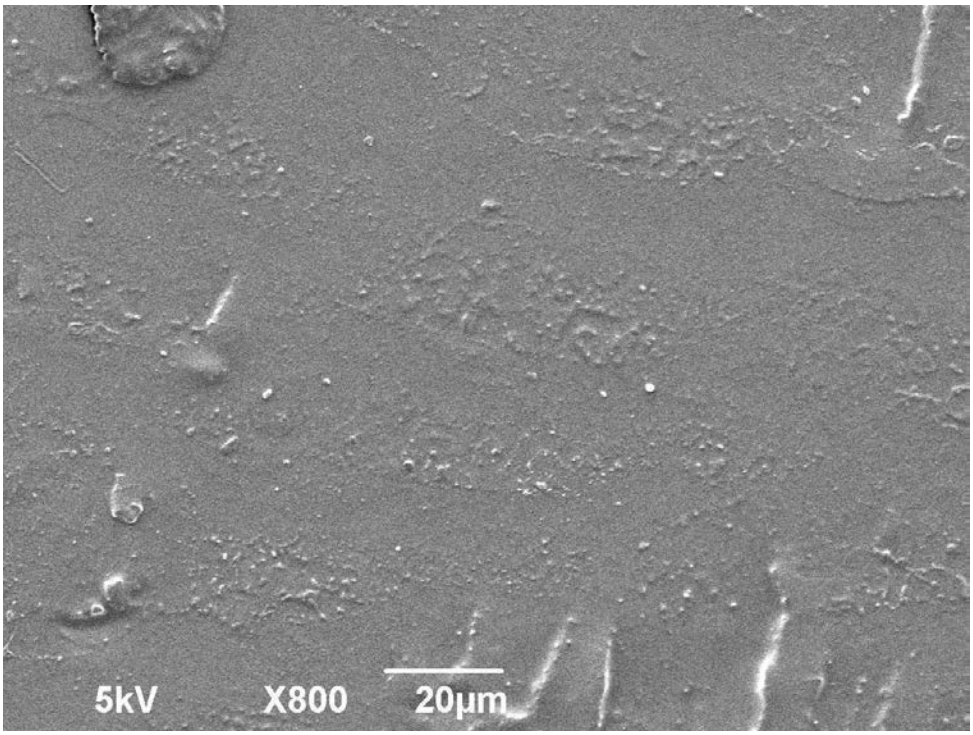

Figure 5.12 SEM fractograph of PLA after impact fracture testing.

Figure 5.12 shows the PLA fracture surface is smooth without obvious plastic deformation indicating a brittle fracture occurred in the impact fracture testing.

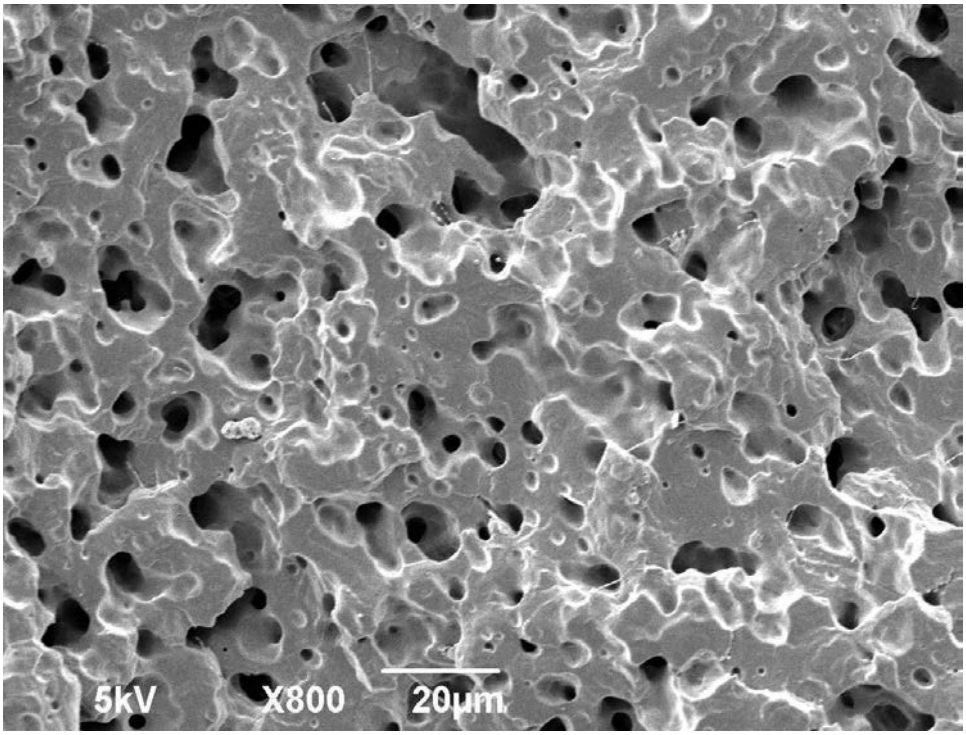

Figure 5.13 SEM fractograph of PBA/PLA (20/80) specimen after impact fracture testing.

For the PBA/PLA (20/80) blends, which is indicated in Figure 5.13, the fracture surfaces were more rough, they were found to consist of numerous spherical 'dimples' besides the pores. These 'dimples' are characteristic of fracture resulting from uniaxial tensile failure. Each dimple is one half of a microvoid that formed and then separated during the fracture process.

Upon addition of the PBA elastomer to the PLA matrix, stress whitening could be clearly observed after test and the fracture surface also shows a marked difference from that of neat PLA. Some fibrils can be observed for the PBA/PLA (20/80) (Figure 5.13) and PBA-2%LRD-Si/PLA (20/80) (Figure 5.14) blends, which implies that shear yielding of the PLA matrix has taken place.

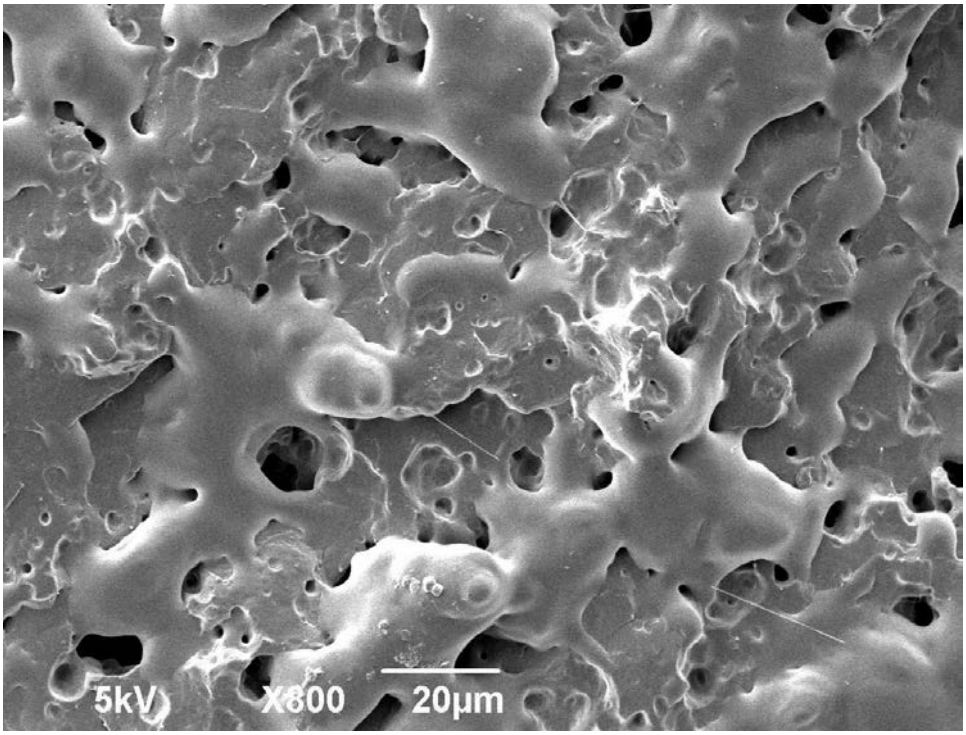

Figure 5.14 SEM fractograph of PBA-2%LRD-Si/PLA (20/80) specimen after impact fracture testing.

3. PLA and core-shell particles blends

3.1. Mechanical tests

By the encapsulation of LRD-Si in PBA particles, the interlayer spacing of the clay increases, even the exfoliation would take place. Furthermore, when the PBA-LRD-Si/PMMA core-shell was obtained, as the PMMA is partially miscible with PLA, the interaction between PBA and PLA would be improved. With the large interlayer spacing of clay and strong interaction of PBA in the PLA matrix, the corresponding properties of the resulting nanocomposites were investigated.

Figure 5.15 show s the tensile strength, the Young's modulus and impact strength for the pure PLA, PBA/PLA blends as well as (PBA/PMMA)/PLA blends. The blends of core-shell nanoparticles with PLA matrix had the significantly improved impact resistance (about 3 times comparing to that of pure PLA) while their tensile properties only decreased about 25% comparing to pure PLA.

The core-shell particles modified PLA maintains quite high tensile modulus and

tensile strength with the obviously increased impact strength, which means that the obtained material having a good stiffness-toughness balance. Furthermore, it can be expected that the blends exhibit increased heat resistance as compared with neat PLA due to the increased relaxation temperature (or glass transition temperature), as discussed in the DMTA results.

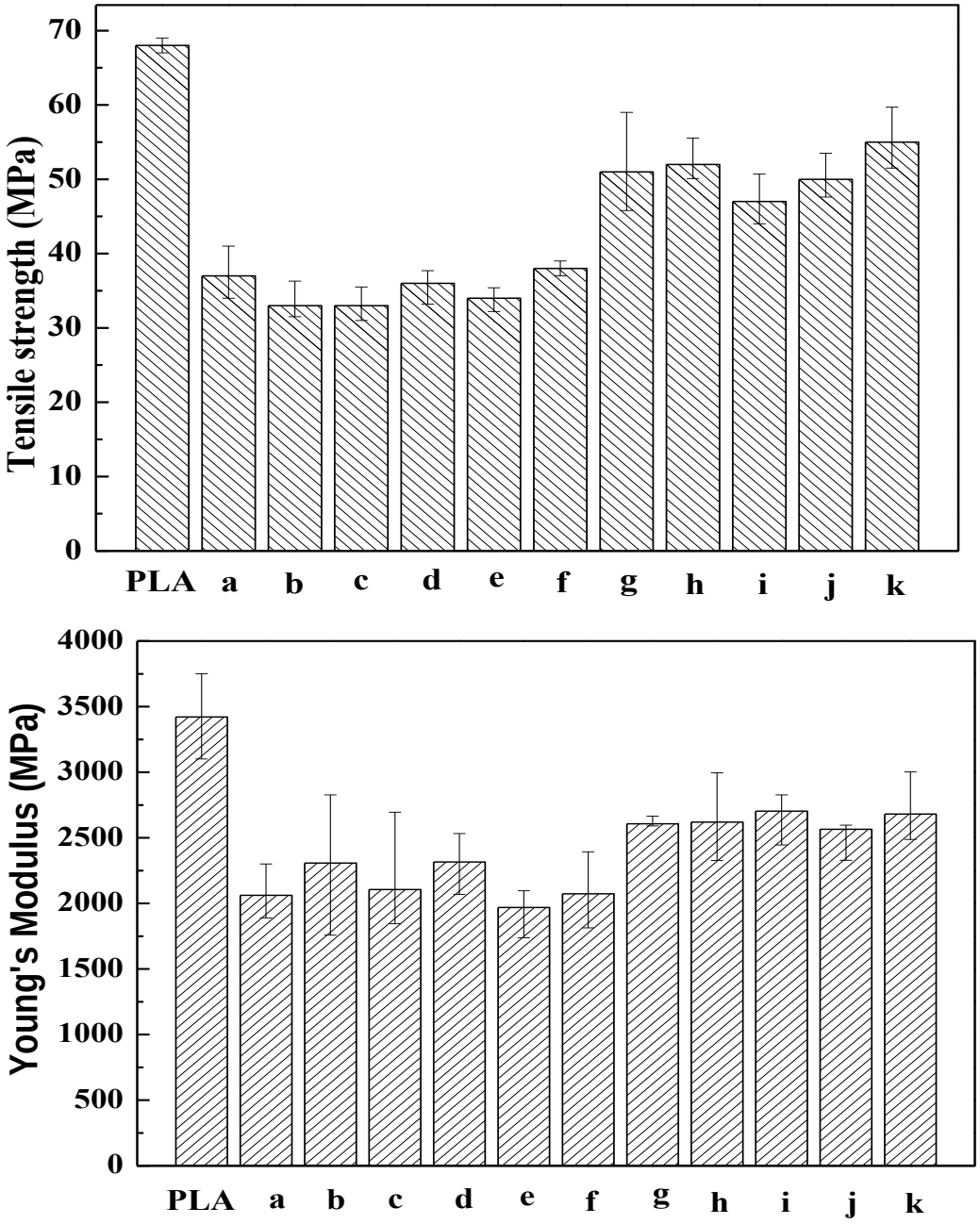

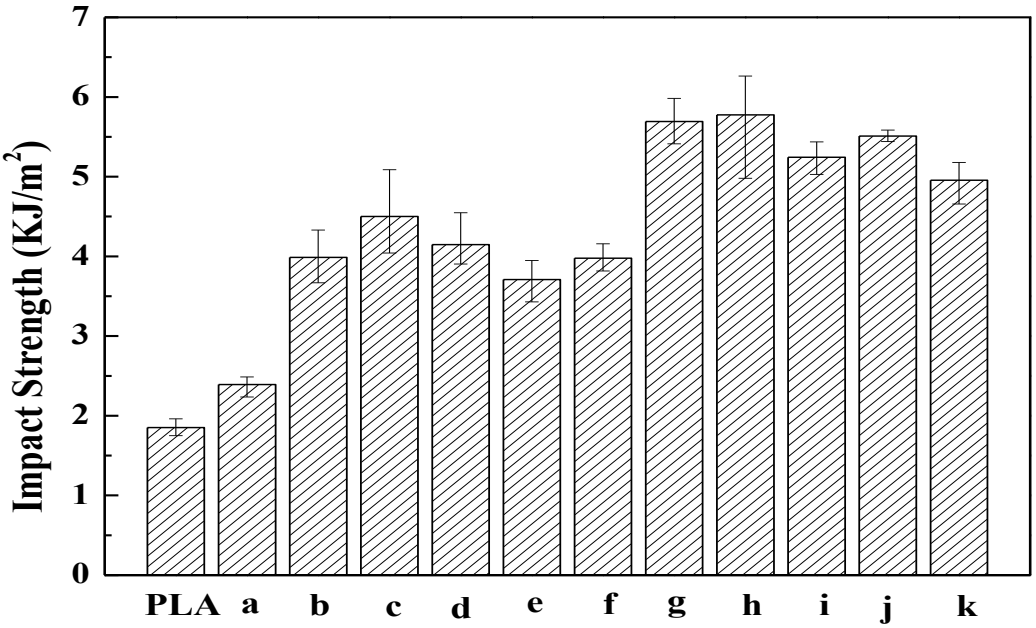

Figure 5.15 Tensile strength, Young's modulus, and impact strength of pure PLA, PBA/PLA blends and (PBA/PMMA)/PLA blends: (a) PBA/PLA (20/80) blend, (b) PBA-2%LRD-Si/PLA (20/80) blend, (c) PBA-5%LRD-Si/PLA (20/80) blend, (d) PBA-5%LRD/PLA (20/80) blend, (e) LRD/PLA/PBA (1/79/20) blend, and (f) PBA-3%LRD-Si-3G/PLA (20/80) blend, (g) (PBA/PMMA)/PLA (10/10/80) blend, (h) (PBA-2%LRD-Si/PMMA)/PLA (10/10/80) blend, (i) (PBA-5%LRD-Si/PMMA)/PLA (10/10/80) blend, (j) (PBA-5%LRD/PMMA)/PLA (10/10/80) blend, (k) LRD/PLA/(PBA/PMMA) (1/79/10/10) blend.

The strong hydrogen bonding between the ester-groups of PMMA chains and the PLA matrix made the nanoparticles disperse well in the matrix and greatly increased toughness of the composites.

The rubbery core consists of PBA, which was slightly crosslinked by LRD-Si could retain its spherical morphology and size during the processing and molding of the blends. In the case of good interfacial adhesion, the interfacial adhesion strength is strong enough to endure the build-up of sufficient stress around the particles, which induces crazing of the matrix, voiding in the rubber particles or cavity formation around interface at some critical stress level.

Avella et al. [14] have used PMMA as dispersed phase in blend with PLLA, the blends are prepared in reactive (R-type blends) as well as non-reactive (NR-type blends) methodologies, respectively. The tensile and impact properties of blends are summarized in Table 5.2.

Table 5.2 Flexural tests [14].

Sample	Modulus in MPa	Ultimate strength in MPa	Fracture energy in KN
PLLA	2900	15	0.0216
PLLA/PMMA 80/20 R	3200	4	0.005
PLLA/PMMA 70/30 R	3400	6	0.009
PLLA/PMMA 70/30 NR	3100	17	0.0217

The results of Avella et al. [14] indicated with the addition of PMMA in PLA matrix, without any chemical reaction between these two components, the existing of PMMA could improve the tensile strength and the modulus of the blend while without influence for increasing the blend's impact resistance. When we compared their results with our (PBA/PMMA)/PLA blends, it is clearly that the improvement of impact resistance for (PBA/PMMA)/PLA blends was all attributed to the soft core particles (PBA particles).

Meanwhile, the mean diameter of the PBA particles was about 350 nm in the PLA matrix with the help of PMMA. Furthermore, Udagama et al. [44] found the mechanical property improvements of an impact modifier depend on the properties of the rubbery core, the thickness of the PMMA shell and the particle size distribution of the latex (preferably no bigger than 200nm). When in our study, when the particle size of PBA core was decreased from 1~2 micron to ~350 nm within the PLA matrix, the reinforcing effect of PBA particles for impact resistance was enhanced.

Therefore, firstly, the existence of PMMA shell made up the loss of tensile property of PLA blends causing by introducing of PBA core particles; secondly, the PMMA shell acting like a compatibilizer had improved the dispersion of PBA particles within the PLA matrix.

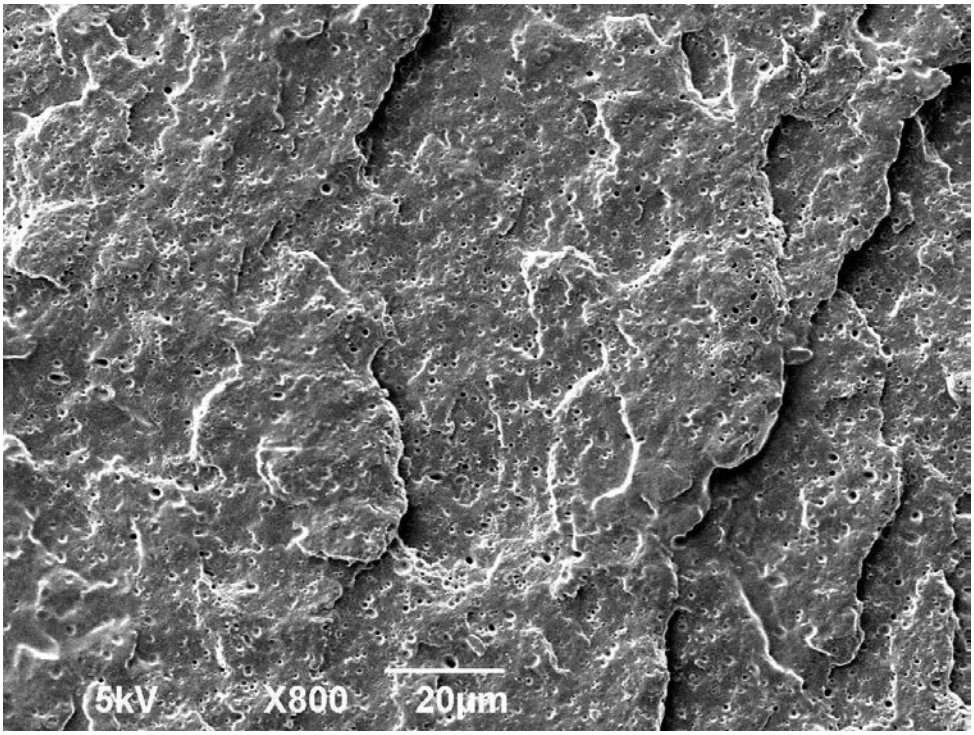

Figure 5.16 SEM fractograph of (PBA/PMMA)/PLA (10/10/80) specimen after impact fracture testing.

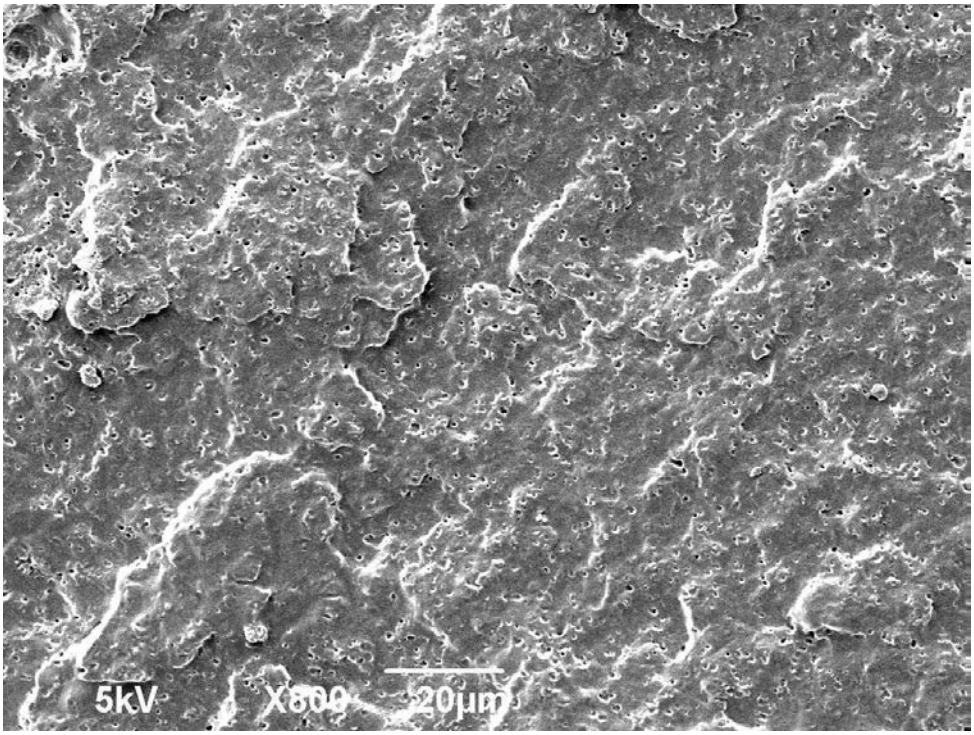

Figure 5.17 SEM fractograph of (PBA-2%LRD-Si/PMMA)/PLA (10/10/80) specimen after impact fracture testing.

The fracture for PBA/PLA blends tested by the Izod impact resistance shows no big

differences in comparison to the fracture surfaces of core-shell/PLA blends. This result suggests that the deformation mechanism of both blends is essentially the same.

3.2. Dynamic mechanical properties

Figure 5.18 shows the dynamic mechanical properties curves for neat PLA and PBA/PMMA/PLA based blends over a temperature range of -90°C~160°C.

Figure 5.18A exhibits the E' values for neat PLA and (PBA/PMMA)/PLA based blends. Similar to PBA/PLA based blends, the E' drops rapidly due to the glass-rubber transition, reaching a minimum value around 80°C.

Interestingly, below the T_g of PLA (~60°C), the PBA/PLA based blends exhibited higher E' value compared to (PBA/PMMA)/PLA based blends. This difference observed in E' was unexpected inasmuch as PMMA has a higher Young's modulus than PLA and the blending of soft PBA particles with stiff PLA matrix should decrease the stiffness of the blend more than the blending of (PBA/PMMA)/PLA does. The reduction of stiffness observed from tensile strength and Young's modulus (Figure 5.15A and 5.15B) in mechanical properties of PLA and (PBA/PMMA)/PLA based blends also contradicts these findings in E' curve. It should be noted that tensile test implies a much slower and direct strain rate, whereas a fast and amplitude type of strain is applied in DMTA. Thus, the presences of PBA composite particles in PLA seem to reduce more of the stiffness of PLA if a direct and slow rate of load is applied (in tensile test). Nevertheless, PBA/PMMA composites particles decrease the stiffness of PLA much faster when a rapid and cyclic type of load is applied (in DMTA).

It can be clearly observed that the E' values for (PBA/PMMA)/PLA based blends were maintained higher than pure PLA above T_g of PLA (~60°C) in which exhibiting the reinforcement effect of PMMA.

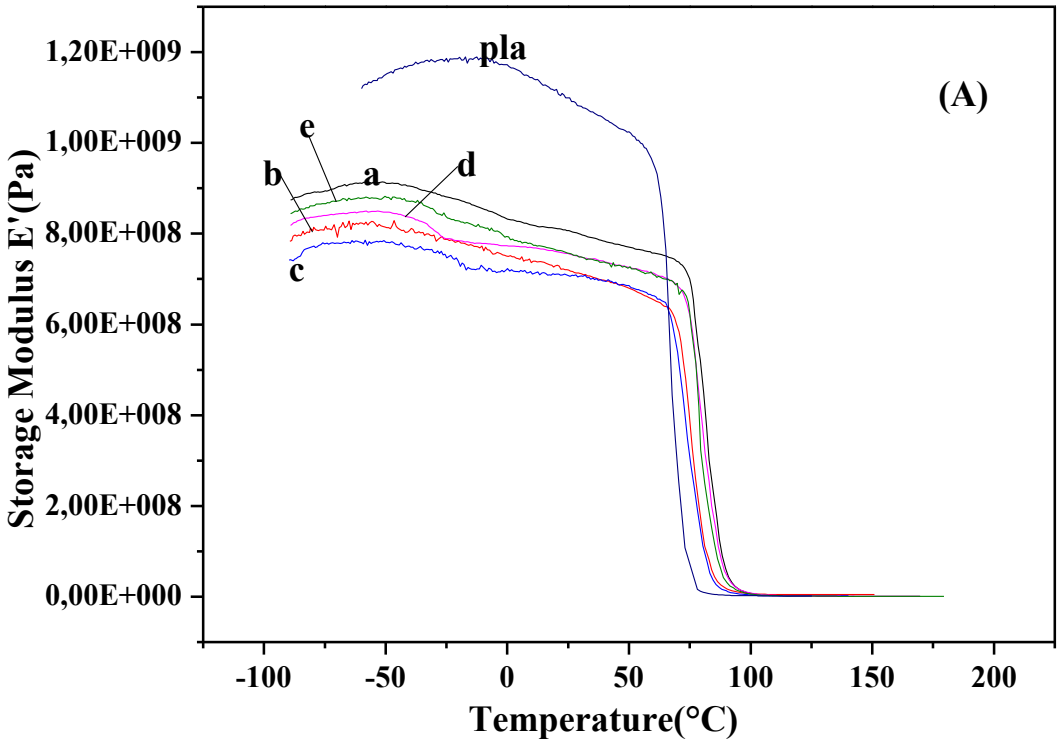
Storage Modulus E'(Pa)
1,20E+009
1,00E+009
8,00E+008
6,00E+008
4,00E+008
2,00E+008
0,00E+000
-100
-50
0
50
100
150
200
Temperature(°C)
pla
(A)
a
b
c
d
e

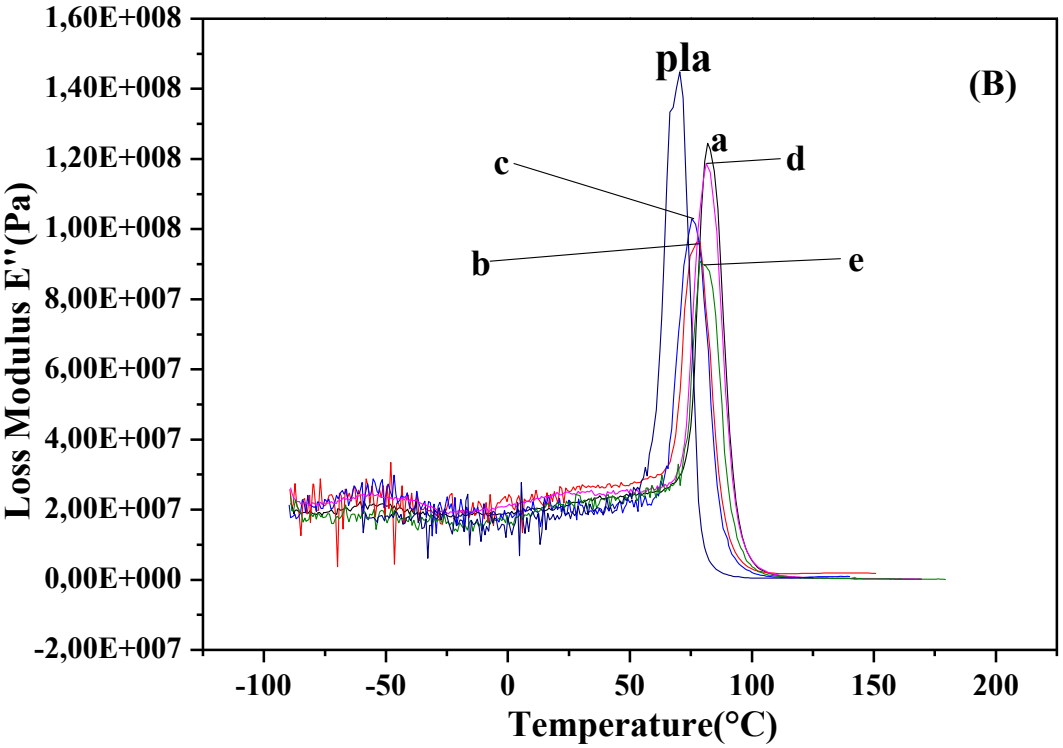
Loss Modulus E''(Pa)
1,60E+008
1,40E+008
1,20E+008
1,00E+008
8,00E+007
6,00E+007
4,00E+007
2,00E+007
0,00E+000
-2,00E+007
-100
-50
0
50
100
150
200
Temperature(°C)
pla
(B)
a
b
c
d
e

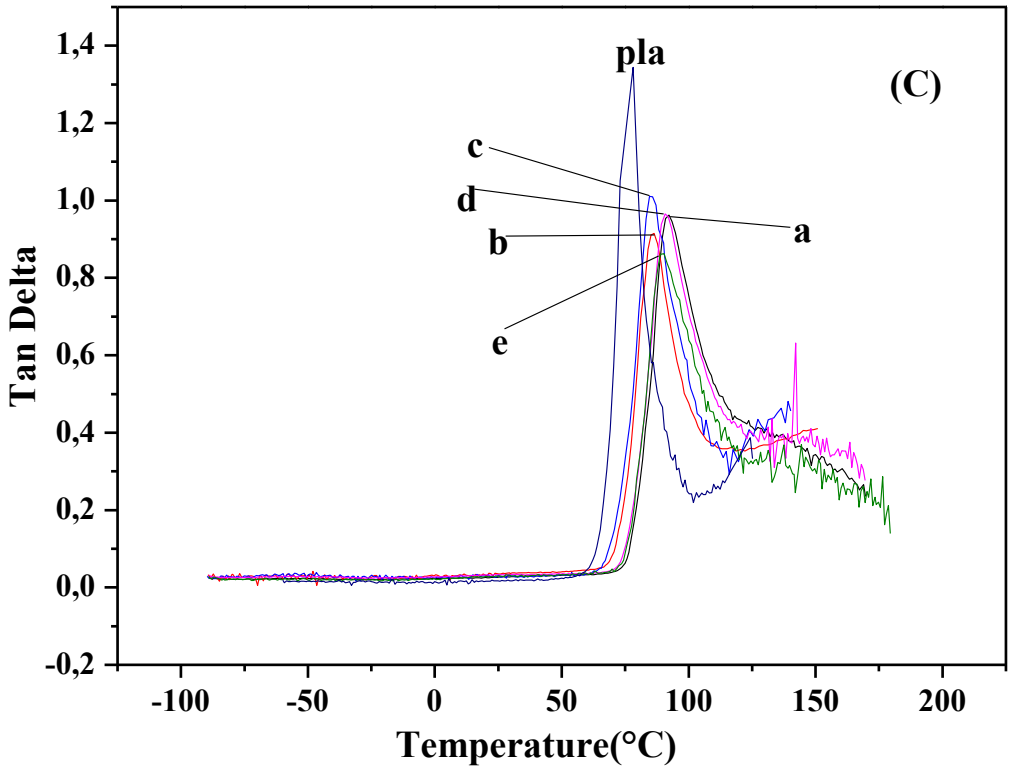

Figure 5.18 Temperature dependence of (A) storage modulus, (B) loss modulus and (C) tangent delta of pure PLA and (PBA-LRD/PMMA)/PLA or (PBA-LRD-Si/PMMA)/PLA composites: (a) (PBA/PMMA)/PLA (10/10/80) blend, (b) (PBA-2%LRD-Si/PMMA)/PLA (10/10/80) blend, (c) (PBA-5%LRD-Si/PMMA)/PLA (10/10/80) blend, (d) (PBA-5%LRD/PMMA)/PLA (10/10/80) blend, and (e) LRD/PLA/(PBA/PMMA) (1/79/10/10) blend.

Loss modulus E'' of the pure PLA and (PBA/PMMA)/PLA based composites are shown in Figure 5.18B indicating T_α of the blends with core-shell PBA/PMMA particles shift to higher temperatures. From Figure 5.18B and 5.18C, T_α of PBA phase or PMMA phase is not clear from the DMTA curves because the concentration of these two phases was low which had only 10%. T_α of PLA increased with adding the compatibilizers PMMA which enhances the shift. The uncompatibilized PBA/PLA blends show almost same T_α corresponding to the each component, indicating the thermodynamic immiscibility between PLA and PBA. The addition of PMMA clearly changes the peak positions of PLA. From Table 5.3, the T_α of PLA shift toward to higher temperature, suggesting the compatibilities between PLA and PMMA. The DMTA results are consistent with those by SEM. It can be explained based on the retardation in the relaxation of amorphous regions imparted by the enhanced physical

interaction with the reinforcing phase and the PLA matrix. The increase of T_α is associated with the decreased mobility of the matrix chains, which indicates enhanced interfacial adhesion between the PBA core and the PLA matrix.

Table 5.3 The relaxation temperatures (T_α) obtained from the peaks of Tan δ curves.

Blends	***T_α*** **(°C)**
Pure PLA	78
(PBA/PMMA)/PLA (10/10/80)	92
(PBA-2%LRD-Si/PMMA)/PLA (10/10/80)	86
(PBA-5%LRD-Si/PMMA)/PLA (10/10/80)	85
(PBA-5%LRD/PMMA)/PLA (10/10/80)	91
LRD/PLA/(PBA/PMMA) (1/79/10/10)	89

The ratio of loss modulus to storage modulus is defined as mechanical loss factor or tan δ. The damping properties of the material give the balance between the elastic phase and viscous phase in a polymeric structure. A good interface will bear a greater stress and a less energy dissipation. However, composite material with poor interfacial bonding will tend to dissipate more energy showing high magnitude of damping peak in comparison to a material with strongly bonded interface. By comparing Figure 5.18C and Figure 5.9C, they show that the damping peak in the (PBA/PMMA)/PLA based blends decrease in comparison to neat PLA and PBA/PLA based blends. It indicates that compatibility between PLA matrix and PBA particles is much improved by PMMA.

4. Conclusion

The incorporation of the PBA nanoparticles in the PLA increases the impact strength of the PLA while significantly reducing its tensile properties. When laponite is incorporated in the PBA nanoparticles, the tensile properties of the PLA are further improved. Furthermore, while the PBA-laponite nanocomposite are encapsulated by PMMA shell which not only has better tensile properties than but also better compatibility with the PLA, the impact strength of the resulting

(PBA-LRD-PMMA)/PLA blends is significantly higher (3 times) than that of the PLA, with a minimum decrease (~25%) in tensile properties.

Conclusions and perspectives

PBA nanoparticles have been prepared by miniemulsion polymerization. Several parameters for miniemulsion polymerization have been examined. Several surfactants such as SDS, Brij78 and Brij700 were used to form stable miniemulsion systems, with the final particle size around 100 nm.

With the addition of OMMT in the PBA miniemulsion, only unstable latex could be obtained after the polymerization. The size of OMMT particles was too large (~300 nm in length) to be encapsulated in the nanoparticles PBA. However, another kind of clay-laponite RD (LRD) (~25 nm in length and ~1 nm in thickness) was a better choice for the encapsulation within the nanosize PBA particles.

3-Methacryloxypropyltrimethoxysilane (MPTMS) was confirmed to be a very useful coupling agent for LRD. Because after the modification of LRD, the double bonds of MPTMS were capable to react with BA monomer and linked the LRD sheets with PBA chains. The encapsulation of laponite in PBA particles was formed by the aid of MPTMS. The LRD particles with grafted MPTMS acted as a crosslinking agent during BA polymerization. The degree of crosslinking was enhanced with increasing the load of modified-LRD. Meanwhile, cationic surfactant was necessary to obtain a convenient dispersion of laponite in the monomer which was a key point in order to achieve the encapsulation of LRD. It was clear that laponite in the PBA particle was not forming stack but well exfoliation which was confirmed by TEM images.

PBA particles in the PLA matrix had smooth, distinct particle interfaces indicating an incompatible polymer blend. Agglomeration of PBA phase caused by the melt blending was very clear. Attempts for improving the dispersion of PBA particles in the PLA matrix by using polymer surfactant like poly(ethylene glycol) methyl ether methacrylate (PEGMEM, Mn=950) were not successful. It was presumed that the quantity of PEGMEM molecules sticking to the PBA particles was not enough to produce a significantly improved dispersion of PBA in the blend. For further study, the amount of the PEGMEM in the complex surfactant to insure a better dispersion of elastomer particles in the matrix can still be explored. On the other side, the weakness

of tensile strength of PEGMEM in the polymer matrix should be also taken into account for the further exploration.

Furthermore, two other silanes, 3-Aminopropyltriethoxy silane (3A) and 3-Glycidoxypropyltrimethoxy silane (3G), were used to modify LRD-Si in order to improve interfacial properties of PBA particles with PLA matrix because the functional groups on the silane molecule would react with hydroxyl groups of the PLA. From the SEM images, the latter silane (3G) has a better influence for improving the interfacial properties of PBA particles and PLA matrix.

Because poly(methyl methacrylate) (PMMA) was partially miscible with PLA, PBA/PMMA core-shell latexes with or without LRD (or LRD-Si) were prepared by seeded emulsion polymerization in order to improve compatibility between nanoparticles and PLA matrix. The incorporation of the PBA nanoparticles in the PLA increased the impact strength of the PLA while significantly reducing its tensile properties. When laponite was incorporated into the PBA nanoparticles, the tensile properties of the PLA were further improved. On the other hand, when the PBA-laponite nanocomposite nanoparticles were encapsulated by PMMA shell which not only had better tensile properties than but also possessed better compatibility with the PLA, the impact strength of the resulting (PBA-LRD/PMMA)/PLA blends was significantly higher (3 times) than that of the PLA, with a minimum decrease (about 25%) in tensile properties.

However, for achieving a better enhancement of PLA matrix and obtaining an improved dispersion of PBA particles in the matrix, the thickness and the structure of PMMA shell in the core-shell particles should be further studied.

References

[1] H. S. Yongjin Li, "Improvement in toughness of poly (l-lactide) (PLLA) through reactive blending with acrylonitrile-butadiene-styrene copolymer (ABS): Morphology and properties," *European Polymer Journal,* vol. 45, pp. 738-746, 2009.

[2] A. H. M. U. W. A. Y. S. B. A. R. Harintharavimal Balakrishnan, "Novel toughened polylactic acid nanocomposite: Mechanical, thermal and morphological properties," *Materials and Design,* vol. 31, pp. 3289-3298, 2010.

[3] D. M. V. K. O. T. T. T. F. T. F. Ryoko Tokoro, "How to improve mechanic properties of polylactic acid with bamboo fibers," *Journal of Materials Science,* vol. 43, pp. 775-787, 2008.

[4] J. Q. M. L. S. D. L. S. S. L. G. Z. Y. Z. X. F. Lijun Qin, "Mechanical and thermal properties of poly (lactic acid) composites with rice straw fiber modified by poly (butyl acrylate)," *Chemical Engineering Journal,* vol. 166, pp. 772-778, 2011.

[5] R. N. K. C. T. D. Y. I. Sachiko Ishida, "Toughening of Poly (L-lactide) by Melt Blending with Rubbers," *Journal of Applied Polymer Science,* vol. 113, pp. 558-566, 2009.

[6] H. Y. M. Q. Y. L. J. K. W. W. H. G. Q. F. Shi, "Influence of Heat Treatment on the Heat Distortion Temperature of Poly(lactic acid)/Bamboo Fiber/Talc Hybrid Biiocomposites," *Journal of Applied Polymer Science,* vol. 123, pp. 2828-2836, 2012.

[7] H. S. Yongjin Li, "Toughening of Polylactide by Melt Blending with a Biodegradable Poly(ether)urethane Elastomer," *Macromolecular Bioscience,* vol. 7, pp. 921-928, 2007.

[8] A. D. S. F. P. D. M. A. P. D. Marius Murariu, "Polylactide compositions. Part 1: Effect of filler content and size on mechanical properties of PLA/calcium sulfate composites," *Polymer,* vol. 48, pp. 2613-2618, 2007.

[9] A. K. J. L. C. C. S. G. L.-S. T. Srikanth Pilla, "Microcellular processing of polylactide-hyperbranched polyester-nanoclay composites," *Journal of materials science,* vol. 45, pp. 2732-2746, 2010.

[10] A. D. S. F. M. P. L. B. M. A. P. D. Marius Murariu, "Polylactide (PLA)-CaSO4 composites toughened with low molecular weight and polymeric ester-like plasticizers and related performances," *European polymer Journal,* vol. 44, p. 3842–3852, 2008.

[11] S. S. H. R. Sathya Kalambur, "Biodegradable and Functionally Superior Starch–Polyester Nanocomposites from Reactive Extrusion," *Journal of Applied Polymer Science,* vol. 96, pp. 1072-1082, 2005.

[12] B. H. S. S. Rafael Auras, "An Overview of Polylactides as Packaging Materials," *Macromolecular Bioscience,* vol. 4, pp. 835-864, 2004.

[13] W. Y. R. K. Y. L. Dean Shi, "Study of nanocomposites containing core-shell fibers with rigid nano-SiO2 core in PMMA matrix," *Journal of Materials*

Science, vol. 43, pp. 1162-1165, 2008.

[14] M. E. E. B. I. M. M. L. F. L. P. Maurizio Avella, "Radical polymerization of methyl methacrylate in the presence of biodegradable poly (L-lactic acid). Preparation of blends, chemical-physical characterization and morphology," *Macromolecular Chemistry and Physics,* vol. 201, pp. 1295-1302, 2000.

[15] M. E. E. B. I. M. M. E. M. L. P. L. F. Maurizio Avella, "Radical polymerization of poly(butyl acrylate) in the presence of poly(L-lactic acid), 1 Synthesis, characterization and properties of blends," *Die Angewandte Makromolekulare Chemie,* no. 246, pp. 49-63, 1997.

[16] S. K. L. W. S. Chow, "Thermal properties of poly(lactic acid)/organo-montmorillonite nanocomposites," *Journal of Thermal Analysis and Calorimetry,* vol. 95, pp. 627-632, 2009.

[17] P. M. M. O. K. Y. a. K. U. Suprakas Sinha Ray, "New Polylactide/Layered Silicate Nanocomposites. 1. Preparation, Characterization, and Properties," *Macromolecules,* vol. 35, pp. 3104-3110, 2002.

[18] Y.-z. B. Z.-m. H. Z.-x. W. Dong-ming Qi, "Synthesis and Characterization of Poly(butyl acrylate)/Silica and Poly(butyl acrylate)/Silica/Poly(methyl methacrylate) Composite Particles," *Journal of Applied Polymer Science,* vol. 99, pp. 3425-3432, 2006.

[19] L. L. W. Z. Y. F. Yu Li, "A new hybrid nanocomposite prepared by graft copolymerization of butyl acrylate onto chitosan in the presence of organophilic montmorillonite," *Radiation Physics and Chemistry,* vol. 69, pp. 467-471, 2004.

[20] J.-L. P. L. D. a. E. B.-L. Norma Negrete-Herrera, "Polymer/Laponite Composite Colloids through Emulsion Polymerization: Influence of the Clay Modification Level on Particle Morphology," *Macromolecules,* vol. 39, pp. 9177-9184, 2006.

[21] Y. D. Zhaohui Tong, "Synthesis of polystyrene encapsulated nanosaponite composite latex via miniemulsion polymerization," *Polymer,* vol. 48, pp. 4337-4343, 2007.

[22] Y. D. Zhaohui Tong, "Synthesis of Water-Based Polystyrene-Nanoclay Composite Suspension via Miniemulsion Polymerization," *Industrial & Engineering Chemistry Research,* vol. 45, pp. 2641-2645, 2006.

[23] M. W. Z. Z. X. G. Y. F. Tao Wang, "Preparation of core (PBA/layered silicate)-shell (PS) structured complex via γ-ray radiation seeded emulsion polymerization," *Materials Letters,* vol. 60, pp. 2544-2548, 2006.

[24] J.-L. P. L. D. F. D. H. E. B.-L. Norma Negrete-Herrera, "Polymer/Laponite composite latexes: Particle morphology, film microstructure, and properties," *Macromolecular Rapid Communications,* vol. 28, pp. 1567-1573, 2007.

[25] J. D. H. Alexander B. Morgan, "Exfoliated polystyrene-clay nanocomposites synthesized by solvent blending with sonication," *Polymer,* vol. 45, pp. 8695-8703, 2004.

[26] P. J. C. a. S. A. F. B. Severine Cauvin, "Pickering stabilized miniemulsion polymerization: Preparation of clay armored latexes," *Macromolecules,* vol. 38,

pp. 7887-7889, 2005.

[27] K. L. H. F. Bodo zu Putlitz, "The generation of "armored latexes" and hollow inorganic shells made of clay sheets by templating cationic miniemulsions and latexes," *ADVANCED MATERIALS,* vol. 13, pp. 500-503, 2001.

[28] B.-L. E, "Organic-inorganic nanostructured colloids," *Journal of nanoscience and nanotechnology,* vol. 2, pp. 1-24, 2002.

[29] a. J. V. Y.J. Chou. M.S. El Aasser, «Mechanism of emulsification of styrene using hexadecyltrimethyl ammonium bromide-cetyl alcohol mixtures,» *Journal of Dispersion Science and Technology,* vol. 1, pp. 129-150, 1980.

[30] J. M. W. I. Higuchi, "Physical degradation of emulsions via the molecular diffusion route and the possible prevention thereof," *Journal of Pharmaceutical Science,* vol. 51, pp. 459-466, 1962.

[31] M. S. E.-A. G. W. P. J. W. V. D. P. Durbin, «Influence of monomer preemulsification on formation of particles from monomer drops in emulsion polymerization,» *Journal of Applied Polymer Science,* vol. 24, p. 703–707, 1979.

[32] J. M. Asua, "Miniemulsion polymerizatioin," *Progress in Polymer Science,* vol. 27, pp. 1283-1346, 2002.

[33] J. Z. S. W. D. S. Guobao Zhang, "Miscibility and Phase Structure of Binary Blends of Polylactide and Poly (methyl methacrylate)," *Journal of Polymer Science: Part B: Polymer Physics,* vol. 41, pp. 23-30, 2003.

[34] M. J. F.-B. J. S. R. Jose Luis Eguiburu, "Graft copolymers for biomedical applications prepared by free radical polymerization of poly (L-lactide) macromonomers with vinyl and acrylic monomers," *Polymer,* vol. 37, no. 16, pp. 3615-3622, 1996.

[35] S. R. Sahoo Prafulla K., "Fire retardancy and biodegradability of poly(methyl methacrylate)/ montmorillonite nanocomposite," *Polymer degradation and stability,* vol. 92, pp. 1700-1707, 2007.

[36] C. B. M. L. a. H. W. S. Katharina Landfester, "Characterization of Interfaces in Core-Shell Polymers by Advanced Solid-State NMR Methods," *Macromolecules,* vol. 29, pp. 5972-5980, 1996.

[37] D. d. W.-R. R. D. S. B. K. Andre J. P. van Zyl, «The role of surfactant in controlling particle size and stability in the miniemulsion polymerization of polymeric nanocapsules,» *European Polymer Journal,* vol. 40, pp. 2717-2725, 2004.

[38] Y. J. G. Z. L. Y. Zeng Zhong, "Preparation and application of cross-linked core-shell PBA/PS and PBA/PMMA nanoparticles," *Frontiers of Chemistry in China,* vol. 4, pp. 459-464, 2006.

[39] A. P. J. S. D. S. S. Kirsch, "Control of particle morphology and film structures ofcarboxylated poly (n butylacrylate)/poly (methyl methacrylate) composite latex particles," *Colloids and Surfaces A: Physicochemical and Engineering Aspects,* Vols. 183-185, pp. 725-737, 2001.

[40] D. L. a. P. S. Dongxia Huo, "Morphology of poly(butyl acrylate)/poly(styrene-co-methyl methacrylate) latex prepared by starved emulsion polymerization: II. Development of particle morphology," *Polymer International,* vol. 51, pp. 1417-1421, 2002.

[41] V. L. D. M. S. E.-A. Katharina Landfester, "The evaluation of the size and the structure of the interphase in composite particles containing a macromonomer studied by solid-state NMR," *Macromolecular Chemistry and Physics,* vol. 203, pp. 1772-1780, 2002.

[42] M. S. E.-A. A. K. E. S. D. a. J. E. R. V. Nelliappan, "Compatibilization of the PBA/PMMA Core/Shell Latex Interphase. I. Partitioning of PMMA Macromonomer in the PBA Seed Latex," *Journal of Polymer Science: Part A: Polymer Chemistry,* vol. 34, pp. 3173-3181, 1996.

[43] J. Y. a. C. E. P. Kilwon Cho, "The effect of interfacial adhesion on toughening behaviour of rubber modified poly (methyl methacrylate)," *Polymer,* vol. 38, pp. 5161-5167, 1997.

[44] T. F. L. M. R. Udagama, "Strategies for the Production of High Solids Acrylic/Methacrylic Core-Shell Latices," *Journal of Applied Polymer Science,* vol. 115, pp. 2668-2676, 2010.

[45] A. P. K. L. O. S. M. S. E.-A. Stefan Kirsch, "Particle Morphology of Carboxylated Poly (n-butyl acrylate)/Poly (methyl methacrylate) Composite Latex Particles," *Macromolecular Symposia,* vol. 151, pp. 413-418, 2000.

[46] J. Y. C. E. P. Kilwon Cho, "The effect of rubber particle size on toughening behaviour of rubber-modified poly (methyl methacrylate) with different test methods," *Polymer,* vol. 39, p. 3073–3081, 1998.

[47] W. M. a. A. M. v. H. D. J. Voorn, "Clay Platelets Encapsulated Inside Latex Particles," *Macromolecules,* vol. 39, pp. 4654-4656, 2006.

[48] R. P. B. R. P. C. J. Wootthikanokkhan, "Effect of Acrylic Diblock Copolymer upon Interfacial Adhesion," *Journal of Applied Polymer Science,* vol. 62, pp. 835-844, 1996.

[49] K. L. Shyang CW, "Flexural, morphological and thermal properties of polylactic acid/organo-montmorillonite nanocomposites," *Polymers & polymer composites,* vol. 16, pp. 263-270, 2008.

[50] Y. D. Zhaohui Tong, "Kinetics of Miniemulsion Polymerization of Styrene in the Presence of Organoclays," *Macromolecular Materials and Engineering,* vol. 293, pp. 529-537, 2008.

[51] J. M. A. M. P. J. R. L. Gabriela Diaconu, "High-Solids Content Waterborne Polymer-Clay Nanocomposites," *Macromolecular Symposia,* vol. 259, pp. 305-317, 2007.

[52] Y. D. Z. L. W. Qunhui Sun, "Synthesis and Characterization of Polystyrene-Encapsulated Laponite Composites via Miniemulsion Polymerization," *Macromolecular Materials and Engineering,* vol. 289, pp. 288-295, 2004.

[53] M. P. J. R. L. Gabriela Diaconu, "Towards the synthesis of high solids content waterborne poly(methyl methacrylate-co-butyl acrylate)/montmorillonite nanocomposites," *Polymer,* vol. 49, pp. 2444-2454, 2008.

[54] A. M. S. P. C. O. F. C. T. S. M. d. A. T. S. V. N. R. D. Raul P. Moraes, "Poly(styrene-co-butyl acrylate)-Brazilian Montmorillonite Nanocomposites, Synthesis of Hybrid Latexes via Miniemulsion Polymerization," *Macromolecular Symposia,* Vols. 245-246, pp. 106-115, 2006.

[55] M. S. E.-A. Peter A. Lovell, *Emulsion Polymerization and Emulsion Polymers,* 1997.

[56] C. A. F. Henry Warson, *Applications of Synthetic Resin Latices,* 2001.

[57] K. T. Dieter Urban, *Polymer Dispersions and Their Industrial Applications,* 2002.

[58] A. J. M., "Emulsion polymerization: from fundamental mechanisms to process developments.," *Journal of polymer science. Part A. Polymer chemistry,* vol. 42, pp. 1025-1041, 2004.

[59] J. L. Gardon, "Mechanism of Emulsion Polymerization," *Rubber Chemistry and Technology,* vol. 43, pp. 74-94, 1970.

[60] I. Piirma, *Emulsion polymerization,* New York, 1982.

[61] G. W. Poehlein, «Emulsion polymerization,» *ACS Symposium Series,* vol. 285, p. 131–150, 1985.

[62] D. J. D. G. W. Poehlein, "Continuous emulsion polymerization," *Rubber Chemistry and Technology,* vol. 50, p. 601–639, 1977.

[63] F. J.Ugelstad, "Kinetics and mechanism of emulsion polymerization," *Rubber chemistry and technology,* vol. 49, p. 536–612, 1976.

[64] W. D. Harkins, "A general theory of the mechanism of emulsion polymerization," *Journal of the American Chemical Society,* vol. 69, p. 1428–1444, 1947.

[65] R. H. E. W. V. Smith, "Kinetics of emulsion polymerization," *Journal of Chemical Physics,* vol. 16, p. 592–600, 1948.

[66] D. H. N. A. E. Alexander, "Emulsion polymerization," *Progress in Polymer Science,* vol. 3, p. 145–197, 1971.

[67] D. C. Blackley, *Emulsion Polymerization,* New York, 1982.

[68] M. G. E. C. S. P. J. H. Baxendale, "The mechanism and kinetics of the initiation of polymerisation by systems containing hydrogen peroxide," *Transactions of the Faraday Society,* vol. 42, p. 675–684, 1946.

[69] M. G. E. J. K. K. J. H. Baxendale, "The kinetics of polymerisation reactions in aqueous solution," *Transactions of the Faraday Society,* vol. 42, p. 668–675, 1946.

[70] W. J. Priest, "Partice Growth in the Aqueous Polymerization of Vinyl Acetate," *The Journal of Physical Chemistry,* vol. 56, p. 1077–1082, 1952.

[71] C. P. Roe, "Surface chemistry aspects of emulsion polymerization," *Industrial &*

Engineering Chemistry Research, vol. 60, p. 20–33, 1968.

[72] C. H. T. R. M. Fitch, *Polymer Colloids,* New York, 1971.

[73] R. M. Fitch, "The homogeneous nucleation of polymer colloids," *British Polymer Journal,* vol. 5, pp. 467-483, 1973.

[74] R. G. G. D. H. N. Gottfried Lichti, "The mechanisms of latex particle formation and growth in the emulsion polymerization of styrene using the surfactant sodium dodecyl sulfate," *Journal of Polymer Science: Polymer Chemistry Edition,* vol. 21, pp. 269-291, 1983.

[75] N. D. H. G. R. G. Feeney P. J., "Coagulative nucleation and particle size distributions in emulsion polymerization," *Macromolecules,* vol. 17, pp. 2520-2529, 1984.

[76] B. R. M. D. H. N. R. G. G. Ian A. Maxwell, "Entry of free radicals into latex particles in emulsion polymerization," *Macromolecules,* vol. 24, p. 1629–1640, 1991.

[77] M. S. E.-A. J. W. V. J. Ugelstad, "Emulsion polymerization: Initiation of polymerization in monomer droplets," *Journal of Polymer Science: Polymer Letters Edition,* vol. 11, pp. 503-513, 1973.

[78] D. H. N. R. G. G. Bruce J. Chamberlain, "Polymerization within styrene emulsion droplets," *Journal of the Chemical Society, Faraday Transactions 1: Physical Chemistry in Condensed Phases,* vol. 78, pp. 591-606, 1982.

[79] K. H. K. F. K. H. A. B. J. Ugelstad, "Absorption of low molecular weight compounds in aqueous dispersions of polymer-oligomer particles, 2. A two step swelling process of polymer particles giving an enormous increase in absorption capacity," *Makromol. Chem.,* vol. 180, p. 737–744, 1979.

[80] H. R. M. P. C. M. T. E. A. B. R. S. L. H. A. J. F. K. H. K. N. J. Ugelstad, "Preparation and application of monodisperse polymer particles," *Journal of Polymer Science: Polymer Symposia,* vol. 72, pp. 225-240, 1985.

[81] H. F. F. K. H. T. E. J. Ugelstad, «Studies on the emulsion polymerization of vinyl chloride by seed polymerization,» *Journal of Polymer Science: Polymer Symposia,* vol. 42, pp. 473-485, 1973.

[82] E. B. O. J. U. F. K. Hansen, *Theory and Practice of Emulsion Technology,* New York, 1976.

[83] J. U. F. K. Hansen, "Particle nucleation in emulsion polymerization. III. Nucleation in systems with anionic emulsifier investigated by seeded and unseeded polymerization," *Journal of Polymer Science: Polymer Chemistry Edition,* vol. 17, pp. 3047-3067, 1979.

[84] S. K. M. W. A. Maurice Morton, "Swelling of latex particles," *Journal of Colloid Science,* vol. 9, pp. 300-312, 1954.

[85] M. B. Sabine Beuermann, "Rate coefficients of free-radical polymerization deduced from pulsed laser experiments," *Progress in Polymer Science,* vol. 27, pp. 191-254, 2002.

[86] J. Y. H. S. K. S. D. C. Sundberg, "Diffusion-controlled kinetics in the emulsion polymerization of styrene and methyl methacrylate," *ACS Symposium Series,* vol. 165, p. 327–343, 1981.

[87] G.-R. L. G. R. N. D. G. J. H. A. H. D. O. K. O. O. S. J. S. D. M. G. S. M. T. M. W. M. Buback M., "Consistent values of rate parameters in free radical polymerization systems," *Journal of Polymer Science. Part C, Polymer Letters,* vol. 26, pp. 293-297, 1988.

[88] F. J. S. D. T. Barnette, "Continuous miniemulsion polymerization," *Chemical Engineering Science,* vol. 83, pp. 25-30, 1987.

[89] A. E. H. N. Friis, "Kinetics of styrene emulsion polymerization," *Journal of Polymer Science Part A: Polymer Chemistry,* vol. 11, p. 3321–3325, 1973.

[90] W. H. R. J. B. Rawlings, "The modeling of batch and continuous emulsion polymerization reactors. Part I: Model formulation and sensitivity to parameters," *Polymer Engineering & Science,* vol. 28, pp. 237-256, 1988.

[91] W. H. R. J. B. Rawlings, "The modeling of batch and continuous emulsion polymerization reactors. Part II: Comparison with experimental data from continuous stirred tank reactors," *Polymer Engineering & Science,* vol. 28, pp. 257-274, 1988.

[92] R. G. G. D. H. N. P. J. P. P. W. O. J. H. O. Mathew J. Ballard, "Propagation rate coefficients from electron spin resonance studies of the emulsion polymerization of methyl methacrylate," *Macromolecules,* vol. 19, pp. 1303-1308, 1986.

[93] S. K. S. D. Soh, "Diffusion-controlled vinyl polymerization. I. The gel effect," *Journal of Polymer Science: Polymer Chemistry Edition,* vol. 20, pp. 1299-1313, 1982.

[94] D. C. S. S. K. Soh, "Diffusion-controlled vinyl polymerization. III. Free volume parameters and diffusion-controlled propagation," *Journal of Polymer Science: Polymer Chemistry Edition,* vol. 20, pp. 1331-1344, 1982.

[95] F. K. H. S. L. John Ugelstad, «Emulsion polymerization of styrene with sodium hexadecyl sulphate/hexadecanol mixtures as emulsifiers. Initiation in monomer droplets,» *Die Makromolekulare Chemie,* vol. 175, pp. 507-521, 1974.

[96] R. M. Fitch., *Polymer Colloids II,* New York, 1980.

[97] G. H. J.E Carlessa, "The viscosity of emulsifying agents at oil-water interfaces," *Journal of Colloid and Interface Science,* vol. 26, pp. 75-88, 1968.

[98] C. J. Hallworth GW, "Stabilization of oil-in-water emulsions by alkyl sulfates. Influence of the nature of the oil on stability," *Journal of Pharmacy and Pharmacology,* vol. 24, pp. 71-83, 1972.

[99] C. J. Hallworth GW, "Stabilization of oil-in-water emulsions by alkyl sulfates," *Journal of Pharmacy and Pharmacology,* vol. 25, pp. 85-95, 1973.

[100] A. L. Smith, *Theory and Practice of Emulsion Technology,* New York, 1976.

[101] T. J. C. C.S Chern, "Effect of ostwald ripening on styrene miniemulsion stabilized by reactive cosurfactants," *Colloids and Surfaces A: Physicochemical*

and Engineering Aspects, vol. 138, p. 65–74, 1998.

[102] M. S. E.-A. E. D. S. J. W. V. Y. T. Choi, "Polymerization of styrene miniemulsions," *Journal of Polymer Science: Polymer Chemistry Edition,* vol. 23, p. 2973–2987, 1985.

[103] P.-H. N. J.-A. L. X.-L. Z. Zhang-Qing Yu, "Miniemulsion copolymerization of methyl methacrylate and butyl acrylate in the presence of vinyl siloxane rubber," *Colloids and Surfaces A: Physicochemical and Engineering Aspects,* vol. 242, pp. 9-15, 2004.

[104] K. L. Markus Antonietti, "Polyreactions in miniemulsions," *Progress in Polymer Science,* vol. 27, pp. 689-757, 2002.

[105] J. Ugelstad, "Swelling capacity of aqueous dispersions of oligomer and polymer substances and mixtures thereof," *Die Makromolekulare Chemie,* vol. 179, pp. 815-817, 1978.

[106] P. J. Flory, *Principles of Polymer Chemistry,* New York, 1953.

[107] P. M. J. Ugelstad, "Swelling of oligomerpolymer particles. New methods of preparation," *Advances in Colloid and Interface Science,* vol. 13, p. 101–140, 1980.

[108] M. C. W. G. W. P. Lars H. Jansson, "High swelling of latex particles without the utilization of swelling agents," *Journal of Polymer Science: Polymer Letters Edition,* vol. 21, pp. 937-943, 1983.

[109] C. L. Y. C. T. M. J. V. F. F. M.S. El-Aasser, "Interfacial aspects of miniemulsions and miniemulsion polymers," *Colloids and Surfaces,* vol. 12, pp. 79-97, 1984.

[110] F. C. C. P. A. E. H. T. Y. X. J. B. V. V. J. G. M. V. D. H. R. D. Hunkeler, "Heterophase polymerizations: A physical and kinetic comparison and categorization," *Advances in Polymer Science,* vol. 112, pp. 115-133, 1994.

[111] S. R. SAHOO Prafulla K., "Fire retardancy and biodegradability of poly(methyl methacrylate)/ montmorillonite nanocomposite," *Polymer degradation and stability,* vol. 92, pp. 1700-1707, 2007.

[112] J. M. H. A. D. A. S. C. G'Sell, "Video-controlled tensile testing of polymers and metals beyond the necking point," *Journal of materials science,* vol. 27, pp. 5031-5039, 1992.

[113] J.-M. L. J.-L. P. L. D. a. E. B.-L. Negrete, "Aqueous dispersions of silane-functionalized laponite clay platelets. A first step toward the elaboration of water-based polymer/clay nanocomposites," *LANGMUIR,* vol. 20, pp. 1564-1571, 2004.

[114] M. P. J. R. L. Gabriela Diaconu, "High-Solids Content Waterborne Acrylic/Montmorillonite Nanocomposites by Miniemulsion Polymerization," *Macromolecular Reaction Engineering,* vol. 2, pp. 80-89, 2008.

[115] G. Taylor, «The formation of emulsions in definable fields of flow,» *Proceedings of the Royal Society of London,* vol. A146, pp. 501-523, 1934.

[116] A. D. S. A. Plochocki, «The interface in binary mixtures of polymers containing

a corresponding block copolymer: effects of industrial mixing processes and of coalescence,» *Polymer Engineering and Science,* vol. 30, pp. 741-52, 1990.

[117] B. C. J. Favis, «The effect of viscosity ratio on the morphology of propylene/ polycarbonate blends during processing,» *Polymer Engineering and Science,* vol. 27, pp. 1591-600, 1987.

[118] U. M. C. Sundararaj, «Drop breakup and coalescence in polymer blends: The effects of concentration and compatibilization,» *Macromolecules,* vol. 28, pp. 2647-2657, 1995.

[119] B. Favis, «The effect of processing parameters on the morphology of an immiscible binary blend,» vol. 39, p. 285, 1990.

Etude de l'élaboration de nano-particules élastomères et application de celles-ci en tant qu'agents renforçants pour le poly(acide lactique)

Résumé

Le poly(acide lactique) (PLA), est un polymère synthétisé à partir de ressources renouvelables, qui est l'objet de beaucoup d'études à l'heure actuelle mais qui souffre d'une faible résistance au choc. Le but de ce travail est de rechercher des pistes permettant la préparation d'un matériau à base de PLA avec une résistance au choc améliorée tout en minimisant la perte de résistance à la traction.

Les travaux présentés ici ont étudié le rôle de nanoparticules élastomères de poly(acrylate de butyle) (PBA) chargées de laponite (LRD) (PBA-LRD) ainsi que de nanocomposites cœur-écorce (PBA-LRD)/poly(méthacrylate de méthyle) (PMMA) en tant qu'agents de renforcement d'une matrice de PLA. Ces nanoparticules ont été dispersées dans la matrice PLA à l'état fondu. La synthèse de ces nanoparticules a été effectuée par polymérisation en émulsion ou miniémulsion. La laponite a été incorporée dans les nanoparticules afin de minimiser la perte de la rigidité tout en améliorant la résistance au choc de PLA. Trois types de tensioactifs et des modifications de surface de la laponite ont été testées pour améliorer l'adhérence entre les particules de PBA et la matrice de PLA. Enfin une écorce de PMMA a été utilisée pour assurer la bonne adhérence entre les particules de PBA et de matrice PLA. Nous avons montré que les particules cœur-écorce ont permis d'augmenter la résistance au choc au 3 fois du PLA tout en réduisant la diminution du module d'Young et la perte de résistance à la traction (~25%).

Les propriétés de les particules synthétiques et les propriétés des mélange du PLA avec les particules PBA ou particules cœur-écorce ont été étudiées par diverses techniques de caractérisation (DLS, FTIR, ATG, MET, MEB, RMN ^{1}H, DSC, DMTA…).

Mot-clé : Poly(acide lactique) ; Laponite ; Poly(acrylate de butyle), Propriétés mécaniques ; Polymérisation en mini-émulsion ; Poly (méthacrylate de méthyle) ; Nanoparticules cœur-écorce.

Study of the development of elastomer nanoparticles and their application as reinforcing agents for poly(lactic acid)

Abstract

Poly(lactic acid) (PLA), come from renewable resources, one of the most important biopolymers, suffers from weak impact resistance. The aim of this work is to develop a process that will allow preparing a PLA with improved impact resistance while minimizing loss in tensile strength.

The work presented here examined in detail the synthesis of poly(butyl acrylate) (PBA) nanoparticles charged with laponite (LRD) (PBA-LRD) and (PBA-LRD)/poly(methyl methacrylate) (PMMA) core-shell nanocomposites. They were dispersed phase in PLA matrix and were synthesized by emulsion or miniemulsion polymerization. The clay such as laponite was included in these nanoparticles to minimize the loss of rigidity while improving the impact resistance of PLA. Note that three types of surfactants and some modify agents for LRD have been tried to improve the adhesion between the PBA particles and matrix PLA, PMMA was finally used to ensure a good adhesion between the PBA particles and the matrix. To this end, we explored successively the PLA blend, using PBA nanocomposites and the PBA/PMMA core-shell nanoparticles as reinforcing agents, with improved impact resistance, showing that core-shell particles allowed increasing of 3 times of impact strength of the PLA with a minimum amount of loss (~25%) in Young's modulus and tensile strength.

The properties of the synthetic particles and the properties of PLA blends have been demonstrated by various characterization techniques (DLS, FTIR, TGA, TEM, SEM, 1H-NMR, DSC, DMTA ...).

Keyword: Poly(lactic acid); Laponite; Poly(butyl acrylate); Mechanical properties; Miniemulsion polymerization; Poly(methyl methacrylate); Core-shell nanoparticles.